NUREG/CP-0149
Vol. 1

Proceedings of the U.S. Nuclear Regulatory Commission

Twenty-Third Water Reactor Safety Information Meeting

Volume 1
- Plenary Session
- High Burnup Fuel Behavior
- Thermal Hydraulic Research

Held at
Bethesda Marriott Hotel
Bethesda, Maryland
October 23–25, 1995

U.S. Nuclear Regulatory Commission

Office of Nuclear Regulatory Research

Proceedings prepared by
Brookhaven National Laboratory

AVAILABILITY NOTICE

Availability of Reference Materials Cited in NRC Publications

Most documents cited in NRC publications will be available from one of the following sources:

1. The NRC Public Document Room, 2120 L Street, NW., Lower Level, Washington, DC 20555-0001

2. The Superintendent of Documents, U.S. Government Printing Office, P. O. Box 37082, Washington, DC 20402-9328

3. The National Technical Information Service, Springfield, VA 22161-0002

Although the listing that follows represents the majority of documents cited in NRC publications, it is not intended to be exhaustive.

Referenced documents available for inspection and copying for a fee from the NRC Public Document Room include NRC correspondence and internal NRC memoranda; NRC bulletins, circulars, information notices, inspection and investigation notices; licensee event reports; vendor reports and correspondence; Commission papers; and applicant and licensee documents and correspondence.

The following documents in the NUREG series are available for purchase from the Government Printing Office: formal NRC staff and contractor reports, NRC-sponsored conference proceedings, international agreement reports, grantee reports, and NRC booklets and brochures. Also available are regulatory guides, NRC regulations in the *Code of Federal Regulations*, and *Nuclear Regulatory Commission Issuances*.

Documents available from the National Technical Information Service include NUREG-series reports and technical reports prepared by other Federal agencies and reports prepared by the Atomic Energy Commission, forerunner agency to the Nuclear Regulatory Commission.

Documents available from public and special technical libraries include all open literature items, such as books, journal articles, and transactions. *Federal Register* notices, Federal and State legislation, and congressional reports can usually be obtained from these libraries.

Documents such as theses, dissertations, foreign reports and translations, and non-NRC conference proceedings are available for purchase from the organization sponsoring the publication cited.

Single copies of NRC draft reports are available free, to the extent of supply, upon written request to the Office of Administration, Distribution and Mail Services Section, U.S. Nuclear Regulatory Commission, Washington, DC 20555-0001.

Copies of industry codes and standards used in a substantive manner in the NRC regulatory process are maintained at the NRC Library, Two White Flint North, 11545 Rockville Pike, Rockville, MD 20852-2738, for use by the public. Codes and standards are usually copyrighted and may be purchased from the originating organization or, if they are American National Standards, from the American National Standards Institute, 1430 Broadway, New York, NY 10018-3308.

DISCLAIMER NOTICE

NUREG/CP-0149
Vol. 1

Proceedings of the U.S. Nuclear Regulatory Commission

Twenty-Third Water Reactor Safety Information Meeting

Volume 1

- Plenary Session
- High Burnup Fuel Behavior
- Thermal Hydraulic Research

Held at
Bethesda Marriott Hotel
Bethesda, Maryland
October 23–25, 1995

Manuscript Completed: February 1996
Date Published: March 1996

Compiled by: Susan Monteleone

C. Bonsby, NRC Project Manager

Office of Nuclear Regulatory Research
U.S. Nuclear Regulatory Commission
Washington, DC 20555–0001

Proceedings prepared by
Brookhaven National Laboratory

ABSTRACT

This three-volume report contains papers presented at the Twenty-Third Water Reactor Safety Information Meeting held at the Bethesda Marriott Hotel, Bethesda, Maryland, October 23-25, 1995. The papers are printed in the order of their presentation in each session and describe progress and results of programs in nuclear safety research conducted in this country and abroad. Foreign participation in the meeting included papers presented by researchers from France, Italy, Japan, Norway, Russia, Sweden, and Switzerland. The titles of the papers and the names of the authors have been updated and may differ from those that appeared in the final program of the meeting.

PROCEEDINGS OF THE
23rd WATER REACTOR SAFETY INFORMATION MEETING

October 23-25, 1995

Published in Three Volumes

GENERAL INDEX

VOLUME 1

VOLUME 2

VOLUME 3

REGISTERED ATTENDEES (NON-NRC)
23RD WATER REACTOR SAFETY INFORMATION MEETING

D. AGARWAL
U.S. DEPARTMENT OF ENERGY
NE-50/GTN-E478
WASHINGTON, DC 20585 USA

M. AHMED
WESTINGHOUSE ELECTRIC CORP.
4350 NORTHERN PIKE
MONROEVILLE, PA 15146-2886 USA

T. AL-HUSSAINI
DUKE POWER CO.
1010 SHORELINE CO.
STANLEY, NC 28164 USA

M. ALLEN
SANDIA NATIONAL LABORATORY
PO BOX 5800
ALBUQUERQUE, NM 87185-1137 USA

C. ALLISON
IDAHO NATIONAL ENGINEERING LAB
PO BOX 1625, MS 3840
IDAHO FALLS, ID 83415 USA

A. ALONSO
SONSEJO DE SEGURIDAD NUCLEAR
JUSTO DORADO, 11
MADRID, 28040 SPAIN

R. ANDERSON
NORTHERN STATES POWER CO.
414 NICOLLET MALL
MINNEAPOLIS, MN 55401 USA

A. ANKRUM
PACIFIC NORTHWEST LAB
PO BOX 999, MS K826
RICHLAND, WA 99352 USA

K. ARAI
TOSHIBA NUCLEAR ENGINEERING LAB
4-1, UKISHIMA-CHI, KAWASAKI-KU
KAWASAKI, 210 JAPAN

P. ARNOLD
PJA ENGINEERING
FORCHHEIMERSTR. 31
ERLANGEN, 91056 GERMANY

V. ASMOLOV
RRC "KURCHATOV INSTITUTE"
KURCHATOV SQUARE 1
MOSCOW, 123182 RUSSIA

S. AZUMI
KANSAI ELECTRIC POWER CO., INC.
2001 L ST., N.W., SUITE 801
WASHINGTON, DC 20036 USA

M. BALE
B&W FUEL COMPANY
3315 OLD FOREST RD
LYNCHBURG, VA 24506-0935 USA

A. BARATTA
PENN STATE UNIVERSITY
231 SACKETT
UNIVERSITY PARK, PA 16803 USA

J. BARDELAY
IIPSN/CEA
60-68 AV. DU GEN. LECLERC PG6
FONTENAY AUX ROSES, 92265 FRANCE

R. BARI
BROOKHAVEN NATIONAL LABORATORY
BLDG. 197C, PO BOX 5000
UPTON, NY 11973-5000 USA

M. BEAUMONT
WESTINGHOUSE ELECTRIC CORPORATION
11921 ROCKVILLE PIKE - SUITE 450
ROCKVILLE, MD 20852 USA

J. BECKHAM
SOUTHERN NUCLEAR-GEORGIA POWER CO.
PO BOX 1295
BIRMINGHAM, AL 35201 USA

L. BELBLIDIA
SCANDPOWR, INC.
101 LAKE FOREST BLVD, #340
GAITHERSBURG, MD 20877 USA

D. BERRY
SANDIA NATIONAL LABORATORY
P.O. BOX 5800
ALBUQUERQUE, NM 87185-0744 USA

C. BEYER
BATTELLE PNL
11300 W. COURT
PASCO, WA 99302 USA

D. BHARGAVA
VIRGINIA POWER
5000 DOMINION BLVD.
GLEN ALLEN, VA 23060 USA

N. BIXLER
SANDIA NATIONAL LABORATORY
P.O. BOX 5800
ALBUQUERQUE, NM 87185-0739 USA

T. BJORLO
OECD HALDEN REACTOR PROJECT
P.O. BOX 173, OS ALLE 4
N-1751 HALDEN, NORWAY

J. BLASS
OAK RIDGE NATIONAL LABORATORY
236 GUM HOLLOW ROAD
OAK RIDGE, TN 37830 USA

J. BOCCIO
BROOKHAVEN NATIONAL LABORATORY
BLDG. 130, PO BOX 5000
UPTON, NY 11973-5000 USA

L. BOLSHOV
RUSSIAN ACADEMY OF SCIENCES
B. TULSKAYA, 52
MOSCOW, 113191 RUSSIA

M. BONNER
BROOKHAVEN NATIONAL LABORATORY
BLDG. 197C, PO BOX 5000
UPTON, NY 11973-5000 USA

B. BOYACK
LOS ALAMOS NATIONAL LABORATORY
P.O. BOX 1663
LOS ALAMOS, NM 87575 USA

U. BREDOLT
ABB ATOM
ABB ATOM AKTIEBOLAG
VASTERAS S72163 SWEDEN

G. BROWN
AEA TECHNOLOGY
TH5C8, RISLEY WARRINGTON
CHESHIRE, WA36A5 ENGLAND

T. BROWN
SANDIA NATIONAL LABORATORY
PO BOX 5800
ALBUQUERQUE, NM 87185-0748 USA

R. BUDNITZ
FUTURE RESOURCES ASSOCIATES INC.
2039 SHATTUCK AVENUE, SUITE 402
BERKELEY, CA 94704 USA

S. CALPENA
DIR. FOR SAFETY OF NUCLEAR INSTALLATIONS
60-64 AV. DE LA DIVISION LECLERC
FONTENAY AUX ROSES, 92265 FRANCE

A. CAMP
SANDIA LABS.
P.O. BOX 5800, MS 0747
ALBUQUERQUE, NM 87185 USA

G. CAPPONI
ANPA
VIA VITALIANO BRANCATI, 48
ROME, 00144 ITALY

R. CARLSON
LAWRENCE LIVERMORE NATIONAL LAB.
PO BOX 808, L634
LIVERMORE, CA 94551 USA

M. CARLSSON
STUDSVIK NUCLEAR AB
S-611 82 NYKOPING
NYKOPING, S-611 82 SWEDEN

D. CASADA
OAK RIDGE NATIONAL LABORATORY
P.O. BOX 2009
OAK RIDGE, TN 37831-8065 USA

N. CAVLINA
U. OF ZAGREB, ELECT. ENG'G & COMPUTING
UNSKA 3
ZAGREB, 10000 CROATIA

S. CHAKRABORTY
SWISS FEDERAL NUCLEAR SAFETY
INSPECTORATE
VILLIGEN, CH-5232 SWITZERLAND

W. CHEN
ENERGY TECHNOLOGY ENGIN. CENTER
6633 CANOGA AVENUE
CANOGA PARK, CA 91304 USA

F.-B. CHEUNG
PENNSYLVANIA STATE UNIVERSITY
304 REBER BLDG.
UNIVERSITY PARK, PA 16802 USA

D. CHO
ARGONNE NATIONAL LABORATORY
9700 CO. CASS AVE., BLDG. 208
ARGONNE, IL 60439 USA

J-S. CHOI
KOREA INSTITUTE OF NUCLEAR SAFETY
PO BOX 114
YUSUNG, TAEJON, 305-600 KOREA

T. CHU
SANDIA NATIONAL LABORATORY
PO BOX 5800
ALBUQUERQUE, NM 87185-1137 USA

H. CHUNG
ARGONNE NATIONAL LAB
9700 S. CASS AVE
ARGONNE, IL 60439 USA

G. CICCARELLI
BROOKHAVEN NATIONAL LABORATORY
BLDG. 130, PO BOX 5000
UPTON, NY 11973-5000 USA

J. CLAUSS
SANDIA NATIONAL LABORATORY
PO BOX 5800, MS-0741
ALBUQUERQUE, NM 87185-0741 USA

P. COLAIANNI
DUKE POWER CO.
MAIL STOP EC12R P.O. BOX 1006
CHARLOTTE, NC 28201-1006 USA

R. COLE
SANDIA NATIONAL LABORATORY
SANDIA NATIONAL LAB, DEPT. 6421
ALBUQUERQUE, NM 87185-0739 USA

L. CONNOR
STS, INC.
3 METRO CENTER - SUITE 610
BETHESDA, MD 20814 USA

S. COOPER
SCIENCE APPLICATIONS INTERNATIONAL CORP.
11251 ROGER BACON D, M/S R-3-1
RESTON, VA 22090 USA

B. CORWIN
OAK RIDGE NATIONAL LABORATORY
P.O. BOX 2008
OAK RIDGE, TN 37831-6151 USA

M. COURTAUD
COMMISSARIAT A L'ENERGIE ATOMIQUE
CEA/GRENOBLE - 17, RUE DES MARTYRS
GRENOBLE CEDEX 9, 38054 FRANCE

M. CUNNINGHAM
PACIFIC NORTHWEST LAB.
PO BOX 999
RICHLAND, WA 99352 USA

C. CZAJKOWSKI
BROOKHAVEN NATIONAL LABORATORY
BLDG. 130, PO BOX 5000
UPTON, NY 11973-5000 USA

J. DAVIS
BROOKHAVEN NATIONAL LABORATORY
BLDG. 130, PO BOX 5000
UPTON, NY 11973-5000 USA

J. DAVIS
NEI
1776 I ST NW
WASHINGTON, DC 20002 USA

D. DIAMOND
BROOKHAVEN NATIONAL LABORATORY
BLDG. 130, PO BOX 5000
UPTON, NY 11973-5000 USA

S. DINGMAN
SANDIA NATIONAL LABORATORY
PO BOX 5800, MS 0747
ALBUQUERQUE, NM 87185-0747 USA

S. DOROFEEV
RRC "KURCHATOV INSTITUTE"
KURCHATOV SQUARE 1
MOSCOW, 123182 RUSSIA

A. DRAKE
WESTINGHOUSE ELECTRIC CORP.
P.O. BOX 350
PITTSBURGH, PA 15239 USA

J-L. DROULAS
ELECTRICITE DE FRANCE-SEPTEN
12-14, AVENUE DUTRIEVOZ
VILLEURBANNE CEDEX, 69628 FRANCE

J. DUCO
IPSN/DPEI CEA-FAR
BP6
FONTENAY-AUX-ROSES, 92265 FRANCE

M. EL-HAWARY
ATOMIC ENERGY CONTROL BOARD, CANADA
280 SLATER STREET
OTTAWA, ONT K1P 5S9 CANADA

Z. ELAWAR
PALO VERDE NUCLEAR PLANT
PO BOX 52034
PHOENIX, AZ 85072-2034 USA

R. ENNIS
TENERA
1901 RESEARCH BLVD.
ROCKVILLE, MD 20850 USA

P. EWING
OAK RIDGE NATIONAL LABORATORY
PO BOX 2008, MS 6006
OAK RIDGE, TN 37831 USA

R. FENECH
NUCLEAR OPERATIONS, PALISADES PLANT
27780 BLUE STAR MEMORIAL HWY.
COVERT, MI 49043 USA

D. FERETIC
U. OF ZAGREB, ELECT. ENG'G & COMPUTING
UNSKA 3
ZAGREB, 10000 CROATIA

R. FIELDHACK
WISCONSIN ELECTRIC POWER CO.
231 W. MICHIGAN
MILWAUKEE, WI 53201 USA

I. FIERO
ABB COMBUSTION ENGINEERING
1000 PROSPECT HILL RD
WINDSOR, CT 06095 USA

L. FISCHER
LAWRENCE LIVERMORE NATIONAL LAB.
PO BOX 808, L631
LIVERMORE, CA 94551 USA

M. FLETCHER
AECL TECHNOLOGIES
19041 RAINES DRIVE
DERWOOD, MD 20855 USA

K. FOLK
SOUTHER NUCLEAR
P.O. BOX 1295
BINMINGHAM, AL 35201 USA

J. FORESTER
SANDIA NATIONAL LABORATORY
PO BOX 5800, MS 0747
ALBUQUERQUE, NM 87185-0747 USA

E. FOX
OAK RIDGE NATIONAL LABORATORY
P.O. BOX 2009
OAK RIDGE, TN 37832-8063 USA

W. FRID
SWEDISH NUCLEAR POWER INSPECTORATE
UTLANDSGIRO 7, UTSI
STOCKHOLM, S-10658 SWEDEN

T. FUKETA
JAPAN ATOMIC ENERGY RESEARCH INSTITUTE
TOKAI, IBARAKI 319-11
TOKAI, 319-11 JAPAN

W. GALYEAN
IDAHO NATIONAL ENGINEERING LAB
PO BOX 1625
IDAHO FALLS, ID 83415-3850 USA

R. GAMBLE
GE NUCLEAR ENERGY
75 CURTNER AVE., MC 781
SAN JOSE, CA 95125 USA

P. GANGO
IVO INTERNATIONAL LTD.
RAJATORPANTIE 8, VANTAA
IVO, 01019 FINLAND

R. GAUNTT
SANDIA NATIONAL LABORATORY
PO BOX 5800, MS 1139
ALBUQUERQUE, NM 87185 USA

G. GAUTHIER
INST. OF PROTECTION & NUCLEAR SAFETY
DES/SAMS BP 6F
FONTENAY-AUX-ROSES, 92265 FRANCE

R. GAZDZINSKI
OGDEN ENVIRONMENTAL & ENERGY SVCS.
1777 SENTRY PKWY W., STE 300
BLUE BELL, PA 19422 USA

N. GHADIALI
BATTELLE COLUMBUS LABORATORIES
505 KING AVE
COLUMBUS, OH 43201 USA

G. GIGGER
WESTINGHOUSE ELECTRIC
PO BOX 79
WEST MIFFLIN, PA 15122 USA

K. GILLEN
SANDIA NATIONAL LABORATORY
PO BOX 5800, MS 1407
ALBUQUERQUE, NM 87185-1407 USA

R. GILLILAND
OAK RIDGE NATIONAL LABORATORY
PO BOX 2009, MS 8063
OAK RIDGE, TN 37830-8063 USA

J. GLEASON
CONSULTANT TO BNL
1819 CROSS CREEK RD.
HUNTSVILLE, AL 35802 USA

L. GOLDSTEIN
S.M. STOLLER CORP.
485 WASHINTON AVENUE
PLEASANTVILLE, NY 10570 USA

M. GOMOLINSKI
IPSN - FRANCE
BP 6
FONTENAY AUX ROSES, 92265 FRANCE

S. GRAHAM
NAVAL SURFACE WARFARE CENTER
CODE 614, 3A LEGGETT CIR.
ANNAPOLIS, MD 21402 USA

D. GRAND
CEA DRN/DTP/STR
STR CEA-GRENOBLE 17, RUE DES MARTYRS
GRENOBLE-CEDEX 9, 38054 FRANCE

W. GRANT
ATOMIC ENERGY CONTROL BOARD - CANADA
P.O. BOX 1046, STN. B, 280 SLATER STREET
OTTAWA, ONT K1P 5S9 CANADA

M. GREGORIC
SLOVENIAN NUCLEAR SAFETY ADMIN.
VOJKOVA 59
LJUBLJANA, 61113 SLOVENIA

F. GRIFFIN
OAK RIDGE NATIONAL LABORATORY
PO BOX 2009
OAK RIDGE, TN 37831-8057 USA

M. GROUNES
STUDSVIK NUCLEAR AB
S-611 82 NYKOPING
NYKOPING, S-611 82 SWEDEN

K. HADDAD
PENNSYLVANIA STATE UNIVERSITY
215 REBER BLDG.
UNIVERSITY PARK, PA 16802 USA

L. HANES
EPRI
3412 HILLVIEW AVENUE
PALO ALTO, CA 94304 USA

A. HANEVIK
OECD HALDEN PROJECT
OS ALLE 13
1750 HALDEN, NORWAY

D. HARRISON
U.S. DEPT. OF ENERGY
NE-50
WASHINGTON, DC 20545 USA

G. HART
PERFORMANCE CONTRACTING INC.
4025 BONNE INDUSTRIAL
SHAWNEE, KS 66226 USA

H. HASHEMIAN
ANALYSIS & MEASUREMENT SERVICES CORP.
AMS 9111 CROSS PARK DR.
KNOXVILLE, TN 37923 USA

K. HASHIMOTO
JAPAN ATOMIC ENERGY RESEARCH INSTITUTE
TOKAI-MURA
IBARAKI-KEN, 319-11 JAPAN

G. HECKER
ALDEN RESEARCH LABORATORY, INC.
30 SHREWSBURY STREET
HOLDEN, MA 01520 USA

G. HEUSENER
FORSCHUNGSZENTRUM KARLSRUHE
POSTFACH 3640
KARLSRUHE, 76021 GERMANY

J. HIGGINS
BROOKHAVEN NATIONAL LABORATORY
BLDG. 130, PO BOX 5000
UPTON, NY 11973-5000 USA

L. HOCHREITER
WESTINGHOUSE ELECTRIC CORP.
P.O. BOX 355
PITTSBURGH, PA 15230 USA

P. HOFMANN
FORSCHUNGSZENTRUM KARLSRUHE
POSTFACH 3640
KARLSRUHE, 76021 GERMANY

S.W. HONG
SANDIA NATIONAL LABORATORY
PO BOX 5800, MS 1139
ALBUQUERQUE, NM 87185 USA

E. HONTANON
C.I.E.M.A.T. RESEARCH CENTER
AVDA. COMPLUTENSE, 22
MADRID, 28040 SPAIN

W. HORIN
WINSTON & STRAWN
1400 I ST. N.W.
WASHINGTON, DC 20005 USA

L. HORVATH
BROOKHAVEN NATIONAL LABORATORY
BLDG. 130, P.O. BOX 5000
UPTON, NY 11973 USA

R. HOUSER
WESTINGHOUSE BETTIS ATOMIC POWER LAB.
PO BOX 79
WEST MIFFLIN, PA 15122 USA

T. HSU
VIRGINIA POWER
5000 DOMINION BLVD.
GLEN ALLEN, VA 23060 USA

A. HUERTA
CNSNS
DR. BARRAGAN 779; COL. NARVARIC
MEXICO D.F., MEXICO 03020 MEXICO

J. HUTCHINSON
EPRI PLANT SUPPORT ENGINEERING
1300 W. HARRIS BLVD
CHARLOTTE, NC 28262 USA

Y.D. HWANG
KOREA ATOMIC ENERGY RESEARCH INSTITUTE
POWER REACTOR DEVELOPMENT TEAM
YUSUNG-GU, TAEJUN KOREA

T. HYRSKY
IVO INTERNATIONAL LTD.
RAJATORPANTLE 8, VANTAA
IVO, 01019 FINLAND

J. HYVARINEN
FINNISH CENTRE FOR RAD. & NUC. SAFETY
PO BOX 14
HELSINKI, FIN-00881 FINLAND

K. IDO
SHIKOKU ELECTRIC POWER CO., INC.
6-1-2 MINATOMACHI
MATSUYAMA, 790 JAPAN

J. IRELAND
LOS ALAMOS NATIONAL LABORATORY
PO BOX 1663, MS F606
LOS ALAMOS, NM 87545 USA

M. ISHII
PURDUE UNIVERSITY
1290 NUCLEAR ENGINEERING BLDG.
WEST LAFAYETTE, IN 47907-1290 USA

K. ISHIJIMA
JAPAN ATOMIC ENERGY RESEARCH INSTITUTE
TOKAI, IBARAKI 319-11
TOKAI, 319-11 JAPAN

R. ISLAMOV
RUSSIAN ACADEMY OF SCIENCES
B. TULSKAYA, 52
MOSCOW, 113191 RUSSIA

T. ITO
JAPAN INSTITUTE OF NUCLEAR SAFETY
FUJITA KANKO TORANOMON BLDG. 4F
MINATO-KU, TOKYO 105 JAPAN

R. JAMES
ELECTRIC POWER RESEARCH INSTITUTE
3412 HILLVIEW AVENUE
PALO ALTO, CA 94304 USA

F. JANSKY
BTB-JANSKY GMBH
GERLIUGER STR. 151
LEONBERG, 71229 GERMANY

M. JIMINEZ
FLORIDA POWER & LIGHT
700 UNIVERSE BLVD.
JUNO BEACH, FL 33408 USA

R. JOHNSON
PACIFIC GAS & ELECTRIC CO.
PO BOX 770000, MC A10A
SAN FRANCISCO, CA 94177 USA

W. JOHNSON
UNIVERSITY OF VIRGINIA
REACTOR BUILDING, UNIVERSITY OF VIRGINIA
CHARLOTTESVILLE, VA 22903 USA

S. KARIMIAN
PSE&G
PO BOX 236
HANCOCK'S BRIDGE, NJ 08038 USA

T. KASSNER
ARGONNE NATIONAL LAB
9700 S. CASS AVE
ARGONNE, IL 60439 USA

S. KERCEL
OAK RIDGE NATIONAL LABORATORY
PO BOX 2008, MS 6318
OAK RIDGE, TN 37831 USA

S. KIKKAWA
NUCLEAR POWER ENGINEERING CORP.
3-CHOME TORANOMON, 8F, 17-1
MINATO-KU, TOKYO 105 JAPAN

K. KILPI
VTT ENERGY
PO BOX 1604, FIN-02044 VTT
ESPOO 15, 02150 FINLAND

B. KIM
KOREA INSTITUTE OF NUCLEAR SAFETY
PO BOX 114
YUSUNG, TAEJON, 305-600 KOREA

H. KIM
KOREA INSTITUTE OF NUCLEAR SAFETY
PO BOX 114
YUSUNG, TAEJON, 305-600 KOREA

H.C. KIM
KOREA INSTITUTE OF NUCLEAR SAFETY
PO BOX 114
YUSUNG, TAEJON, 305-600 KOREA

H.Y. KIM
KOREA INSTITUTE OF NUCLEAR SAFETY
PO BOX 114
YUSUNG, TAEJON, 305-600 KOREA

S.B. KIM
KOREA ATOMIC ENERGY RESEARCH INSTITUTE
P.O. BOX 105, YUSEONG
TAEJON, KOREA

S. KINNERSLY
AEA TECHNOLOGY
UK WINFRITH
DORCITESTER, DORSET U.K.

A. KISSELEV
RUSSIAN ACADEMY OF SCIENCES
B. TULSKAYA, 52
MOSCOW, 113191 RUSSIA

M. KITAMURA
NUCLEAR POWER ENGINEERING CORP.
3-13, 4-CHOME TORANOMON, MINATO-KU
TOKYO, 105 JAPAN

J. KLAPPROTH
GENERAL ELECTRIC
PO BOX 780, MC J26
WILMINGTON, NC 28409 USA

L. KLEIN
ATOMIC ENERGY CONTROL BOARD CANADA
PO BOX 1046, STA. B, 280 SLATER ST.
OTTAWA, ONT K1P 5S9 CANADA

J. KLUGEL
SWISS FEDERAL NUC. SAFETY INSPECTORAT
VILLIGEN, CH-5232 SWITZERLAND

N. KOJIMA
MITSUBISHI HEAVY INDUSTRIES, LTD.
1-1, WADAMISAKI-CHO, 1-CHOME
HYOGO-KU, KOBW JAPAN

K. KORSAH
OAK RIDGE NATIONAL LABORATORY
PO BOX 2008, MS 6010
OAK RIDGE, TN 37831 USA

D. KOSS
PENNSYLVANIA STATE UNIVERSITY
202A STEIDLE BLDG.
UNIVERSITY PARK, PA 16802 USA

F. KRAMER
CONSULTANT TO MITSUBISHI HEAVY IND.
5427 FAIR OAKS ST.
PITTSBURGH, PA 15217 USA

B. KUJAL
NUCLEAR RESEARCH INSTITUTE
NUCLEAR POWER & SAFETY DIV.
REZ, 25068 CZECH REPUBLIC

Y. KUKITA
JAPAN ATOMIC ENERGY RESEARCH INSTITUTE
TOKAI, IBARAKI 319-11
TOKAI, 319-11 JAPAN

K. KURODA
NUCLEAR POWER ENGINEERING CORP.
3-CHOME TORANOMON, 8F, 17-1
MINATO-KU, TOKYO 105 JAPAN

K. KUSSMAUL
MPA, UNIVERSITY OF STUTTGART
PFAFFENWALDRING 32
STUTTGART, 70569 GERMANY

J. LA CHANCE
SCIENCE APPLICATIONS INTERNATIONAL CORP.
2109 AIR PARK RD SE
ALBUQUERQUE, NM 87106 USA

P. LACY
UTILITY RESOURCE ASSOCIATES CORP.
51 MONROE ST., STE 1600
ROCKVILLE, MD 20850 USA

J. LAKE
IDAHO NATIONAL ENGINEERING LABORATORY
BOX 1625, MS 3860
IDAHO FALLS, ID 83415-3860 USA

S. LANGENBUCH
GRS - GERMANY
FORSCHUNGSGELANDE
GARCHING, 85748 GERMANY

H-K. LEE
NUCLEAR TECH DEPT.
ATOMIC ENERGY COUNCIL
TAIPEI, TAIWAN ROC

J. LEE
KOREA INSTITUTE OF NUC. SAFETY
P.O. BOX 114 YUSUNG
TAEJON, KOREA

S. LEE
ONTARIO HYDRO
700 UNIVERSITY AVENUE
TORONTO, ONTARIO M5G 1X6 CANADA

Y-W. LEE
KOREA INSTITUTE OF NUCLEAR SAFETY
PO BOX 114
YUSUNG, TAEJON, 305-600 KOREA

J. LEHNER
BROOKHAVEN NATIONAL LABORATORY
BLDG. 130, PO BOX 5000
UPTON, NY 11973-5000 USA

S. LEVINSON
B&W NUCLEAR TECHNOLOGIES
3315 OLD FOREST RD.
LYNCHBURG, VA 24501 USA

R. LICCIARDO
PROFESSIONAL ENGINEER & ECONOMIST
11801 ROCKVILLE PIKE, SUITE 1405
NO. BETHESDA, MD 20852 USA

M. LIVOLANT
IPSN
CE/FAR BP6
FONTENAY-AUX-ROSES CEDEX, 92265 FRANCE

K. LOCKWOOD
KNOLLS ATOMIC POWER LABORATORY
PO BOX 1072 (P3-172)
SCHENECTADY, NY 12301-1072 USA

R. LOFARO
BROOKHAVEN NATIONAL LABORATORY
BLDG. 130, PO BOX 5000
UPTON, NY 11973-5000 USA

J.-L. LUC
DIR. FOR SAFETY OF NUCLEAR INSTALLATIONS
4 IMPASSE MATHIEU
PARIS, 75015 FRANCE

W. LUCKAS
BROOKHAVEN NATIONAL LABORATORY
BLDG. 130, PO BOX 5000
UPTON, NY 11973-5000 USA

D. MAGALLON
CEC-JRC-ISPRA
JRC-EURATOM ISPRA
ISPRA, 20120 ITALY

H. MAGLEBY
IDAHO NATIONAL ENGINEERING LAB
PO BOX 1625, MS 3870
IDAHO FALLS, ID 83415 USA

B. MAGONDEAUX
ELECTRICITE DE FRANCE-SEPTEN
12-14, AVENUE DUTRIEVOZ
VILLEURBANNE CEDEX, 69628 FRANCE

J. MARN
U. OF MARIBOR, FAC. OF MECHANICAL ENG'G.
PO BOX 224
MARIBOR, SI62000 SLOVENIA

R. MARTINEZ, JR.
JUPITER CORPORATION
STE 900, 2730 UNIVERSITY BLVD. W.
WHEATON, MD 20902 USA

T. MATSUMOTO
NUCLEAR POWER ENGINEERING CORP.
5F 17-1, TORANOMON, MINATO-KU
TOKYO, 105 JAPAN

G. MEYER
B&W FUEL COMPANY
3315 OLD FOREST RD
LYNCHBURG, VA 24506-0935 USA

P. MEYER
SWISS FEDERAL NUC. SAFETY INSPECTORATE
(HSK)
VILLIGEN, AG CH-5232 SWITZERLAND

T. MIEDA
ISHIKAWAJIMA-HARIMA HEAVY INDUSTRIES
1, SHIN-NAKAHARA-CHO, ISOGO-KU
YOKOHAMA, 235 JAPAN

P. MILELLA
ANPA
VIA VITALIANO BRANCATI 68
ROME, 00144 ITALY

J. MILLER
SCIENTECH
11140 ROCKVILLE PIKE, SUITE 500
ROCKVILLE, MD 20874 USA

R. MILLER
WESTINGHOUSE ELECTRIC CORP.
PO BOX 355
PITTSBURGH, PA 15230 USA

S. MIRSKY
SCIENCE APPLICATIONS INTERNATIONAL CORP.
20201 CENTURY BLVD.
GERMANTOWN, MD 20770 USA

S. MODRO
IDAHO NATIONAL ENGINEERING LABORATORY
P.O. BOX 1625, MS 3895
IDAHO FALLS, ID 83415 USA

S. MONTELEONE
BROOKHAVEN NATIONAL LABORATORY
BLDG. 130, PO BOX 5000
UPTON, NY 11973-5000 USA

M. MONTGOMERY
NUCLEAR FUEL INDUSTRIES, LTD.
3845 NORWOOD CT.
BOULDER, CO 80304 USA

D. MOON
WASHINGTON PUBLIC PWR SUPPLY SYS
PO BOX 968 (MD PE21)
RICHLAND, WA 99352 USA

E. MOREL
FRAMATOME
TOUR FIAT
PARIS LA DEFENSE, 92084 FRANCE

A. MOTTA
PENNSYLVANIA STATE UNIVERSITY
231 SACKETT BLDG.
UNIVERSITY PARK, PA 16802 USA

M. MUHLHEIM
OAK RIDGE NATIONAL LABORATORY
P.O. BOX 2009
OAK RIDGE, TN 37831-8065 USA

M. MUNTZING
MORGAN LEWIS & BOCKIUS LLP
1800 M ST., NW
WASHINGTON, DC 20036 USA

Y.W. NA
KOREA ATOMIC ENERGY RESEARCH INSTITUTE
PO BOX 105, YUSONG
TAEJON, 305-600 KOREA

A. NAKAMURA
NUCLEAR POWER ENGINEERING CORP.
3-13. 4-CHOME, TORANOMON.MINATO-KU
TOKYO, 105 JAPAN

Y. NARUSE
TOSHIBA CORP.
8, SHINSUGITA-CHO, ISOGO-KU
YOKOHAMA, 235 JAPAN

D. NAUS
OAK RIDGE NATIONAL LABORATORY
P.O. BOX 2009
OAK RIDGE, TN 37831-8065 USA

U. NAYAK
WESTINGHOUSE ELECTRIC CORP.
PO BOX 355
PITTSBURGH, PA 15230 USA

G. NIEDERAUER
LOS ALAMOS NATIONAL LABORATORY
MS K575 LANL
LOS ALAMOS, NM 87545 USA

A. NUNEZ
CNSNS
DR. BARRAGAN 779; COL. NARVARIC
MEXICO D.F., MEXICO 03020 MEXICO

S. ONO
HITACHI WORKS, HITACHI LTD.
1-1 SAIWAI-CHO 3-CHOME, HIMCHI-SHI
IBARAKI-KEN, 317 JAPAN

N. ORTIZ
SANDIA NATIONAL LABORATORY
PO BOX 5800, MS 0736
ALBUQUERQUE, NM 87185-0736 USA

D. OSETEK
LOS ALAMOS TECHNICAL ASSOCIATES
BLDG. 1 SUITE 400, 2400 LOUISIANA BLVD. NE
ALBUQUERQUE, NM 87110 USA

F. OWRE
OECD HALDEN REACTOR PROJECT
DS ALLE 13
N 1751 HALDEN, NORWAY

Q. OZER
EPRI
PO BOX 10412
PALO ALTO, CA 94303-0813 USA

J. PAPIN
IPSN
CE CADARACHE
ST PAUL LEZ DURANCE, 13108 FRANCE

K-B. PARK
KOREA ATOMIC ENERGY RESEARCH INST.
PO BOX 105, YUSONG
TAEJON, 305-600 KOREA

M. PARKER
IL DEPT. OF NUCLEAR SAFETY
1035 OUTER PARK DRIVE
SPRINGFIELD, IL 62704 USA

J. PELTIER
IPSN
C.E. FONTENAY - AUX - ROSES BP6
FONTENAY-AUX-ROSES, 92965 FRANCE

W. PENNELL
OAK RIDGE NATIONAL LABORATORY
PO BOX 2009, MS-8056
OAK RIDGE, TN 37830-8056 USA

A. PEREZ-NAVARRO
UNIV. ALFONSO X EL SABIO
AVDA D E LA UNIVERSIDAD, 1
MADRID, 28691 SPAIN

V. PETENYI
NUC. REG. AUTHORITY OF SLOVAK REPUBLIC
BAJKALSKA 27, PO BOX 24
BRATISLAVA, 820 07 SLOVAKIA

M. PILCH
SANDIA NATIONAL LABORATORY
PO BOX 5800
ALBUQUERQUE, NM 87185-1137 USA

A. POOLE
OAK RIDGE NATIONAL LABORATORY
Y12 PLANT, BLDG. 9102-1 BEAR CREEK RD.
OAK RIDGE, TN 37831-8038 USA

V. PROKLOV
RRC "KURCHATOV INSTITUTE"
KURCHATOV SQUARE 1
MOSCOW, 123182 RUSSIA

J. PUGA
UNESA
FRANCISCO GERVAS 3
MADRID, 28020 SPAIN

C. PUGH
OAK RIDGE NATIONAL LABORATORY
PO BOX 2009, MS 8063
OAK RIDGE, TN 37831 USA

E. PURVIS
10105 CLEAR SPRING ROAD
DAMASCUS, MD 20872 USA

L. RANEY
COMMONWEALTH EDISON CO.
1400 OPUS PL.
DOWNERS GROVE, IL 60515 USA

V. RANSOM
PURDUE UNIVERSITY
SCHOOL OF NUCLEAR ENGINEERING - NUCL 140
WEST LAFAYETTE, IN 47907 USA

D. RAPP
WESTINGHOUSE BETTIS ATOMIC POWER LAB.
PO BOX 79
WEST MIFFLIN, PA 15122 USA

J. RASHID
ANATECH RESEARCH CORP.
5435 OBERLIN DR.
SAN DIEGO, CA 92121 USA

S. RAY
WESTINGHOUSE ELECTRIC CORP.
PO BOX 355
PITTSBURGH, PA 15230 USA

P. REGNIER
INST. OF PROTECTION & NUCLEAR SAFETY
DES/SAMS BP 6F
FONTENAY-AUX-ROSES, 92265 FRANCE

K. REIL
SANDIA NATIONAL LABORATORY
PO BOX 5800, MS 1139
ALBUQUERQUE, NM 87185-1139 USA

M. REOCREUX
IPSN
CE CADARACHE
ST PAUL LEZ DURANCE, 13108 FRANCE

W. RETTIG
DEPARTMENT OF ENERGY
1574 LOLA STREET
IDAHO FALLS, ID 83402 USA

J. REYES, JR.
OREGON STATE UNIVERSITY
RADIATION CENTER C116
CORVALLIS, OR 97331-5902 USA

M. RHATIB-RAHBAR
ENERGY RESEARCH INC.
P.O. BOX 2034
ROCKVILLE, MD 20854 USA

U. ROHATGI
BROOKHAVEN NATIONAL LABORATORY
BLDG. 475B, PO BOX 5000
UPTON, NY 11973-5000 USA

P. ROTHWELL
HM NUCLEAR INSTALLATIONS INSPECTORATE
ST. PETER'S HOUSE, BALLIOL RD., BOOTLE
LIVERPOOL, L20 3LZ UNITED KINGDOM

J. ROYEN
OECD NUCLEAR ENERGY AGENCY
12 BLVD. DES ILES
ISSY-LES-MOULINEAUX, F-92130 FRANCE

K. RUSSELL
IDAHO NATIONAL ENGINEERING LABORATORY
PO BOX 1625, MS 3779
IDAHO FALLS, ID 83415 USA

O. SANDERVAG
SWEDISH NUCLEAR POWER INSPECTORATE
KLARABERGSVIADUKTEN 90
STOCKHOLM, 10658 SWEDEN

H. SASAJIMA
TOSHIBA CORP.
8, SHINSUGITA-CHO, ISOGO-KU
YOKOHAMA, 235 JAPAN

M. SATTISON
LOCKHEED IDAHO TECHNOLOGIES CO.
PO BOX 1625, MS 3850
IDAHO FALLS, ID 83415-3850 USA

N. SCHAUKI
SIEMENS/WYLE
445 UPSHIRE CIRC.
GAITHERSBURG, MD 20878 USA

P. SCHEINERT
WESTINGHOUSE BETTIS ATOMIC POWER LAB.
PO BOX 79
WEST MIFFLIN, PA 15122 USA

E. SCHMIDT
NUS CORP.
910 CLOPPER ROAD
GAITHERSBURG, MD 20878 USA

F. SCHMITZ
IPSN
CE CADARACHE
ST PAUL LEZ DURANCE, 13108 FRANCE

W. SCHOLTYSSEK
FORSCHUNGSZENTRUM KARLSRUHE
POSTFACH 3640
KARLSRUHE, 76021 GERMANY

M. SCHWARZ
IPSN
CE CADARACHE
ST PAUL LEZ DURANCE, 13108 FRANCE

M. SEITO
JAPAN INSTITUTE OF NUCLEAR SAFETY
FUJITA KANKO TORANOMON BLDG. 7F
MINATO-KU, TOKYO 105 JAPAN

P. SEONG
KOREA ADVANCED INST. OF SCIENCE & TECH.
373-1 GUSONG-DONG YUSONG-KU
TAEJON, 305-701 KOREA

S. SETH
THE MITRE CORPORATION
MS:W779, 7525 COLSHIRE DRIVE
MC LEAN, VA 22102 USA

W. SHA
ARGONNE NATIONAL LABORATORY
9700 S. CASS AVENUE
ARGONNE, IL 60439 USA

W. SHACK
ARGONNE NATIONAL LAB
BLDG. 212
ARGONNE, IL 60439 USA

J. SHEFFIELD
OAK RIDGE NATIONAL LABORATORY
PO BOX 2008
OAK RIDGE, TN 37831-6248 USA

S. SIM
KOREA ATOMIC ENERGY RESEARCH INSTITUTE
DUKJIN-DONG 150, KAERI
TAEJON, KOREA

L. SIMPSON
ATOMIC ENERGY OF CANADA LTD.
WHITESHELL LABORATORIES
PINAWA, MANITOBA ROE 1LO CANADA

W. SLAGLE
WESTINGHOUSE ELECTRIC CORP.
PO BOX 355
PITTSBURGH, PA 15230 USA

L. SLEGERS
SIEMENS-KWU
P.O. BOX 101063, BERLINER STR. 295
OFFENBACH, D63067 GERMANY

S. SLOAN
IDAHO NATIONAL ENGINEERING LABORATORY
PO BOX 1625
IDAHO FALLS, ID 83415-3895 USA

V. SMIRNOV
RRC "KURCHATOV INSTITUTE"
KURCHATOV SQUARE 1
MOSCOW, 123182 RUSSIA

F. SOUTO
SCIENCE & ENGINEERING ASSOCIATES, INC.
6100 UPTOWN BLVD. NE, STE 700
ALBUQUERQUE, NM 87110 USA

K. ST. JOHN
YANKEE ATOMIC ELECTRIC CO.
580 MAIN ST.
BOLTON, MA 01741 USA

R. STEELE, JR.
IDAHO NATIONAL ENGINEERING LAB
PO BOX 1625
IDAHO FALLS, ID 83415-3870 USA

P. STOOP
NETHERLANDS ENERGY RES. FOUNDATION
PO BOX 1, 1755 ZG PETTEN
WESTERDUINWEG 3, PETTEN,
THE NETHERLANDS

M. STRAND
SCIENTECH, INC.
11140 ROCKVILLE PIKE, SUITE 500
ROCKVILLE, MD 20852 USA

V. STRIZHOV
RUSSIAN ACADEMY OF SCIENCES
B. TULSKAYA, 52
MOSCOW, 113191 RUSSIA

E. STUBBE
TRACTEBEL ENERGY ENGINEERING
AVENUE ARIANE 7
BRUSSELS, 1200 BELGIUM

W. STUBLER
BROOKHAVEN NATIONAL LABORATORY
BLDG. 130, PO BOX 5000
UPTON, NY 11973-5000 USA

S. SUNG
KOREAN NUCLEAR FUEL CO.
HYUPSIN-MEMSION #101,
177-9 YONGDUZ-DONG JUNG-GU,
TAEJON, SOUTH KOREA

H. TAGAWA
NUPEC
BROOKHAVEN NAT. LAB., APT. 4C
UPTON, NY 11973 USA

M. TAKAYASU
NUCLEAR FUEL INDUSTRIES, LTD.
950, OHAZA NODA KUMATORI-CHO
SENNAN-GUN, OSAKA 590-04 JAPAN

T. TANAKA
SANDIA NATIONAL LABORATORY
PO BOX 5800, MS 0737
ALBUQUERQUE, NM 87185-0737 USA

J. TAYLOR
BROOKHAVEN NATIONAL LABORATORY
BLDG. 130, PO BOX 5000
UPTON, NY 11973-5000 USA

C. THIBAULT
WYLE LABORATORIES
7800 HIGHWAY 20 WEST
HUNTSVILLE, AL 35807-7777 USA

H. THORNBURG
CONSULTANT
901 S. WARFIELD DR.
MT. AIRY, MD 21771 USA

E. TITLAND
MATERIALS & ENERGY ASSOCIATES, INC.
512 IDLEWILD RD., PO BOX 1107
BEL AIR, MD 21014 USA

J. TONG
ATOMIC ENERGY CONTROL BOARD, CANADA
280 SLATER STREET
OTTAWA, ONT KIP 5S9 CANADA

L. TOTH
KFKI ATOMIC ENERGY RESEARCH INST.
PO BOX 49
BUDAPEST, H-1525 HUNGARY

R. TREGONING
NAVAL SURFACE WARFARE CENTER
CODE 614, 3A LEGGETT CIR.
ANNAPOLIS, MD 21402 USA

R. VALENTIN
ARGONNE NATIONAL LABORATORY
9700 S. CASS AVENUE - BLDG. 308
ARGONNE, IL 60439 USA

K. VALTONEN
FINNISH CENTRE FOR RAD. & NUC. SAFETY
PO BOX 14
HELSINKI, FIN-00881 FINLAND

T. VAN ETTEN
KNOLLS ATOMIC POWER LABORATORY
PO BOX 1072 (P3-172)
SCHENECTADY, NY 12301-1072 USA

M. VESCHUNOV
RUSSIAN ACADEMY OF SCIENCES
B. TULSKAYA, 52
MOSCOW, 113191 RUSSIA

Y. WAARANPERA
ABB ATOM
NUCLEAR SYSTEMS DIV.
VASTERAS, S-72163 SWEDEN

N. WAECKEL
EDF SEPTEN
12-14 AVENUE DUTRIEVOZ
VILLEURBANNE, 69628 FRANCE

J. WATKINS
IDAHO NATIONAL ENGINEERING LAB
PO BOX 1625
IDAHO FALLS, ID 83415-3870 USA

M. WETZEL
BECHTEL CORP.
9801 WASHINGTONIAN BLVD.
GAITHERSBURG, MD 20878 USA

K. WHITT
SOUTHERN NUCLEAR
40 INVERNESS CENTER PKWY.
BIRMINGHAM, AL 35201 USA

W. WIESENACK
OECD HALDEN REACTOR PROJECT
P.O. BOX 171
HALDEN, NORWAY

G. WILKOWSKI
BATTELLE COLUMBUS
505 KING AVENUE
COLUMBUS, OH 43201 USA

S. WILLIAMS
DOMINION ENGINEERING, INC.
6862 ELM ST.
MC LEAN, VA 22101 USA

R. WOOD
OAK RIDGE NATIONAL LABORATORY
PO BOX 2008, MS 6010
OAK RIDGE, TN 37831 USA

J. WREATHALL
WREATHWOOD GROUP
4157 MACDUFF WAY
DUBLIN, OH 43016 USA

J. WRIGHT
MODELING & COMPUTING SERVICES
6400 LOOKOUT ROAD
BOULDER, CO 80301 USA

G. WROBEL
ROCHESTER GAS & ELECTRIC CORP.
89 EAST AVENUE
ROCHESTER, NY 14649 USA

L. WUNDERLICH
KNOLLS ATOMIC POWER LABORATORY
PO BOX 1072 (D2-221)
SCHENECTADY, NY 12301-1072 USA

G. YADIGAROGLU
SWISS FED. INST. OF TECH. &
PAUL SCHERRER INST.
ETH-ZENTRUM, CLT
ZURICH, CH-8092 SWITZERLAND

L. YEGOROVA
RRC "KURCHATOV INSTITUTE"
KURCHATOV SQUARE 1
MOSCOW, 123182 RUSSIA

K-J. YOO
KOREA ATOMIC ENERGY RESEARCH INST.
PO BOX 105, YUSONG
TAEJON, 305-600 KOREA

M. YOUNG
SANDIA NATIONAL LABORATORY
PO BOX 5800
ALBUQUERQUE, NM 87185-0748 USA

T. ZAMA
TOKYO ELECTRIC POWER CO., INC.
1901 L ST., NW, SUITE 720
WASHINGTON, DC 20036 USA

G. ZIGLER
SCIENCE & ENGINEERING ASSOCIATES, INC.
6100 UPTOWN BLVD. NE, STE 700
ALBUQUERQUE, NM 87110 USA

PROCEEDINGS OF THE
23rd WATER REACTOR SAFETY INFORMATION MEETING
October 23-25, 1995

CONTENTS - VOLUME 1

UNITED STATES
NUCLEAR REGULATORY COMMISSION
Office of Public Affairs
Washington, D.C. 20555

No. S-95-20
Tel. 301-415-8200
Internet:opa@nrc.gov

THE ROLE OF RESEARCH IN NRC REGULATORY PROGRAMS

BY

DR. SHIRLEY ANN JACKSON, CHAIRMAN
U.S. NUCLEAR REGULATORY COMMISSION

TO

THE 23RD WATER REACTOR SAFETY INFORMATION MEETING
BETHESDA, MARYLAND
OCTOBER 23, 1995

INTRODUCTION

Good morning, ladies and gentlemen. I am pleased to welcome you to the twenty-third Water Reactor Safety Information Meeting. The long history of these meetings suggests that they provide important opportunities for enhancing our common understanding of safety issues related to current and advanced reactor designs. In this regard, I am particularly gratified to see representatives from the U.S. nuclear industry and a large presence from the international community. After reviewing the agenda for this meeting, I am confident that there will again be opportunities for valuable exchanges of information.

I have been Chairman of the NRC for four months, but I have spent most of my career in research and development and understand the role that research plays in the fulfillment of agency and corporate missions. Clearly, valid regulatory decisions must be based on the firm technical understanding that comes from research.

NRC research programs provide a strong independent technical capability for our regulatory programs. Without this strong technical component, our decision making capability would be diminished and public safety could be compromised. It is this independent capability that has made the NRC preeminent in nuclear reactor regulation around the world.

The concept of research to ensure an independent technical capability was defined by Congress in the Energy Reorganization Act of 1974, and the soundness of that concept is beyond dispute. In practice, our research programs must also anticipate the needs of the regulators and the problems

that may occur in the future in the systems that we license. In addition, we must sustain a technical base that allows us to react in the event of abnormal events. Careful planning and priority setting, as well as prudent investments are essential to NRC's research program if we are to maintain technical credibility.

INDUSTRY USE OF NRC RESEARCH

I have studied and have received several briefings on NRC research programs since coming to the agency. I believe the programs have not only provided strong technical support to the NRC, but have also provided valuable information to the industry we regulate. The research programs have provided significant enhancements to data bases of all kinds, and they have produced analytical methods and measurement techniques that have been very useful to the nuclear industry.

Let me take a few minutes to cite some examples.

Behavior of Emergency Core Cooling Systems

In the early 1970s, NRC conducted a major hearing on the behavior of emergency core cooling systems (ECCS) during loss-of-coolant accidents. As a result, NRC undertook a number of research programs to confirm judgments that were made in the hearings. Without the promise of that comprehensive research program, it is quite possible that no construction permits or operating licenses would have been issued in the mid 1970s. In that decade, our research confirmed the conservatism in oxidation kinetics, decay heat levels, embrittlement criteria and other requirements. Arguments over ECCS analyses no longer held up licensing activities.

There are other legacies of our research on loss-of-coolant accidents besides the solution of problems which hindered the licensing process. Much of the data generated in these NRC programs are still used today by reactor manufacturers and utilities as the basis for their analytical models: core reflood data from LOFT, SEMISCALE, and the 2D/3D program; ballooning and rupture data from the Multi Rod Burst Tests; and fuel rod performance data from NRC rigs in the Halden test reactor, among others. And then there are the large thermal-hydraulic computer codes: RELAP, TRAC, and COBRA. All U.S. reactor vendors use NRC-developed computer codes, with some modification, in their technical activities. And almost every major U.S. nuclear utility uses NRC-developed codes in their routine technical studies and core management. In fact, ten of these utilities are full-fledged members of our RELAP users group today.

Heavy Section Steel Research

In another area, where work was started early by our predecessor-the Atomic Energy Commission, the heavy-section steel program provided essential information on materials properties and fracture behavior of steels and weld materials. Virtually all of the early research on the effects of irradiation on the embrittlement of reactor pressure vessels was performed in NRC research

programs. This work provided a basis for avoiding plant shutdowns at the time the Pressurized Thermal Shock rule was published, and it continues to provide information to support regulatory decisions on reactor pressure vessel safety. The fracture mechanics tools used today in ASME Section III Appendix G for setting pressure-temperature limits were developed and validated under this program.

Piping Integrity Research

NRC's piping integrity research provided much of the basis for relaxing earlier requirements and allowing leak-before-break to be considered. This resulted in significant relaxation in piping restraints in many plants. NRC's research on nondestructive examinations, containment leakage, valve testing, and seismic issues has also contributed significant benefits to industry activities.

Risk Assessment

One of NRC's most important research accomplishments is in the area of risk assessment. It is fair to say that the NRC's research program has had a major impact on the discipline of probabilistic risk analysis and particularly in its application to nuclear reactor safety. While elements of risk assessment had some earlier use in the aerospace industry, the NRC's Reactor Safety Study (WASH-1400) represented the first integrated assessment of nuclear plant risk ever done. Our later assessment of severe accident risks (NUREG-1150) provided better estimates of plant risk based on a more complete understanding of severe accident phenomena. All U.S. nuclear plants have now performed risk assessments and, because of this work, the increased use of risk insights in regulatory activities holds the potential to improve safety and at the same time reduce costs.

Severe Accident Research

WASH-1400 demonstrated that essentially all of the risk from nuclear plants comes from core-melt accidents. Therefore, right after the accident at Three Mile Island, the NRC initiated an aggressive severe accident research program to examine core-melt sequences and subsequent accident phenomena that might challenge containment integrity. The understanding of severe accident phenomena from this research allowed the risk assessment methodology of WASH-1400 to be revisited to produce the credible assessments of NUREG-1150. Although, it may not be generally realized, more than 75 percent of all the severe accident research done in the U.S. has been done by the NRC. The Department of Energy work on the examination of Three Mile Island represents about 10 percent of the severe accident research in the U.S., and a little less than 15 percent was done collectively by the industry under EPRI and the Industry Degraded Core Rulemaking program. This large body of severe accident research has been used by all U.S. utilities as the basis for their risk assessments and Individual Plant Examinations.

Source Term Research

An important spin-off of NRC's severe accident research relates to the source term. The current licensing source term dates back to 1962 and gives an unrealistic portrayal of fission product release during accidents. Because of its assumed instantaneous appearance, this source term places emphasis on plant features that may not be optimum, such as fast acting containment isolation valves and rapid spray initiation. Revised source terms, which have come out of our research program, include a more realistic timing and fission product composition and will provide the basis for the design and operation of plant features to mitigate fission product releases more readily.

Current Research Activities

The NRC is also working in newer areas. Let me identify some of these areas, and you will hear more about them in the technical sessions that will start later today.

Most of you are aware of a recent concern about high-burnup fuel and our current program in that area. We issued an Information Notice to the utilities last year on this subject, and it was discussed last year at this Water Reactor Safety Information Meeting. Using data largely from foreign sources and a strong domestic analytical effort, we are hoping to revise fuel damage licensing criteria without creating undue penalties for the operating utilities.

Our progress on the thermal hydraulics of the advanced pressurized water reactor, the AP-600, has been significant, including scaled testing in the ROSA loop in Japan and in a test loop at Oregon State University, and detailed studies utilizing the RELAP computer code are being performed. Several design changes in the AP-600 have been made by Westinghouse that can be attributed, at least in part, to results from these programs.

Our continuing severe accident research is paying off in several ways. In addition to providing the basis for the utilities' accident management plans and Individual Plant Examinations, it has in some cases led to reductions in potential consequences of severe accidents. Hardened vents in Mark-I containments and provisions for flooding the Mark-I basemat to prevent liner attack are examples of actions taken as a result of our core damage research. Of no less importance, the severe accident research program has provided the basis for <u>not</u> doing anything in other areas. For example, early consideration of the possibility of direct containment heating in PWR containments suggested a high likelihood of early containment failure. More detailed and structured results from this program have indicated that direct containment heating is a very small contributor to public risks at most plants.

Our aging research activities are looking at degradation in pressure vessels, piping, steam generator tubes, reactor internals, valves, cables, and containment structures.

Present work on piping integrity is almost complete for the large baseline programs of the International Piping Integrity Research Group. We are now

pursuing more specialized studies. For example, in collaboration with the Nuclear Engineering Power Corporation (NUPEC) of Japan, we are participating in large-scale seismic tests of main steam and feedwater piping systems on the largest shaking table in the world.

Steam generator tube studies are examining inspection-system capabilities to detect flaws, the effects of primary and secondary side environments, and analysis methods used to assess tube integrity. This program will provide an independent assessment of the inspection and analysis methods being used by the U.S. industry in evaluating steam generator tube integrity.

A final example is our review of aging effects on containment structures. Safety margins may be reduced by corrosion of steel containments and steel liners, breakdown of the seal at the concrete floor, concrete contact with grease, corrosion and relaxation of tensioning cables, etc. We are examining these processes to determine what issues should be included in our research programs, as well as looking at in-service inspections and methodologies to perform assessments of current conditions. These activities are particularly important in light of the promulgation of our new performance-based rule on containment leakage rate tests.

International Safety Research Cooperation

International cooperation in safety research has been going on for a long time. NRC's participation in OECD and IAEA, for example, goes back more than 20 years. However, after the accidents at Three Mile Island and at Chernobyl, nuclear safety has been increasingly recognized as a world-wide concern, and our cooperative programs have intensified. This trend has been further enhanced by the general reduction in research budgets at home and abroad, and the resulting need to pool resources in cooperative programs.

Some of our cooperative programs, like the Halden Project's fuel behavior work and the International Piping Integrity Review Group, have continued over many years, and we are still participating in their activities. Others, like the high-burnup fuel tests in the French CABRI reactor and the containment integrity program with NUPEC in Japan, are relatively new cooperative programs. It is important to note that most of these cooperative international programs also have sponsors from the commercial sector.

Well, that is a sample of what we have done in the past and what we are working on now. What about the future?

THE FUTURE OF THE NRC RESEARCH PROGRAM

In general, we have an obligation to stay strong and to maintain our independent technical capability so we can support the regulation of our 100-plus operating reactors. That means we will continue to work in important areas like thermal-hydraulics, materials, severe accidents, and risk assessment; and we will continue to participate in, and to stay abreast of, international nuclear research programs. There always seem to be issues of the day, such as the integrity of radiation embrittled reactor pressure

vessels and the behavior of reactor fuel at higher burnups. A wide range of these research programs will be discussed in the following technical sessions, and some of the current issues will be addressed in this plenary session in an effort to make sure our research remains on target.

We are now in a period of change at the NRC. The electric utility industry is under strong competitive pressures and is diligently examining means to reduce its costs. NRC has a role to play in reducing the regulatory burden when the safety benefit is marginal.

However, even without external pressure to reduce costs, a new culture, which I refer to as risk-informed, performance-based regulation, is being adopted by the NRC. NRC is becoming less prescriptive and more performance-oriented in its regulatory posture in order to provide greater flexibility to licensees while maintaining adequate protection for the public. Cost-consciousness and cost-effectiveness pervade all of NRC's operations, including research.

NRC's research programs are being reexamined to ensure proper focus under this new paradigm. Research planning must consider the current and prospective level of plant safety, and there should be a reasonable expectation that research projects and their results will be cost beneficial. Among the criteria to evaluate the merits of a research project are the likelihood that the results will improve the effectiveness of regulations and minimize any undue burdens they impose. Some of the rules that the NRC developed conservatively in the 1960's and 1970's because of lack of information can now be modified as a result of improved knowledge that has been gained through investments in research over the past 20 years. Future investments in research will be expected to continue this trend.

As nuclear power plants age, we must examine the standards and operating procedures that have been imposed on critical components, such as the primary coolant system boundary, to assure ourselves and the public that an adequate safety margin still exists. Only through research can we derive dependable estimates against which we can make such judgements. One of our top research priorities is improving our understanding of the aging processes in nuclear power plants with particular focus at the present time on reactor vessels, steam generators, and electrical cables.

Many of the performance standards will be established by drawing on knowledge developed in risk assessments performed both by NRC as well as by licensees.

However, we must acknowledge realities. Careful evaluation is needed to determine the future value of additional research in all areas. We are approaching the point where we can, in some areas, go into a program maintenance mode that includes a very limited experimental program and thoughtful fine-tuning of existing analytical models. Our current international cooperative experimental programs are expected to provide additional data to help make this determination. In doing this, however, we have found that adequate resources and careful planning are still required to avoid losing the important technical skills.

However, further emphasis and new work is needed in important areas related to changing focus of our mission, i.e., risk assessment research to develop and strengthen methodologies for dealing with human/organizational factors and degraded equipment. New methodologies from other fields need to be developed and applied to age related effects in reactors, i.e., going beyond fracture mechanics to relate detailed measurements using new experimental probes to microscopic materials properties in order to make stronger predictive statements about behavior, as well as development of possible in situ probes of key plant systems such as the Reactor Pressure Vessel itself.

Since becoming Chairman, I have come to recognize that there are a number of important research areas associated with aging reactors which possess elements common to reactors in all of the countries relying on nuclear power. I know that countries already share the results of their reactor research and that in some specific technical areas, a number of countries have joined together to address issues of common concern and interest. We need to be certain that our collaborative research projects recognize and build upon the unique areas of specialization and particular expertise each of us has. Through existing institutions, such as the Committee on the Safety of Nuclear Installations of the OECD Nuclear Energy Agency, we must more diligently focus our attention to the planning and integration of our research efforts. At the same time, we should hold these institutions to high performance and efficiency standards so that value is achieved from our investments in them. But, I would like to propose that we go much further. I think that we should consider an international reactor research program focused on aging and risk assessment methodologies in which we seek to integrate the regulatory research activities of various countries within the context of a formal international research program. Each country could specialize in areas of its particular expertise. Thus, we would avoid duplication of effort and meet the common challenges which we are encountering and the common downward pressures on our various regulatory research budgets. In certain areas of mutual interest, a few of which I have already mentioned, this kind of coordinated international research activity has occurred, with excellent outcome. However, this is meant to be a more direct and focused research program than generally exists, internationally. If it can be accomplished with appropriate planning, focus and coordination under the aegis of the existing multilateral structures, then it should happen that way. If not, the task that I propose may be difficult to achieve, but I think that it at least should be carefully considered and explored. Consideration of such an activity will be part of the NRC strategic assessment and rebaselining initiative that I recently announced, and which I will now discuss further.

Strategic Assessment and Rebaselining

Changes in the industries we regulate ultimately affect the regulator, and the NRC is no exception. Although I believe that the NRC has earned its reputation as the foremost nuclear regulatory body in the world, we still need to develop a strategic vision that allows us to adapt to a changing environment and to budgetary constraints, to carry out our regulatory programs more effectively, to take on possible new missions, to conduct effective resource planning, while remaining responsive to the public and the regulated industries. The first phase of the strategic initiative, the "strategic

assessment," involves identifying and examining the sources of the mandates that make up our regulatory mission - statutes, executive branch directives, and Commission decisions--so that we can establish a mutual understanding of what the NRC mission is and what is required of us. Also included in this phase is a process of looking at all agency activities to determine whether they are being conducted in response to a specific mandate or whether these activities have some other rationale for their existence, and whether there are areas where we should have ongoing programs to implement a specific mission, but do not. This phase is, as the title implies, essentially a review, categorization, and assessment. This phase is also meant to begin to surface key strategic issues, questions, and decision making points, which the Commission will address.

The subsequent phases -- rebaselining and strategic planning -- flowing from Commission decisions on the key strategic issues, questions and policy alternatives, will address what our programmatic needs are and should be, and what resource levels should be assigned to them. The first phase will drive and provide input to the following phases and ultimately to budget and human resource planning, which is the final phase. I believe that this review is necessary to position us to meet effectively the challenges we face and to guide intelligently our activities and decision-making in the future.

CONCLUSION

I hope my remarks give you some of my perspectives on the role and value of the NRC research programs. I believe both the nuclear industry and the NRC are facing a series of interrelated challenges that, taken together, could change substantially how the electric power industry continues to develop and how it will be regulated. How we solve today's problems can, and will, affect the role that nuclear energy will play in the nation's energy mix in the future. Our mutual goal should be to view our challenges as opportunities and address them proactively rather than reactively. The NRC's research program can assist us in addressing some of the challenges.

Let me close my remarks by again expressing my appreciation for your interest in our work and to encourage your active participation in this important meeting. Thank you for your attention and I hope you will have an enjoyable and successful meeting.

CURRENT ISSUES WITH RESEARCH SUPPORT

William T. Russell
U. S. Nuclear Regulatory Commission

It would be difficult to condense current issues in nuclear reactor regulation to just a few minutes. So, let me start off by saying that I have not tried to give a comprehensive listing of issues that are currently facing the reactor program, but rather to select those that I thought were relevant as they relate to research activities. Use of probabilistic risk assessment in regulatory decisions; materials aging issues concerning steam generators and reactor vessels; high burnup fuels; accident management; and digital instrumentation and control, are just a sampling of the important issues that I want to talk about.

Probabilistic Risk Assessment (PRA)

The Commission in August passed a major milestone with the publication of a policy statement on the use of probabilistic safety assessment in regulation. We had been for some years using probabilistic safety assessment techniques starting with WASH 1400. Shortly after Three Mile Island, the "Lewis" report reviewed the use of PRA in regulation. We back away a little bit from use of PRA in regulatory activities. Concerns were that the state of the art had not sufficiently progressed, and there were significant uncertainties. There were questions about using PRA alone as a basis for licensing decisions.

In the intervening years, from 1980 to 1995, there has been substantial progress made in the use of PRA, and this is recognized in the Commission's policy statement, which encourages, to the extent supported by data and by the state of the art, the use of PRA in expanding regulatory activities.

A precedent was set when four NRC office directors got together and developed an overall plan for how the agency should proceed. These four offices were NMSS, RES, NRR, and AEOD. We proposed that there be an agency-wide action plan for coordinating these activities. Within that plan, there are a few areas that should be highlighted that relate to the future use of PRA and our interface with the NRC research program.

One area in particular deals with in-service testing requirements. These requirements flow from Section XI of the ASME Code. We are examining techniques to apply probabilistic thinking to such things as the frequency of testing and prioritizing testing activities within the Code.

Another area that NRR is working on very hard and that we have had feedback on is implementation of the new maintenance rule. We have completed in NRR the development of the inspection procedures, and held a number of workshops on pilot inspection results. Licensees are in the process of implementing their internal procedures and developing the requirements that they will follow when the rule goes into effect this July.

An important part of implementation of the maintenance rule is the use of risk insights on a plant-specific basis to develop the list of those systems, trains, and selected components that have a relatively high risk significance and to monitor and trend their performance.

This risk prioritization also relates to the draft reliability data reporting rule. We believe that the implementation of the maintenance rule essentially requires the data to be available on a site-specific basis. We are now looking at taking the next step and having the data reported nationally. This is very important for establishing trends and feedback from industry operating experience. It is also critical if we are to proceed to expand the use of PRA in a regulatory context. The data upon which we are basing these decisions need to be publicly available.

We have some pilot activities going on, particularly in the in-service inspection area where we are looking at prioritizing, using risk insights, some of the in-service inspection activities. There is a major effort being looked at by the RES to try to develop appropriate standards for a PRA when it is being used in a regulatory context. RES and NRR are respectively working on the development of a Regulatory Guide and Standard Review Plan for various applications of PRA to regulated activities.

Steam Generators

In the aging area, one aging problem--and a real current problem--is the issue associated with steam generators. Proceeding essentially on a case-by-case basis with what I call crisis management, we continue to identify degradation mechanisms in steam generators. This fall has been a particularly heavy time, with the identification of additional circumferential cracking in Combustion Engineering generators, and much more substantial axial cracking in the area of the support plates in Westinghouse generators. In many cases, licensees have not anticipated the degradation sufficiently. Some of them now are in the mode where they do not have sufficient lead time for replacement generators and they are looking at trying to revise their approach to tube repairs with new techniques that are causing quite a bit of additional review on the part of the staff for precedent-setting approaches.

We are trying to put this into a regulatory framework with a rulemaking rather than doing it on a case-by-case basis with facility technical specifications. Our objective for the rulemaking is that it be performance based. That is, we would establish objective criteria, probably along the line of Regulatory Guide 1.121 as it relates to structural integrity margins to be demonstrated. We would allow various inspection techniques to characterize degradation that has occurred and then perform either testing, other correlations, or engineering analysis to show that the sizes of the flaws that exist--with a projected increase for time in service--would remain within allowable sizes to meet the differential pressure requirements for steam line breaks or the differential pressure requirements for normal operation.

We want a rule that will provide incentives for improving inspection techniques. The better you can size and characterize the flaws with more certainty, the less margin you have to have because you need not put that additional margin into your structural analysis.

We want to have an integrated review. We cannot do it just based on materials engineering, inspection techniques, or strength in materials. We have to re-examine the fundamental objectives from a safety standpoint that we are trying to maintain with steam generators. In this context, we have three different issues to examine: (1) normal operation with respect to primary-to-secondary leakage through generators, which is relatively easy to detect with on-line monitoring for radioactive materials leaking through the generators; (2) in the context of accident analysis in the past we have used very conservative approaches, looking at, essentially, one gallon per minute primary-to-secondary leakage through the generator with very conservative calculations for iodine spiking factors and atmospheric dispersion; and (3) severe accidents, particularly for transients resulting from loss of secondary heat sink where you may be either boiling off the primary, ending up with hot gases, or conditions under which you might have high-pressure core melt or core damage sequence.

The implications of a degraded generator and what it means as it relates to a potential containment bypass scenario are significant and need to be examined in an integrated way. We hope to have a three-tiered approach. That is, the performance-based rule would establish the framework and the objectives. Next, we would expect to have a regulatory guide to identify various methodologies for qualifying, for example, inspection techniques and providing guidance on the type of analysis to be done. Below that we would have a number of topical reports for various degradation techniques or for various vendors for the types of inspection techniques that they may use. These reports would be reviewed and compared to the guidelines in the regulatory guide.

We are probably one to two years away from being able to issue the draft rule. We have developed a lot of experience for the degradation mechanism of axial cracking--outside diameter stress corrosion cracking within the support plates on Westinghouse generators. Based upon this work, we believe we have a model for approaching the rulemaking, but we are being stressed right now with the rate of identification of circumferential cracking and various proposals by licensees trying to address circumferential cracking. So we have a resource problem.

This is an area where the research that is needed relates to inspection techniques, qualification of inspectors, and a performance-based approach for qualifying inspections with human beings in the loop. In re-reviews of prior inspection data, we have found missed eddy current and rotating-pancake-coil signals. In some cases, the digital signal processing used did not identify the signals, the analyst did not see it, and the backup analyst did not see it. We are now finding cases where we are in enforcement space for prior missed inspection activities. We need to develop inspection techniques that are more reliable and less dependent upon humans.

Reactor Pressure Vessel

The next issue is a critical one: reactor pressure vessels. The Commission has rulemaking under way to address procedures for annealing. You are aware of the pressurized-thermal-shock (PTS) rule and some of the other requirements of Appendix G, fracture toughness, and of Appendix H, surveillance programs. Recently we found that our knowledge of the actual vessel properties is somewhat lacking. We had to send out a generic letter requesting licensees to gather data, not only on their vessels but on sister vessels that may have been fabricated at

the same time--particularly for those vessels that were manufactured by Combustion Engineering. We generally had a much better data base on vessels manufactured by Babcock & Wilcox.

This vessel information was collated. We published a NUREG report containing the data that have been received by NRC in response to the earlier Generic Letter 92-01. We hope that the industry will take this to the next step and include all data, and that we will resolve the issues with respect to treatment of data as proprietary. Most of you are aware that I have sent out letters to deny withholding of proprietary information on the basis that the information constitutes information important to reactor safety and therefore should be available to the public so the bases for our conclusions on such issues of vessel toughness and the ability to meet the pressurized-thermal-shock rule can be understood.

A major research activity related to vessel annealing demonstrations is critical so that we may be able to conclude that annealing can be safely performed in the United States.

High Burnup Fuel

High burnup fuel is an example of what I think is a success, both on an international level and on a research level. We learned about some testing that had been done in France and also in Japan on transient reactivity behavior of fuel under conditions of high burnup. Some early test results were quite surprising, indicating that you could have a catastrophic failure of a pin with the fuel being dispersed into the coolant. A lot of work is in progress to exchange data to try to understand what caused that failure, to look at some other results from Japan and also more recent results from France. These issues are critical as we look at licensing and going beyond burnups in the range of 60,000 megawatt days per metric ton.

In reviewing the acceptability of higher burnups, we have to be concerned with both the transient reactivity behavior and also the recent experience with the Three Mile Island core. At TMI-1, failures of cladding on first-cycle fuel in a transition core occurred. The combination of high boron/boric acid chemistry along with relatively high heat fluxes caused failures of fuel pins. These issues also relate to the integrity of cladding, which, if this is occurring on first-cycle fuel rather than high- burnup fuel, concerns us.

NRR and RES have major activities going on to re-examine fuel as well as some of the issues associated with reactor physics. We are finding that some reactor licensees and reactor engineers are not as familiar with startups of new cores; operating experiences indicate that reactor engineering activities are not being as well managed as they have been in the past. This is also an inspection area and an interface with the regions. We actually have three separate generic activities going on within NRR to address fuel issues.

Accident Management

Accident management is an issue on which the staff has been patient. We need to mine the severe accident research work, some of the Individual Plant Examination work, and the NUREG-1150 work on severe accidents to try to identify appropriate strategies that can be used in the context of accident management and also to develop aids to assist decision makers, and

to come up with a framework for what I characterize as the Emergency Operations Facility inward aspects of responding to an emergency.

In the conduct of our drills and assessments of licensee performance, we have historically focused on offsite emergency preparedness and how the offsite authorities would respond to radiological releases. As a result, most of the activities focus on a scenario intended for significant radiological releases relatively early so that the offsite activities can be exercised.

We do little inspection related to the direction of onsite activities from the Emergency Operations Facility. That is, the reactor safety assessment and actions that can be taken consistent with Emergency Operating Procedures (EOPs) or, in some cases beyond the EOPs, to address accident management strategies. This is an area where I am very encouraged by what the industry is doing.

The owners groups have become engaged, particularly the BWR owners, in identifying various approaches that could be implemented and developing implementation procedures for such activities as containment flooding. But the actual decision- making process that would reside in the Technical Support Center and the Emergency Operations Facility to decide to flood containment for example has not been as well laid out.

Those activities are ongoing now. We will be conducting some pilot inspections of the industry initiative in this area and factoring the industry work into our ongoing programs.

Digital Instrumentation and Control

In the area of digital instrumentation and control (I&C), I am focusing on a rather narrow aspect. The National Academy of Sciences is looking at the overall approach to instrumentation and control, particularly digital I&C, and the human factors aspects of maintaining software-based protection systems or safety systems. We have had a number of interactions on reliability of software systems, how one handles common-mode failure, and how one addresses diversity within systems.

But in the course of the reviews of those activities and discussion with the Advisory Committee on Reactor Safeguards, we identified environmental issues that go beyond simply the electromagnetic interference that you might have with digital systems that operate at very low voltage and amperage. These other issues are related to smoke, temperature, seismic, and other stressors. Work is ongoing to address these environmental qualification issues. It involves a literature search to see what has been done in the military and other areas, as well as some actual testing. The research work will put us in a good position to address these issues as they come up in future applications and as I&C systems are retrofitted in currently operating reactors.

That completes my sampling of current reactor issues. Thank you.

ANNEALING THE REACTOR VESSEL AT THE PALISADES PLANT

Robert A. Fenech
Consumers Power Company

Good morning. This is my first opportunity to attend a Water Reactor Safety Information Meeting and, as I looked at the attendees, I think it is pretty clear that I am speaking to the technical top guns of the industry here. So, it's a pleasure. I would like to go over what we are about to do with our reactor vessel at Palisades.

In the way of background, Palisades was licensed in 1967 and went commercial in 1971. Jumping to two years ago, we faced at that time three issues that challenged our ability to operate to end-of-license, which would be 2007 without any extensions. The three items were regulatory performance, economic performance, and reactor vessel embrittlement.

We had not been operating the plant with the kind of conservative decisions and with the kind of safety margins that one is expected to operate a plant in the United States at this time. Our economic performance was not satisfactory in that our capacity factor was low and our costs high. In the area of reactor vessel embrittlement, our analysis showed that we would reach the NRC screening criteria for embrittlement in the year 2004.

Over the last two years, we have made significant improvements in the first two areas. Our decision-making has changed. Our performance, especially over the last year and a half, has been excellent. In addition, we have gotten our capacity factors up and our costs under control. Clearly, sustained performance is what is going to carry the day but from what we can see and from where we are, we are in more of a maintenance-of-performance than in a turn-around situation.

On the other hand, in the area of reactor vessel embrittlement, about a year and a half ago we had a bit of a set- back. We had taken material from retired steam generators that had welds identical to the welds in our reactor vessel. When we analyzed the welds from our steam generators, we were given some surprises about the chemistry makeup. When we applied the new information to our analysis, we changed the date on which we would reach our screening criteria from 2004 to late 1999.

After we determined that we would reach the screening criteria in 1999, we were faced with a decision. Where do you go now? Initially, I think you would guess that we thought that we would pursue the Regulatory Guide 1.154 analyses that allow you to use plant-specific data to determine just how tough your reactor is and how long you can operate it. We pretty quickly came to the conclusion that this is really not a viable alternative. Yankee Rowe had tried it and failed. When we talked to the NRC staff, we concluded that the political environment right now would really not support Regulatory Guide 1.154 analyses.

So then we turned to just doing a lot more analysis, get a lot more information, and just keep plugging and chugging here and maybe this will all go away. That alternative dried up very quickly. The more we looked at it, the more we were sure that, although it was possible, we did not have confidence that we could run to end-of-license. Secondly, analysis would not fix anything. We would just be trying to get data to justify continued operations.

What we finally decided was that we needed to bite the bullet and anneal the reactor vessel. We made a decision to do that in 1998--a major undertaking for us. We made the decision for a lot of reasons, but we did feel that it gave us the one success path that would get us to end-of-license with relatively high confidence. It was the only alternative that fixed the problem and didn't just analyze it away.

After we decided to anneal the reactor vessel, we had to decide how. There were two alternatives that we thought were practical and available to us. The first alternative was electric resistance heaters used in Russia and Europe--obviously not in the same areas of the vessel that we are in our annealing, but offering some new and different challenges. The second alternative was indirect gas. Indirect gas involves a series of toruses, doughnuts, stacked vertically in the reactor vessel. You pipe hot gases through each of the toruses and you can control the axial temperature with the temperature in each of the toruses. The gas goes through each torus in a turbulent fashion and then it is exhausted outside the containment.

We chose the indirect gas method. We felt that either method would work, but there are a lot of reasons why we chose indirect gas. The bottom line and the biggest reason was that the gas demonstration project--the annealing of the canceled Marble Hill reactor vessel--was much further along than the other project. We felt that it was imperative that we had the data from at least one demonstration reactor. We had more confidence since that annealing was further along. As a matter of a fact, they intend to anneal Marble Hill in the early spring of 1996, and we will submit our annealing report to the NRC in the early summer of 1996.

You know, technically, annealing is relatively straight- forward. It is less limiting than a typical post-weld heat treatment, and stresses in attached piping can be controlled below code allowables. While it is relatively straightforward, there are many peripheral technical issues that have the potential to bog down the project with little or no real impact on the outcome. Palisades, being the first to anneal in the United States, will have to answer any questions that have the remotest possibility of impacting the process.

Because of that, we could use the NRC's help, and I see it in two areas. The first is research or technical support, and the second is what I call regulatory predictability. In the area of technical support, let me go through some items that you might consider.

The annealing data base needs to be expanded. Most of the data are from high flux environments. There are very limited data on chemistries that are most likely to be annealed. And there is a limited mix of weld fluxes in the data base.

A second area is prediction of re-embrittlement. The current method is highly conservative. The use of surveillance material is not well defined. At Palisades this probably won't be an issue for us. We are expecting to run to 2007. The most we expect to extend our license, if everything goes well with annealing, is to 2011. That would be asking for a four-year extension based on the construction period between 1967 and 1971. Many other plants have had that period approved. At this time we do not see a life extension beyond 2011 in the cards for us.

The high-temperature effects on concrete and the effects of moderately high temperatures are not well defined and questions will have to be answered before we anneal.

The last technical area would be tempered embrittlement, or the migration of impurities to grain boundaries during the radiation and annealing--impurities like phosphorous. We do not expect that this is a problem, but question the amount of analysis necessary to put it to rest.

In the area of regulatory predictability, let me congratulate the NRC. In fact, they did it to me again. My speech had to be considerably changed when Thursday or Friday they passed the annealing rule. I was ready to stomp up and beat on the podium here, and they passed it. The rule is both timely and balances public involvement with loss of control of the process. We were very worried about this. I think it struck the correct balance.

Companies will not be willing to invest the large capital dollars necessary to anneal if they are not confident they can predict the outcome. Palisades offers both the industry and the NRC the opportunity to prove that annealing is both technically straightforward and that you can have regulatory predictability when you go into a process.

Thank you.

NEED FOR HIGHER FUEL BURNUP AT THE HATCH PLANT

J. T. (Tom) Beckham
Southern Nuclear Operating Company

Good morning. This subject has been brought up several times already, but I appreciate the opportunity to give you the views of the Georgia Power Company and the Southern Nuclear Operating Company. Let me just mention that the Hatch plant is operated by Georgia Power. Southern Nuclear is a corporation that we have formed to supply support for several plants, but the actual license is held by Georgia Power for the Hatch plant.

I want to discuss the Hatch plant although Southern Nuclear does supply information to other plants such as Georgia Power's Vogtle plant; we also operate Farley. So much of the information that I will be talking about is relative to both plants although I want to use Hatch as the representative.

Hatch, of course, is a BWR 4 and has been in operation for some time. The first unit became commercial about 1975. Obtaining higher burnups, or higher average discharge exposures, is nothing new at Hatch. Since we have started, the discharge exposure of the plant has increased. Now, of course, we are not approaching the numbers currently being discussed but, as you can see in Fig. 1, the average discharge exposure has increased from around 20,000 MWD/MTU in the early to mid-1980s to 34,000 MWD/MTU in 1994.

I am talking about batch average values. There are also peak bundle and peak rod values. You will have to make the conversions if you think in one way or the other because I am talking in batch averages (Table 1).

During Hatch's operating history we have had some problems with fuel failure. Higher burnup fuel raises a concern about how much fuel failure you are going to have. Fuel failure is, of course, an economic issue with us. Back in the early 1980s, we had a problem with crud-induced localized corrosion, known as CILC. We have gotten over that, but we had some times when it was up around 27 fuel failures a year. That is not a pleasant time to live through because it is not what you want from an economic viewpoint or any other.

We have gotten that down. We have had some fuel failures recently, but they have not been related to fuel burnup or to corrosion. In fact, as shown in Fig. 2, the number of failures has decreased from the early 1980s to the 90s even though burnup increased during that time. The fuel failures are more debris-related-type failures.

In addition to increasing burnups, utilities are actively evaluating or have already incorporated power uprate and longer fuel cycles (e.g., 2-year cycles). The goal is to balance out the higher power density, longer cycles, higher burnup, and to have no leakers. Why do we as an industry want to have higher burnup fuel? That is what I want to tell you a little bit about.

The incentives can be divided into several categories. Obviously, reduced fuel costs is one. The onsite spent fuel storage cost can also be reduced, and we can get longer cycles.

Let's talk just a minute about reduced fuel cost. If you would assume that there is a constant energy cycle, the number of fuel assemblies per reload can be reduced by increasing the enrichment of the assemblies. Reducing the number of assemblies, while increasing enrichment, will reduce fuel costs for today's projected burnup levels and costs of nuclear materials and services. All this works even better if there are some nuclear materials and services that can be reduced such as the uranium costs and the enrichment services.

But that is not something that goes on forever and ever. There appears to be a limit on how far this concept can be extended because of higher fabrication costs and some nonlinear costs that are associated with the enrichment.

As shown in Fig. 3, it appears that the projected savings start to diminish past about 38,000 MWD/MTU with today's environment. No one knows for sure that you may not have a situation similar to the one of buying a pocket computer years ago when some of you may have paid $200 or $300 for one similar to what you can buy for $1.99 now at the grocery store. Whether that will actually happen, we don't know. There obviously could be some changes in the way things are done and possibly this number would change.

The second incentive to have higher burnup fuel is, of course, reduced storage costs. Obviously, if you do not have as many bundles to store, it doesn't cost you as much to store them. That cost could be somewhat significant--somewhere between $2 million to $4 million per cycle.

If you put the lower storage cost on this curve (the lower line of Fig. 3) you do get some benefit by having the higher burnup.

The other thing that utilities need is higher energy cycles. Some utilities have already gone to 24-month cycles, and other utilities are considering it. At Hatch, we need to go to the longer cycles if we possibly can for cost reasons, but you must increase the discharge exposure to do that. There is an efficient batch size to which you must be limited. You cannot just put in more and more fuel because pretty soon you are putting in fuel at the wrong places and you are using new fuel where you do not need new fuel. The maximum efficient batch size is somewhere in the 36 to 40 percent range. Our projections right now say that to get the 24-month cycle, we need to be in the 47,000 MWD/MTU burnup range for this batch size.

For our use, considering all the above, we will probably project our limit in the 45,000 to 50,000 MWD/MTU range for average discharge exposure. All this needs to be done with reliability efforts-- some of which you are doing and some of which we are doing.

There are ongoing programs to monitor fuel cladding performance, and to use lead-use assemblies in the reactors. We have been doing that for some period of time. When we put those lead-use assemblies in, we monitor them to see what they do during operation and we also examine them during the refueling with high magnification video inspections, corrosion thickness measurements, and anything else that we can determine would show us whether the fuel is going to perform the way we had predicted. So far the cladding in our lead-use assemblies appears to be doing rather well.

These inspections, along with our normal inspections of the fuel, give us confirmation of acceptable cladding performance with such things as hydrogen water chemistry and feedwater zinc injection, both of which the Hatch plant has.

We work with EPRI and General Electric to address these issues through these inspections and through water chemistry measurements to make certain that we understand what is actually happening.

Some consideration is being given to an ultra high burnup lead-use assembly program. That could go as high as 60,000 MWD/MTU batch average. We have not yet reached a decision on that. If we do that, those lead-use assemblies would use cladding with better corrosion resistance, at least according to GE, and better resistance to hydrogen pickup. Its pellets would have an enhanced pellet grain size and would have an enhanced thermal conductivity. As our fuel people are trying to decide whether we should do this, we are trying to participate in gathering data--getting information that is necessary to make the right decision.

What does the NRC Office of Research need to do in this regard? We think that you need to gather whatever data that you need so when we come to you, you can make an informed decision. You should not wait until the industry comes to NRC and then say you have to do research on it. Because in today's competitive environment, we have to be able to make the decision and move on. We hope you will be able to get the data that you need to do the confirmation or whatever type of research so that when it is requested, whether it is the Hatch plant or some other utility, you will only need to find what the utility is really talking about and not need to do primary research to understand the program.

The industry today is in a very competitive environment. In fact, some utilities are fighting for their very existence. Those of us who operate nuclear power plants, of course, have to watch out for the public health and safety, make conservative decisions, and do the right thing. But we also do not want to be shut down so we want to do what is right as well as having whatever tools in our tool box for being competitive. And use of higher burnup fuel is one of those tools.

I appreciate the opportunity to give you an industry perspective of higher burnup. I don't think I said anything that was not fairly obvious to you. But sometimes just having an industry representative say what we might be considering is of value.

Thank you very much.

Table 1. Approximate Exposure Relationships
MWD/MTU

Batch Average	Peak Bundle	Peak Rod
38,000	43,000	48,000
45,000	50,000	60,000

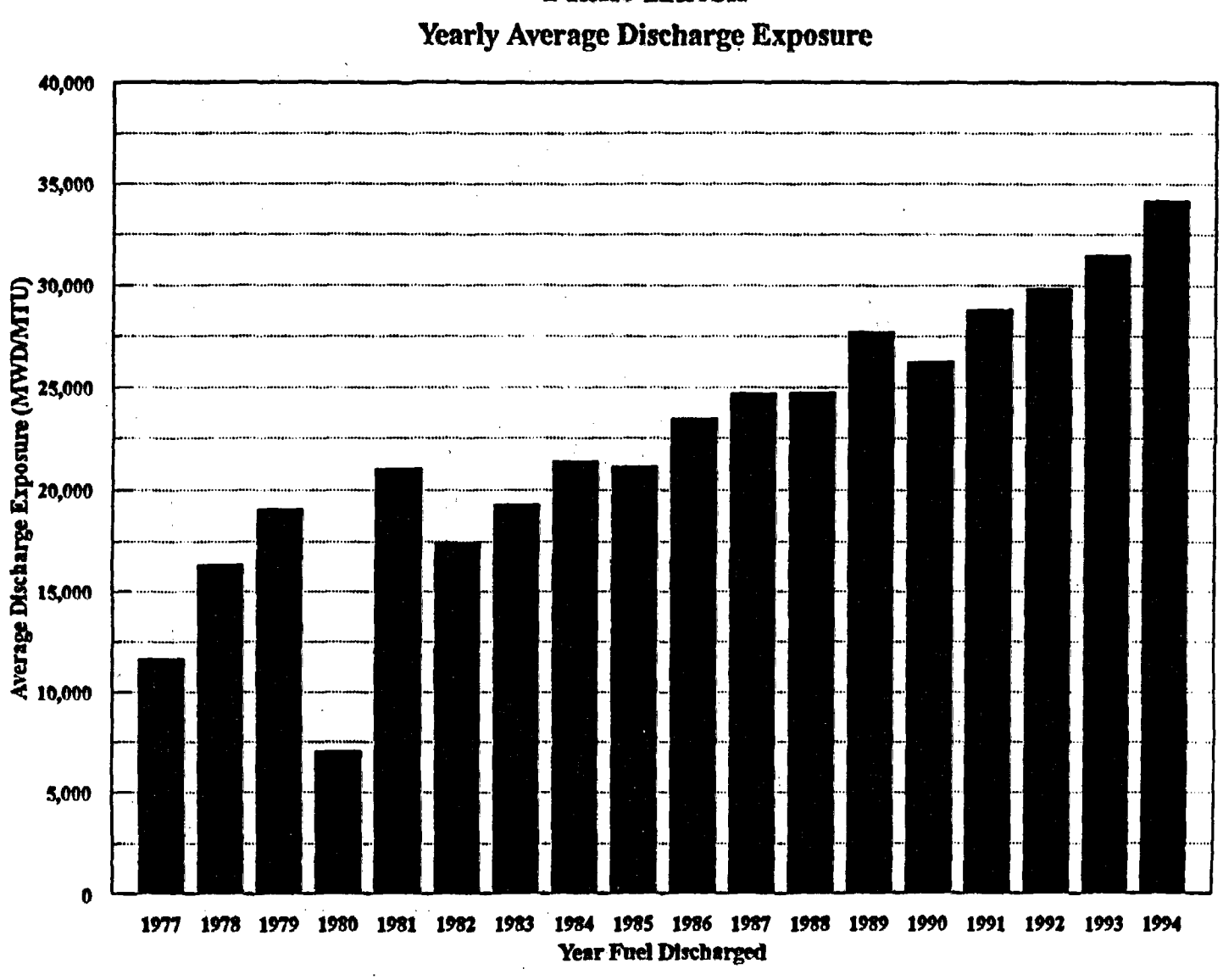
Plant Hatch
Yearly Average Discharge Exposure
Average Discharge Exposure (MWD/MTU)
40,000
35,000
30,000
25,000
20,000
15,000
10,000
5,000
0
1977 1978 1979 1980 1981 1982 1983 1984 1985 1986 1987 1988 1989 1990 1991 1992 1993 1994
Year Fuel Discharged

Figure 1

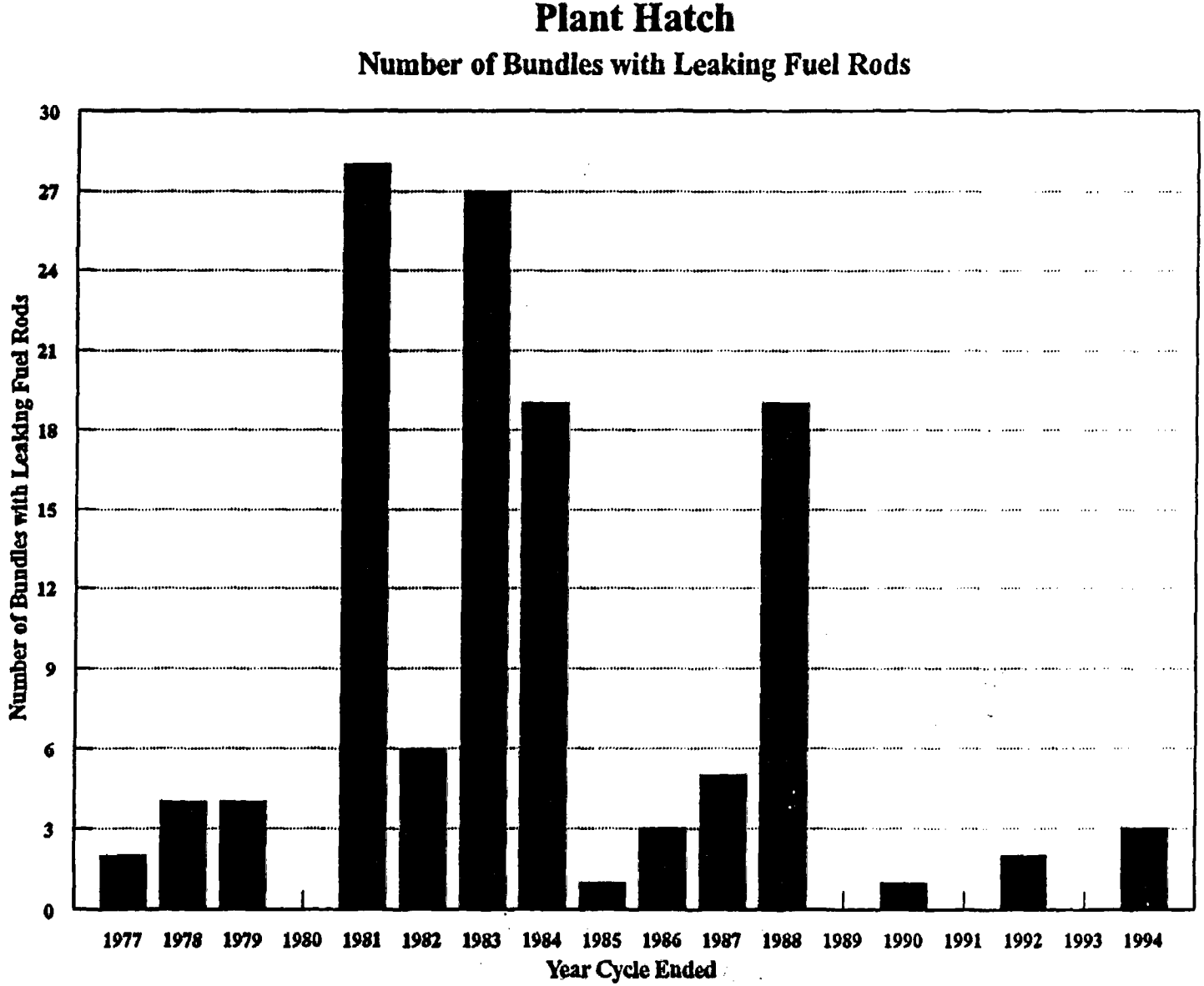
Plant Hatch
Number of Bundles with Leaking Fuel Rods
Number of Bundles with Leaking Fuel Rods
30
27
24
21
18
15
12
9
6
3
0
1977
1978
1979
1980
1981
1982
1983
1984
1985
1986
1987
1988
1989
1990
1991
1992
1993
1994
Year Cycle Ended

Figure 2

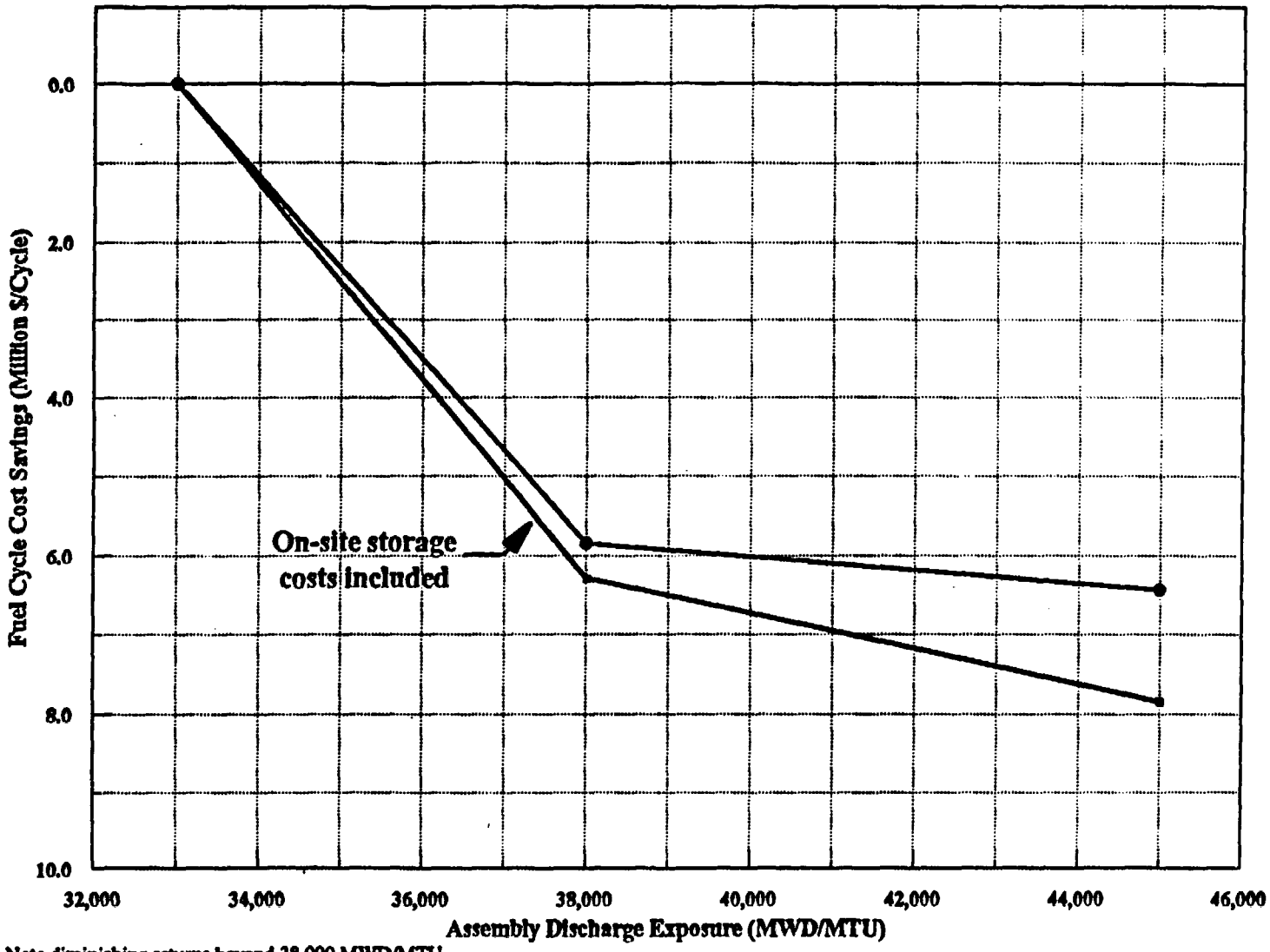

Note diminishing returns beyond 38,000 MWD/MTU.

Figure 3. Increased Burnup Effect on Fuel Cycle Costs

LUNCHEON REMARKS
OF
JAMES M. TAYLOR
EXECUTIVE DIRECTOR FOR OPERATIONS
U.S. NUCLEAR REGULATORY COMMISSION

INTRODUCTION

Good afternoon!

It is a pleasure to welcome so many of our colleagues from the United States and abroad to this 23rd Water Reactor Safety Information Meeting. I hope that you have found these last three days of sessions interesting and stimulating. You have heard presentations and research results on a diverse group of topics.

It remains clear that nuclear safety research continues to play a vital role in our agency's approach to accomplish its regulatory mission. For research not only may uncover potential problem areas, as is the case with high burnup fuel, but also offers the potential to provide the solution to such problems, as with reactor pressure vessel annealing.

I want to briefly talk to you this afternoon on three topics where reactor safety research has played, and continues to play, an important role. These areas are the increased use of probabilistic risk assessment methods in regulatory activities, thyroid cancer studies arising from the Chernobyl accident, and recent developments in reactor pressure vessel annealing.

PROBABILISTIC RISK ASSESSMENT METHODS

On August 6, 1995, the NRC published its Final Policy Statement on the Use of Probabilistic Risk Assessment Methods in Nuclear Regulatory Activities.

This policy statement represents the logical conclusion to a long and successful application of probabilistic risk assessment, or PRA, methods in nuclear safety research and analysis. In this final policy statement, the Commission stated that an overall policy on the use of PRA methods in nuclear regulatory activities should be established so that the many potential applications of PRA could be implemented in a consistent and predictable manner and would promote regulatory stability and efficiency. I'd like to briefly remind you of the background and events that led to this policy and touch on the key points of the policy itself.

PRA Background

The NRC has generally regulated nuclear power plants and the use of nuclear material based on a deterministic approach. In this approach, a set of challenges to safety is determined, and an acceptable level of mitigation is defined. This leads to the so-called design basis accident, or DBA, approach.

An example is the postulated Loss-of-coolant-accident, or LOCA. Here, the safety challenge is a postulated coolant pipe rupture, up to and including the largest coolant pipe in the reactor coolant system. The level of mitigation required is that the fuel cladding temperature not exceed a specified temperature in the face of this challenge. Another aspect of the LOCA postulates the occurrence of a fission product release within containment as the safety challenge, and requires that the plant design and site characteristics be such that a hypothetical individual located at the exclusion area boundary would not receive a radiation dose in excess of prescribed limits.

Although this approach appears not to be related to a probabilistic risk approach, in fact, probability and risk have been implicitly considered from the beginning. One of the basic findings made during the safety review, and required before reactor licensing is one of "...no undue risk to the health and safety of the public." However, until the Three Mile Island accident, the NRC used explicit probabilistic criteria in only a few selected areas of licensing.

In 1975, the Reactor Safety Study, or WASH-1400, was published. This was the first systematic assessment of reactor risk that used modern probabilistic methods, and this report represents a seminal event in reactor risk assessment. Risk assessment techniques and applications advanced rapidly in the years following the TMI accident. More recently, we have seen the issuance of NUREG-1150 in 1990, which used improved PRA techniques to assess the risks associated with five U.S. nuclear power plants. This study has been noted as a significant turning point in the use of risk-based concepts in the regulatory process.

Recent PRA Applications

PRA methods have been successfully applied in a number of regulatory activities, acting as a complement to the traditional deterministic process. A number of recent Commission Policies or rules have been based, in part, on PRA methods. It may be appropriate to mention just a few of these.

These include the Backfit Rule, 10 CFR 50.109, the Commission's Safety Goal Policy, the Commission's Severe Accident Policy, and the Commission's Policy on Technical Specification Improvement. PRA methods have also been used in developing regulations regarding anticipated transients without scram (ATWS), the station blackout rulemaking, and in support of generic issue prioritization and resolution.

The NRC is also currently using PRA techniques to assess the safety importance of operating reactor events and as a part of the design certification review for advanced reactor designs. As many of you are aware, the Individual Plant Examination (IPE) Program which resulted from the Commission's Severe Accident Policy has resulted in power reactor licensees using risk assessment methods to identify potential plant vulnerabilities.

PRA is also being applied in performance assessment methods for low-level and high-level waste facilities, as well. This has involved the development of conceptual models and computer codes to model the disposal of waste. Because these systems are passive, the methods used to analyze active systems such as those found in PRA studies for reactors had to be adapted for the performance assessment of the potential geologic repository at Yucca Mountain.

PRA Policy Statement

I will briefly summarize the major points covered in this policy statement. First, the Commission has stated that the use of PRA technology should be increased in all regulatory matters to the extent supported by the state of the art in PRA methods and data and in a manner that complements the NRC's deterministic approach and supports the NRC's traditional defense-in-depth philosophy.

Second, the Policy states that PRA and associated analyses should be used in regulatory matters, where practical within the bounds of the state-of-the-art, to reduce unnecessary conservatism associated with current regulatory requirements, regulatory guides, license commitments, and staff practices. Where appropriate, PRA should be used to support proposed additional requirements in accordance with the provisions of the Backfit Rule (10 CFR 50.109). Appropriate procedures for including PRA in the process for changing regulatory requirements should be developed and followed. It is understood that the intent of this policy is that existing rules and regulations shall be complied with unless they are revised.

Third, the Policy states that PRA evaluations in support of regulatory decisions should be as realistic as practicable and appropriate supporting data should be publicly available for review.

Finally, the Policy concludes that the Commission's safety goals for nuclear power plants and subsidiary numerical objectives are to be used with appropriate consideration of uncertainties in making regulatory judgments on the need for proposing and backfitting new generic requirements on nuclear power plant licensees.

In conclusion, with this Policy statement, the NRC is affirming its belief that PRA methods can be used to derive valuable insights, perspectives, and general conclusions as a result of an integrated examination regarding design, operation, and the interactions between the facility and its staff. The NRC also recognizes, and encourages, continuation by industry to improve still further the application of PRA methods, data collection, and support in this very important area.

STUDY OF CHILDHOOD THYROID CANCER FROM THE CHERNOBYL NUCLEAR ACCIDENT

Another area that could potentially have significant benefit to the industry has been the US Government efforts in conducting epidemiologic studies of radiation induced thyroid disease in Belarus and Ukraine.

These studies focus on the incidence of thyroid disease, especially cancer, resulting from the 1986 accident at the Chernobyl nuclear power plant. Two scientific protocols have been signed. The first was signed with Belarus on May 26, 1994 and recently, the second, with Ukraine on May 10, 1995, during the President's visit to Kiev. The purpose of these thyroid studies is to assess the risk of thyroid cancer and hypothyroidism among persons, particularly children, who were exposed to iodine radioisotopes, especially I-131, during and/or following the Chernobyl accident. These scientific protocols will involve approximately 15,000 children in Belarus and about 70,000 Ukrainian children.

The release of radioiodine is likely to figure prominently in any nuclear power plant accident. This is especially significant considering that little is known of its carcinogenic potency. This new research of the Chernobyl accident provides a unique opportunity to understand and quantify the thyroid cancer risk of exposure to radioiodine and the role of potential cofactors, especially dietary iodine deficiency. It is expected that the analyses will contribute new knowledge of the carcinogenic effectiveness of I-131 in

comparison with that of x-ray and gamma radiation. This information will fill a major gap in the world's knowledge of radiation effects and contribute to improvement in public health policies wherever nuclear reactors are in operation.

These studies originated under the auspices of a 1988 memorandum of cooperation between the United States and the former Soviet Union concerning civilian nuclear reactor safety following the Chernobyl accident.

Currently the studies are being primarily implemented by the National Cancer Institute with support from the Department of Energy and the Nuclear Regulatory Commission in cooperation with the Ministries of Health of Belarus and Ukraine and several scientific institutes in these countries.

Presently, NRC, DOE and NCI continue to provide all the financial support for the implementation of the studies. Considering present U.S. Government budget issues, international participation may be welcome in the future.

I'd like to turn next to another topic of great current interest - thermal annealing of nuclear reactor pressure vessels.

ANNEALING OF NUCLEAR REACTOR PRESSURE VESSELS

Introduction

Assuring the structural integrity of the reactor pressure vessel is fundamental to the safe operation of nuclear power plants. It has been long recognized that neutrons escaping from the reactor core can embrittle the pressure vessel materials, and, as plants age, can limit the safe operating life of a reactor pressure vessel.

The criteria in 10 CFR 50, Appendix G, and the Pressurized Thermal Shock (PTS) rule provide continued assurance of pressure vessel integrity. However, there are a few plants that will approach these criteria before the end of their current license, and there are several more plants that may approach these criteria if the plants operate for an additional 20 years. Thus, embrittlement of the reactor vessel could limit the useful operating life of some plants.

The NRC, U.S. industry, and the international community have made significant progress in developing the analytical methods and supporting data needed to make realistic estimates of pressure vessel embrittlement. The technical community has developed analysis capabilities necessary to quantify the level of embrittlement and to assess the ability of embrittled pressure vessels to withstand normal operating loads and accident loads.

Refining our analytical techniques can lead to a better definition of the limits of safe operation, but performing analyses does not make the pressure vessel any safer. We need methods to mitigate the deleterious effects of neutron irradiation. Today, thermal annealing of the reactor pressure vessel is the only known technique for mitigating neutron irradiation embrittlement.

Description of Thermal Annealing

Our research has shown that neutron irradiation allows some elements, particularly copper and nickel, to change their distribution and cause an increase in hardness and a reduction in fracture toughness. Thermal annealing consists of heating the pressure vessel beltline materials to temperatures of about 850 to 900'F, well above the normal operating temperature of the pressure vessel, and holding them there for an extended period, typically about one week. Heating effectively relieves the damage to the steel's microstructure and restores the ductility of the material to nearly its unirradiated level. The annealing temperature must be high enough to allow atomic diffusion to take place and restore the embrittlement damage but not so high as to cause geometric distortion of the vessel or affect the original heat treatment of the vessel materials. While the idea is simple, and the metallurgical evidence for recovery of at least part of the embrittlement is conclusive, other considerations must also be addressed, including fire protection, and assurance that important systems, structures, and components are not degraded by the higher-than-normal temperatures.

Thermal annealing of a commercial reactor pressure vessel has never been accomplished in the U.S. However, reactor pressure vessels in 13 Russian designed plants in Russia and Eastern Europe have been successfully annealed. This experience lends significant credibility that thermal annealing in the U.S. is feasible from an engineering point of view. The NRC staff has witnessed the thermal annealing of a Russian reactor pressure vessel. This experience has helped to provide guidance to assure a successful annealing operation in the U.S.

Annealing Demonstration

The engineering feasibility of thermal annealing is being addressed through two Annealing Demonstration Projects, being jointly funded by the U.S. Department of Energy and the nuclear industry, including some international support. Currently, the two demonstration projects are planned using the reactor pressure vessels of two cancelled PWR plants. One plant, Marble Hill in Indiana, is a typical Westinghouse design, while the other, Midland in Michigan, is a typical B&W design.

Both plants will be instrumented and detailed analyses will be performed for comparison to the measurements. Through these demonstrations, we expect that key questions regarding the engineering feasibility of thermal annealing for U.S. designs will be answered, and that they will provide validation of the analytical methods used to predict temperatures and deformations in the overall system. Currently, the demonstrations are scheduled to be completed by mid to late 1996.

The NRC is working closely with the Department of Energy (DOE) in reviewing the annealing demonstration projects. We are also performing independent analyses and evaluations of the demonstration projects. Through this close review and evaluation, we expect to develop our independent assessment capability of the engineering feasibility of thermal annealing for U.S. designs, and to develop information that will be directly relevant to NRC review of any proposed annealing of a U.S. commercial power reactor vessel.

Palisades Nuclear Power Plant

As you heard earlier this week, the licensee of one plant, Palisades, has declared its intent to anneal the reactor pressure vessel. The limiting weld for the Palisades pressure vessel is projected to reach the pressurized thermal shock (PTS) screening criterion specified in our regulations in late 1999. The licensee has committed to annealing the pressure vessel prior to this time. The licensee currently projects

that recovery of the embrittlement will be sufficient to enable safe operation of the plant through at least the original end of license date, 2007, with a high probability that the plant could be operated well beyond 2011.

We anticipate that the licensee will begin submitting its thermal annealing report to the NRC shortly. This will be the first application of the new thermal annealing rule and Regulatory Guide once they are approved.

In conclusion, the NRC has made significant commitments to develop an environment for thermal annealing procedures that will result in the successful recovery of reactor pressure vessel toughness. The goal of these efforts is to ensure that thermal annealing in U.S. plants becomes a straightforward, safe alternative to maintain the integrity of the reactor pressure vessel throughout plant life.

Closing

I would like to close my remarks by reminding you once again of the importance of confirmatory safety research to the NRC's mission. I hope that this discussion of two recent examples in this regard as well as the topics presented in this meeting has made that clear. Thank you!

New Results from Pulse Tests in the CABRI Reactor

-:-:-:-:-

F. SCHMITZ, J. PAPIN, M. HAESSLER
Institut de Protection et de Sûreté Nucléaire, CADARACHE
Commissariat à l'Energie Atomique
F 13108 Saint Paul Lez Durance - France

N. WAECKEL
Electricité de France, SEPTEN
F 69628 Villeurbanne - France

Abstract

At the 21st and 22nd WRSM (1,2), the motivation and objectives of the French program on the behaviour of high burnup PWR fuel under RIA conditions in the CABRI test reactor has been presented.

The major results of the three first tests of the test matrix were presented and in particular REP-Na1, which failed at an unexpected low level of fuel enthalpy, was exposed to the community of nuclear safety research. At this time, no final understanding was reached for the origin of the failure. This objective is reached now.

Two further tests, REP-Na4 and 5, have been performed in 1995, they demonstrated a satisfactory and safe behaviour by resisting to the early phase of severe loading during the RIA pulse test.

Further examination work and analytical testing is in progress and the next tests with MOX fuel are being prepared.

1. Introduction

At the 21st and 22nd WRSM, generic papers have been presented on the motivation, objectives and first results of the program to investigate the behaviour of high burn-up PWR fuel under RIA conditions in the CABRI test reactor (1,2).

This year, we present progress in further test realisation, examination work and analysis.

In particular, we present experimental results from post-test examination and arguments giving a plausible explanation for the failure mechanism of REP-Na1, which is the « Hydride Assisted PCMI Failure Mechanism » (HAP), already observed in other RIA tests (3) and various clad loading situations (4).

This understanding, together with the results from the further tests, in particular clad straining and transient fission gas release and fuel fragmentation, give some clear partial understanding basis and valuable data for modeling and code validation, they are insufficient however, for the transposition to the real reactor case. The unprototypical coolant conditions in CABRI (low pressure sodium) give only for a very short time, representative clad temperature conditions. Under reactor conditions, high sustained contact pressures and important fission gas release might play a major role when clad temperatures increase rapidly. Under PWR conditions, DNB might be reached and, if lasting sufficiently long time,

will cause clad temperatures to run up fast and decrease rapidly the mechanical resistance of the clad material.

Improved clad material, on the other side, will better resist to PCMI loading because of lower corrosion and associated hydrogen pick-up. Fuel loading and clad resistance factors are presently badly known. Considerable improvement of the theoretical tools is needed in this field. An additional experimental programme is underway to assess the effects of localized hydrides and high strain rates on the mechanical behaviour of the irradiated claddings.

Clad to coolant transient heat transfer is another subject which needs consideration, a research programme is in progress in France to improve the present situation. So, the originally intended demonstration tests in CABRI revealed insufficiencies of mechanistic understanding and a need for scientific support work. In a later stage, according to the results obtained from the additional experimental programmes, more representative tests would be needed.

2. New CABRI tests

In 1995, two further tests have been performed and four tests are remaining to be done. In Table 1, the major test parameters of all five tests performed up to now are presented.

2.1. REP-Na4

This very important test is to be compared directly with REP-Na1. With regard to the first test, two major parameters have been changed :

- the ramp rate, 65ms (efficient) pulse width, compared to 9,5ms in REP-Na 1,
- the clad corrosion behaviour, 80μ mean corrosion thickness for both but heavy spalling for REP-Na1 and a dense continuous oxide without spalling for REP-Na4.

Burnup level and fuel state are very close to REP-Na1. The injected energy was of 95 cal/g at 1.2s and the pin resisted to this significant power transient, no rod failure was observed.

2.2. REP-Na5

For almost identical loading conditions (burnup, pulse shape, energy injection) compared to REP-Na1, this test was performed with a test pin which was cut off from the lower part of a GRAV 5c pin. The oxide layer was 20μ thick and the local hydrogen content is estimated to be 200 ppm, compared to 800 ppm in REP-Na1.

The test rod did not fail indicating the predominant role of the residual clad ductility in the early phase of PCMI loading.

3. Post-test examination work

3.1. Status

The non-destructive examination work is terminated for REP-Na1 to 3. The work is in progress for REP-Na5 and also REP-Na4 will be terminated before end of 1995.

TABLE 1 : MAIN CHARACTERISTICS OF THE TESTS

	REP Na1	REP Na2	REP Na3	REP Na4	REP Na5
Test fuel rod fissile length (mm)	EDF/Fabrice 569	BR3 rod 1000	EDF/segmented 440	EDF/Fabrice 571	EDF/Fabrice 571
Cladding	standard	standard	improved	standard	standard
Pint-Pchannel (b)	0.	0.	2.	2.	2.
Enrichment (%)	4.5	6.85	4.5	4.5	4.5
Burn-up (Gwd/t) (max. rod)	63.8	33.	52.8	62.3	64.3
Corrosion thickness (μ)	80	4	40	80	20
Gap gas composition	83.3% He + 16.7% Xe	He	He	He	He
Test energy deposition (cal/g) at 0.4 s	110	211	120	95 (at 1.2 s)	105
Power pulse width (ms)	9.5	9.5	9.5	# 60.	9.
Diametral maximum clad strain (mean value, %)	-	3.5	2.1	not yet available	1.06
Rod failure	yes	no	no	no	no
Maximal clad elongation (mm)	-	10	6	not yet available	6.3
Maximal fuel elongation (mm)	-	4	not available	not yet available	-
Transient FGR (%)		5.5	13.4	not yet available	17.2 %

Major destructive examination work is terminated for REP-Na1 and 2 and in progress for REP-Na3. Detailed work like rupture surface analysis by scanning electron microscobe (SEM) and fuel examination by microprobe analysis (MPA) is still under way.

3.2. Major results

Except REP-Na1, there was no further failure observed in the tests. So the major observations concerning the response of the test rod to the power transient are to be expected from the post test examinations.

- **Failure mechanism of REP-Na1** : the failure mechanism of REP-Na1 is the Hydride Assisted PCMI (HPA).

Local hydride accumulations are detected as well on the father rod cladding as on REP-Na1 after the test (Fig. 1). These accumulations result from cold spots on the cladding outside, at the location of the spalling of the corrosion layer of ZrO_2 occuring during irradiation.

Cracking of the brittle hydride is initiated during rapid transient heating and cracks may propagate locally into the underlaying ZIRCALOY which also is embrittled due to its high mean hydrogen concentration.

In REP-Na1, the very early failure gives a clear hint for a significant contribution of transient fuel swelling most probably to be situated in the RIM zone. In fact, at failure time, the bulk of the fuel is still cold and does not exceed nominal operation temperature. Also the clad loading stress at failure time resulting from thermal expansion only, is much lower than the contact pressure values which are reached under load follow conditions. So it is important to recall that the father rod of REP-Na1 was operated under load follow during the last cycles. Furthermore, the observed hydride accumulations have been generated with certainty during operation in the reactor.

- **Clad straining** : Profilometry data are available for REP-Na2, 3 and 5. These data are of high value for the validation of thermal/mechanical behaviour modelling. The homothetical following of the axial power shape is a valuable indication for the mechanistic loading behaviour. Characteristic 3D effects are observed in REP-Na2 (bamboo effect) as a result of the high energy injection (5).

In REP-Na3 and 5, the preirradiation spikes persist after the additional transient deformation without major change. This more uniform additional deformation might be due to the increasing contribution from gas swelling to the clad straining (Fig. 2).

- **Fission gas release** : The rod-puncturing after test and profilometry allows to collect the fill-gas and determine the fractional gas release. Simultaneously, the pin free volume is determined, so the post-transient pressure level in the pin can be determined.

- **Detailed fuel and clad structure and composition analysis** : The metallographic and ceramographic examination work reveals structural changes resulting from transient high burnup phenomena. Radial and azimuthal gross cracking and peripheral micro-cracking give hints on transient phenomena. Once the phenomena are well established, this heavy examination work can be considerably reduced.

A similar statement applies to scanning electron microscopy and microprobe analysis.

Fig 1 : REPNA1 Clad at 168.5 mm BFC

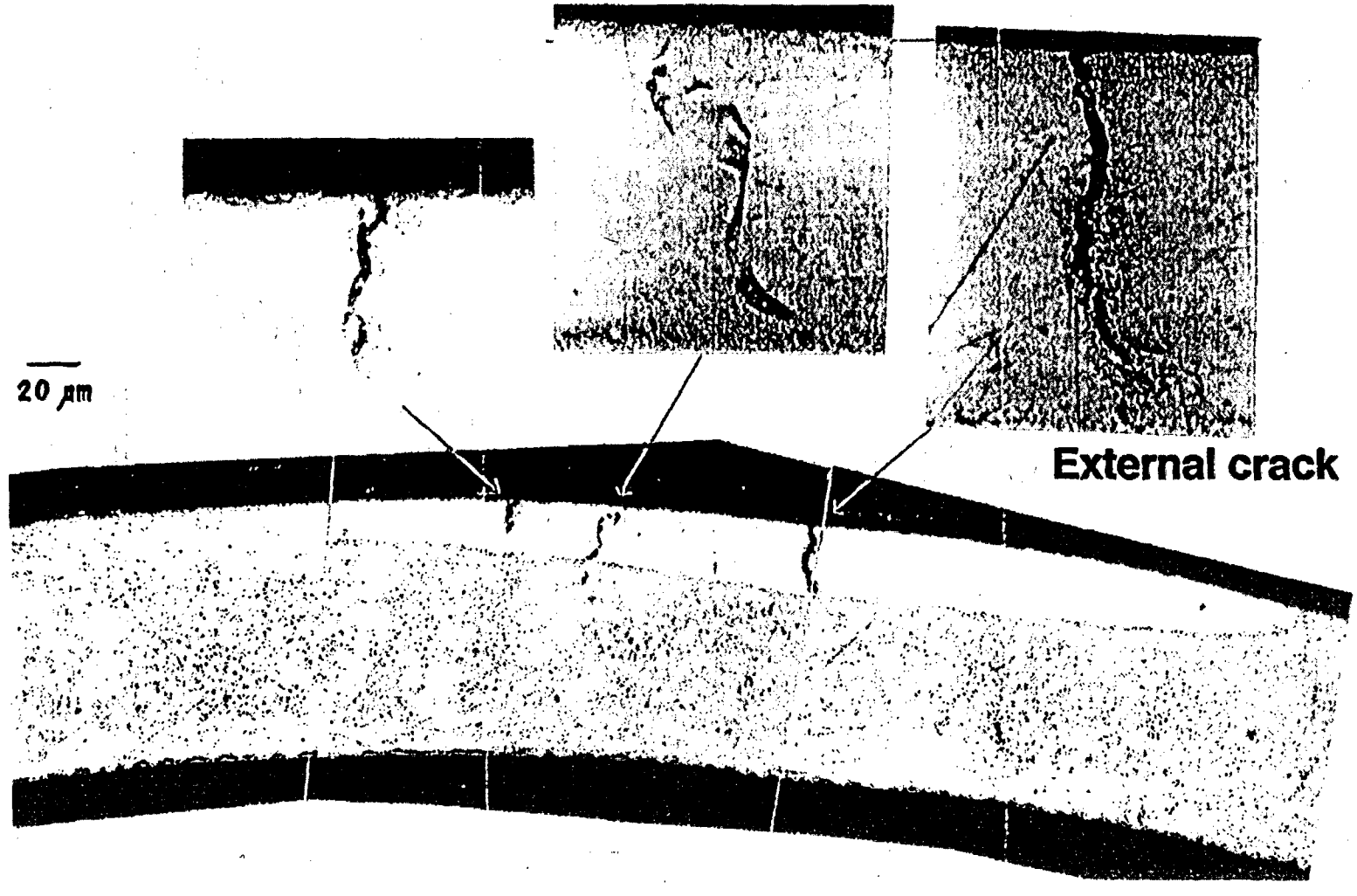

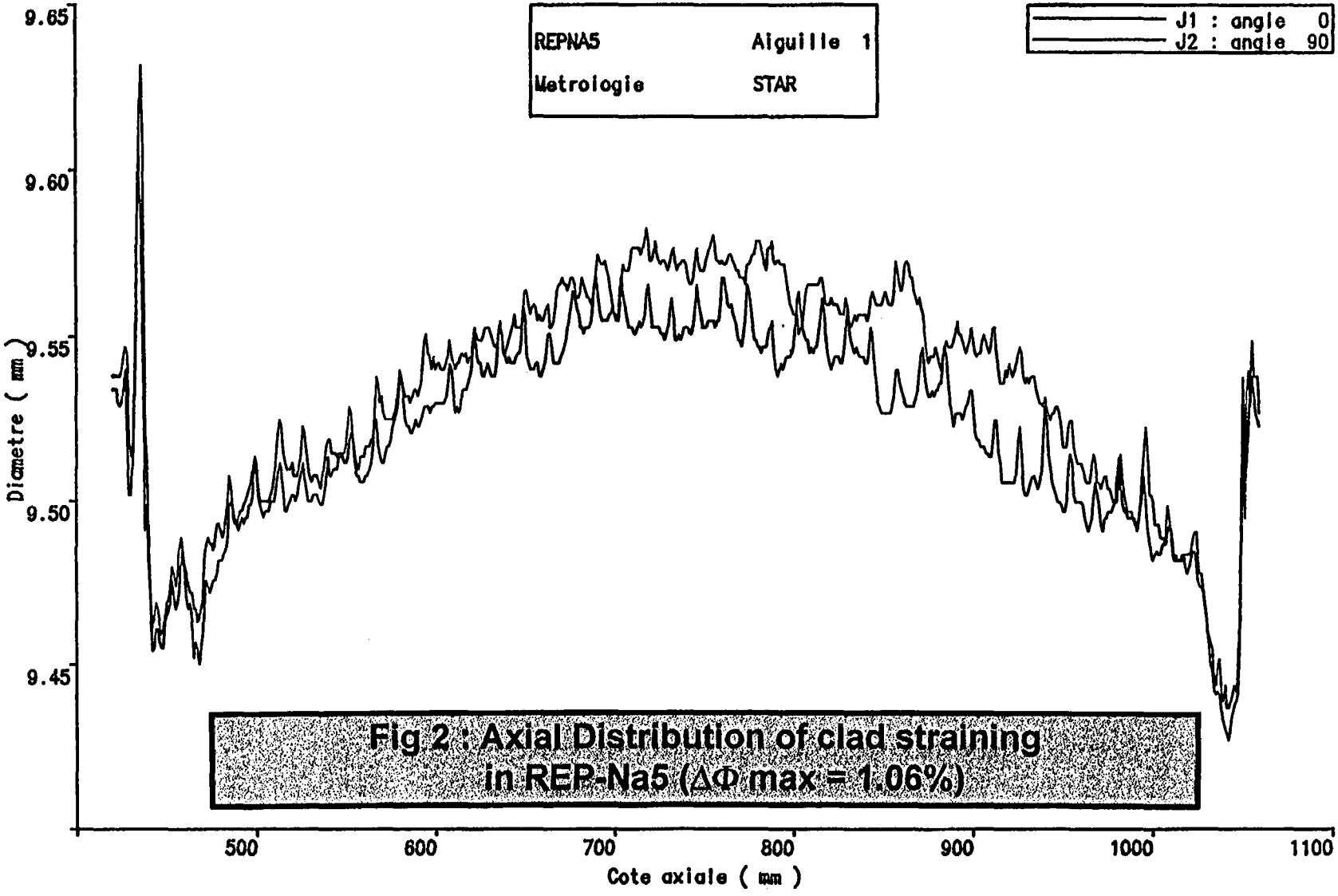

Fig 2 : Axial Distribution of clad straining in REP-Na5 ($\Delta\Phi$ max = 1.06%)

4. Analysis work

The IPSN code SCANAIR is the major analysis tool for precalculation and interpretation of the REP-Na tests (6). The initial state (t_0.state) is calculated with the CEA/DRN code system METEOR.

- **Thermal state :** The thermal state of the fuel, including the RIM region as well as the clad temperature, are believed to be well calculated.

The important thermal desequilibrium of the RIM zone disappears when the pulse width becomes larger than ~ 25ms.

- **Fuel swelling and clad straining :** The present understanding is that the fuel swelling energy and the clad strain energy are the parameters which set up the failure criterion. REP-Na3 and REP-Na5 strains seem to indicate that transient fission gas swelling represents a significant contribution to the straining on top of the thermal fuel expansion.

- **Fission gas release :** The transient release of retained fission gas increases strongly with burn-up. Despite a much higher energy input, the release in REP-Na2 is less than in REP-Na3 (5,5% compared to 13,4%). These results are fully coherent with NSRR results (7). Code calculation do not allow presently to simulate the observed release at high burn-up.

5. Next coming tests of the matrix

The updated matrix of the CABRI REP-Na tests is shown in table 2. From the four remaining tests, three are MOX-fuel experiments, the next two tests and the last one. The last UO_2 test at high burnup is to be performed with a test pin elaborated from a high burnup reactor fuel rod of advanced design.

The MOX fuel, resulting from the MIMAS fabrication procedure, will be tested at three different burnup stages. Compared to UO_2 fuel, the MOX fuel is characterized by some significant heterogenity. The product specification allows explicitely grain clusters with the Pu concentration of the initial masterblend powder (e.g. 30%Pu). A small fraction of the clusters may have a size of up to 400 microns according to the fabrication specifications but the largest clusters which have been measured are less than 200 microns.

During irradiation, these clusters burn more rapidly than the fuel average, they also diffuse into the matrix. During nominal operation, the clusters are in close to equilibrium thermal conditions.

During a fast power ramp, the clusters may reach much higher temperatures than the bulk of the fuel, due to the locally high fission density which results from the high fissile concentration.

In large clusters, the local burnup will be several times larger than the fuel mean burnup and under rapid transient heating, local melting or even fuel vaporization could be reached.

The effect of this possible scenario will be studied in the three REP-Na Mox tests.

The pulse width of the MOX power transient is still not defined, it is expected that reactor calculations will find a width of 25 to 40ms.

TABLE 2 : RIA TESTS MATRIX IN CABRI SODIUM LOOP

Name (date)	Fuel Rod	Maximum mean fuel enthalpy (cal/g)	Remarks
REP Na1 (11/93)	EDF, 63 Gwd/t (4.5 %) grid levels 5/6 Fabrice rod : 569 mm	115	failure fast pulse
REP Na2 (06/94)	BR3, 33 Gwd/t (6.85 %) no rod conditioning (1 m length)	200	no failure fast pulse
REP Na3 (10/94)	EDF, 52 Gwd/t (4.5 %) grid levels 5/6 segmented rod (440 mm)	125	no failure fast pulse
REP Na4 (07/95)	EDF, 63 Gwd/t (4.5 %) grid levels 5/6 Fabrice rod : 571 mm	~ 100	no failure reactor type ramp
REP Na5 (05/95)	EDF, 63 Gwd/t (4.5 %) grid levels 2/3 Fabrice rod : 571 mn	115	no failure fast pulse
REP Na6 (95)	Mox 3 cycles Fabrice rod	≤ 190	ramp to be defined
REP Na7 (96)	Mox 4 cycles Fabrice rod	≤ 175	ramp to be defined
REP Na8 (96)	EDF, ≥ 58 Gwd/t (4.5 %) grid level 4/5	~ 125	ramp to be defined
REP Na9 (96)	Mox 2 cycles Fabrice rod	≤ 200	ramp to be defined

It can easily be understood that the thermal heterogenity effect of the MOX fuel will be highest at the beginning of the irradiation when the Pu concentration is still high and the spot burnup already important. Mechanical effects resulting from high local burnup could shift the critical burnup, where the specific MOX behaviour reaches its maximum, to higher burnup. The first MOX test REP-Na6 will be performed at the medium burnup of three cycles.

REP-Na7 will be performed with a four cycle rod, at this level the heterogenity effects are expected to be less pronounced.

The test pins for these two experiments have been selected and the pin fabrication is in progress presently. The safety case for these specific experiments is also prepared presently for presentation to the safety authority.

The two last tests REP-Na8 and 9 are not defined in the last detail presently. For the improved advanced fuel design of the fuel rod chosen for the last UO_2 test, low corrosion parameters and no spalling are expected up to a maximum local burn-up of 55GWd/tU. So, the presently satisfactory behaviour of REP-Na 4 would a priori envelop the behaviour of the improved fuel. However, the PTE results of REP-Na4 might give arguments to perform REP-Na8 under the same conditions as REP-Na4. Otherwise, this test could be devoted to still open questions remaining after a coherent interpretation of the previous tests (e.g. high corrosion with some spalling and large pulse $\geq$ 40ms).

For the definition of the last MOX test, REP-Na-9, some feedback from the two other MOX tests and calculation data will be used to optimize the choice of the test fuel and the parameters of this test.

6. Conclusion

The major issue to be solved in the interpretation of the REP-Na tests is to identify and quantify the driving forces of clad straining and finally failing.

The thermal fuel expansion represents the obvious and unrefutable contribution. The correct thermal calculation, together with the thermomechanical fuel/clad interaction, are determined principally by the fuel and clad thermal and mechanical properties.

In addition to this basic loading mechanism, the contribution from transient gas swelling and, in particular, the RIM effect, which are the real high burnup effects, must be quantified.

This work is not terminated presently. Clear hints however, from the REP-Na1 failure first and furthermore, from the amplitude of the observed plastic strain and gas release observation from the other tests, lead to the conclusion that swelling phenomena contribute significantly to the clad loading at high burnup.

The behaviour of the MOX fuel under RIA conditions will be studied in the next-coming tests. The global behaviour will be compared to UO_2 fuel rod behaviour and special attention will be given to the local effects resulting from the plutonium rich grain clusters. It is in particular not known presently whether the critical burnup which might result from the specific MOX behaviour as a consequence of local fuel heterogeneities, is to be situated at begin of life or at high burnup.

7. Summary and outlook

The REP-Na test series is defined to study high burn-up effects during the early loading phase of the RIA scenario.

Separate effect tests and material property measurements at high burn-up contribute to improve the predictive capabilities of computer codes.

Code development and application on global test results allow to validate the understanding of interdependant physical phenomena inside the parameter range of the experiments.

Presently available test facilities are still far from representativity for reactor conditions :

- the pressurized water DNB and post DNB phenomena cannot be studied :
  - *failure
  - *fuel dispersal
  - *fuel coolant interaction

The international LWR safety R&D community needs a test facility offering close to representative, high quality experimental conditions :

- nominal temperature pressurized water-loop
- adequate performances :
  - * energy input
  - * pulse width
- instrumentation for key parameters and events :
  - * fuel and clad expansion
  - * temperature measurements
  - * coolant flow and pressure
  - * failure detection and dating
  - * fuel dispersal detection and dating
  - * fuel coolant interaction detection and quantification

A project study has been undertaken concluding that the implementation of a pressurized water loop into CABRI is possible and core and instrumentation performances are adequate to satisfy the requirements.

8. Acknowledgments

The authors express their thanks to the important contributions from CEA/DRN laboratories in Cadarache, Saclay and Grenoble and, in particular, to Patrick MENUT, Didier LESPIAUX, Maria TROTABAS and Claude LEMAIGNAN.

9. References

(1) J. PAPIN, J.P. MERLE « Irradiated Fuel Behaviour During Reactivity Initiated Accidents in LWRs. Status of Research and Development Studies in France » - 21st WRSM, Bethesda (1993)

(2) F. SCHMITZ, J. PAPIN, M. HAESSLER, JC. NERVI, P. PERMEZEL « Investigation of the Behaviour of High Burnup PWR Fuel under RIA Conditions in the CABRI Test Reactor » - 22nd WRSM, Bethesda, 24-26/10-1994

(3) R.K. McCARDELL, R.O. MEYER « Primary Factors Causing the Failure of High Burnup LWR Fuel Rods during Simulated Reactivity Initiated Accidents » - CSNI Specialist Meeting on Transient Behaviour of High Burnup Fuel , Cadarache 12-14/9-1995

(4) A.M. GARDE « Effects of Irradiation and Hydriding on Mechanical Properties of ZIRCALOY 4 at High Fluence » - Zirconium in the Nuclear Industry ASTM STP 1023, SWAM and EUCKEN Eds

(5) T. FUKETA, Y. MORI, H. SASAJIMA,K. ISHIJIMA and T. FUJISHIRO « Behaviour of High Burnup PWR Fuel under a Simulated RIA Condition in NSRR » - CSNI Specialist Meeting on Transient Behaviour of High Burnup Fuel , Cadarache 12-14/9-1995

(6) J. PAPIN, H. RIGAT, J.P. BRETON « The Behaviour of Irradiated Fuel under RIA Transients : Interpretation of the CABRI Experiments » - CSNI Specialist Meeting on Transient Behaviour of High Burnup Fuel , Cadarache 12-14/9-1995

(7) J.C. LATCHE, F. LAMARE, M. CRANGA « Computing Reactivity Initiated Accidents in PWRs » - SMIRT Conference, Porto Allègre, 1995.

New Results from the NSRR Experiments with High Burnup Fuel

Toyoshi FUKETA, Kiyomi ISHIJIMA, Yukihide MORI,
Hideo SASAJIMA and Toshio FUJISHIRO

Department of Reactor Safety Research
Japan Atomic Energy Research Institute
Tokai, Ibaraki 319-11 Japan

23rd Water Reactor Safety Information Meeting
Bethesda, U.S.A., October 23, 1995

Results obtained in the NSRR power burst experiments with irradiated PWR fuel rods with fuel burnup up to 50 MWd/kgU are described and discussed in this paper. Data concerning test method, test fuel rod, pulse irradiation, transient records during the pulse and post irradiation examination are described, and interpretations and discussions on fission gas release and fuel pellet fragmentation are presented. During the pulse-irradiation experiment with 50 MWd/kgU PWR fuel rod, the fuel rod failed at considerably low energy deposition level, and large amount of fission gas release and fragmentation of fuel pellets were observed.

INTRODUCTION

To provide a data base for the regulatory guide of light water reactors, behavior of reactor fuels during off-normal and postulated accident conditions such as reactivity-initiated accident (RIA) is being studied in the Nuclear Safety Research Reactor (NSRR) program of the Japan Atomic Energy Research Institute (JAERI). Numerous experiments using pulse irradiation capability of the NSRR have been performed to evaluate the thresholds, modes, and consequences of fuel rod failure in terms of the fuel enthalpy, the coolant conditions, and the fuel design. The current safety evaluation guideline for the reactivity-initiated events in light water reactors (LWRs) was established by the Nuclear Safety Commission of Japan in 1984, and based mainly on the results of the NSRR experiments. In the guideline, an absolute limit of fuel enthalpy during an RIA is defined as 963 J/g fuel (230 cal/g fuel) to avoid mechanical forces generation. The guideline also defines an allowable limit of fuel enthalpy for fuel design as a function of difference between rod internal pressure and system pressure. When fuel rod internal pressure is lower than external pressure, the limit is 712 J/g fuel (170 cal/g fuel). All of the NSRR data used for the guideline were limited to those derived from the experiments with fresh, i.e. un-irradiated fuel rods. For this reason, the current Japanese guideline adopted a peak fuel enthalpy of 356 J/g fuel (85 cal/g fuel) as a provisional failure threshold of pre-irradiated fuel rod during an RIA; and this failure threshold is used to evaluate number of failed pre-irradiated fuel rods, and to assess source term regarding fission gas release in a postulated RIA. This failure threshold enthalpy of 356 J/g fuel was derived from only one experiment, i.e. the test 859 performed in the Special Power Excursion Reactor Test program in the Capsule Driver Core facility (SPERT/CDC)[1,2], and hence the current guideline noted that the failure threshold should be revised by the NSRR experiments with pre-irradiated fuel rods. In addition to the requirements for the regulation, the burnup effect becomes one of a primary concern in the field of fuel behavior study since economics and prudent utilization of natural resources have provided strong incentives for extending the burnup levels of fuel operating in commercial power-producing LWRs. The burnup limits in Japan have been increased from 39 MWd/kgU to 48 MWd/kgU for PWRs and 50 MWd/kgU for BWRs, and further increase of the limits to 55 MWd/kgU

is in consideration. In these conditions, a series of experiments with pre-irradiated fuel rods were newly initiated in July 1989 as a part of the NSRR program after the completion of necessary modifications of the experimental facilities. This paper describes the results obtained from the NSRR experiments with irradiated PWR fuels, including 50 MWd/kgU PWR fuels (the HBO fuels).

EXPERIMENTAL METHOD AND TEST CONDITION

Pulse Irradiation in the NSRR

The NSRR is a modified TRIGA-ACPR (Annular Core Pulse Reactor) of which salient features are the large pulsing power capability which allows the moderately enriched fuel to be heated by nuclear fission to temperature above the melting point of UO_2; and large (22 cm in diameter) dry irradiation space located in the center of the reactor core which can accommodate a sizable experiment. **Figure 1** shows NSRR power histories of \$4.6, \$3.6 and \$3.0 reactivity insertion, which are recorded during tests HBO-3, -4 and -2, respectively. Shape of reactor power history depends on the inserted reactivity, and the smaller pulse becomes broader. While the full width at half maximum (FWHM) in \$4.6 pulse is 4.4 ms, that in \$3.0 pulse is 6.9 ms.

Energy Deposition and Peak Fuel Enthalpy

The energy deposited to a test fuel during pulse irradiation, is a key attribute among test conditions, which represents magnitude of power burst. To evaluate the energy deposition, number of fissions generated during the pulse irradiation is obtained from gamma-ray measurement of sample solution from post-pulse fuel pellet. Because additional burnup during the pulse irradiation is much smaller than that accumulated during base irradiation in a commercial power-producing reactor, only short life fission products are used for evaluating the number of fissions during the pulse irradiation. Fission product Ba-140, with a half life of 12.75 days, is selected for the evaluation. In order to reduce high gamma ray background from Cs-137 and other fission products, chemical separation scheme is applied to the sample solution. Unless otherwise noted, the "energy deposition", Q_t, denotes the radial average total energy deposition per unit mass of fuel (J/g fuel or cal/g fuel) in this paper. Since the energy deposition includes an energy released during runout phase, one should know an amount of energy promptly generated at pulse for assessment of fuel behavior. The prompt energy deposition, Q_p, can be calculated by using a ratio Q_p/Q_t, which is provided from an analysis[3] with EUREKA code as a function of an inserted reactivity. Since the NSRR transient is extremely fast, the prompt energy deposition becomes identical to peak fuel enthalpy under adiabatic assumption.

Test Capsule and Instrumentation

The experimental capsule used in the pulse irradiation is a newly developed double-container system for the irradiated fuel rod test in the NSRR. **Figure 2** shows a schematic diagram of the capsule. The outer capsule is a sealed container of 130 mm in inner diameter and 1,250 mm in height, and the inner capsule is a sealed pressure vessel of 72 mm in inner diameter and 680 mm in height. In terms of the design of the capsule, the easiness of assembling and disassembling works by the remote handling system is one of primary concern as well as the structural strength. The capsule contains an instrumented test fuel rod with stagnant water at atmospheric pressure and ambient temperature.

The instrumentation used in the pulse irradiation is illustrated in **Fig. 3**. Cladding surface temperatures are measured by 0.2 mm bare-wire R type (Pt/Pt-13%Rh) thermocouples (T/Cs) spot-welded to the cladding at three elevations. Coolant water temperature is measured by sheathed K type (CA) thermocouples (1 mm in diameter) near the cladding surface at top of the test fuel rod and/or center of the fuel stack. A strain gauge type pressure sensor is installed at the bottom of the inner capsule to measure the increase of capsule internal

pressure. A foil type strain gauge was attached at axial center on the outer surface of the inner capsule wall to measure the deformation of capsule. In some experiments, sensors for axial elongations of pellet stack and cladding tube are instrumented.

Test Fuel Rod

In a series of the irradiated PWR fuel experiments, four different test fuels have been refabricated from full-size commercial reactor fuels, and subjected to the pulse irradiation in the NSRR. The test fuels consist of the MH, GK, OI and HBO test fuels (acronyms for the fuels irradiated in the Mihama, Genkai, Ohi reactors and High Burnup fuels irradiated in the Ohi reactor, respectively). Irradiation history in the commercial reactor is a key attribute in this program. Fuel burnup and linear heat generation rate (LHGR) during the base-irradiation are listed in **Table 1**. Preceding to the extension of PWR fuel burnup limit from 39 MWd/kgU to 48 MWd/kgU, the demonstration program of high burnup fuel had been performed in the Ohi unit #1 reactor. The HBO test fuel had been irradiated in this program, and the fuel burnup reached 50.4 MWd/kgU.

As-fabricated, initial fuel specifications are listed in **Table 2**. The MH and GK fuels are 14×14 PWR type, and have the same dimensional configurations. While the OI and HBO fuels are 17×17 type, they have different cladding thickness and pellet outer diameter since fuel manufacturer of each fuel is different. It should be noted that the HBO fuel was not newly designed and manufactured for the high burnup application.

Dimensional data of the short-sized test fuel rods are listed in **Table 3**. The radial distance between cladding inner surface and fuel pellet (P/C gap) listed in the table is obtained from metallography for arbitrary horizontal cross-section (round slice). As it can be seen in this table, the P/C gap of the HBO test fuels is smaller than those of the other test fuels, since creep down of the cladding exceeded and the linear heat generation rate in the last irradiation cycle is lower in the high burnup HBO test fuel. The HBO test fuel rod is illustrated in **Fig. 4**. Since the HBO test fuel in each experiment was sampled from different elevation, oxide film thickness in cladding outer surface and concentration of absorbed hydrogen have variation. **Figure 5** shows the oxide film thickness of the HBO test fuels and the hydrogen concentration in the vicinity of the fuels.

Pulse-Irradiation Condition

The pulse-irradiation conditions including the energy deposition and peak fuel enthalpy are listed in **Table 4**. The Tests HBO-1, HBO-3 and OI-2 were performed with the maximum pulse of the NSRR. Because of high burnup and small number of residual fissile in the HBO fuel, peak fuel enthalpy was restricted to 310 J/g fuel (74 cal/g fuel). The Test KF-1 (referred as GK-3 in some documents) is excluded from the table, since the experiment is atypical. The fuel rod used in the Test KF-1 was exposed to excessive load follow operations with several hundred cycles in the Japan Materials Testing Reactor (JMTR).

RESULTS AND DISCUSSION

Appearance of Post-test Fuel Rod

The first test in a series of experiments with the HBO fuels, the Test HBO-1, resulted in fuel failure, while the other irradiated PWR experiments, including the Tests HBO-2, -3 and -4, remained no failure. **Figure 6** shows post-test appearance of the HBO-1 test fuel. Axial cracking of the cladding in entire region corresponding to the fuel stack occurred. The fractures are similar to those occurred by hydride-assisted PCMI in the SPERT 859 experiment. **Figure 7** shows horizontal cross-section of the failed cladding. Considerable hydride deposition and oval deformation can be seen in the figure. Residual hoop strain at a failed position is estimated as approximately 2%, which is much larger than that observed in un-irradiated fuel experiments. This could be caused by severe creep down of the cladding and large transient swelling of the high burnup fuel. Many small cracks vertical to the

cladding outer surface were also found in outside oxide layer and radially localized hydride layer. Large wall-through cracks were originated from some of these crack tips and showed a feature of ductile fracture in the inner cladding region, as shown in **Fig. 8.**

All of fuel pellets did not stay inside the rod, and were found in the capsule water as fragmented debris. Since the collected fuel pellets are finely fragmented, it can be thought that the fuel pellets are expelled from the fractured opening during the pulse. However, it can be also expected that the pellets dropped from the horizontal break after the pulse. The break can be seen at the bottom end of fuel active region.

Transient Record

Figure 9 illustrates the transient records of the reactor power, cladding surface temperature, fuel rod internal pressure and capsule internal pressure during the pulse-irradiation of the Test HBO-1 with the peak fuel enthalpy of 305 J/g fuel (73 cal/g fuel). Thermo-couple failure and spikes in capsule and fuel rod internal pressure histories observed simultaneously. This indicates an occurrence of cladding failure. The energy deposition at failure is approximately 250 J/g fuel (60 cal/g fuel). The early failure when the cladding surface temperature remains about 50 deg C indicates cladding cracking caused by pellet cladding mechanical interaction (PCMI). Although all of the fuel pellets was expelled or dropped from the rod and was recovered as finely fragmented debris, the transient records did not show pressure generation indicating an occurrence of molten fuel-coolant interaction. Because of the fuel failure in the Test HBO-1, pellet stack and cladding elongations were not successfully measured.

Fuel Deformation

Residual hoop strain was obtained from dimensional measurements on the post-test fuel rods. The residual hoop stain is shown in **Fig. 10** as a function of the peak fuel enthalpy. The strain becomes larger in the increased peak fuel enthalpy. In relatively low peak fuel enthalpy range, 250 J/g fuel (60 cal/g fuel) or lower, the Tests HBO resulted in larger strain than those in the Tests MH, as it was expected from the thinner pre-pulse P/C gap in the HBO test fuel. On the other hand, the strain of the Test HBO-3 with the peak fuel enthalpy of 310 J/g fuel (74 cal/g fuel) was almost same with that in the Test MH-3 with the peak fuel enthalpy of 280 J/g fuel (67 cal/g fuel). It should be noted that the Tests GK-1 and OI-2 resulted in no failure although the strains in these experiments exceeded 2% and 4%, respectively.

Fission Gas Release

After the pulse irradiation, rod-average fission gas release was destructively measured for the test rod by rod puncture and gas analysis. The fission gas release during the pulse-irradiation is shown in **Fig. 11** as a function of the peak fuel enthalpy. Fission gas release from the HBO fuel during base-irradiation was 0.49%. On the other hand, significant fission gas release occurred in the pulse-irradiation of the Tests HBO. Fission gas release is 17.7% even in the Test HBO-2 with the peak fuel enthalpy of 157 J/g fuel (37 cal/g fuel), and reaches 22.7% in the Test HBO-3. It should be noted that the fission gas release in the Test HBO-2 is higher than the release in the Test GK-1 with the peak fuel enthalpy of 389 J/g fuel (93 cal/g fuel). The data shown in Figs. 8 and 9 indicate that the significant fission gas release in the Tests HBO occurred with relatively small fuel swelling. **Figure 12** shows the fission gas release as a function of the fuel burnup. Higher fuel burnup correlates with the higher fission gas release.

Fuel Pellet Structural Change

Metallographical examinations on the post-test HBO fuel rods are being extensively performed. Since the fuel pellets of the Test HBO-1 were finely fragmented, horizontal round slice and vertical division could not be sampled from the test fuel. As for the Tests

HBO-2, -3 and -4, round slices and vertical divisions were subjected to the examinations. Figure 13 shows horizontal and radial cross-sections of the Test HBO-3 fuel. In the horizontal cross-section, number of radial and circumferential cracks can be seen in the fuel pellet periphery. The radial crackings in the peripheral region were observed also in other irradiated fuel experiments, i.e. MH, GK OI and JM test series. On the other hand, the post-test HBO fuel is characterized by the circumferential crackings. The vertical cross-section also shows numerous cracks can in the vicinity of the dish. The crackings seem stream-lines between source and sink in both ends of the dish, or magnetic-lines between positive and negative poles. A part of fuel pellet was collapsed during the pulse-irradiation. X-ray photograph showing the post-test HBO-3 fuel rod indicated that the collapse of fuel pellets in both ends of the fuel stack.

Fuel Pellet Fragmentation

The fuel pellets were found as finely fragmented particles after the Test HBO-1. A particle size distribution of the Test HBO-1 fuel is given in Table 5. The fragmented fuel debris were sieved to obtain the particle size distribution. Since the fuel was highly radioactive, the variation of mesh size was restricted to only two, and the mesh openings for the sieves were 500 μm and 50 μm. The result shows an occurrence of intensive fragmentation. About 90% of recovered particles are smaller than 500 μm, and a half or more is smaller than 50 μm. Regarding destructive forces generation, fragmented particle size distribution has been examined also in NSRR high energy deposition experiments[4] with fresh, un-irradiated fuels. In the fresh fuel experiment with an energy deposition of 1600 J/g fuel (380 cal/g fuel) or higher, partly molten fuel ejected from the rod and fragmented fuel particles were recovered. As for fresh fuel rods, more than a half of debris are larger than 100 μm even in the experiment with an energy deposition of 2100 J/g fuel (500 cal/g fuel). The fuel recovered in the Test HBO-1 became the finest particles in the NSRR program. Optical and scanning electron microscopy (SEM) and electron probe microanalysis (EPMA) are in planning stage for relatively large fragmented fuel particle.

The radially averaged peak fuel enthalpy in the Test HBO-1 is only 306 J/g fuel (73 cal/g fuel), and corresponding fuel temperature is well below the melting point. It is naturally accepted that the fuel pellets of the Test HBO-1 have not melted during the experiment. During the PIE process, once-molten, spherical particle was not observed. Hence, one can hardly expect an occurrence of molten fuel-coolant interaction, or steam explosion. However, it seems premature to deny the possibility of mechanical forces generation caused by vigorous boiling. Since surface area of the finely fragmented fuel particles is considerably large, prompt contact of the particles with coolant water may generate mechanical force, especially under stagnant and high subcooling coolant and atmospheric pressure conditions of the NSRR experiment.

Grain Boundary Separation

The significantly large fission gas release, the fuel fragmentation producing extremely fine particles and pre-existing small porosity in fuel pellets of the Test HBO-1 indicate the grain boundary separation[5] occurred almost instantaneously. Figure 14 illustrates the postulated scheme. Fission gas pores are accumulated along grain boundaries during the base-irradiation. Rapid expansion of fission gas accumulated in the small pores may cause weakening of the boundaries and subsequent grain boundary separation, and then results in fission gas release and fuel fragmentation.

Fuel Failure

Figure 15 summarizes fuel burnup of subjected test fuels and peak fuel enthalpy during transients in RIA experiments.[6,7] Fuel integrity have been demonstrated at the peak fuel enthalpy below 450 J/g fuel (108 cal/g fuel) for the fuel burnup of 42 MWd/kgU or lower. The data in the figure, however, suggests decreased failure threshold in high burnup region

in terms of peak fuel enthalpy. Fission gas accumulation and its rapid expansion may contribute to the significant fuel swelling which has been observed in the NSRR experiments. The swelling has a potential to cause PCMI, and possibly in combination with decreased cladding integrity, to generate the cladding failure.

SUMMARY AND CONCLUSIONS

The Test HBO-1 with a 50 MWd/kgU PWR fuel resulted in fuel failure at the energy deposition of approximately 250 J/g fuel (60 cal/g fuel). The results suggest possible reduction of failure threshold for high burnup fuels, and indicate that PCMI with swelling of the fuel pellets leads to the failure. Rapid thermal expansion of accumulated fission gas can intensify the swelling and fission gas release, and subsequent fuel fragmentation to extremely small particles.

The 50 MWd/kgU fuel rods in three experiments following to the Test HBO-1 survived through the transients with peak fuel enthalpy ranged from 157 to 310 J/g fuel (37 to 74 cal/g fuel). However, significant fission gas release up to 22.7% occurred.

Further investigations on fuel failure mechanisms through in-pile integrated experiments, out-of-pile separate effect tests and phenomenological modeling could contribute to "accident-conscious" fuel design to avoid fuel failure and excessive fission gas release.

Acknowledgements

The HBO test series have been performed as a collaboration program between JAERI and Mitsubishi Heavy Industries, LTD. by using fuel rods transferred from Kansai Electric Power Company. The authors would like to acknowledge and express their appreciation for the time and effort devoted by numerous engineers and technicians in Reactivity Accident Research Laboratory, NSRR Operation Division, Department of Hot Laboratories and Analytical Chemistry Laboratory, JAERI. They also acknowledge the support and help of individuals and other organizations too numerous to cite, whose contribution were critical to the success of the program.

REFERENCES

(1) Miller, R. W., "The Effects of Burnup on Fuel Failure: I. Power Burst Tests on Low Burnup UO_2 Fuel Rods", IN-ITR-113, Idaho Nuclear Corporation (July 1970).

(2) Miller, R. W., "The Effects of Burnup on Fuel Failure: Power Burst Tests on Fuel Rods with 13,000 and 32,000 MWd/MTU Burnup", ANCR-1280/TID-4500, R63, Aerojet Nuclear Company (Jan. 1976).

(3) Ohnishi, N. and Inabe, T., "Evaluation of Effective Energy Deposition in Test Fuel during Power Burst Experiment in NSRR", *J. Nucl. Sci. Technol.*, **19** [7], 528 (1982).

(4) Fuketa, T. and Fujishiro, T., "Generation of Destructive Forces During Fuel/Coolant Interactions Under Severe Reactivity Initiated Accident Conditions", *Nucl. Eng. Des.*, **146**, 181 (1994).

(5) Fuketa, T., Mori, Y., Sasajima, H., Homma, K., Tanzawa, S., Ishijima, K., Kobayashi, S., Kikuchi, T. and Sakai, H., "Behavior of Pre-irradiated Fuel Under a Simulated RIA Condition [Results of NSRR Test JM-4]", JAERI-Research 95-013 (Mar. 1995).

(6) MacDonald, P. E., Seiffert, S. L., Martinson, Z. R., McCardel, R. K., Owen, D. E. and Fukuda, S. K., "Assessment of Light-Water-Reactor Fuel Damage During a Reactivity-Initiated Accident", *Nucl. Safety*, **21**, 582 (1980).

(7) Schmitz, F., Papin, J., Haessler, M., Nervi, J. C. and Permezel, P., "Investigation of the Behaviorof High Burn-up PWR Fuel Under RIA Conditions in the CABRI Test Reactor", *22nd Water Reactor Safety Information Mtg.*, Bethesda, Maryland, Oct. 24-26, (1994).

Table 1 Base-irradiation conditions

Test Fuel ID	Reactor	Initial Enrichment (%)	Irradiation cycle	Start of irradiation	End of irradiation	Fuel burnup (MWd/kgU)	LHGR (kW/m)	
							Average	Last cycle
HBO	Ohi unit #1	3.2	4	June, 1981	Dec., 1987	50.4	16.1	15.4
OI	Ohi unit #2	3.2	2	Dec., 1985	Aug., 1988	39.2	20.7	20.5
MH	Mihama unit #2	2.6	4	June, 1978	Aug., 1983	38.9	19.8	19.3
GK	Genkai unit #1	3.4	3	Feb., 1975	Feb., 1979	42.1	20.1	19.8

Table 2 As-fabricated fuel rod specifications

Fuel ID	Fuel type	Cladding			Fuel pellet			Radial P/C gap
		O.D.	I.D.	Thickness	O.D.	Height	Shape	
HBO	17×17	9.5	8.36	0.57	8.19	13.5	Dished & Chamfered	0.084
OI		9.5	8.22	0.64	8.05	9.5	Dished & Chamfered	0.085
MH, GK	14×14	10.72	9.48	0.62	9.29	15.2	Dished & Chamfered	0.095

(unit : mm)

Table 3 Test fuel rod specifications

Test Fuel ID	Total Length	Active Fuel Stack	Cladding O.D.	Radial P/C gap
HBO	.308	135	9.444±0.002	<0.01
OI	.306	133	9.470±0.002	0.02
MH	300	121.6	10.656±0.001	0.02
GK	300	121.6	10.666±0.002	0.02

Table 4 Pulse-irradiation condition

Test ID	Fuel Burnup (MWd/kgU)	Date of Pulse	Inserted Reactivity ($)	Energy Deposition (J/g fuel)	(cal/g fuel)	Peak Fuel Enthalpy (J/g fuel)	(cal/g fuel)
HBO-1	50.4	Feb. 16, 1994	4.6	390	93	305	73
HBO-2		Mar. 25, 1994	3.0	215	51	157	37
HBO-3		Oct. 19, 1994	4.6	397	95	310	74
HBO-4		Jan. 24, 1995	3.6	279	67	211	50
OI-1	39.2	Nov. 10, 1992	4.5	571	136	444	106
OI-2		Jan. 27, 1993	4.6	581	139	453	108
MH-1	38.9	Nov. 28, 1989	3.4	262	63	196	47
MH-2		Mar 8, 1990	3.8	301	72	228	55
MH-3		Oct. 31, 1990	4.3	363	87	280	67
GK-1	42.1	Mar. 12, 1991	4.3	505	121	389	93
GK-2		Mar. 17, 1992	4.2	490	117	377	90

Table 4 Particle size of recovered fragmented fuel in the Test HBO-1

		Mass (g)	% in initial mass	% in total collected
Collected fuel particles	$d \geq 500\ \mu m$	4.78	6.5	9.7
	$500\ \mu m \geq d \geq 50\ \mu m$	17.81	24.3	36.0
	$50\ \mu m \geq d$	26.84	36.7	54.3
	Total collected	49.43	67.5	100
Un-collected fuel pellets		23.78	32.5	
Initial mass (fuel pellets before pulse)		73.21	100	

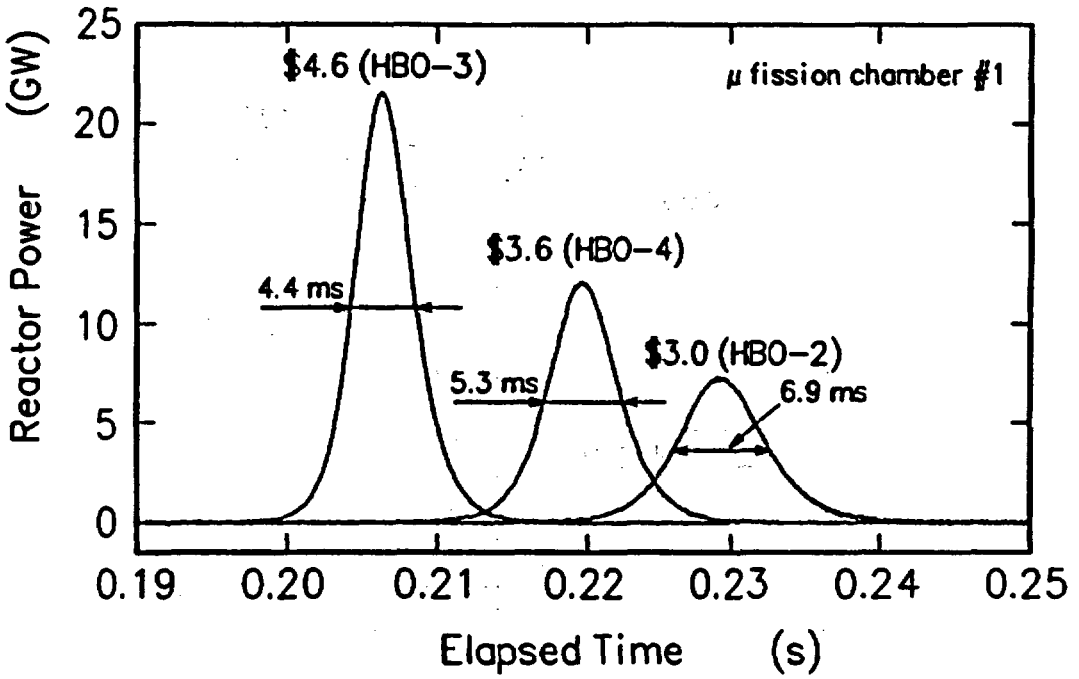

Fig. 1 Power histories during pulse-irradiations for the Tests HBO-2, -3 and -4

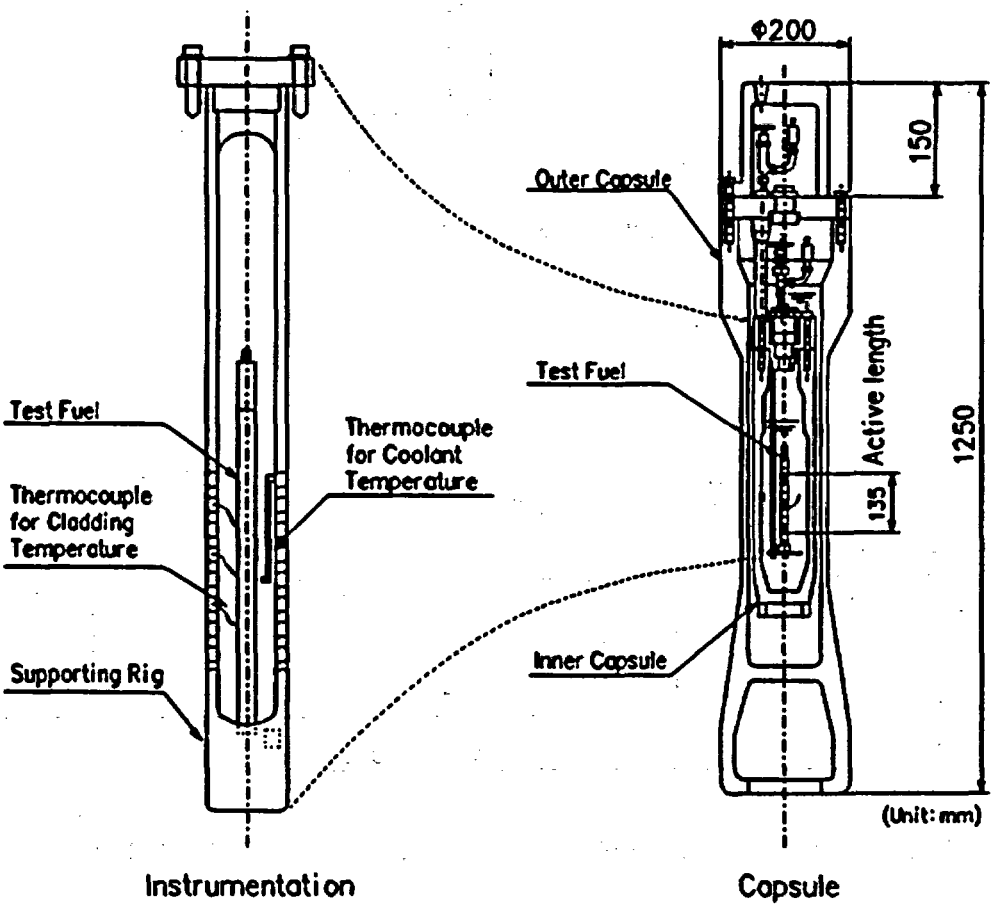

Fig. 2 Schematics of experimental capsule for pulse-irradiation

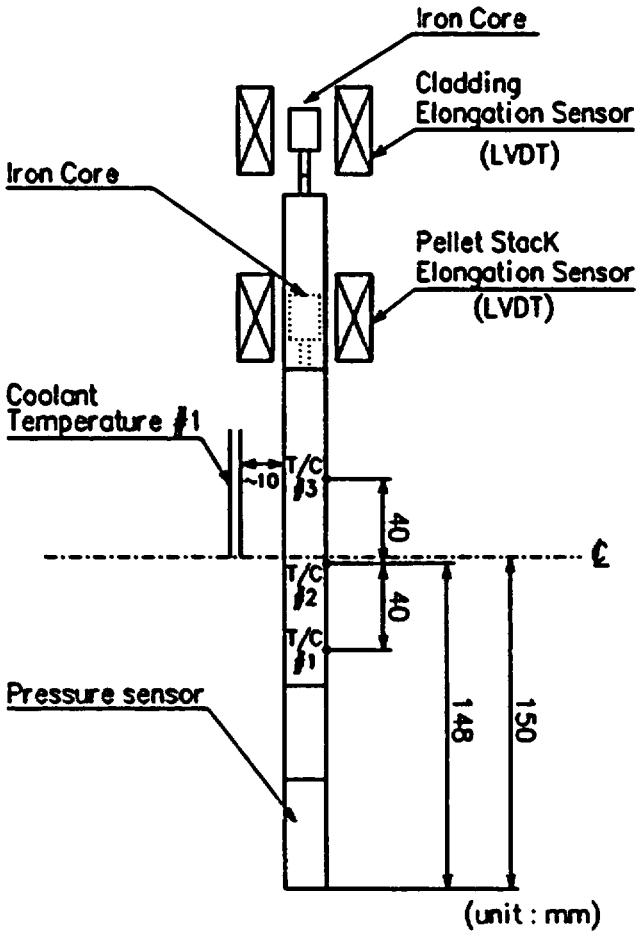

Fig. 3 Instrumentations for pulse-irradiation experiment

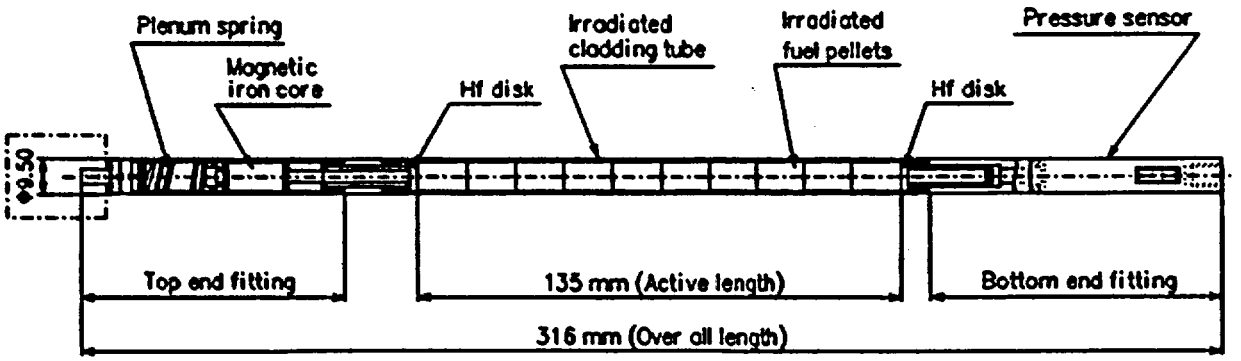

Fig. 4 Schematics of the HBO test fuel (segmented 50 MWd/kgU PWR fuel)

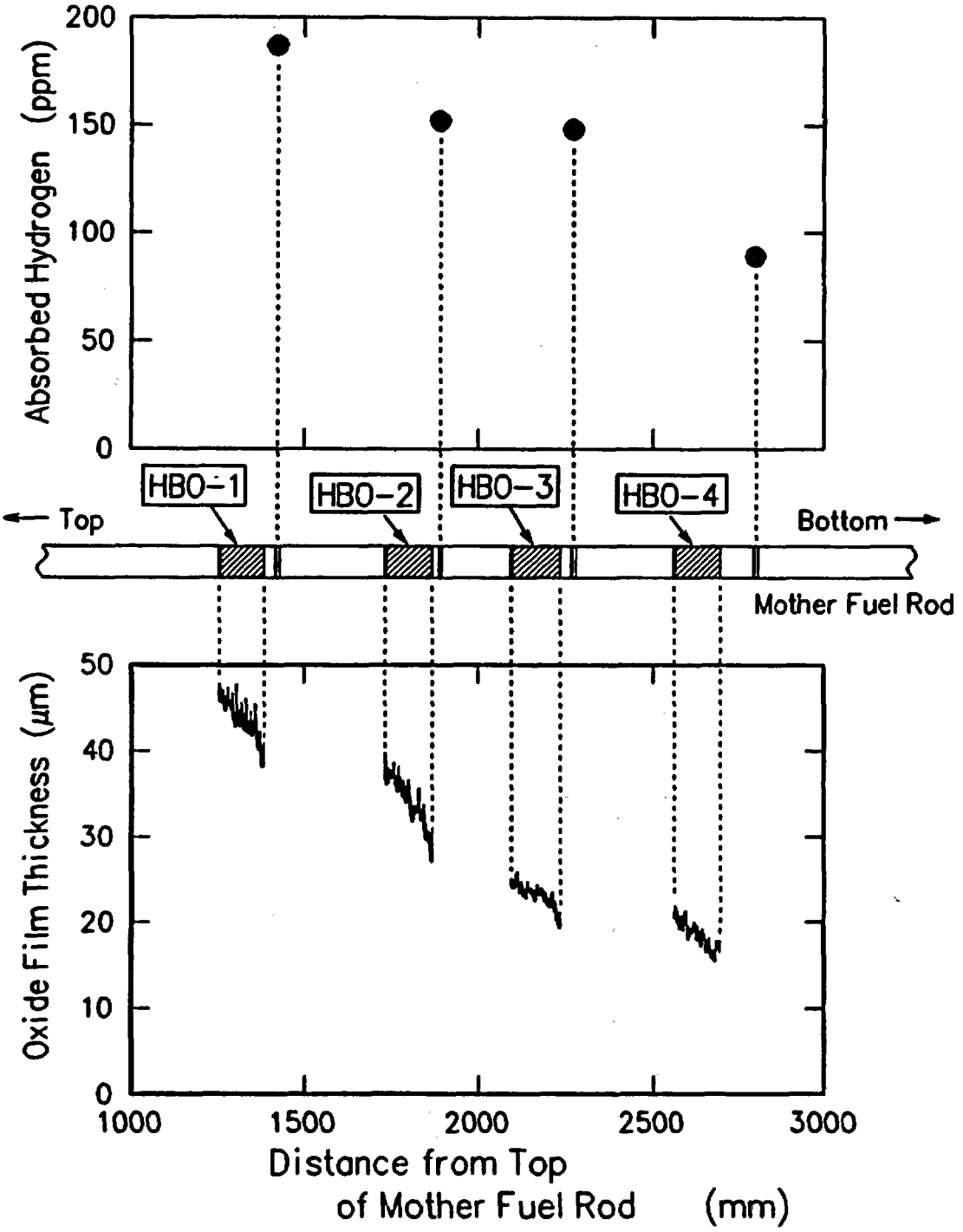

Fig. 5 Oxide film thickness and hydrogen concentration in HBO test fuels

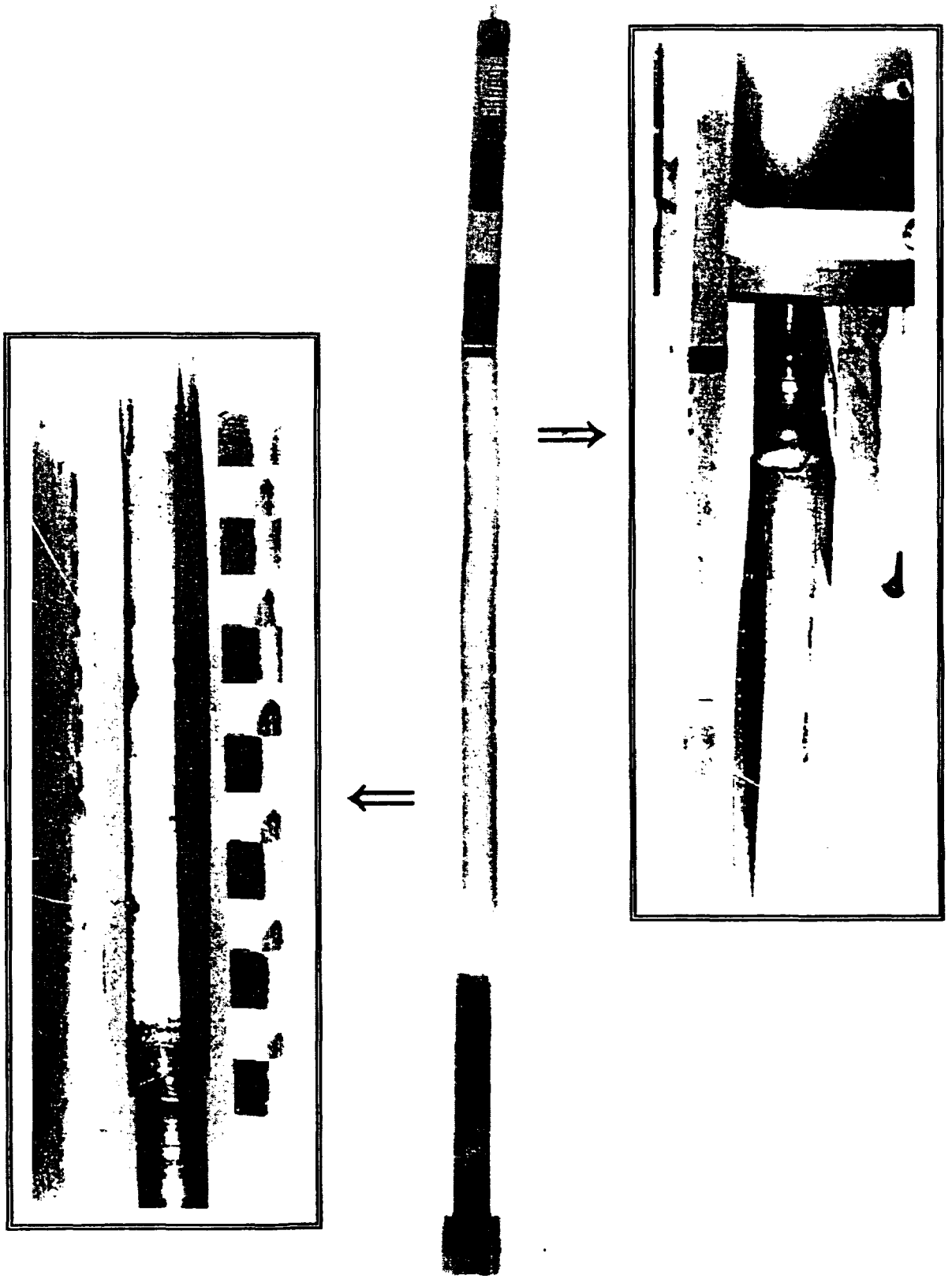

Fig. 6 Post-test appearance of the HBO-1 test fuel

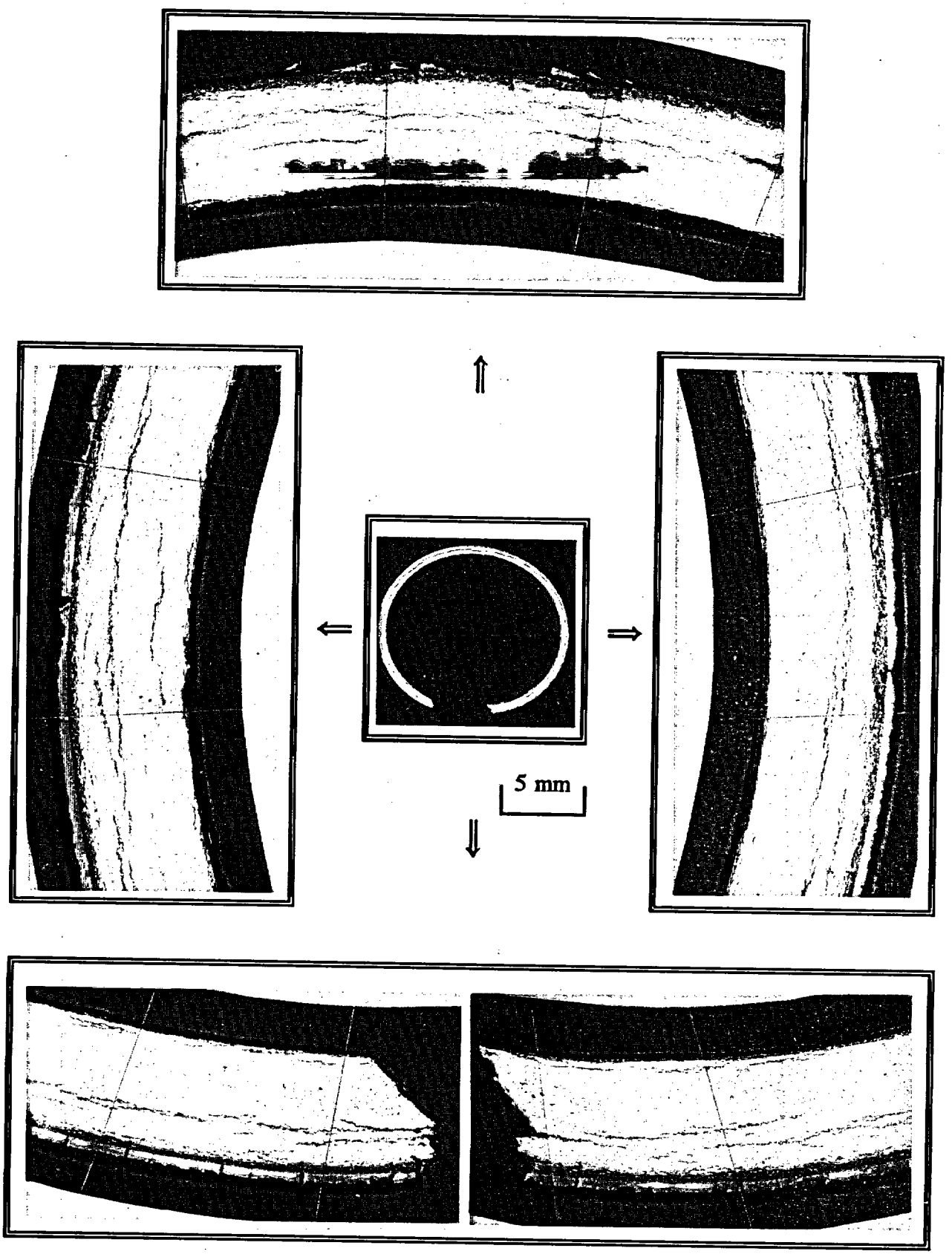

Fig. 7 Horizontal cross-section of the cladding failed in the test HBO-1

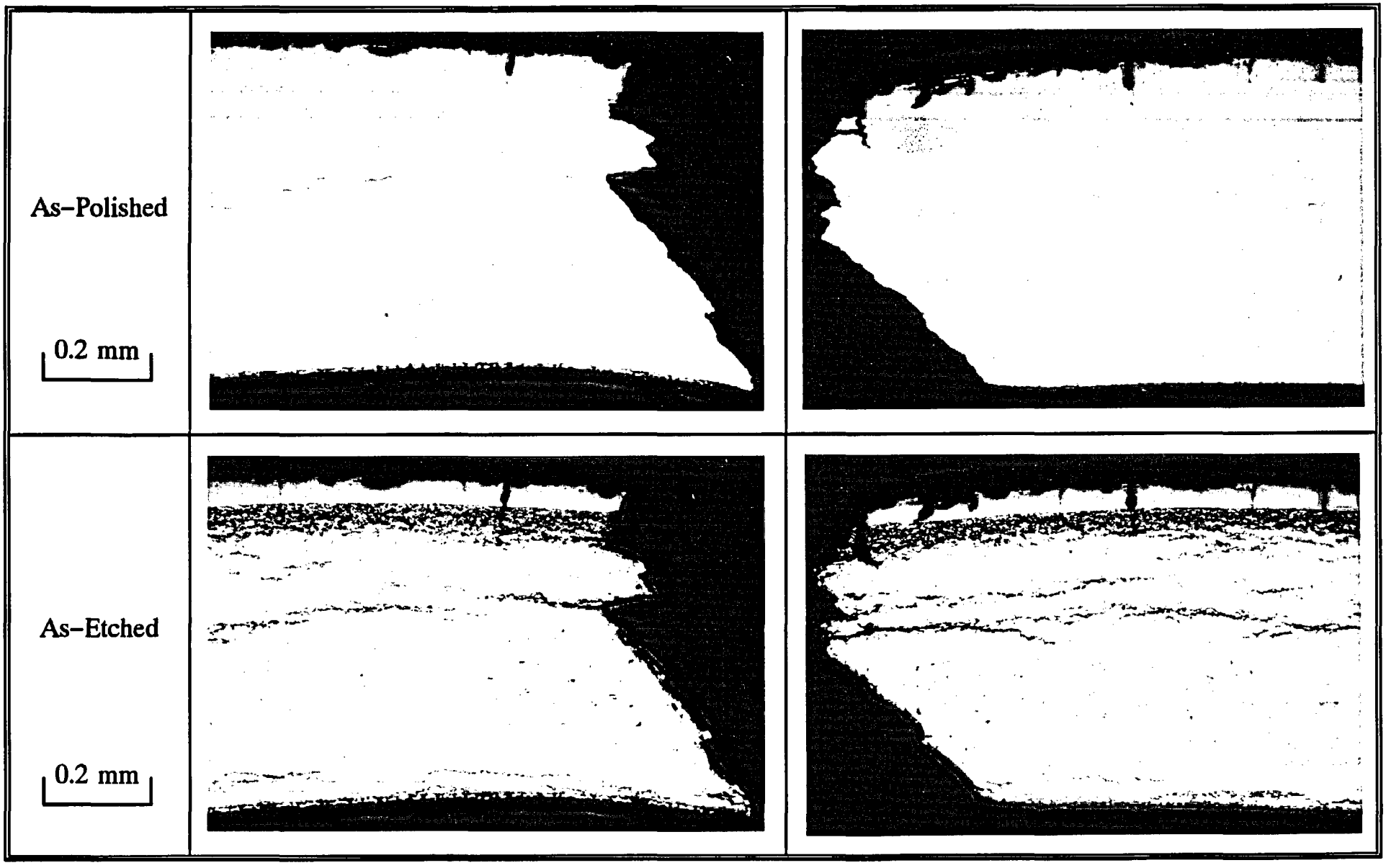

Fig. 8 Cracking in the post-test cladding in the Test HBO-1

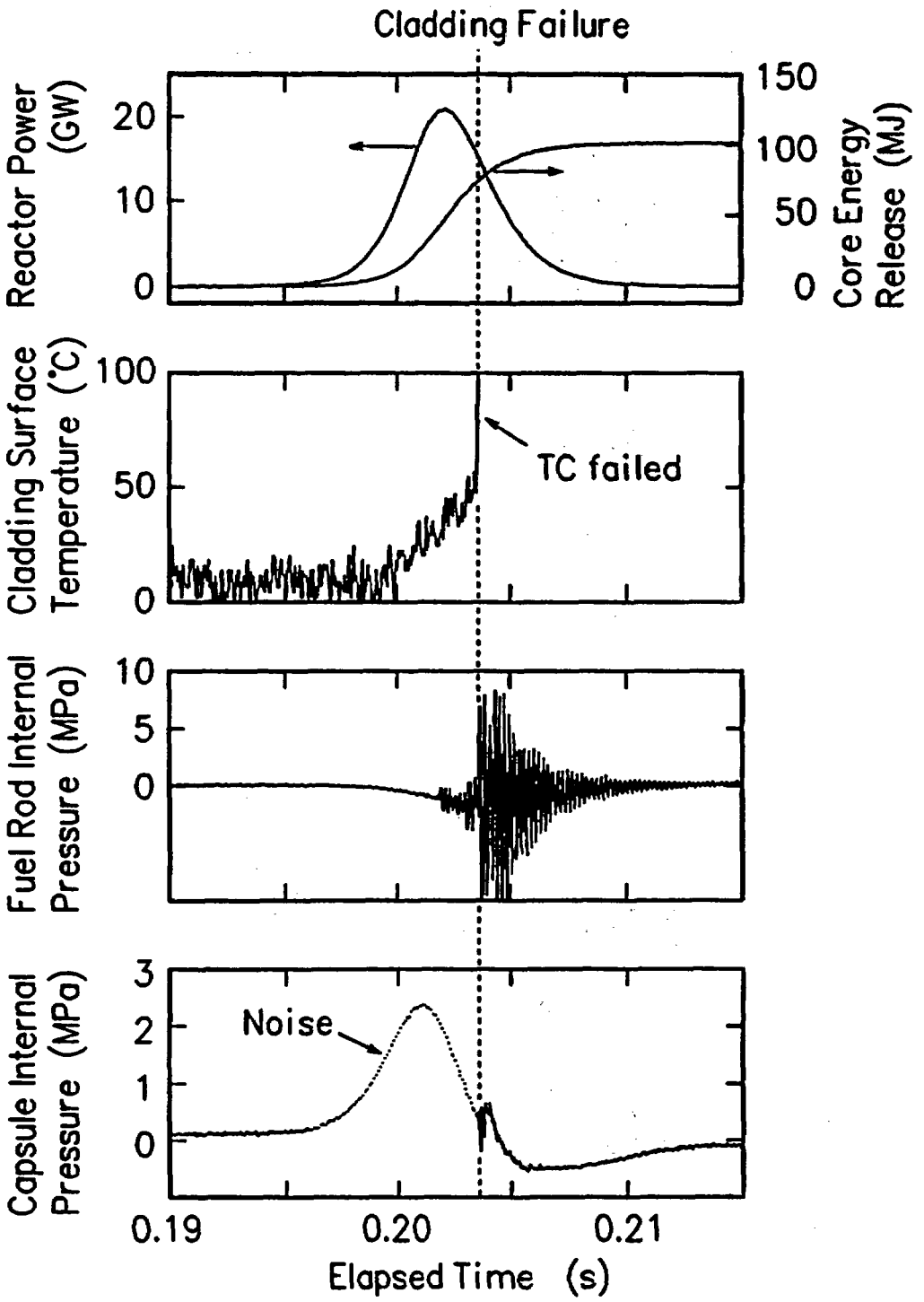

Fig. 9 Transient records of reactor power, cladding surface temperature, fuel rod internal pressure and capsule internal pressure during the pulse-irradiation of the Test HBO-1

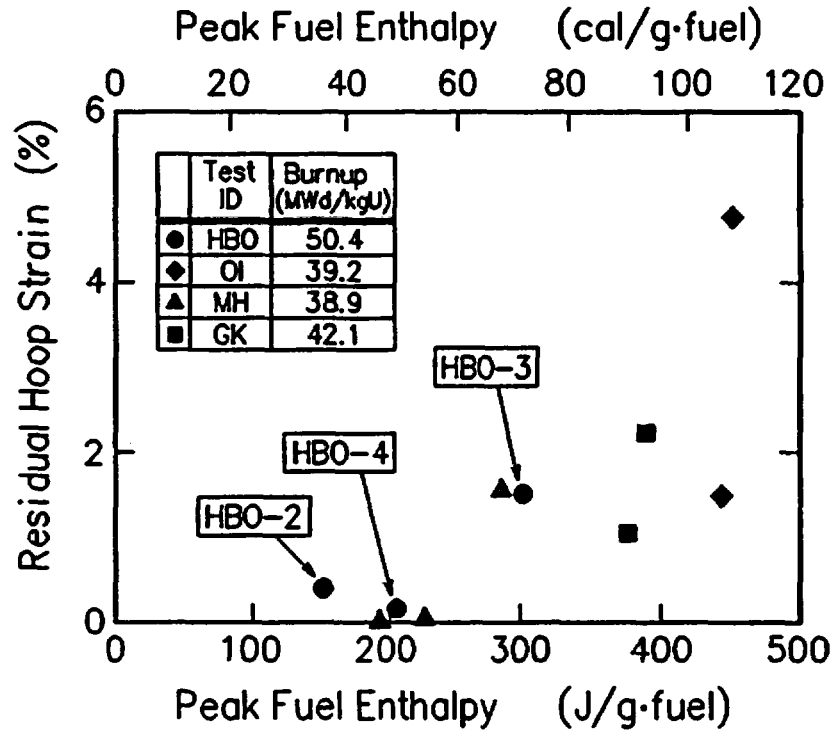

Fig. 10 Residual hoop stain as a function of peak fuel enthalpy

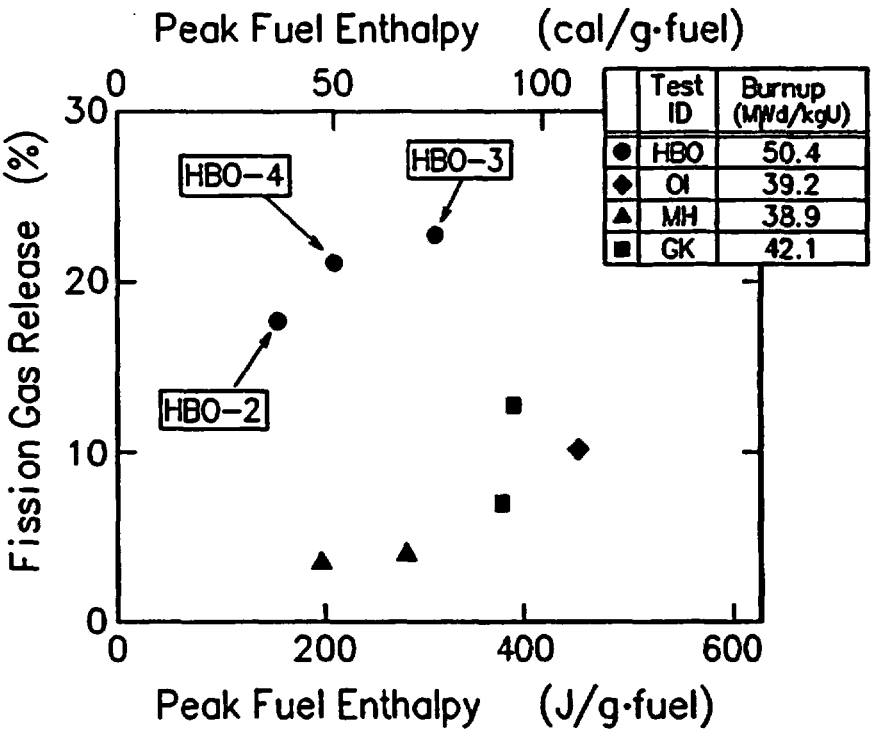

Fig. 11 Fission gas release during the pulse-irradiation as a function of the peak fuel enthalpy

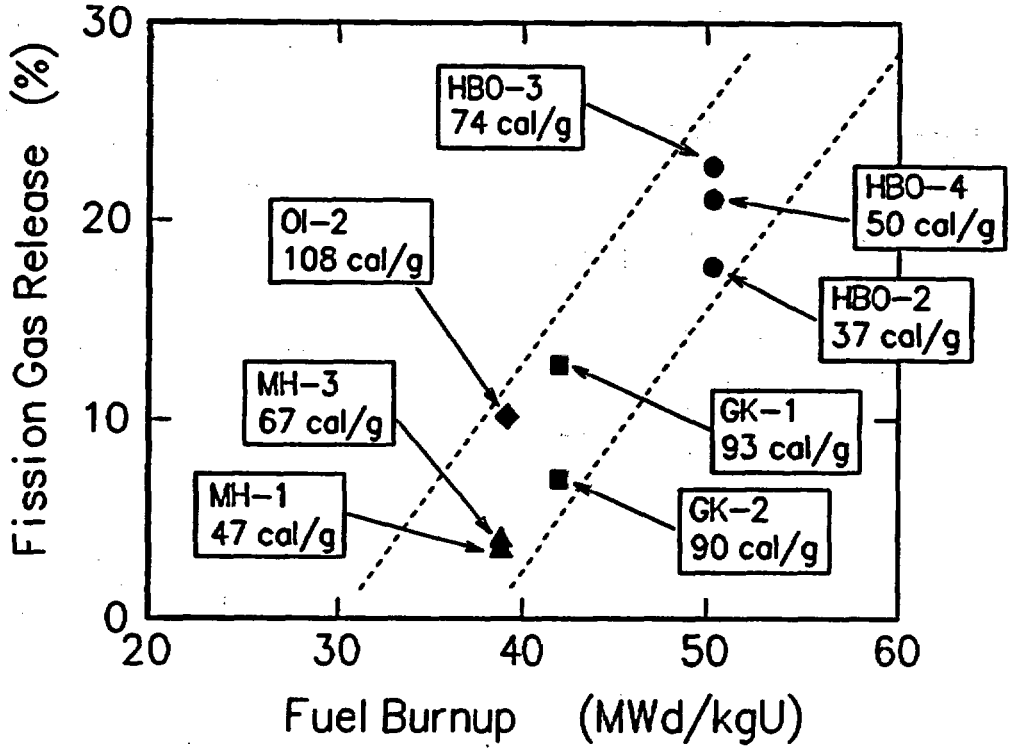

Fig. 12 Fission gas release as a function of fuel burnup

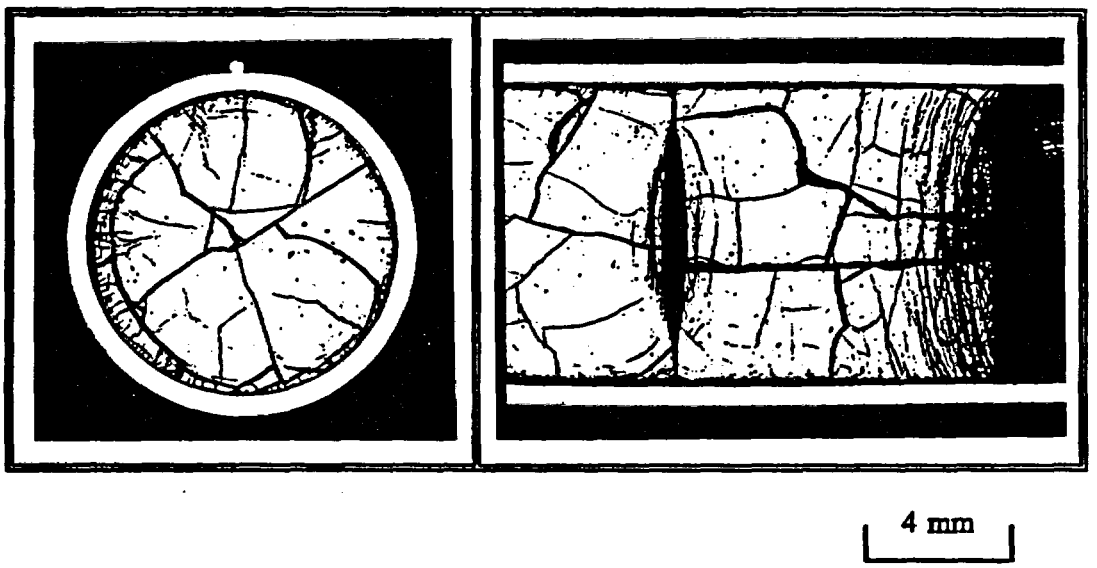

Fig. 13 Metallographies showing horizontal and vertical cross-sections of the post-test HBO-3 fuel

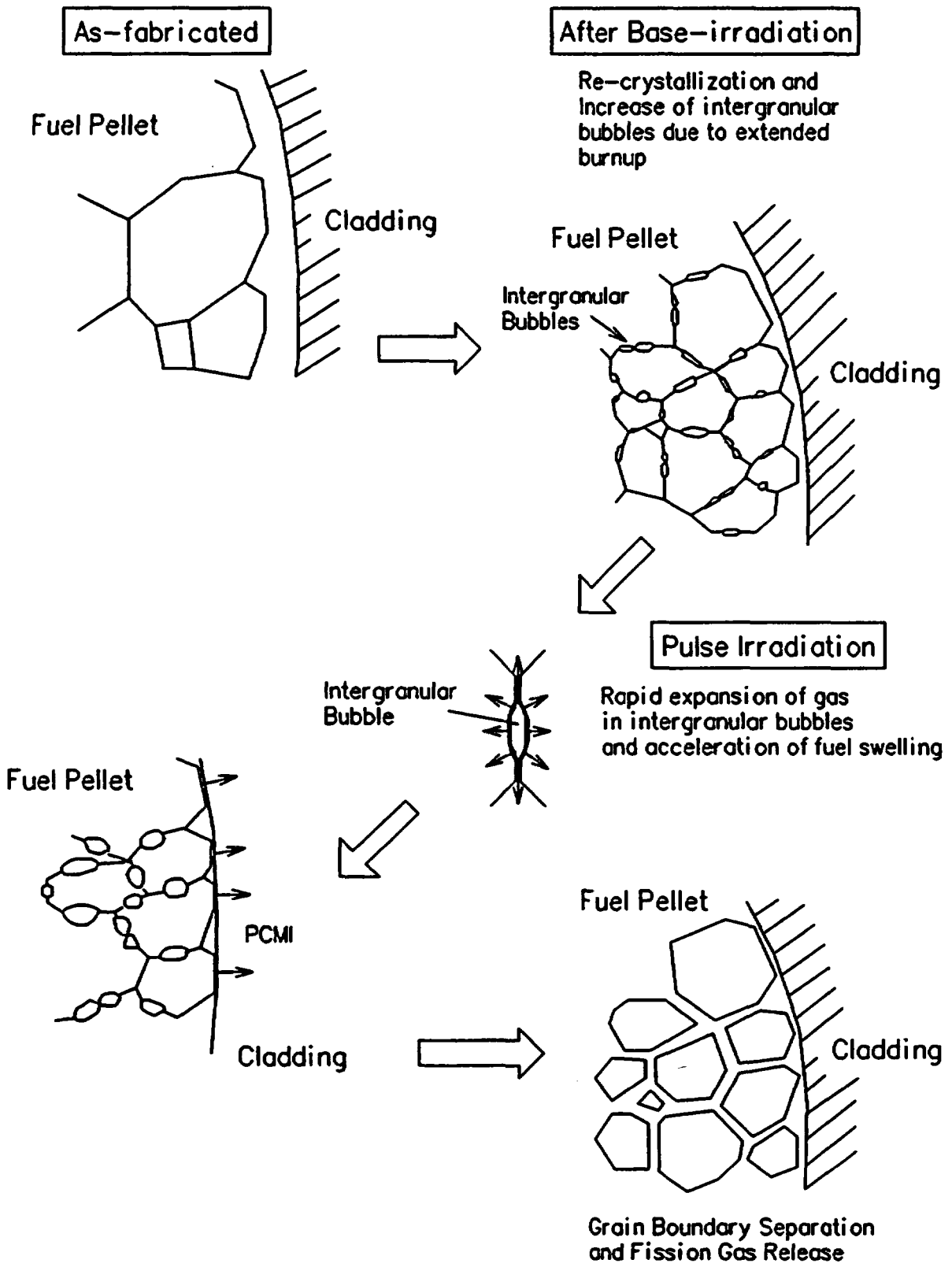

Fig. 14 Postulated grain boundary separation resulting in pellet swelling, fission gas release and fuel fragmentation

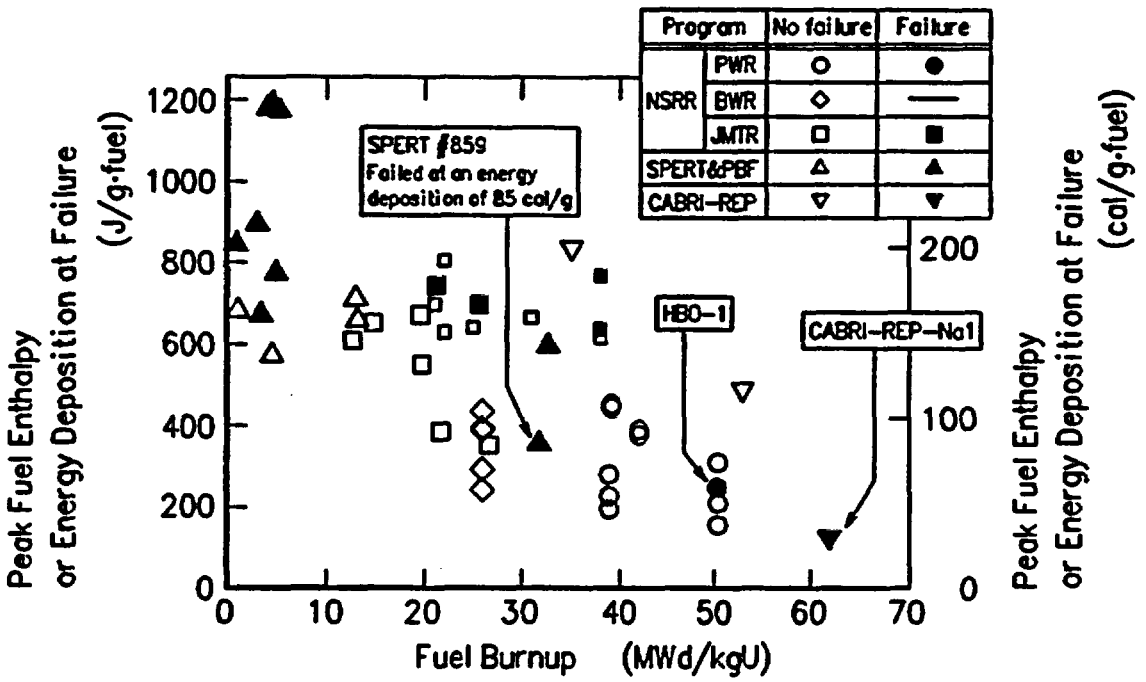

Fig. 15 Fuel burnup and peak enthalpy in irradiation fuel experiments

RECENT VIEW TO THE RESULTS OF PULSE TESTS IN THE IGR REACTOR WITH HIGH BURN-UP FUEL

V. Asmolov, L. Yegorova
Nuclear Safety Institute
Russian Research Centre "Kurchatov Institute"
Moscow, Russia

Within the time period of 1990-1992, the specialists of the Russian Research Centre "Kurchatov Institute," in cooperation with a number of research institutes of the former USSR, prepared for and carried out an experimental program to study the behavior of fuel elements under reactivity-initiated-accident (RIA) conditions with fresh fuel and with irradiated fuel from commercial Russian reactors of the VVER type having average burnups of 48 MWd/kgU. Testing of 43 fuel elements (13 fuel elements with high burn-up fuel, 10 fuel elements with preirradiated cladding and fresh fuel, and 20 non-irradiated fuel elements) was carried out in the IGR pulse reactor with a half width of the reactor power pulse of about 0.7 sec. Tests were conducted in capsules with no coolant flow and with standard initial conditions in the capsule of 20°C and 0.2 MPa. Two types of coolant were used: water and air.

One purpose of the test program was to determine the thresholds and mechanisms of fuel rod failure under RIA conditions for VVER fuel rods over their entire exposure range, from zero to high burn-up. These failure thresholds are often used in safety analyses. The tests and analyses were designed to reveal the influence on fuel rod failure of (a) the mechanical properties of the cladding, (b) the pellet-to-cladding gap, (c) fuel burn-up, (d) fuel-to-coolant heat transfer, and other parameters. The resulting data base can also be used for validation of computer codes used for analyzing fuel rod behavior.

Three types of test specimens were used in the tests, and diagrams of these specimens are shown in Fig. 1. "Type-C" specimens were re-fabricated from commercial fuel rods of the VVER-1000 type that had been subjected to many power cycles of operation in the Novovoronezh Nuclear Power Plant (NV NPP).

"Type-D" specimens were fabricated from the same commercial fuel rods used above, but the high burn-up oxide fuel was removed from the cladding and was replaced with fresh oxide fuel pellets. "Type-D" specimens thus provided a means of separating the effects of the cladding and the oxide fuel pellets and were used to examine cladding effects only.

"Type-E" specimens were manufactured from fresh cladding and fresh oxide fuel pellets according to original specifications of the other VVER-1000 fuel rods. These specimens were used to

examine fuel rod behavior at zero burn-up for comparison with the high burn-up results. Initial characteristics of all three types of specimens are given in Fig. 2.

Tests were performed in the Impulse Graphite Reactor in Semipalatinsk, Kazakstan. A photograph of this test reactor is shown in Fig. 3. The test capsule, which could be filled with either water or air, is shown in Fig. 4. Two test rods could be tested simultaneously in this capsule, but no instrumentation penetrations through the capsule were permitted for safety reasons. Dimensions in the figure are given in millimeters.

A series of specimens were tested with increasingly energetic power pulses to determine the threshold for cladding failure. Figure 5 shows several of the reactor power pulses used in these tests. Pulse width at half maximum varied from a little over 0.5 sec to almost 0.9 sec as the height of the pulse was varied, with a typical value around 0.7 sec.

Results for the 13 irradiated specimens (Type-C) and the 10 specimens with fresh oxide fuel and irradiated cladding (Type-D) are shown in Fig. 6. This figure shows the local energy deposited in each of the test rods in calories per gram of fuel. Because of the large pulse width, the energy depositions are not adiabatic, and local fuel enthalpies will be lower. For some of the air-cooled specimens, it is seen that fragmentation occurred at the highest energies.

The main test results for the eight high burn-up fuel specimens (Type-C) are shown in Fig. 7. This plot shows the radially averaged fuel enthalpy at the elevation of peak local power (peak fuel enthalpy) in calories per gram of fuel. These values are obtained by correcting the local deposited energy values for heat transfer to the water to get the amount of energy retained in the fuel rod. It can be seen from this figure that the threshold for cladding failure is about 140 cal/g.

Figure 8 shows a photograph of the "Type-C" specimen that failed at 151 cal/g. The large ballooning strain that is evident and the high enthalpy of this failure exhibit the same ductile rupture characteristics of rod failure under loss-of-coolant conditions. Figure 9 shows a cross section of this rod at different magnifications.

Figure 10 summarizes the failure thresholds for the various types of specimens and test conditions investigated. Two of the IGR test data for "Type-C" specimens in water are shown in Fig. 11. These two data points are for the lowest failure enthalpy and the highest non-failure enthalpy found in these tests. Figure 11 is the typical enthalpy-vs-burnup plot with data from other test programs as well. The dashed lines connect the points of lowest failure enthalpy and the points of highest non-failure enthalpy from a larger population of data, all of which are not shown in this figure.

Results from the RIA tests with VVER-1000 fuel rods are thus different from results found by other investigators with PWR and BWR fuel rods. These differences may be due to differences in fuel rod design and to differences in test conditions. Figure 12 compares some of the fuel rod design differences between VVER and PWR fuel rods that may affect the results, and Fig. 13 compares different test conditions of the major RIA test programs. The exact cause of the different results is not known at this time.

The following conclusions have been reached:

- High temperature bursting of the cladding is the mode of failure for VVER fuel rods at high burn-up.
- Failure enthalpies for VVER rods are as follows:

  140 cal/g for high burn-up rods cooled by water;

  195 cal/g for fresh rods cooled by water;

  <85 cal/g for fuel rods of all types cooled by gas.
- There were no qualitative differences in the mode of failure for the three types of fuel rods tested.
- Experimental values of failure enthalpy for VVER high burn-up fuel is higher than for PWR fuel rods.
- Detailed analysis of SPERT, PBF, NSRR, CABRI, and IGR data should be done using computer codes and recent experimental results to reach final conclusions and make recommendations for failure criteria under RIA conditions.

Additional work is planned in this program to investigate the relationship between failure threshold characteristics (fuel enthalpy, burst temperature and pressure, etc.) and several fuel rod parameters (e.g., initial pellet-to-cladding gap, ZrO_2 thickness, H_2 content in cladding, coolant conditions, pressure drop across cladding, and pulse width). Additional out-of-pile and in-pile testing may be performed, and analyses comparing results from other RIA test programs are planned.

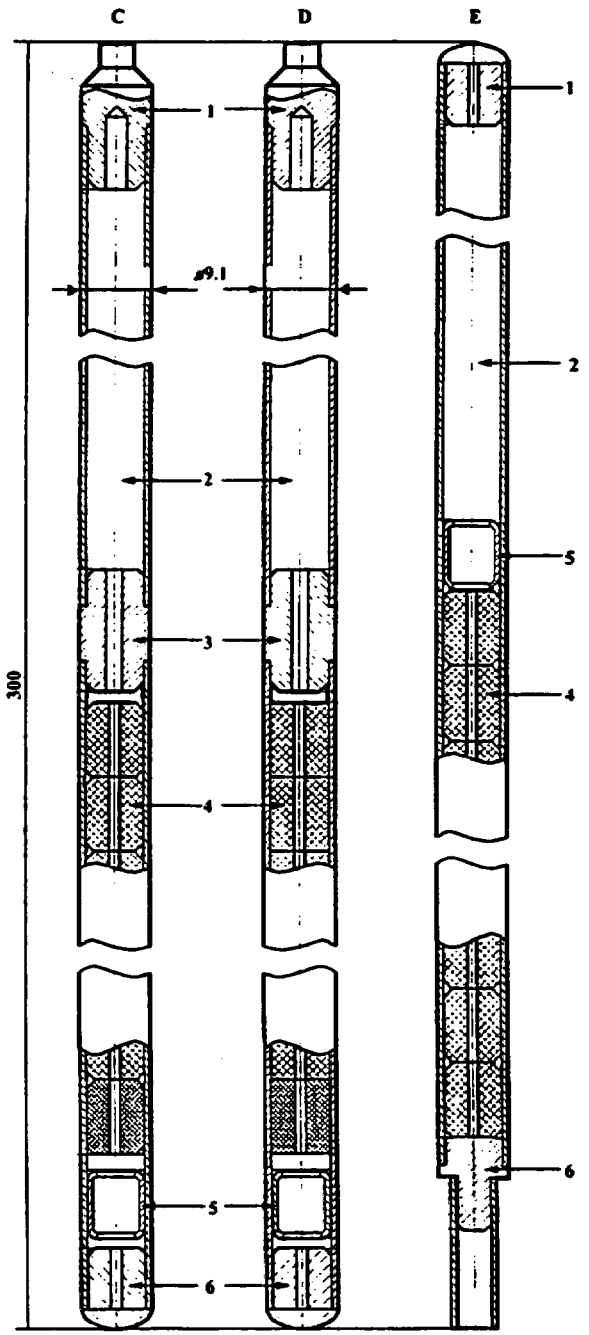

1. Upper cap; 2. Plenum; 3. Connector; 4. Fuel pellet; 5. Coil spring; 6. Low cap.

Fig. 1. Types of fuel specimens tested in the IGR test reactor.

Parameter	Fuel rod type		
	C	D	E
1. *Fuel*			
1.1 Initial composition before power operation	UO_2	UO_2	UO_2
1.2 Initial enrichment, %	3.58	4.46-4.47	4.46-4.47
1.3 Burn-up, MWd/kgU	41.0-49.7	0	0
1.4 Outer pellet diameter, mm	7.55-7.60	7.56	7.56-7.69
1.5 Density, g/cm^3	10.31-10.32	10.50-10.60	10.50-10.60
1.6 Fuel stack length, mm	148-167	141-143	142-144
2. *Cladding*			
2.1 Initial composition before power operation	Zr-1%Nb	Zr-1%Nb	Zr-1%Nb
2.2 Outer cladding diameter, mm	9.13	9.11	9.15
2.3 Inner cladding diameter, mm	not measured	not measured	7.75
2.4 Oxide thickness, um	5-6	5-6	3-5
3. *Fuel rod*			
3.1 Fuel rod length, mm	300	300	300
3.2 Initial fill gas pressure, MPa	2	2	2
3.3 Gas composition	He	He	He
3.4 Free gas volume, cm^3	6.11	5.80	6.59
3.5 Fuel-cladding gap, mm	0.03-0.15	not measured	0.06-0.19
3.6 Number of fuel rods	13	10	20

Fig. 2. Initial characteristics of fuel rods tested in the IGR test reactor.

IGR Appearance

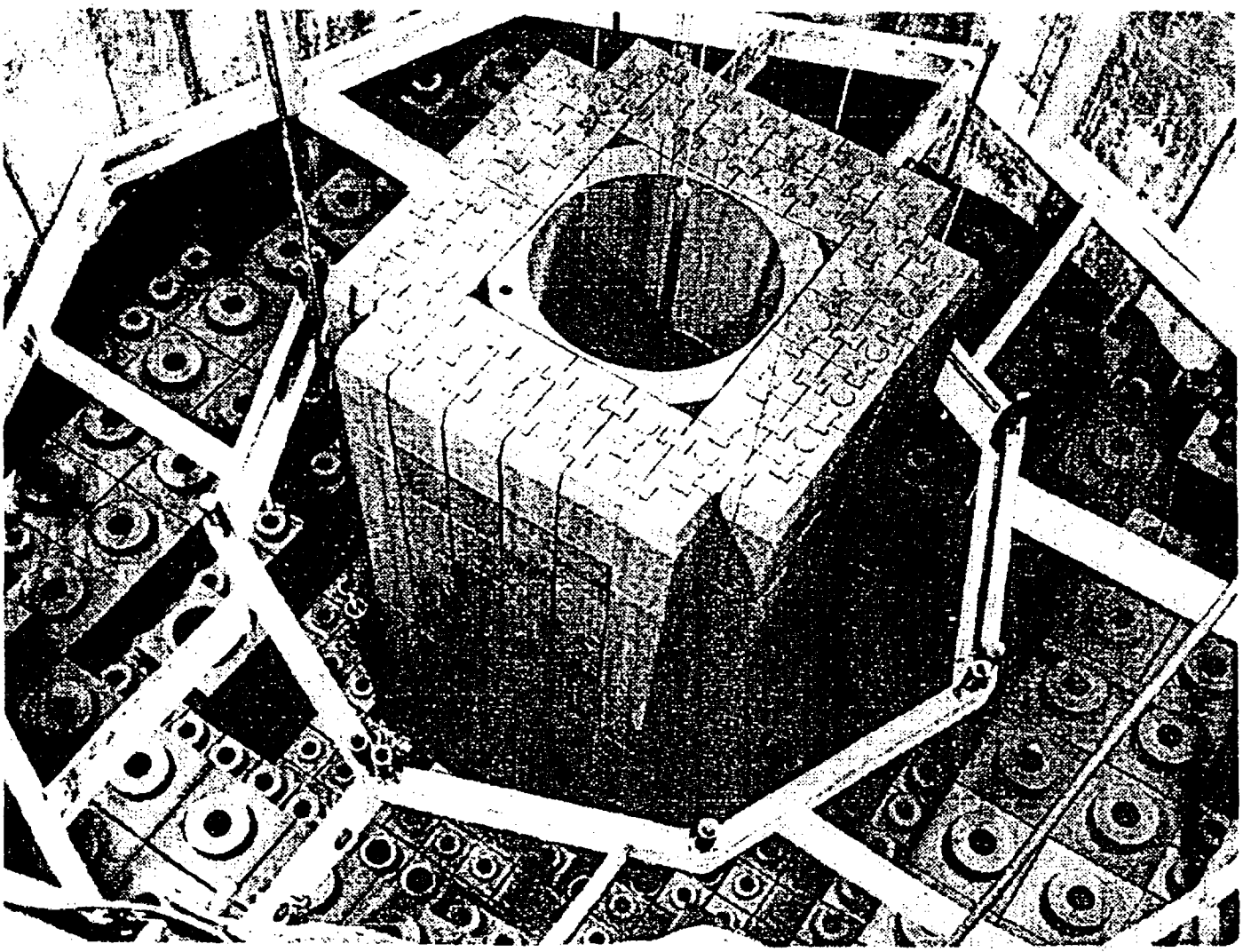

Photographs were prepared by IAE NNC (Semipalatinsk, Kazakstan)

Fig. 3. Photograph of the Impulse Graphite Reactor (IGR) in Semipalatinsk, Kazakstan.

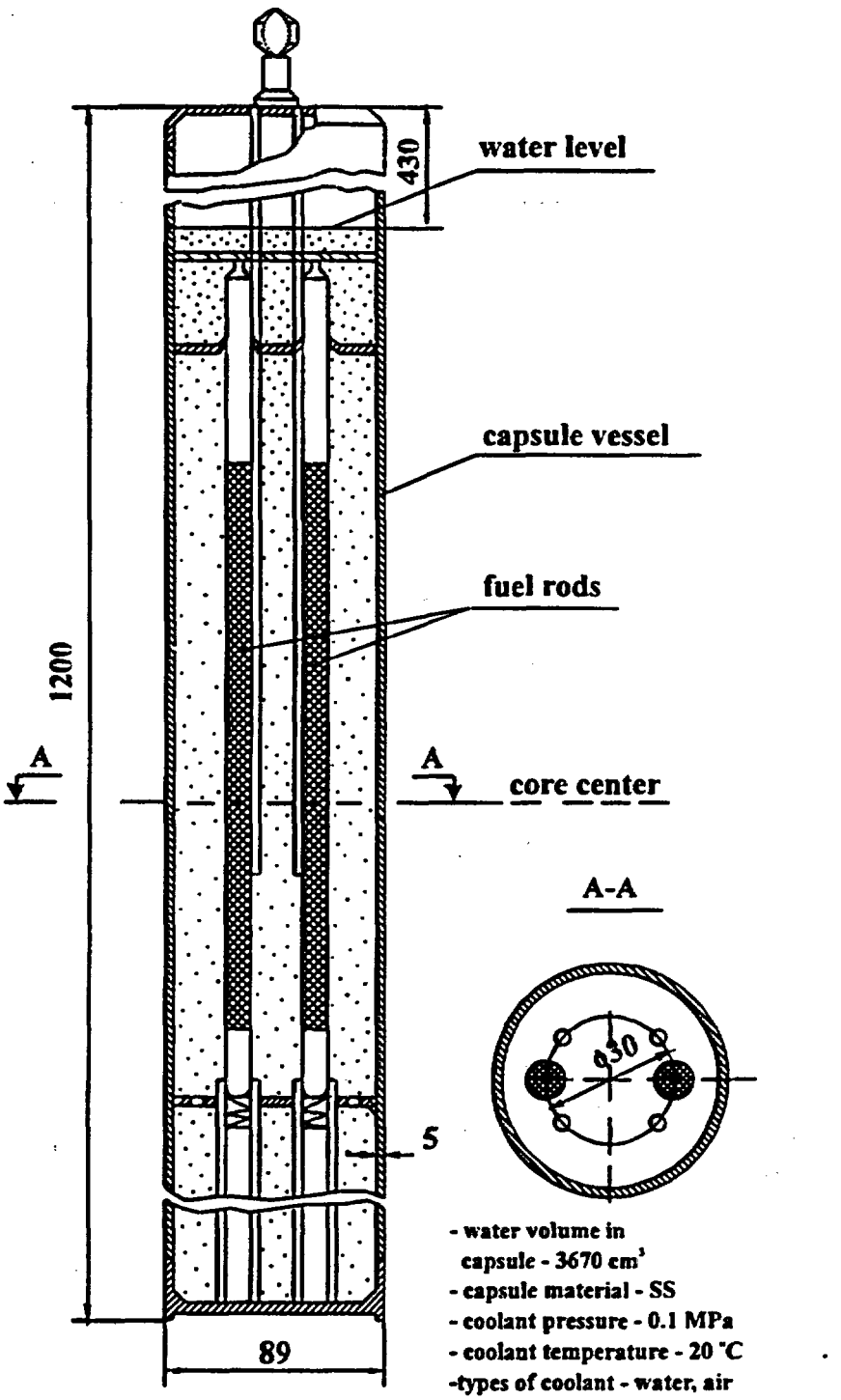

Fig. 4. Test capsule used for RIA tests in the IGR test reactor.

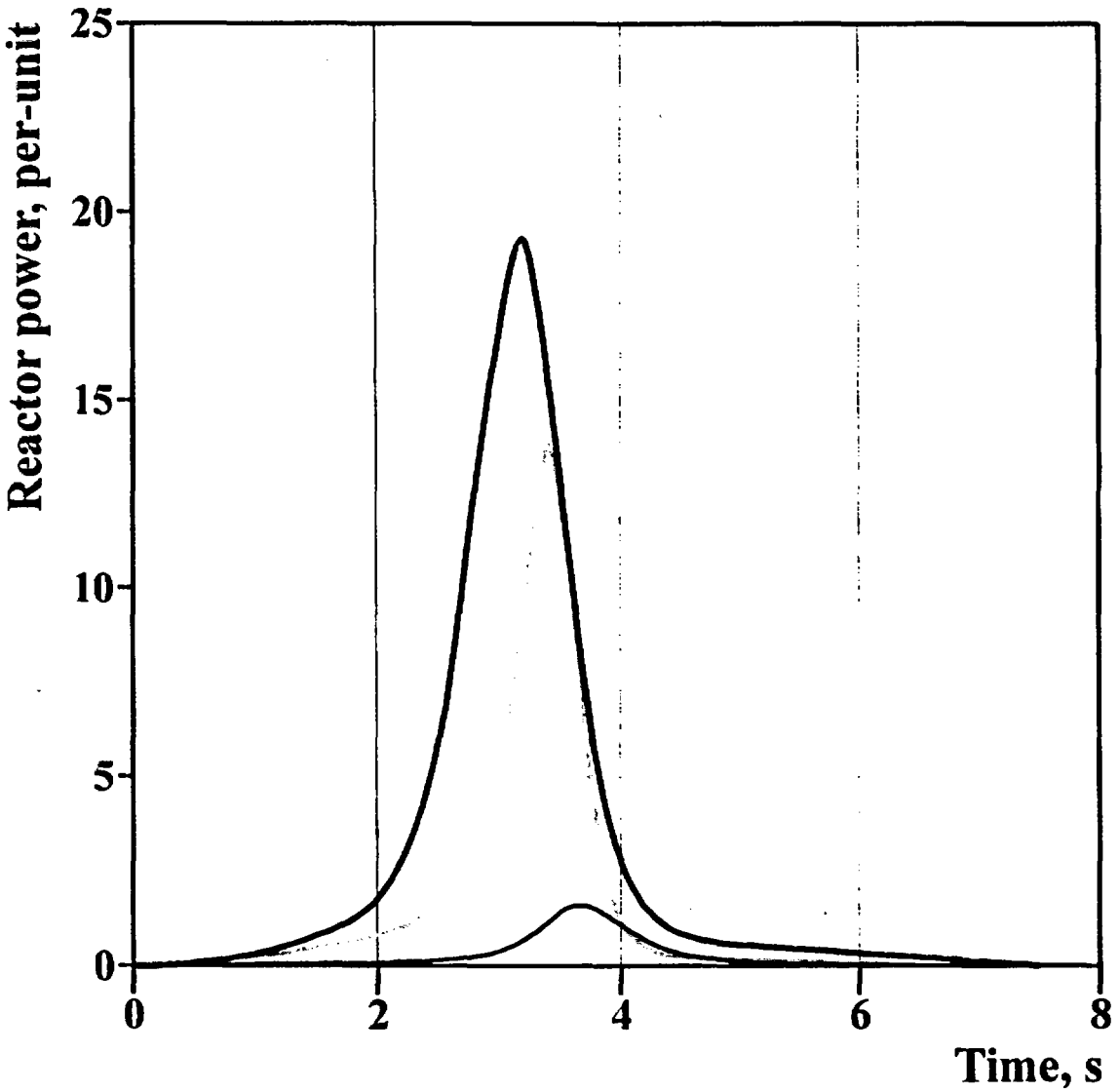

Fig. 5. IGR test reactor power shapes during high burn-up fuel rod tests.

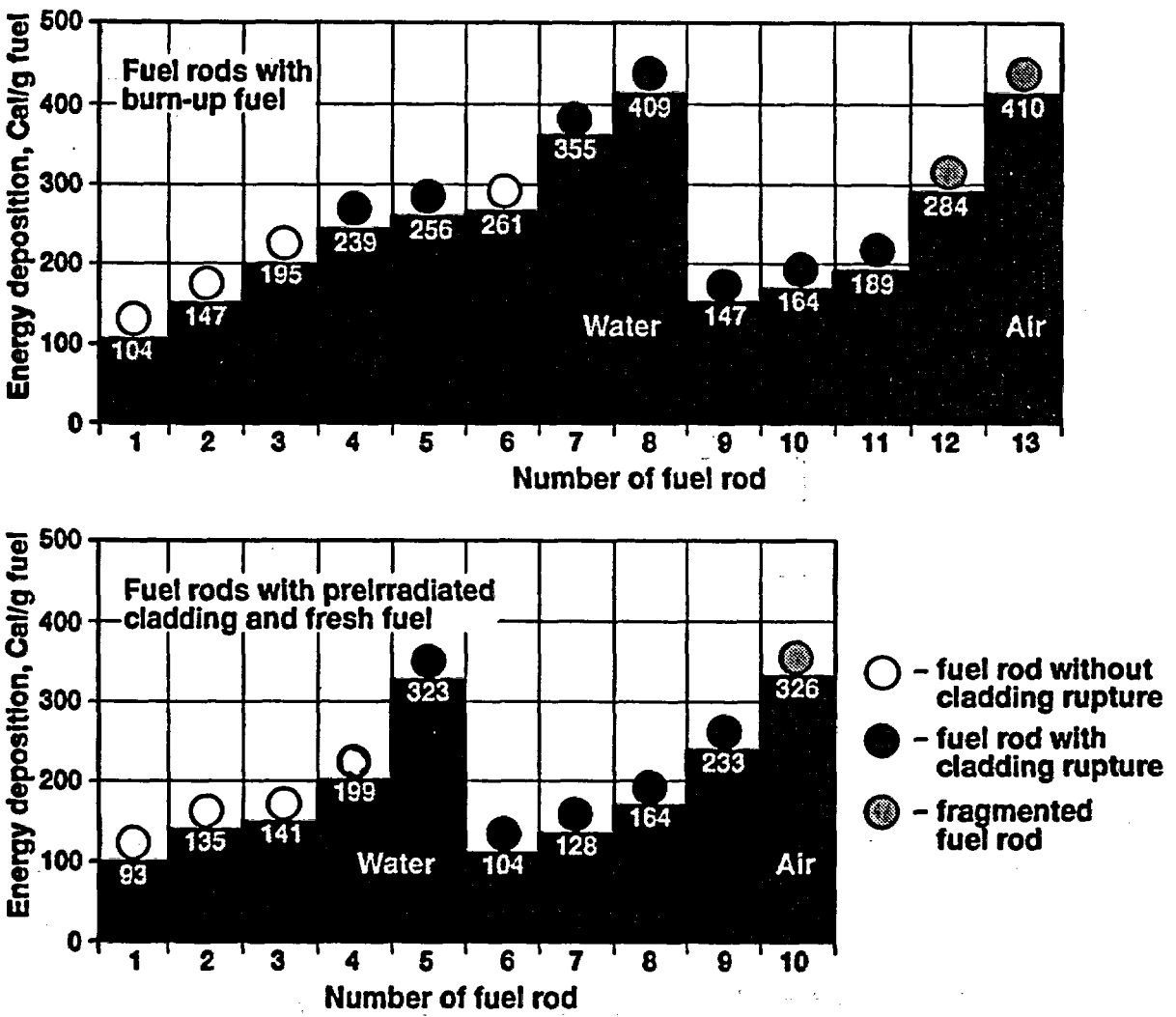

Fig. 6. Results of tests with high burn-up fuel rod and cladding specimens under RIA conditions.

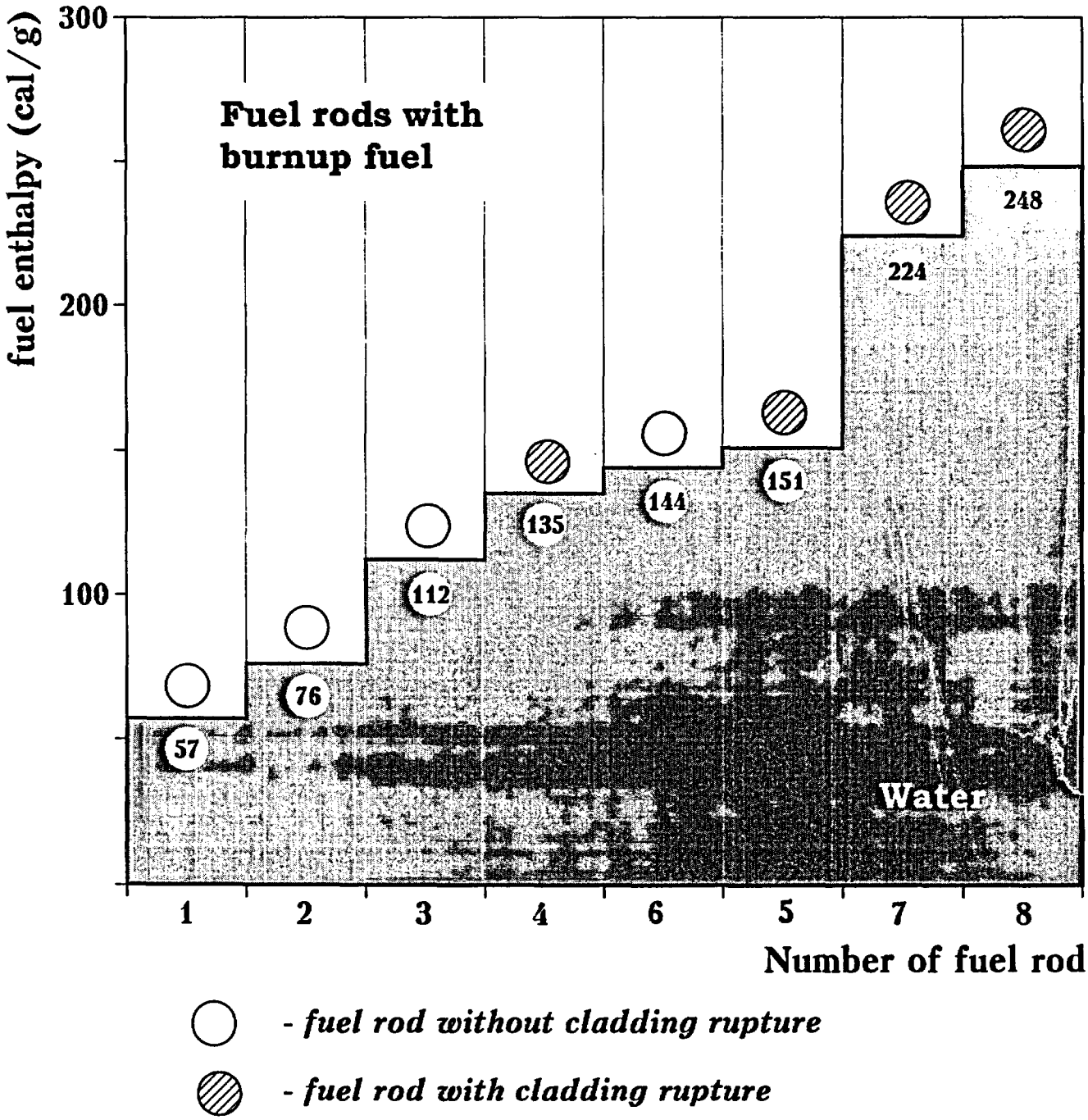

Fig. 7. Radially averaged fuel enthalpy at elevation of peak power for high burn-up specimens tested in water.

Visual View of H7T Fuel Rod Fragments (Preirradiated Fuel Rod)

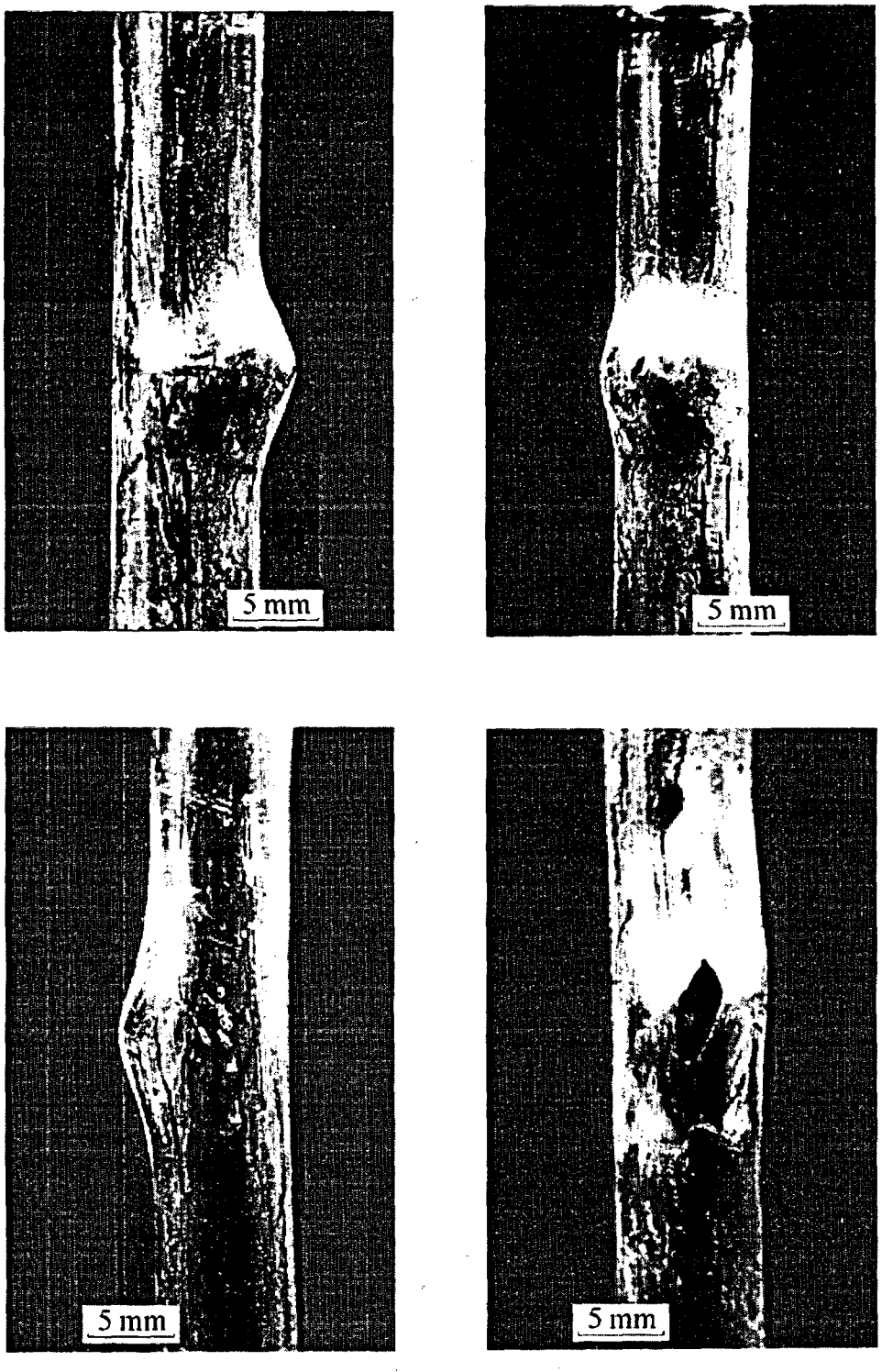

Fig. 8. Photograph of "Type-C" test specimen that failed at 151 cal/g showing large strain (ballooning) at failure location.

Macro and Microphotographs of Cladding Cross-Section #2 for H7T Fuel Rod

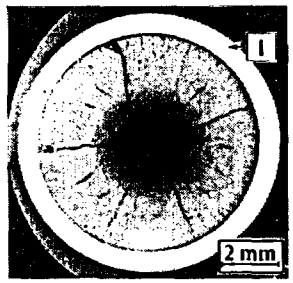

Position 1

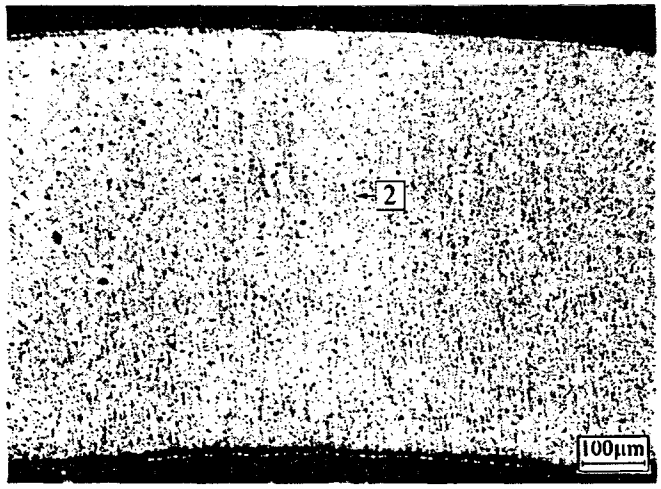

Position 2

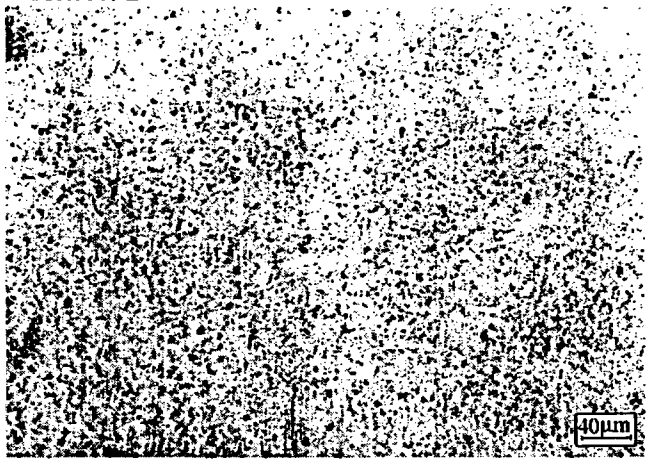

Photographs were prepared by RIAR (Dimitrovgrad, Russia)

Fig. 9. Macro and micro-photographs of cross section of "Type-C" fuel specimen that failed at 151 cal/g.

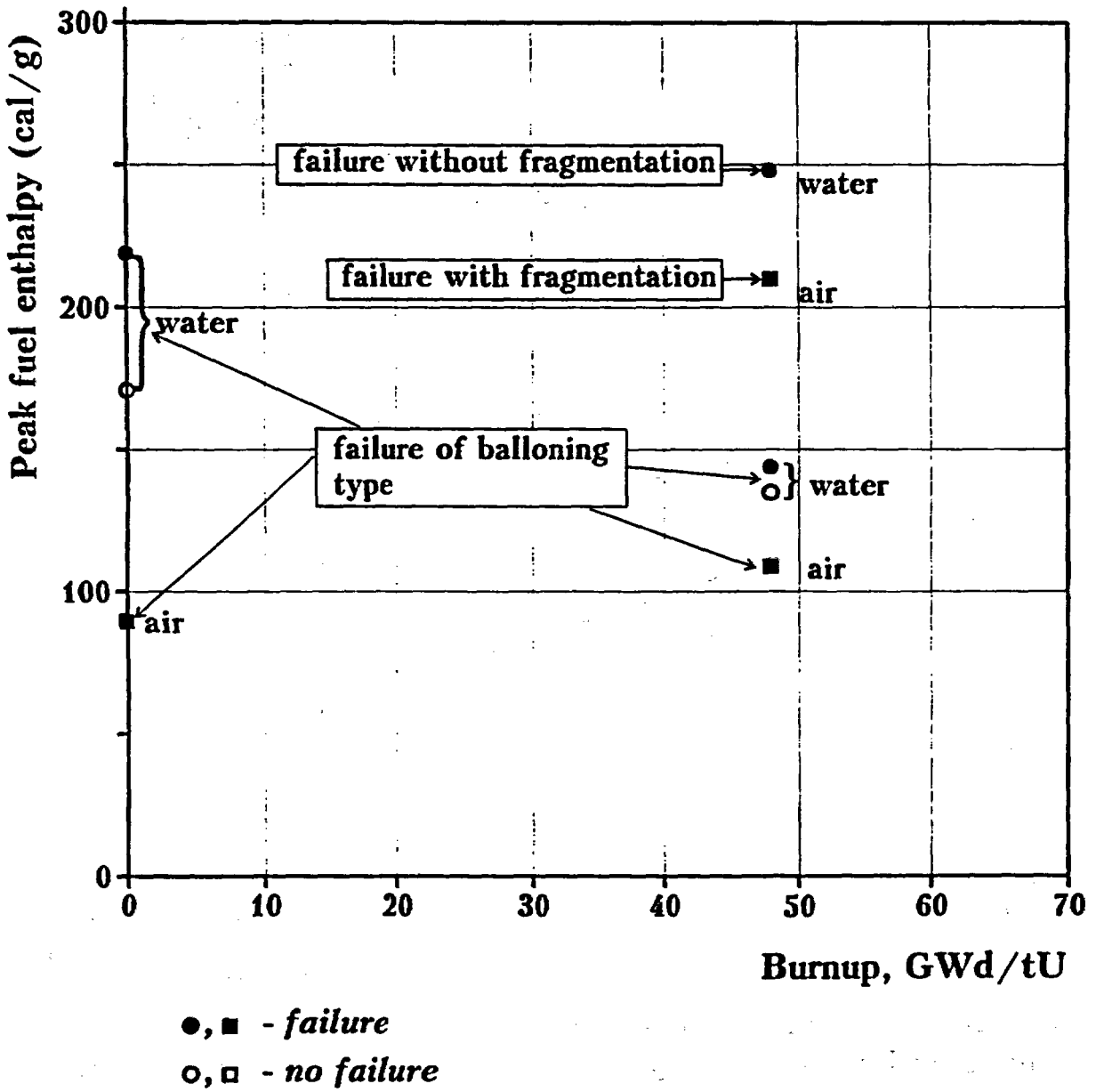

Fig. 10. Summary of failure thresholds for various types of specimens tested in IGR under RIA conditions.

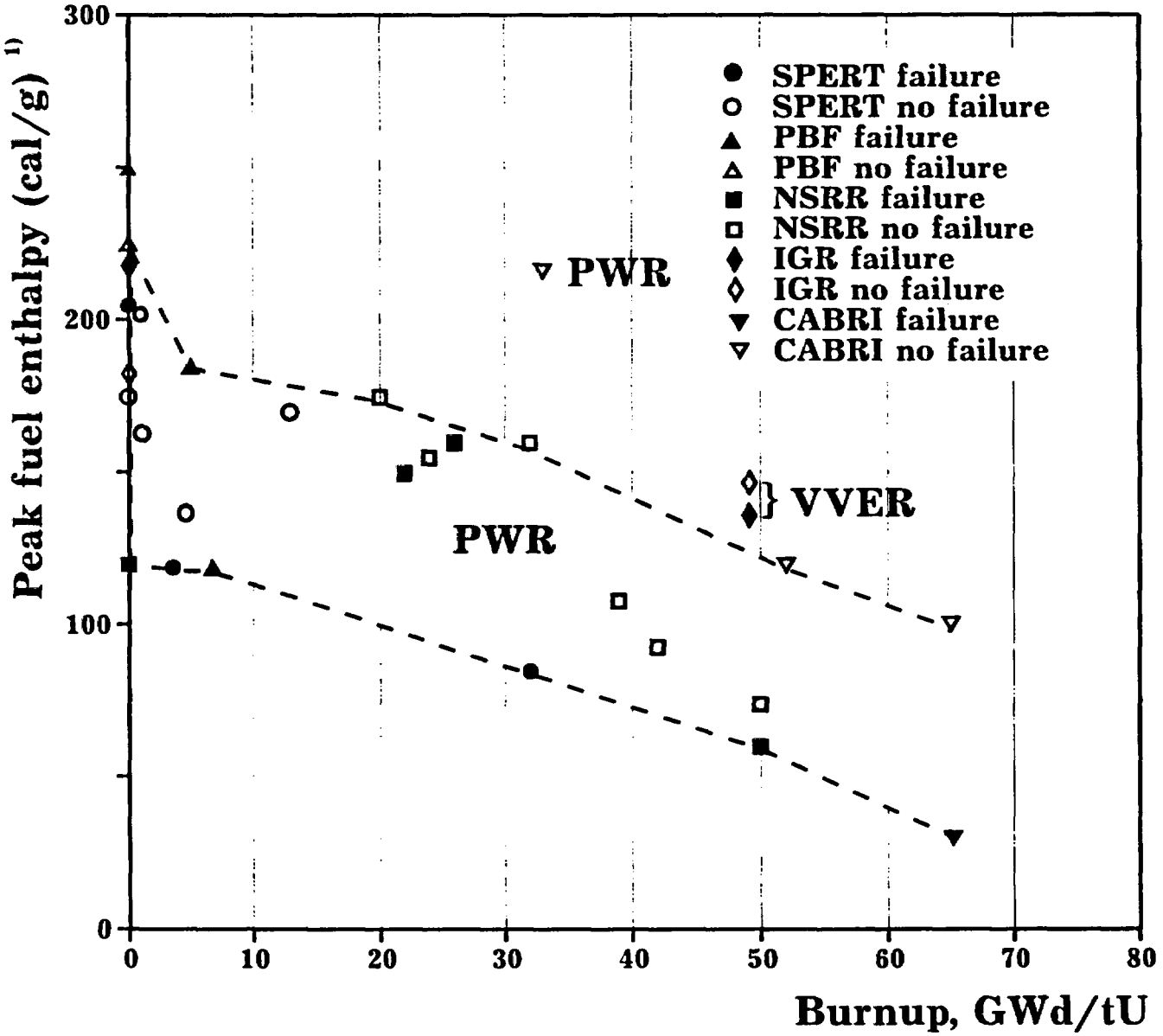

Procedure to obtain plotted data:

- **for each level of burnup was selected the lowest failure enthalpy and the highest no failure enthalpy from the test group**

[1)] ***Failure enthalpy was used for cases which this value was known***

Fig. 11. Typical enthalpy-vs-burnup plot showing selected results from the IGR tests and other RIA test programs.

Burnup ~ 50 GWd/tU

- Type of the pellet
  - PWR → 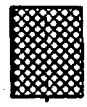
  - VVER → 
- Material of the cladding
  - PWR → Zircaloy
  - VVER → Zr and 1% Nb
- Pellet-cladding gap
  - PWR → 0.01-0.02 mm (NSRR)
  - VVER → 0.03 mm (min)
- ZrO_2 thickness on the cladding
  - PWR → 35-40 μm (NSRR, CABRI)
  - VVER → 5 μm

Fig. 12. Comparison of design differences between VVER and PWR fuel rods.

1. Pressure drop on the cladding	SPERT	0 MPa
	PBF	3.9 - 6.4 MPa
	NSRR	0 - 3.1 MPa
	CABRI	0 - 0.2 MPa
	IGR	1.5 - 1.9 MPa
2. Coolant conditions	SPERT	cold start
	PBF	hot start *(rod inside shroud)*
	NSRR	cold start
	CABRI	specific hot start *
	IGR	cold start
3. Condition of preirradiation	SPERT	research reactor
	PBF	research reactor
	NSRR	research reactor, commercial power plants
	CABRI	research reactor, commercial power plants
	IGR	commercial power plant
4. Half pulse width	SPERT	22 ms
	PBF	18 ms
	NSRR	5 ms
	CABRI	10 ms
	IGR	700 ms

* *300°C; 0.2 MPa; sodium*

Fig. 13. Comparison of different test conditions of the major RIA test programs.

"HIGH BURNUP EFFECTS IN WWER FUEL RODS"

V. Smirnov, A. Smirnov
presented by V. Smirnov

RRC RESEARCH INSTITUTE OF ATOMIC REACTORS

Dimitrovqrad, Russia

Introduction

Since 1987 at Research Institute of Atomic Reactors the examinations of the WWER spent fuel assemblies is carried out. These investigations are aimed to gain information on WWER spent fuel conditions in order to validate the fuel assemblies use during the 3 and 4 years fuel cycle in the WWER-440 and WWER-1000 units respectively.

At present tim,e the aim is to reach an average fuel burnup of 55 MWd/kgU. According to this aim a new investigation program on the WWER spent fuel examinations is started. The main objectives of this program are to study the high burnup effects and their influence on the WWER fuel properties.

This paper presents the main statistic values of WWER-440 and WWER-1000 reactors fuel assemblies and their fragments parameters. Average burnup of fuel in investigated fuel assemblies was in the range of 13 up to 49.7 MWd/kgU. In this case the number of fuel cycles was from 1 to 4 during operation of fuel assemblies.

Results of Investigations

The post irradiation examination programs of individual fuel assemblies may vary in accordance with the objectives of the examinations, but usually the following investigation methods are used:

* visual inspection of fuel assemblies and their elements;
* shape changing of fuel assemblies and fuel rods;
* defectoscopy;
* distribution of radionuclides;
* macro- and microstructure of FA elements;
* mechanical properties of materials;
* gaseous fission product release.

The results of investigations pointed to a possibility of FA shape change during the operation (Fig. 1).

The FEs elongation caused by the cladding growing and its interaction with the fuel pellets (Fig. 2) has considerable deviations for individual FAs and does not depend on FEs location. The typical curve of fuel rod diameter is shown in Fig. 3.

Dependence of the fuel rod average diameter on burnup is shown in Fig. 3 points to slowing down of the diameter decrease rate at burnup more than 35-45 MWd/kgU.

The oxide film on both FEs outer surface and fuel side is insignificant (Fig. 4). It does not exceed 7-10 μm in the whole range of investigated burnups and lightly depends on position along FEs height. Hydrides inclusions have a lamellar form. Total hydrogen content varies in the range of 30 to 60 ppm. Cladding mechanical properties in the whole range of burnups remain high.

The FEs macrostructure during irradiation changes lightly (Fig. 5). Mainly it resultS in the fuel-cladding gap decrease. The central hole diameter does not change. Fuel pellet grain dimension remains constant (Fig. 6).

At burnup more than 43 MWd/kgU the rim-zone on the pellet surfaces, of about 120 μm thickness that characterized by the enhanced porosity and plutonium content become to be appreciable. This zone has a typical "cauliflower" structure (Fig. 7).

Axial distribution of radionuclides (Fig. 8) is caused by axial irregularity of neutron flow. Spacer grids influence is appreciable in the WWER-1000 FEs. Usage of narrow collimator allows to reveal pellet champfers influence on the axial fission product distribution.

Radial distribution of plutonium (Fig. 9) determined by the mass-spectrometry method points to increase of plutonium concentration towards the pellet periphery.

Gaseous fission product release (Fig. 10) increases with burnup lightly and reaches ~3% at burnup of 50 MWd/kgU. In several FEs the increase of gaseous fission product release up to 5-6% is observed.

Conclusion

The statistical values of the main WWER fuel parameters is obtained.

The obtained values of the fuel assemblies and its component parameters pointed to a possibility of the commercial WWER fuel exploitation up to average burnup of about 50 MWd/kgU.

The possibility of the father WWER fuel average burnup increase is the objective of the current investigation.

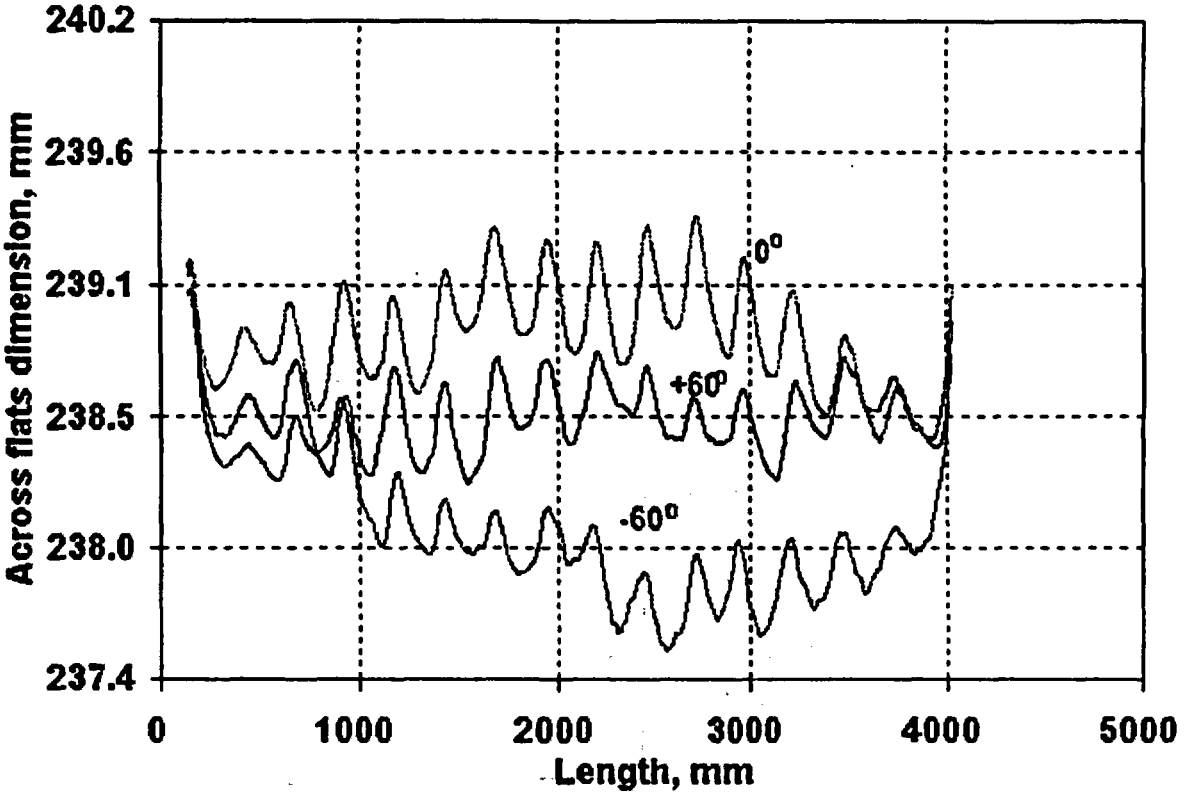

a

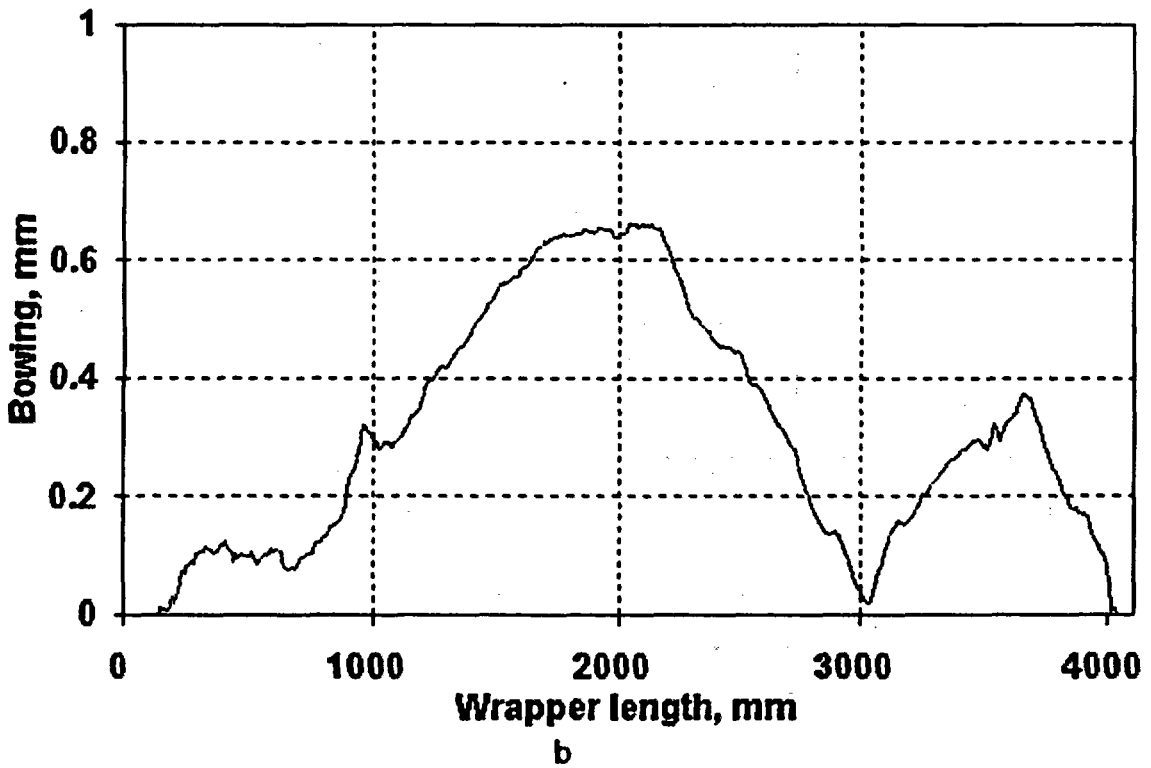

b

Fig 1. WWER-1000 FA form changing
a - across flats dimension, b - FA bowing

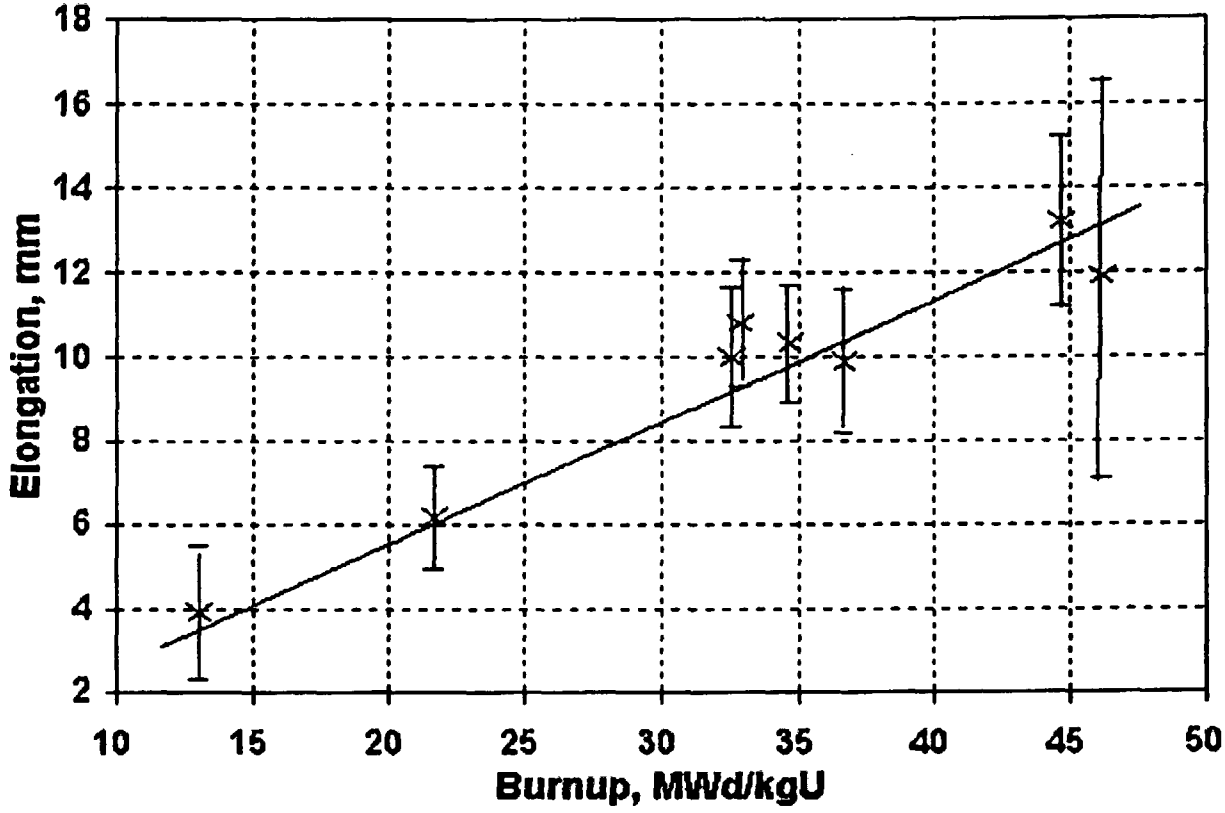

Fig 2. WWER FEs elongation vs burnup

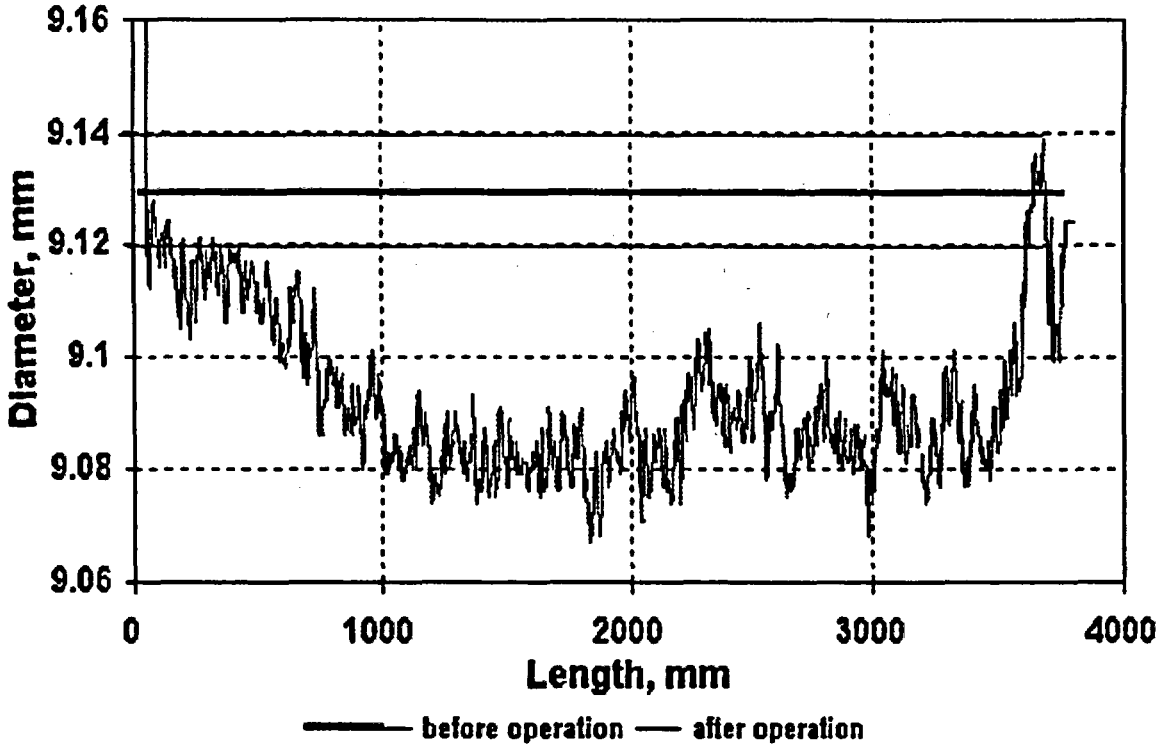

a

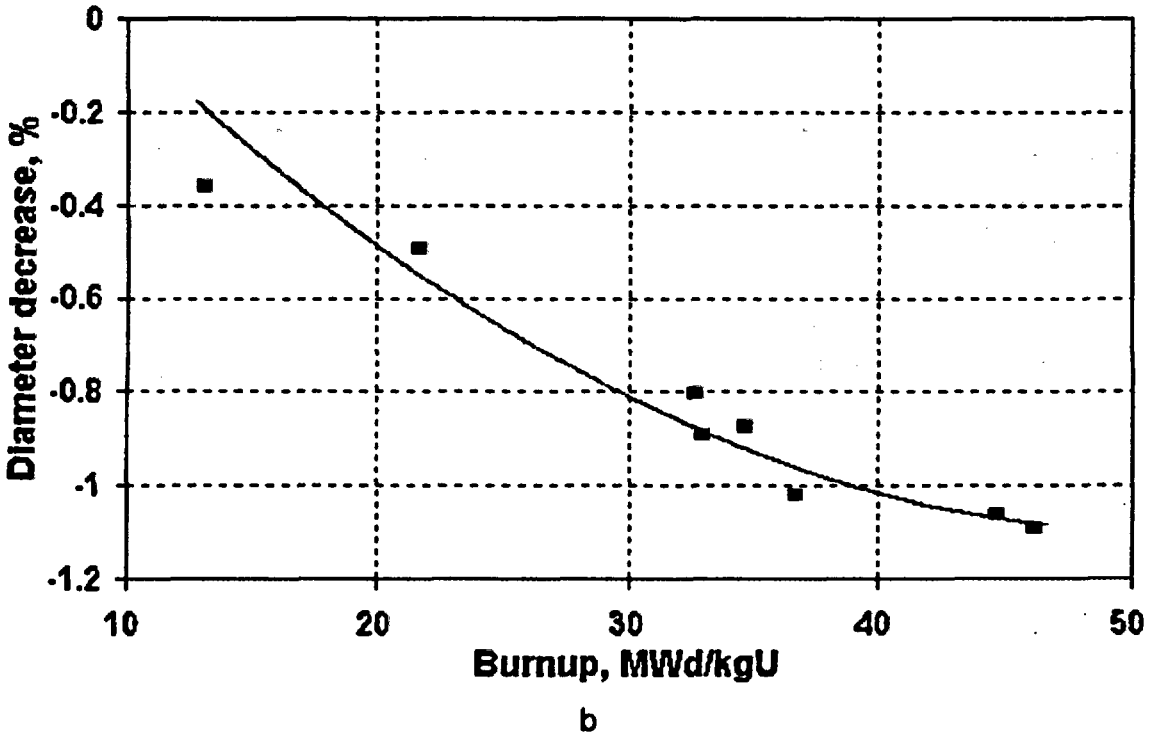

b

Fig 3. FE diameter changing
a - WWER-1000 FE outer diameter longitudinal distribution,
b - diameter dependence on burnup

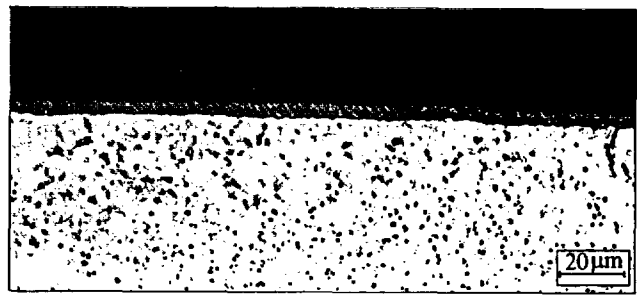

a) Outer cladding surface
B=46.2 MWd/kgU

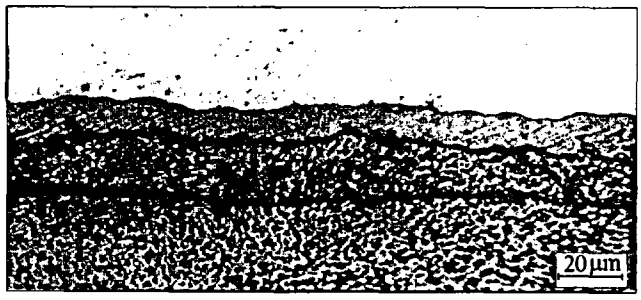

b) Inner cladding surface.
B=46.2 MWd/kgU

c) Inner cladding surface.
B=32.9 MWd/kgU

Fig.4. Oxide films on the WWER fuel rod cladding.

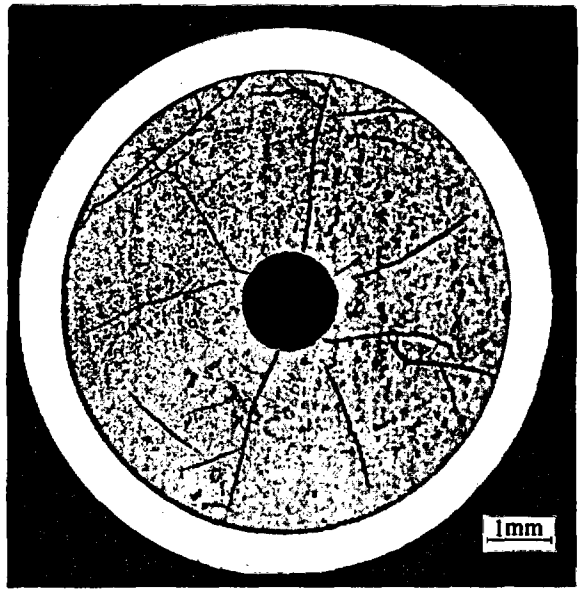

WWER-440
Burnup 49 MWd/kgU

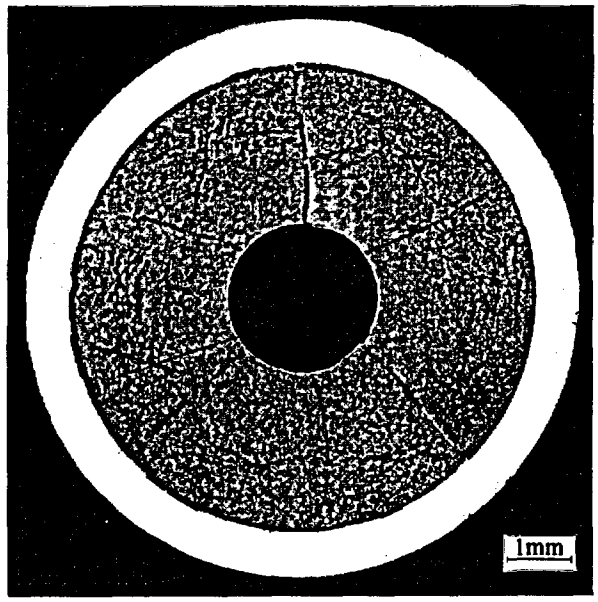

WWER-1000
Burnup 33 MWd/kgU

Fig.5. WWER fuel rod cross-sections.

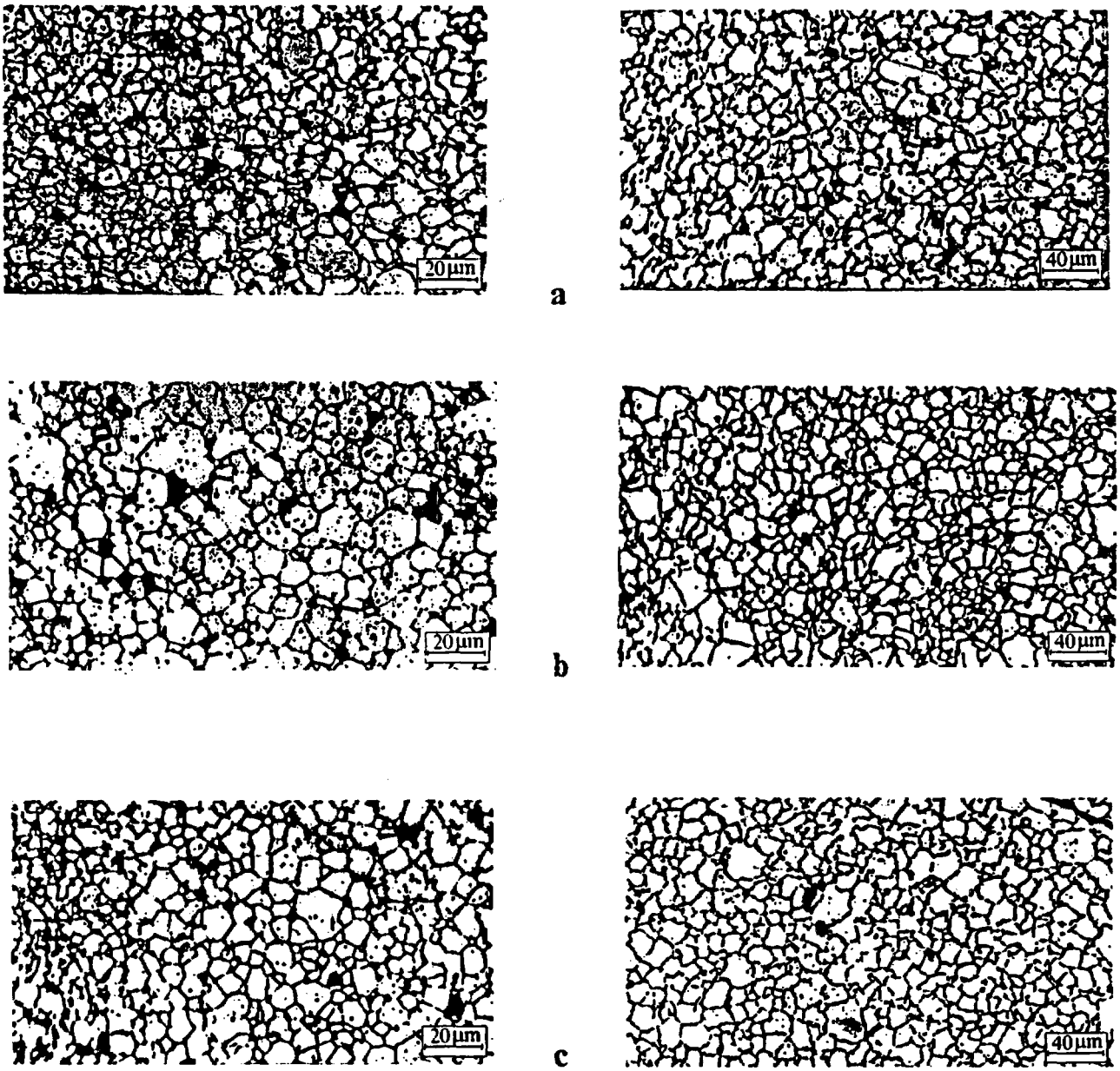

WWER-440
Burnup 54 MWd/kg U

WWER-1000
Burnup 50 MWd/kg U

Fig.6. The microstructure of the spent WWER fuel pellets
a - outer pellet surface; b - center of the pellet;
c - surface of the central hole of the pellet

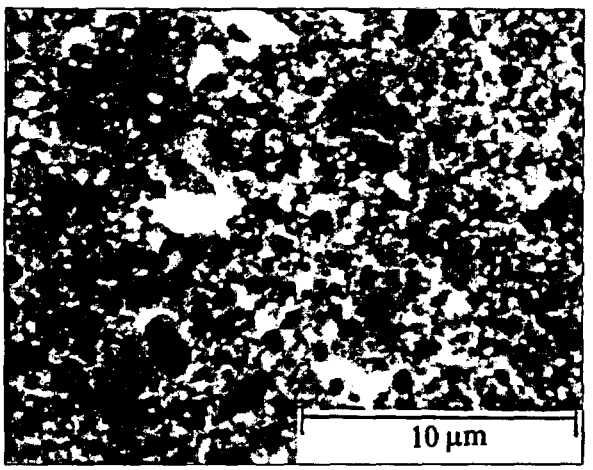

a) R/R_0~0.99

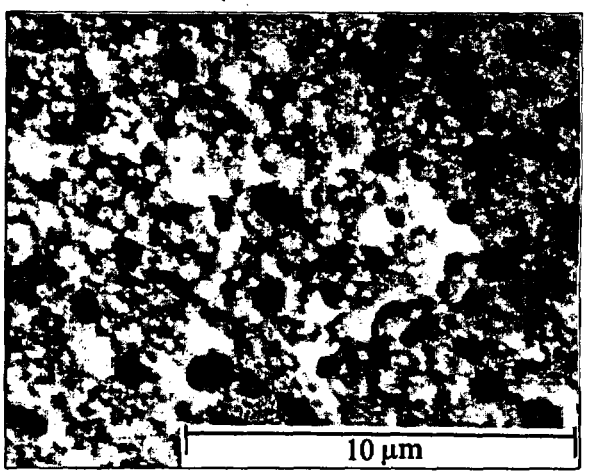

b) R/R_0~0.99

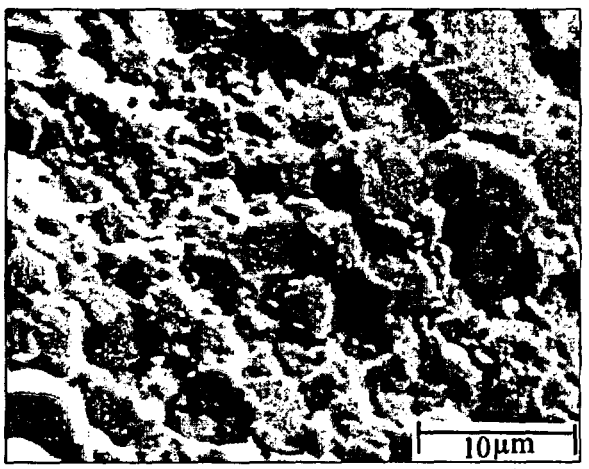

c) R/R_0~0.96

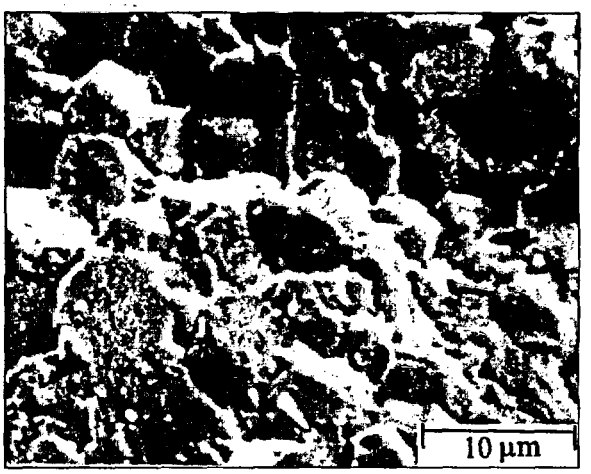

d) R/R_0~0.7

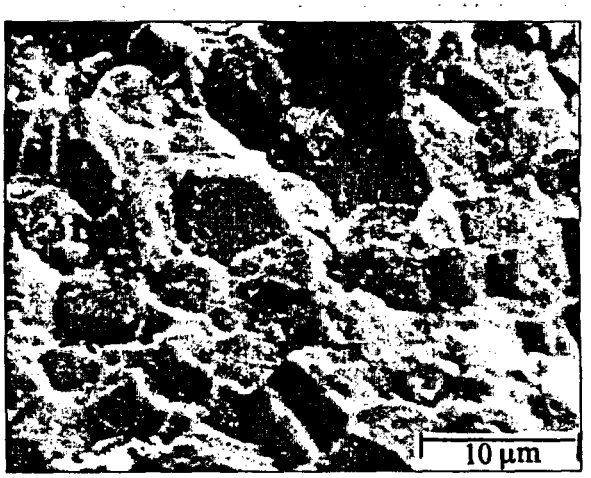

e) R/R_0~0.6

Fig.7. SEM fractography of the WWER-440 fuel pellet of 63.8 MWd/kgU burnup.

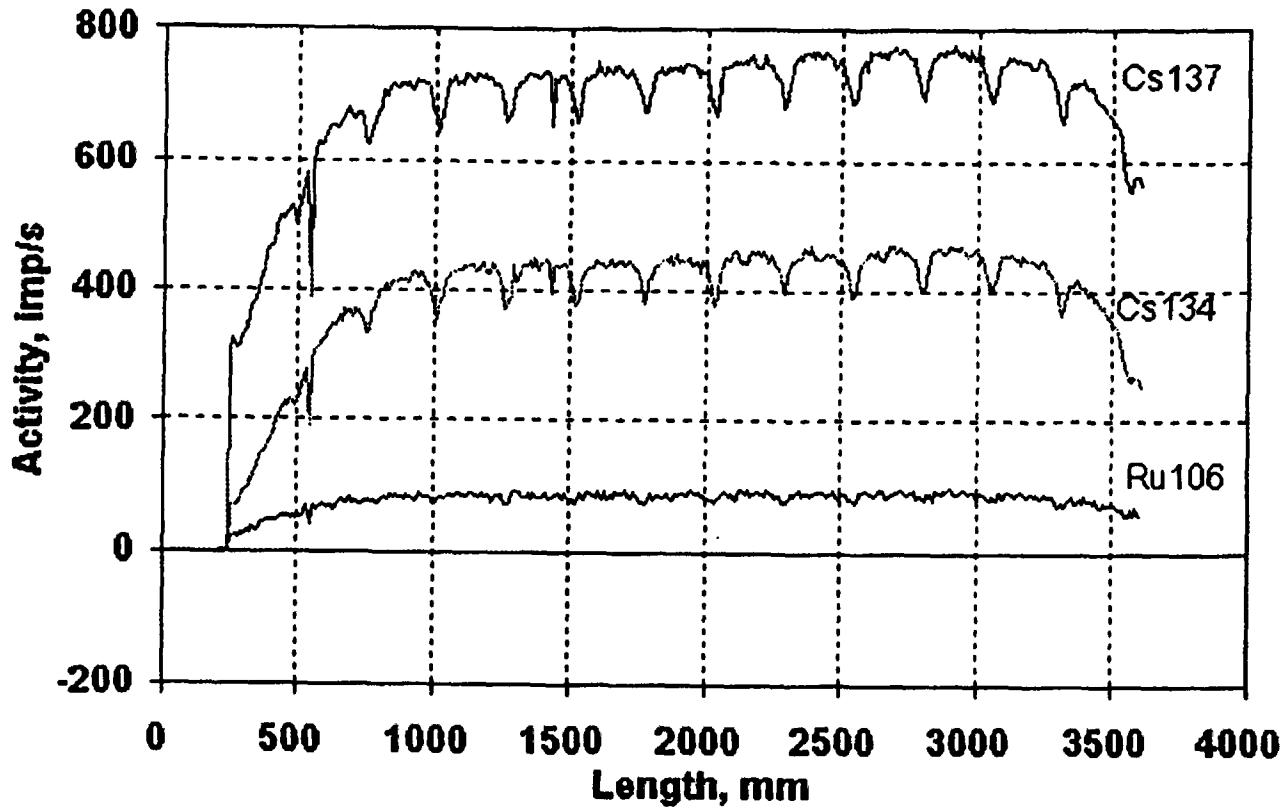

Fig 8. Distribution of fission product gamma activity along the fuel rod length

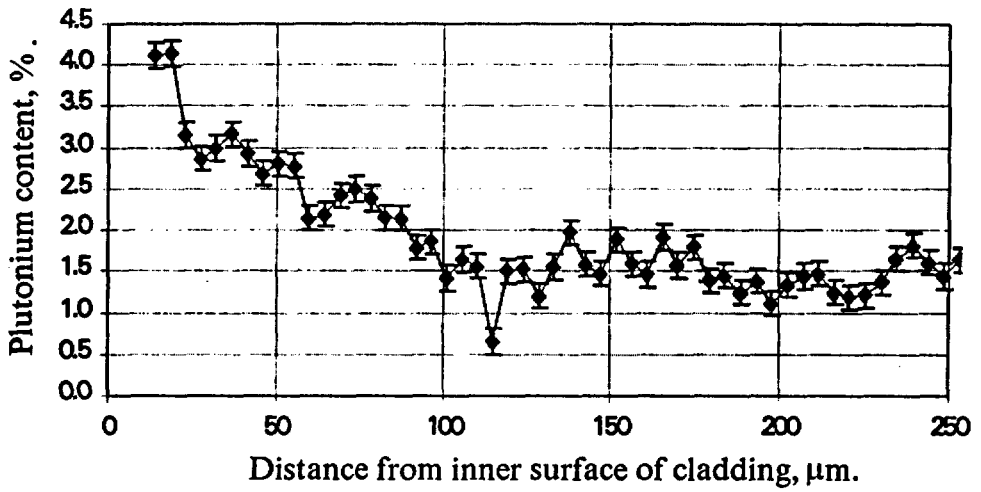

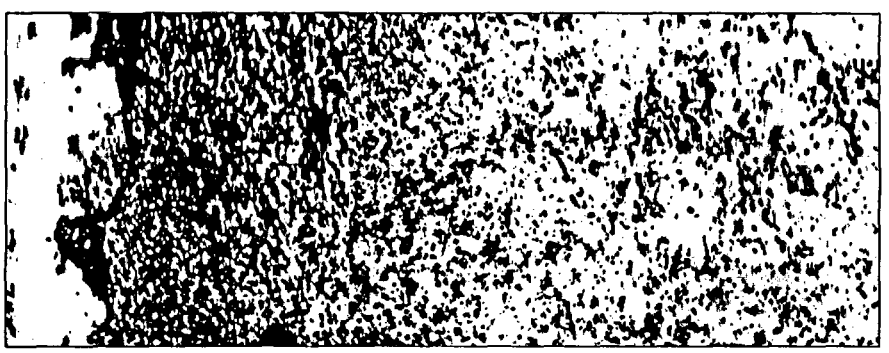

Fig.9. Plutonium distribution along the spent fuel pellet radius.

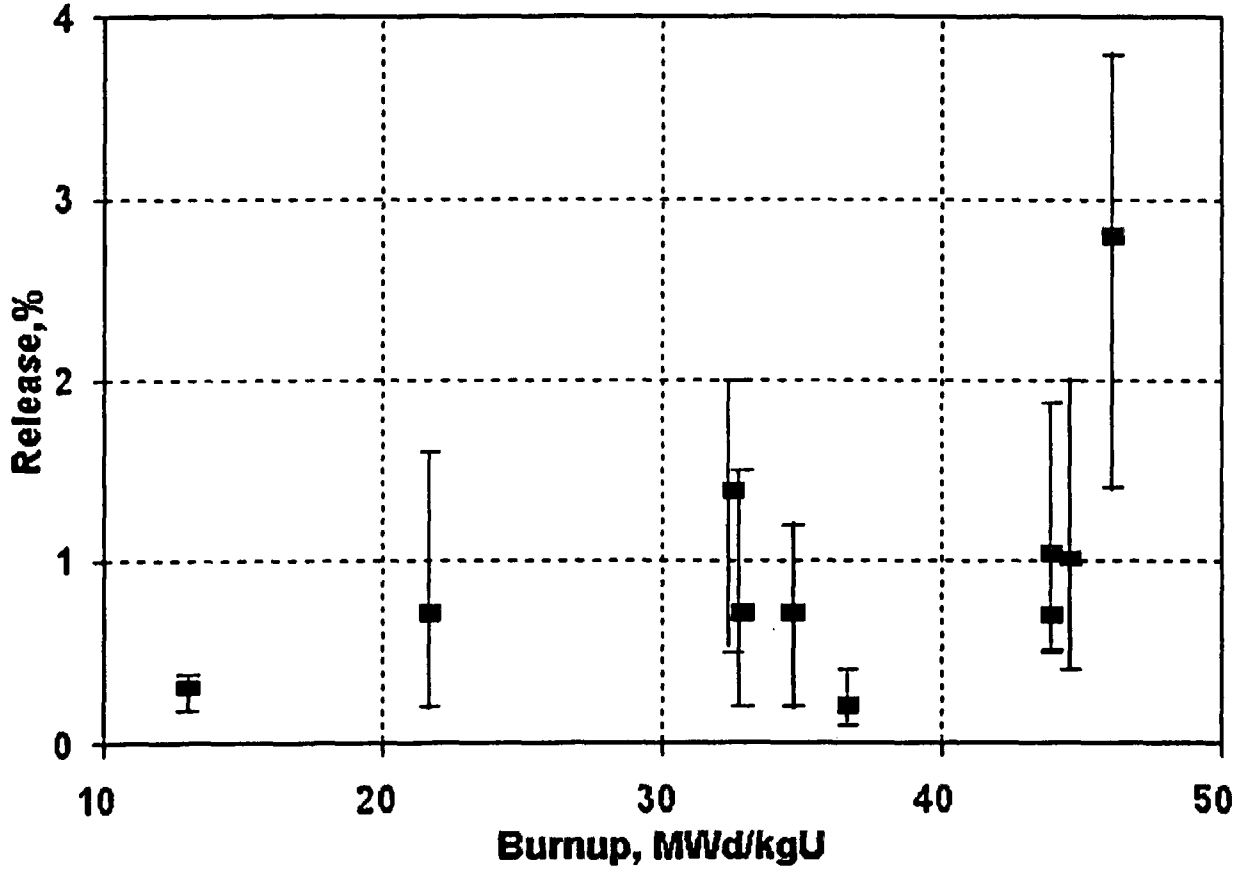

Fig 10. Dependence of gaseous fission product release on burnup

Assessment of Reactivity Transient Experiments with High Burnup Fuel

O. Ozer, R. L. Yang - EPRI
Y.R. Rashid, R.O. Montgomery - ANATECH

I. INTRODUCTION

A few recent experiments aimed at determining the response of high-burnup LWR fuel during a reactivity initiated accident (RIA) have raised concerns that existing failure criteria may be inappropriate for such fuel. In particular, three experiments (SPERT CDC-859[1], NSRR HBO-1[2] and CABRI REP Na-1[3]) appear to have resulted in fuel failures at only a fraction of the anticipated enthalpy levels. In evaluating the results of such "RIA simulation" experiments, however, it is necessary that the following two key considerations be taken into account:

1) Are the experiments representative of conditions that LWR fuel would experience during an in-reactor RIA event?

2) Is the fuel that is being utilized in the tests representative of the present (or anticipated) population of LWR fuel?

Both of these considerations are critical to the correct interpretation of the test results, especially with regard to their applicability to the expected in-reactor LWR fuel behavior. These considerations must therefore be kept in mind when evaluating the validity of the experimentally observed fuel response. For example, conducting experiments under conditions that can not occur in-reactor can trigger response modes that could not take place during in-reactor operation. Similarly, using unrepresentative fuel samples for the tests will produce failure information that is of limited relevance to commercial LWR fuel. This is particularly important for high-burnup fuel since the manner under which the test samples are base-irradiated prior to the test will impact the mechanical properties of the cladding and will therefore affect the RIA response. This can occur even if the initial design and fabrication of the tested samples were representative of commercial fuel. A good example of this effect can be seen in the results of the SPERT CDC-859 test and in the NSRR JM-4[4] and JM-5[5] tests. The conditions under which the fuel used for these tests was fabricated and/or base-irradiated prior to the RIA pulse resulted in the formation of multiple cladding defects in the form of hydride blisters (possibly due to contamination). When this fuel was subjected to the RIA power pulse, it failed by developing multiple cracks that were closely correlated with the locations of the pre-existing hydride blisters. In the case of the JM tests, many of the cracks formed within the blisters themselves and did not propagate beyond the heavily hydrided regions. The information generated by this particular set of tests may be helpful in highlighting the

important role that hydride blisters have on determining the RIA response but can hardly be considered applicable to normal, non-blistered fuel.

The conditions that would be present in a commercial LWR during a RIA event are themselves subject to considerable uncertainty. In particular, whether a sharp power pulse would be generated at all, and if so, its width and magnitude can best be determined by in reactor experiments. However, since control rod drop or rod ejection experiments are unlikely to be carried out in commercial reactors, one must rely on results from RIA simulation experiments conducted under non-ideal conditions in test reactors. An extensive analytic effort is then needed to determine the applicability of results obtained from RIA simulation experiments to commercial fuel.

The challenge of such an analytic effort is to:

1) understand and explain the fuel responses observed in RIA simulation experiments,

2) determine what are the key factors controlling the fuel response,

3) estimate the sensitivity of the observed responses to the conditions under which the experiments are carried out,

4) determine the extent to which the experimental results are relevant to in-reactor fuel.

This paper summarizes observations obtained from a program conducted under the direction of EPRI which analyzed and evaluated the existing database of RIA simulation experiments.

II. OVERVIEW OF THE ANALYTIC APPROACH

A. Analysis of RIA experiments

The initial step of the program consisted of collecting detailed information on selected key RIA experiments. Particular emphasis was given to data from the CABRI tests which involved the highest-burnup fuel, the NSRR HBO test series and the SPERT CDC tests. The CABRI-related data was obtained through an information exchange agreement between EPRI and EDF. Open literature reports and information presented at various conferences was utilized as sources of data for the analysis of the NSRR and SPERT tests.

The anticipated response of the fuel segments during each test was calculated using EPRI's transient fuel behavior code FREY-01[6]. FREY-01 is a two-dimensional, finite element based fuel behavior code ideally suited for calculating the extent of pellet-cladding mechanical interaction (PCMI) and

cladding strains resulting from a power transient. FREY-01 was used to calculate: (a) the evolution of temperature profiles, in the test fuel (pellets, cladding and coolant), (b) the extent of pellet-cladding mechanical interaction, and (c) the stresses and strains in the cladding, before, during and after the RIA power pulse. The pre-test conditions (in particular the status of the pellet-cladding gap resulting from the base-irradiation) were estimated using the EPRI steady-state fuel performance code ESCORE[7]. The recently developed TUBRNP[8] model was used to track the production of plutonium isotopes and the radial power density profiles as a function of burnup. The FREY-01 calculated temperatures and residual cladding strains were compared to measured data and were found to be in reasonably good agreement.

Two enhancements to the analytic approach had to be introduced in order to correctly represent the responses of fuel with burnup levels in excess of ~ 50 GWd/MTU. These enhancements which were described in an earlier paper[9] involved (a) an explicit 3-dimensional representation of the fission gas bubbles trapped in the porous rim region and (b) the development of a "cladding integrity evaluation model" based on the strain energy density (SED) experienced by the cladding during the RIA test.

An explicit rim representation was used to estimate the contribution to pellet-cladding mechanical interaction from expansion of the rim during the pulse. Initial investigators attributed this behavior to the early failure at the CABRI REP Na-1 test and the dispersal of fuel fragments into the coolant after the failure. The explicit analysis indicated that rim instability did not cause the early failure in REP Na-1. Contribution from the rim to cladding strain was found to be negligible at the time when the first indications of failure were measured. The possibility of fuel dispersal was confirmed, but only during the later stages of the energy deposition when the rim region reaches its maximum temperature, and only under the assumption of a failed cladding.

The cladding integrity evaluation model was developed as a means for evaluating the possibility of fuel rod failure. Since the cladding mechanical state is complex during an RIA, methods using traditional parameters such as yield stress, fracture strain, etc. were considered inappropriate, and an approach was developed using the strain energy density experienced by the cladding as the key parameter. The strain energy density concept was used to develop a "critical SED" curve for the evaluation of cladding response in RIA tests. The critical SED curve was constructed as a function of cladding bulk hydrogen content using information from a set of mechanical property tests (axial tensile, ring and burst tests) performed on cladding samples taken from PWR fuel irradiated to burnup levels in excess of 60 GWd/MTU. The SED values that were required to cause failure in the tests were calculated and plotted as a function of cladding (bulk) hydrogen content. Although the mechanical property data exhibited considerable scatter, it was possible to

obtain a best estimate fit curve (referred to as the Rashid curve) shown on Figure 1-a.

The Rashid curve was then applied to the results of the analytical responses obtained for the set of CABRI tests (REP Na-1 through 5). The calculated maximum SED values for the five tests were found to be below their corresponding Rashid curve critical values, indicating expected survival (Figure 1-b). It was also noted that at the time of failure of the REP Na-1 test, its SED was considerably below the range where failure could be expected. Even taking into account the uncertainty inherent in the Rashid curve resulting from the scatter in the underlying mechanical test data, the excessively low failure level of REP Na-1 is clearly inconsistent with cladding mechanical properties. Failure at such a low SED level can be explained either by assuming the presence of pre-existing cladding flaws or by an excessively high level of hydride blistering. Either of these conditions would make the REP Na-1 test fuel sample "untypical" and "unrepresentative".

B. Evaluation of in-reactor conditions during a hypothetical RIA event

In parallel with the analysis of fuel responses in RIA experiments, another analytic effort was aimed at determining representative in-reactor power pulse shapes and magnitudes that could be expected during a hypothetical control rod drop or rod-ejection event. EPRI's best-estimate CORETRAN[10] code system (which consists of a coupled, 3-dimensional transient neutron kinetics and thermal hydraulics capability) was applied to the analysis of a sample PWR and a BWR. Actual core fuel loading configurations and cross-section data were obtained from the respective utilities and the effects of rod ejection (PWR) and rod drop (BWR) events were calculated. This analysis which was summarized in an earlier paper[11] indicated that the results are strongly dependent on the precision of the analytic model and the extent of conservatism assumed in determining the initial status of the event. It was found that three-dimensional best-estimate models yield significantly milder results than those obtained from more conservative models used in original licensing analyses. Even with the more conservative initial-status scenario assumptions, the RIA power pulses were found to reach a magnitude of up to 3 times nominal power over a time interval in excess of 80 ms. Maximum increases in fuel enthalpy were found to be limited to ~ 20 cal/g for the PWR and about ~ 30 cal/g for the BWR cases that were analyzed.

III. SENSITIVITY ANALYSIS OF RIA EXPERIMENTS.

Having developed a fuel behavior analytical model for the interpretation of the RIA experiments, this model was applied to a select set of cases to determine the extent to which the observed fuel response is affected by its experimental environment. In particular, the effects of differences between

the experimental conditions and expected in-reactor conditions were investigated for cases representative of the CABRI REP-Na series, the NSRR-HBO series and the SPERT-CDC series of experiments.
The investigations included: (a) the effects of pulse width differences (4 ms for NSRR, 9 ms for the first four CABRI tests and 17 ms for SPERT CDC-859 were compared to a reference value of 80 ms), and (b) the effects of the coolant type and condition (room-temperature/pressure water for the NSRR and SPERT tests and sodium at 280°C and atmospheric pressure for the CABRI tests compared to a reference condition of water under PWR or BWR pressure/temperatures).

A. Sensitivity analysis of the CABRI tests.

The sensitivity of the CABRI test responses to their experimental environment was estimated by calculating the responses of a PWR fuel rod of 63 GWd/MTU burnup to a gaussian-shaped 100 cal/g enthalpy pulse. The pulse width was varied from a minimum of 9.5 ms out to a maximum of 150 ms. The responses for a rod submerged in sodium at 280°C were compared to those for a rod in 280°C water at a pressure of 15 MPa (PWR conditions). The calculated maximum rim, pellet center and cladding temperatures for each of the cases are compared on Table I. (Since the maxima are reached at different points in time, the time when each of the values is reached is also shown on the table.) As would be expected, the fuel temperatures are insensitive to the coolant conditions and are more strongly influenced by pulse width. Whereas, the cladding temperatures are influenced by the coolant conditions and are only marginally impacted by the pulse width.

In addition to temperatures, Table I contains the maximum hoop strains, the maximum strain energy density (SED) deposited into the cladding during the total duration of the experiment and the SED at the time when cladding hoop strain is at a maximum. Since the maximum SED is delivered over a much longer time (5 to 10 s depending on coolant type) it is the SED at time of maximum hoop strain which is the critical parameter of concern.

Pulse Sensitivity Analysis Results
Coolant - Sodium

	9.5 msec	40 msec	80 msec	150 msec
Max. Rim Temp. (K)	2668/0.506 sec.	2306/0.530 sec	2155/0.57 sec	2041/0.63 sec
Max. Centerline Temp. (K)	1832/1.5 sec	1834/1.5 sec	1834/1.5 sec	1829/1.5 sec
Max. Clad Temp. (K)	865/0.520 sec	822/0.540 sec	757/0.55 sec	714/0.58 sec
Max. Hoop Strain (%)	1.66/0.508 sec	1.65/0.585 sec	1.65/0.61 sec	1.58/0.68 sec
Max. SED (MJ/m^3) SED (MJ/m^3) at time of max. strain	21.0/5 sec 17.5 0.508 sec	19.5/5 sec 16.8/0.585 sec	19.5/5 sec 16.2/0.61 sec	18.0/5 sec 15.1/0.68 sec

Pulse Sensitivity Analysis Results
Coolant - Water (PWR Conditions)

	9.5 msec	40 msec	80 msec	150 msec
Max. Rim Temp. (K)	2615/0.506 sec	2283/0.530 sec	2150/0.57 sec	2037/0.62 sec
Max. Centerline Temp. (K)	1838/2.0 sec	1840/2.0 sec	1839/2.0 sec	1838/2.0 sec
Max. Clad Temp. (K)	1242/0.8 sec	1233/0.8 sec	1222/0.8 sec	1212/0.8 sec
Max. Hoop Strain (%)	1.6/0.509 sec	1.44/0.535 sec	1.34/0.57 sec	1.18/0.63 sec
Max. SED (MJ/m^3) SED (MJ/m^3) at time of max. strain	19.0/10 sec 16.3 0.509 sec	13.8/10 sec 12.7/0.535 sec	11.8/10 sec 11/0.57 sec	10/10 sec 9.3/0.63 sec

Table I. Sensitivity analysis results for RIA tests conducted in the CABRI environment

Two features become evident from an examination of the values presented in Table I:

a) The conditions in sodium coolant are more severe than those in PWR water. Comparing equivalent values calculated for an 80 ms pulse in sodium and in PWR water, one can note that the cladding remains colder in sodium (757 K vs. 1222 K), it experiences higher hoop strain (1.65 % vs. 1.35 %) and higher corresponding SED (16.2 MJ/m^3, vs. 11.0 MJ/m^3).

b) The sensitivity to pulse width variation is less in sodium than in water. Widening the pulse from 9.5 ms to 80 ms reduces the SED by only 1.3 MJ/m^3 (~ 7 %) in sodium (from 17.5 to 16.2 MJ/m^3) whereas the reduction in water is 5.8 MJ/m^3 (~ 38%)

Based on a comparison of SED values, it is possible to conclude that:

- a 100 cal/g (9.5 ms) pulse in CABRI is equivalent to a 159 cal/g (80 ms) pulse in PWR water, and

- widening the pulse from 9.5 ms to 80 ms in CABRI will only produce 25 % of the benefit that pulse widening would produce in PWR water.

B. Sensitivity analysis of the NSRR HBO tests.

The concern with the NSRR series of tests is that they are conducted in 25°C and atmospheric pressure water and involve extremely narrow pulses (4.5 ms). To evaluate the sensitivities of the NSRR HBO test results, the anticipated responses of a 17 x 17 PWR rod were calculated for three separate cases. In Case I, the actual HBO-1 and -3 conditions were modeled. Thus the fuel was assumed to be subjected to a narrow (4.5 ms) gaussian-shaped pulse resulting in a maximum fuel enthalpy rise of 74 cal/g. The cooling environment was assumed to be water at 25 °C and atmospheric pressure. In Case II, the same narrow pulse was assumed to be delivered to a rod cooled by water at 285°C and 15 MPa coolant pressure (PWR conditions). Finally, for Case III, the pulse width was increased to 80 ms. The coolant was again water at PWR conditions.

The results of these calculations are shown on Figures 2-a through 2-d. Figure 2-a shows the initial power pulse, Figure 2-b shows the calculated cladding hoop stresses as a function of time, the cladding temperature distributions at time of failure is given on Figure 2-c, and the SED as a function of time on Figure 2-d. In these figures, the solid line represents the results of Case I (i.e. NSRR experimental conditions), and the dashed lines represent results calculated for Case II (PWR conditions with 4.5 ms pulse). The calculated maximum hoop stresses and SEDs for the above three cases are summarized in Table II.

Case Analyzed	Max. Hoop Stress (MPa)	SED @ end-of-pulse MJ/m^3
Test Capsule (25°C, 4.5 ms)	1100	10.6
PWR Coolant (4.5 ms)	700	8.9
PWR Coolant (80 ms)	490	6.8

Table II. Sensitivity analysis results of RIA experiments conducted in the NSRR HBO-1 & 3 environment

From Table II it can be seen that if the power pulse that was used for the NSRR HBO-1 and -3 tests was delivered to the same rod but in a PWR environment the resulting maximum cladding stresses and SEDs would be significantly lower. Furthermore, if the pulse width is increased to the more representative value of 80 ms, the resulting stresses and SEDs are further reduced (by a factor of 2.2 for maximum hoop stress and a factor of 1.6 for SED). Thus one could claim, on the basis of these comparisons, that the NSRR tests represent conditions that are more severe than those in a PWR by a factor of 1.6 to 2.2, but even this assessment may be an underestimate as discussed in the following section.

From Figure 2-b, it is clear that the experimentally determined failure time corresponds well with the time when the calculated cladding hoop stress is near its maximum. It can be seen in Figure II-c that the cladding temperature at the time of failure is at ~ 25 °C for the external ~ 50 % of the cladding. Only the inner portion has started to heat up, reaching a maximum of ~300 °C at the inner surface. This temperature distribution agrees very well with features observed on metallographic samples of the fractured HBO-1 cladding presented by JAERI[2]. These samples show a brittle fracture originating from the external (cold) surface and propagating inwards. About half-way into the cladding (when it reaches the warmer regions) the brittle crack is transformed into a ductile tear.

This response should be evaluated in view of realistic PWR conditions. As shown on Figure 2-c, the cladding for the realistic case is considerably hotter. Even the coldest temperatures on the cladding OD are above ~ 300 °C, or as high as the hottest (innermost surface) temperature of the preceding case. In HBO-1 the transition from brittle to ductile behavior can be seen to start in the central region of the cladding at temperatures as low as 50 to 100 °C. Therefore, it is unlikely that a brittle crack could have initiated on the outside surface of this rod if it was at 300 °C as it would have been under PWR conditions.

Thus, in addition to the 1.6 to 2.2 severity factor based on cladding strain or SED, all observations from NSRR tests that result in fuel failure must be closely evaluated since the room-temperature environment can induce responses in high-burnup fuel that are not likely to occur under realistic PWR conditions.

C. Sensitivity analysis of the SPERT CDC-859 test.

The RIA test resulting in the third-lowest energy failure is SPERT CDC-859. This test involved a BWR rod with pre-existing cladding blisters. The rod was pulsed in room-temperature, atmospheric pressure water. The pulse amplitude was 158 cal/g and its width was 17 ms.

A sensitivity analysis similar to that for NSRR HBO rods was carried out for the SPERT CDC-859 conditions as well. Again, three cases were analyzed with Case I representing the actual experimental conditions (25°C water, 158 cal/g, 17 ms pulse). In Case II, the pulse was kept the same but the coolant conditions were changed to those of a BWR (238 °C, 7.5 MPa). In Case III, the rod was kept under BWR conditions and the pulse width was extended to 80 ms. The calculated results for Case I (solid lines) and Case II (dashed lines) are shown in Figures 3-a through 3-d. The maximum hoop stress in the cladding was calculated to be 945 MPa for Case I. Going to BWR coolant conditions decreased the maximum hoop stress to 628 MPa. Finally, with the wider pulse and BWR coolant conditions of Case III, the maximum hoop stress was found to be reduced to 540 MPa. This again represents a substantial decrease in severity (factor of ~ 1.5) when comparing the load on the cladding under experimental conditions to those expected under more typical BWR conditions.

IV. CONCLUSIONS

An evaluation of RIA simulation experiments, some of which resulted in fuel failure at low enthalpy levels, has been carried out using a reliable analytic model. The analysis results indicated that the conditions under which RIA simulation experiments are carried out can have a significant impact on the observed fuel response. Based on the analytical results, the experimental conditions used in RIA simulation experiments represent a more severe situation, from a fuel response point of view, than the one that would be present in-reactor during an RIA event. Moreover, the analytical evaluation of certain RIA simulation tests has identified intrinsic deficiencies in their design and execution which negate their validity as benchmarks for establishing RIA criteria. In particular, data from tests on irradiated fuel that resulted in failure should not be utilized since the failure mechanism in those tests may not be possible under realistic conditions. A more appropriate failure limit would be based on the upper range of enthalpies from tests with surviving rods. Values derived from such tests already include a conservatism factor ranging from 1.6 to 2.0 as demonstrated by the analytical results.

REFERENCES

[1] Cook, B.A., et al., "Reactivity Initiated Accident Test Series Test RIA 1-2 Fuel Behavior Report," NUREG/CR-1842, EGG-2073, January 1981.

[2] Ishijima K., et al., "Postulated Mechanisms on the Failure of 50 MWd/kgU PWR Fuel in the Experiment and Related Research Programs in JAERI", Proceedings of Specialists Meeting on Transient Behavior of High Burnup Fuel, Cadarache, France, September 1995.

[3] Schmitz, F., et al., "Investigation of the Behavior of High Burnup PWR Fuel under RIA Conditions in the CABRI Test Reactor," 22nd Water Reactor Safety Meeting, Nuclear Regulatory Commission, October 1994.

[4] Fuketa, T., et al., " Behavior of Pre-Irradiated Fuel Under a Simulated RIA Condition [Results of NSRR Test JM-4], JAERI Research 95-013, March 1995

[5] Fuketa, T., et al., " Behavior of Pre-Irradiated Fuel Under a Simulated RIA Condition [Results of NSRR Test JM-5], JAERI Research 95-078, November 1995

[6] Rashid, Y.R., et al., "FREY-01: Fuel Rod Evaluation System – Volume 1: Theoretical and Numerical Bases," NP-3277, Vol. 1, Rev. 3, August 1994.

[7] Fiero, I.B., "ESCORE – The EPRI Steady State Core Reload Evaluator Code: General Description," NP-5100-L-A, April 1991.

[8] Lassmann, K., O'Carroll, C., et al., "The Radial Distribution of Plutonium in High Burnup UO_2 Fuels," *J. Nuc. Mat.*, 208, 1994, pp. 223-231.

[9] Rashid, Y.R., et al., "Evaluation of RIA Experiments and Their Impact on High-Burnup Fuel Performance", Proceedings of Specialists Meeting on Transient Behavior of High Burnup Fuel, Cadarache, France, September 1995.

[10] "ARROTTA-01 An Advanced Rapid Operational Transient Analysis Computer Code" EPRI NP 7375-CCM, October 1991 and "VIPRE-02 A Two-Fluid ThermalHydraulics Code for Reactor Core and Vessel Analysis", EPRI TR-103931 Final Report, June 1994.

[11] Agee, L.J., et al., " Realistic Scoping Study of Reactivity Insertion Accidents for a Typical PWR and BWR Core", Proceedings of Specialists Meeting on Transient Behavior of High Burnup Fuel, Cadarache, France, September 1995.

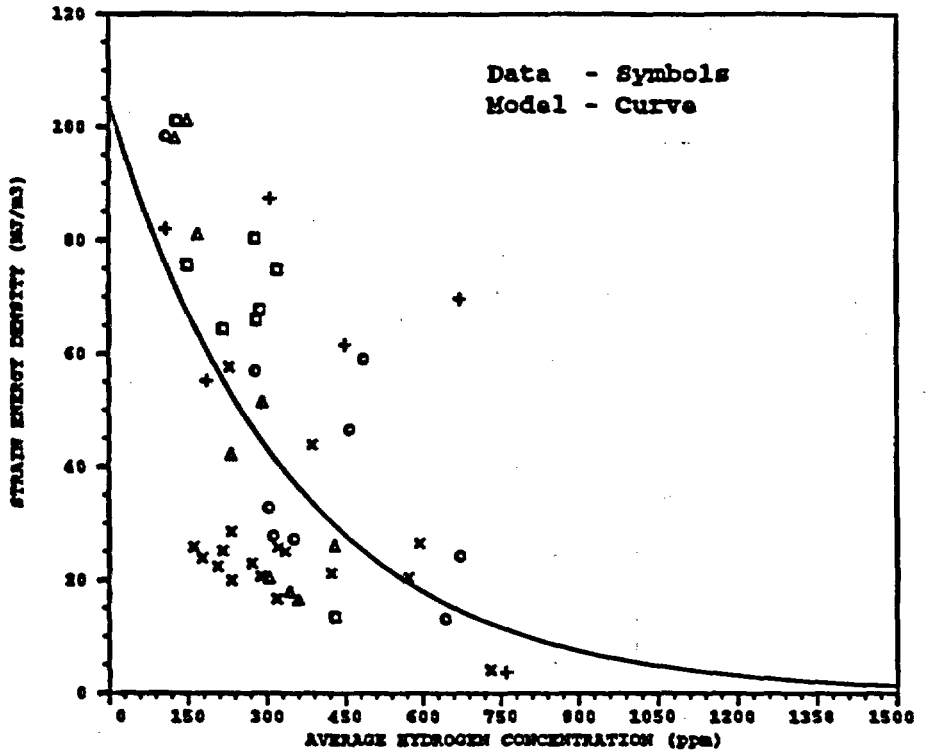

Figure 1a. Cladding Evaluation Model - Comparison to Mechanical Properties Data

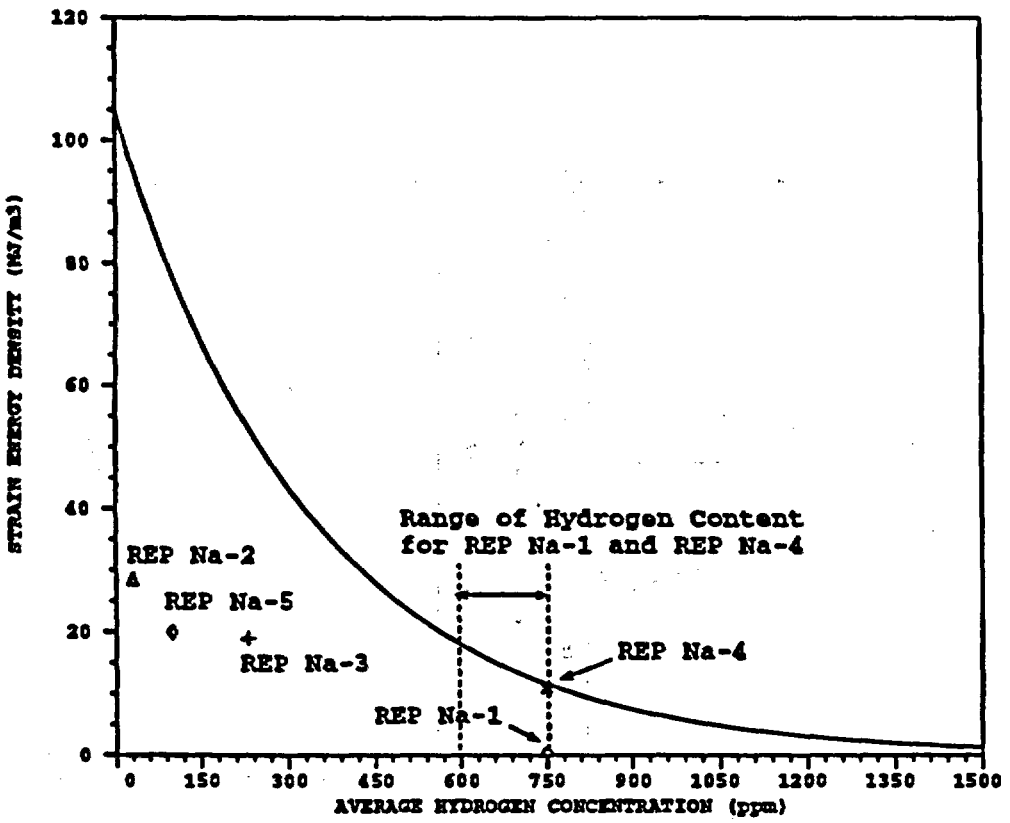

Figure 1b. Comparison of Computed Strain Energy Density With Cladding Integrity Evaluation Model for CABRI Tests

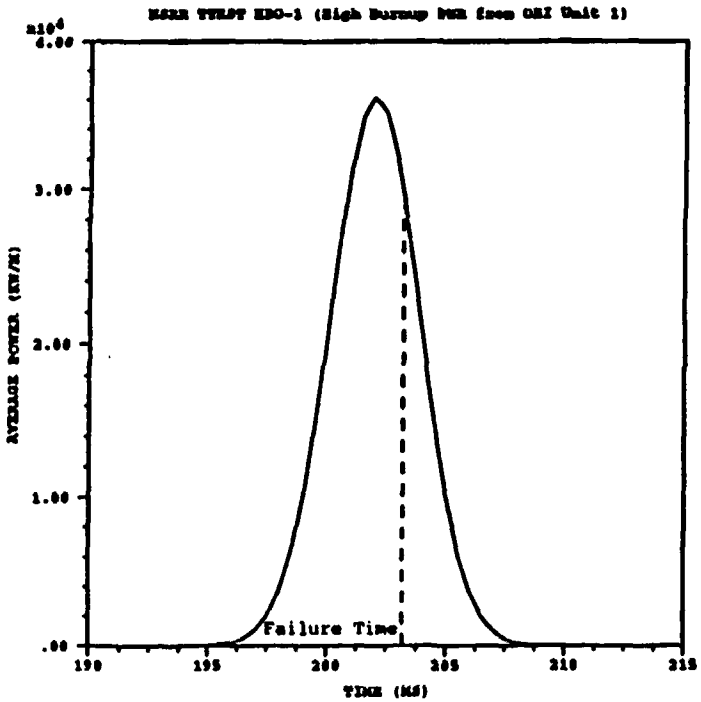

Figure 2a. FUEL ROD PULSE POWER

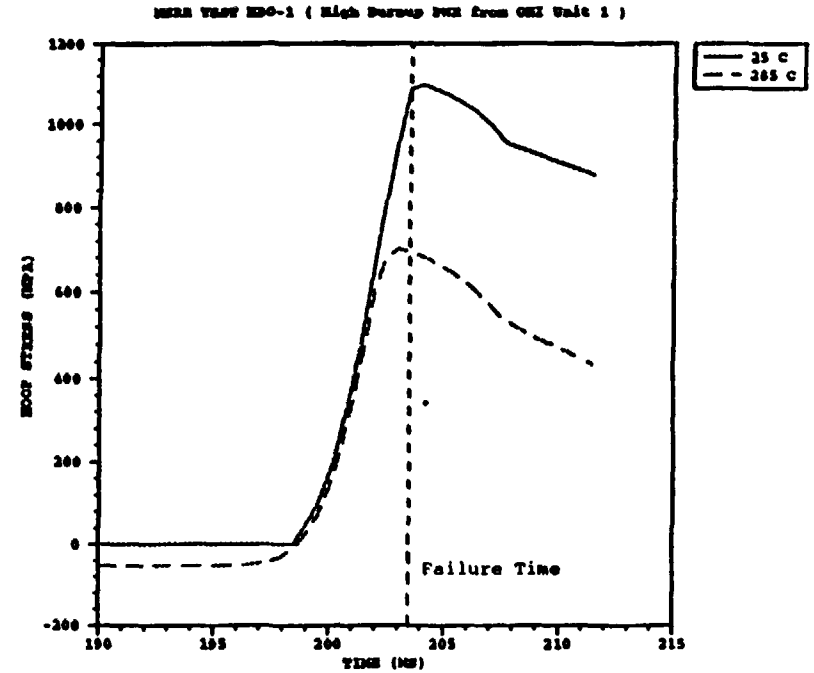

Figure 2b. CLADDING HOOP STRESS @ MAX. PEAK ENTHALPY

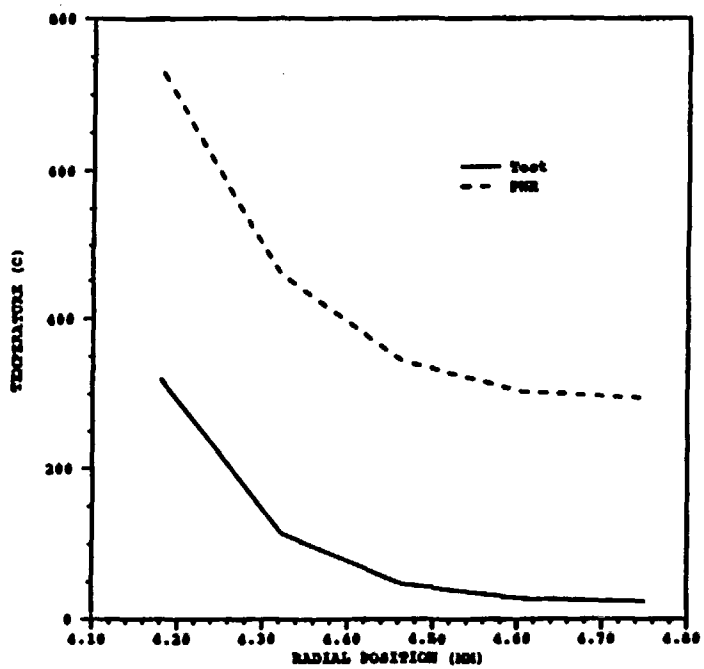

Figure 2c. RADIAL TEMPERATURE PROFILE IN CLADDING AT FAILURE TIME

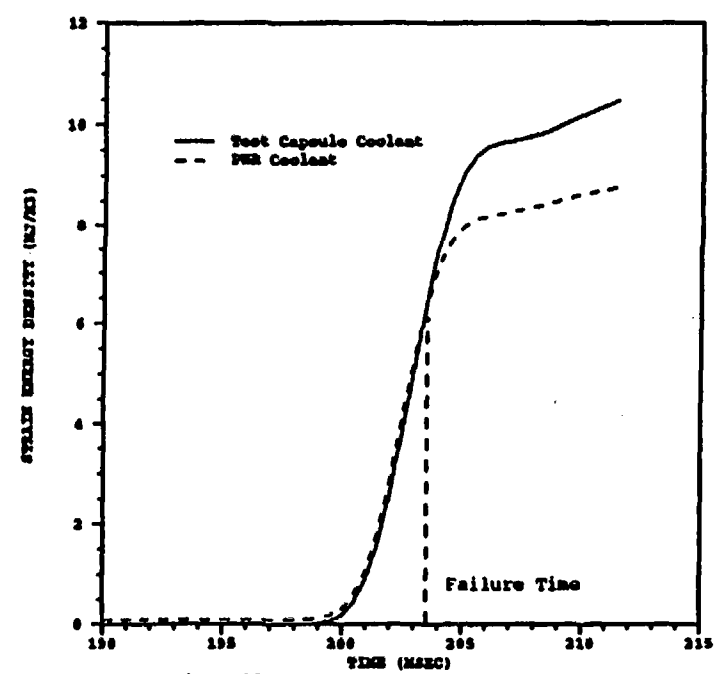

Figure 2d. OUTER CLADDING ZONE -- SED

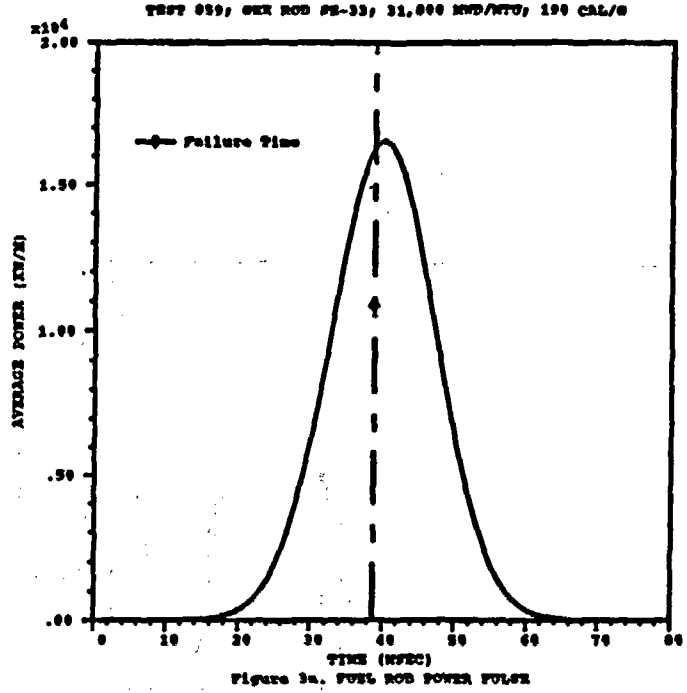

Figure 3a. FUEL ROD POWER PULSE

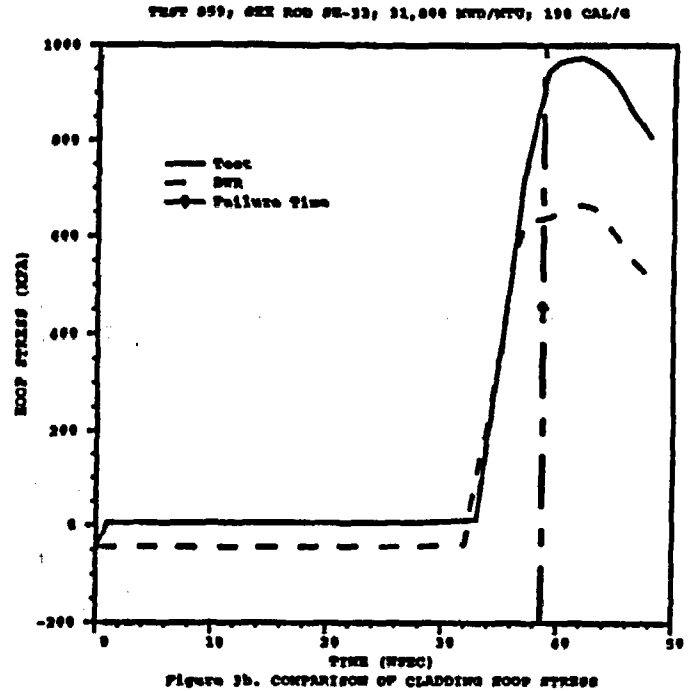

Figure 3b. COMPARISON OF CLADDING HOOP STRESS

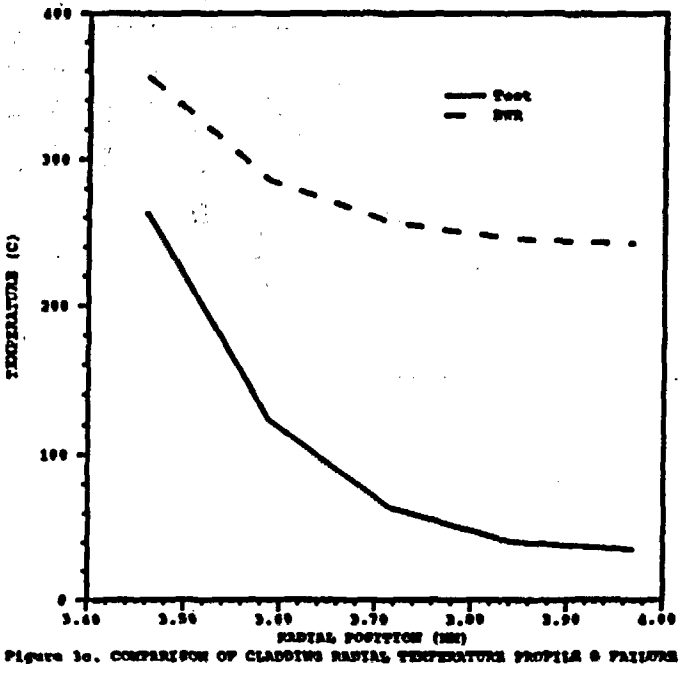

Figure 3c. COMPARISON OF CLADDING RADIAL TEMPERATURE PROFILE @ FAILURE TIME

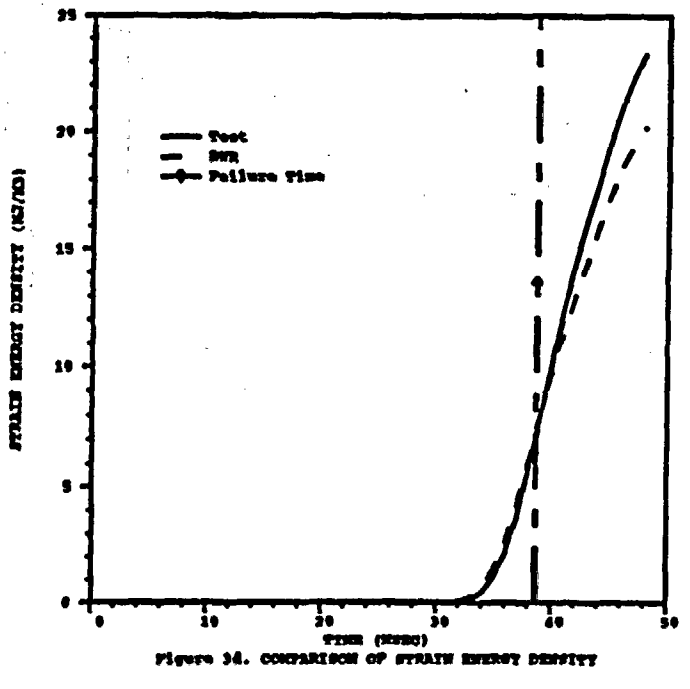

Figure 3d. COMPARISON OF STRAIN ENERGY DENSITY

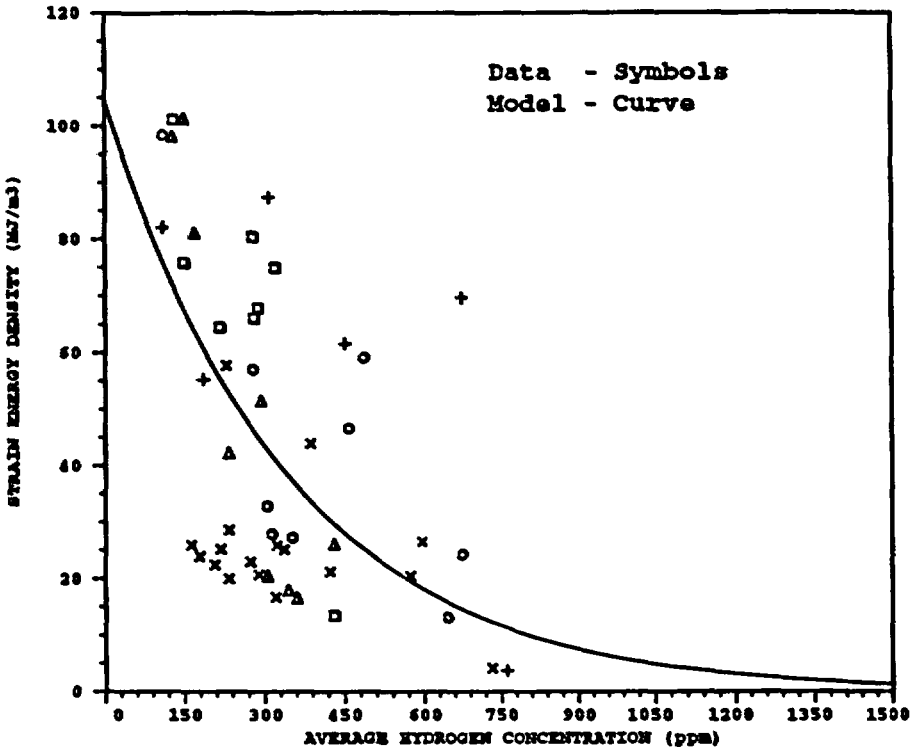

Figure 1a. Cladding Evaluation Model - Comparison to Mechanical Properties Data

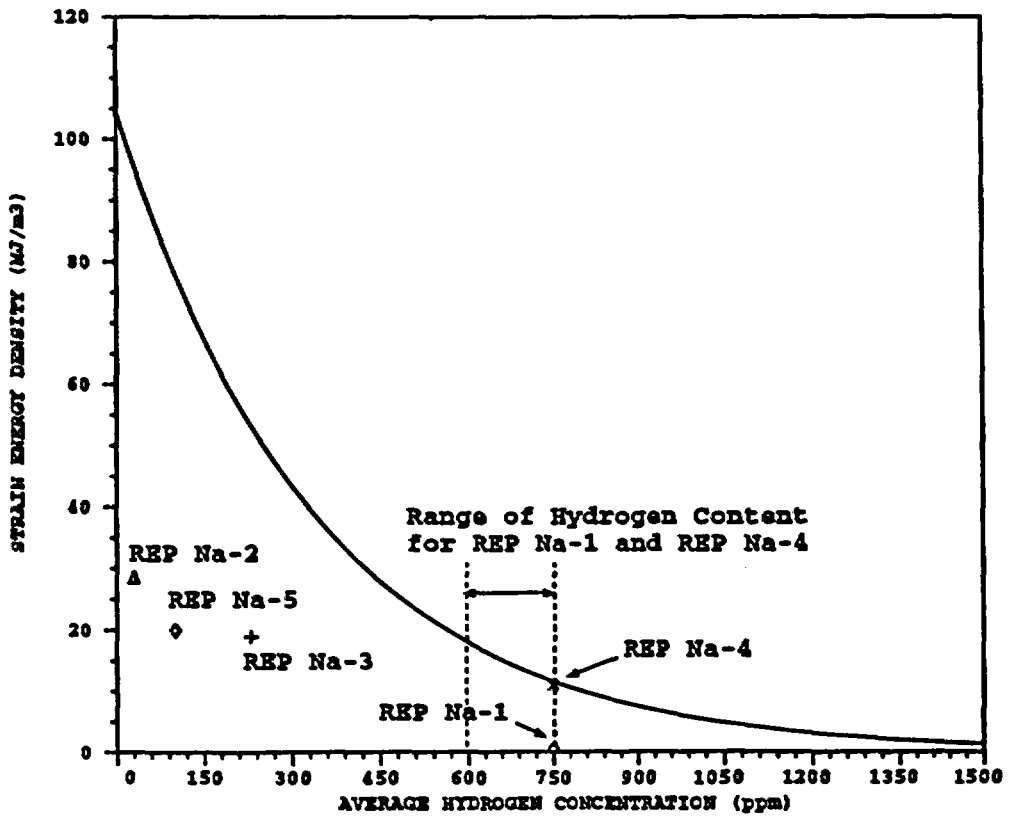

Figure 1b. Comparison of Computed Strain Energy Density With Cladding Integrity Evaluation Model for CABRI Tests

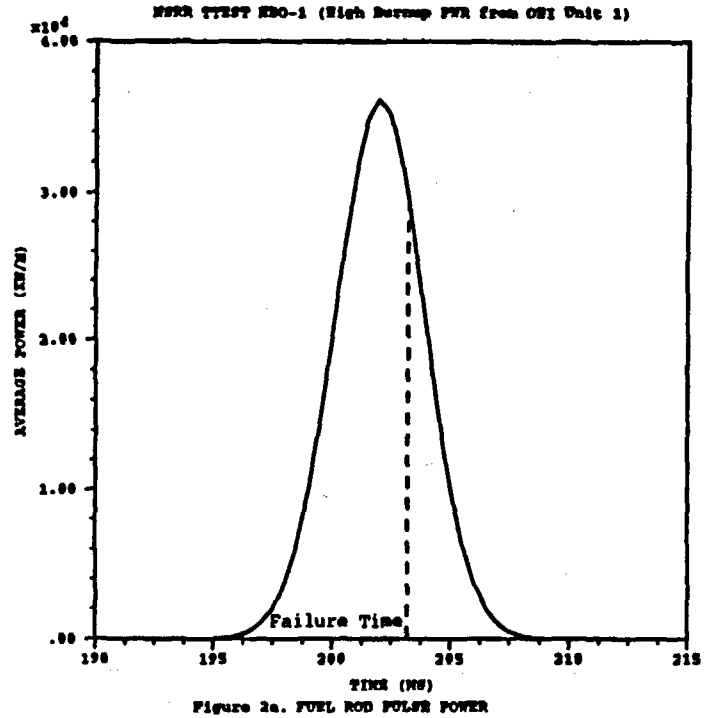

Figure 2a. FUEL ROD PULSE POWER

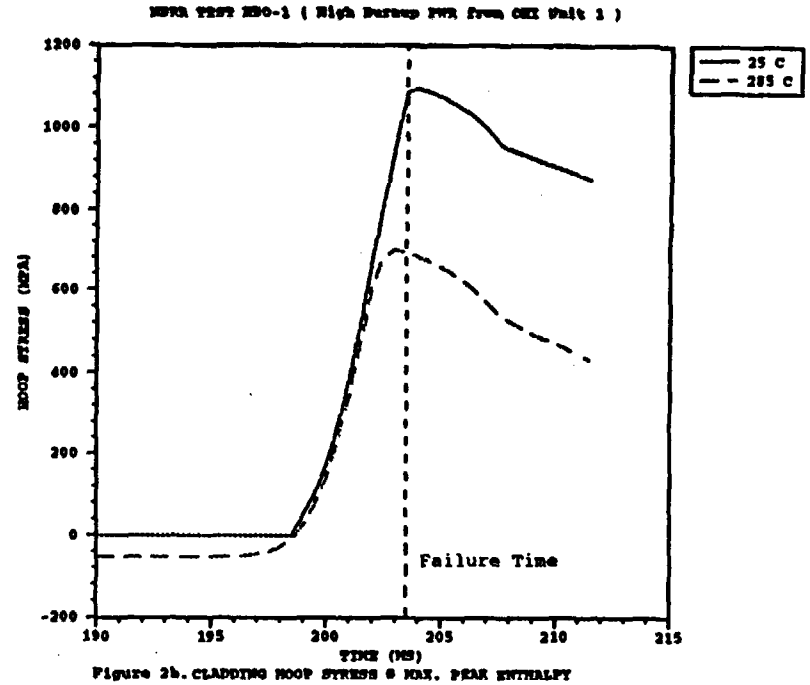

Figure 2b. CLADDING HOOP STRESS @ MAX. PEAK ENTHALPY

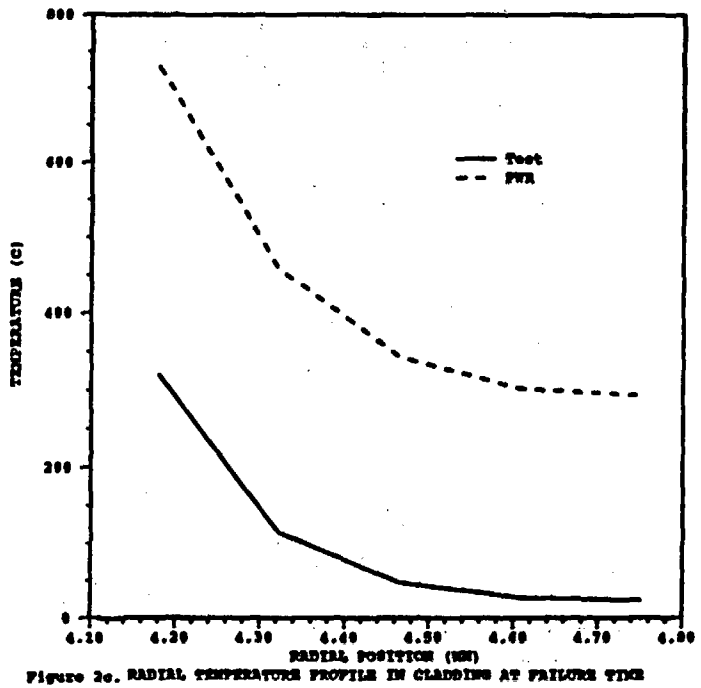

Figure 2c. RADIAL TEMPERATURE PROFILE IN CLADDING AT FAILURE TIME

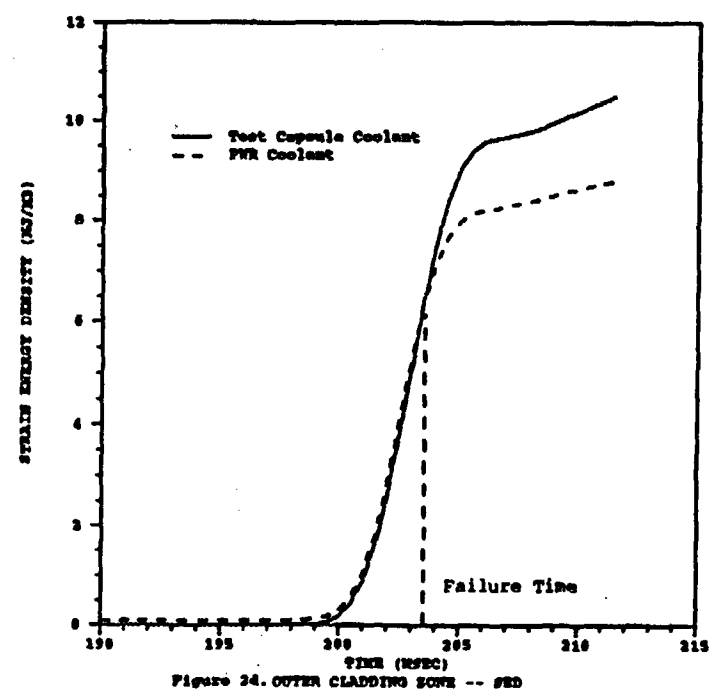

Figure 2d. OUTER CLADDING ZONE -- SED

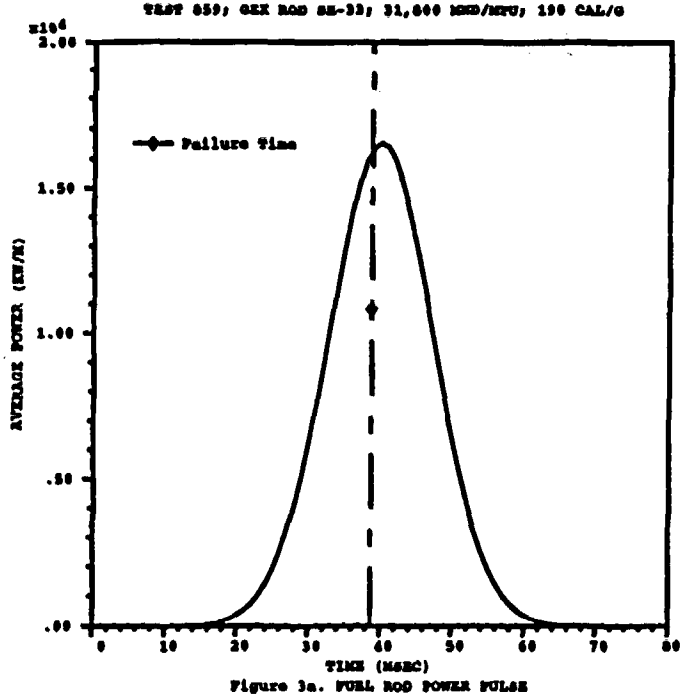

Figure 3a. FUEL ROD POWER PULSE

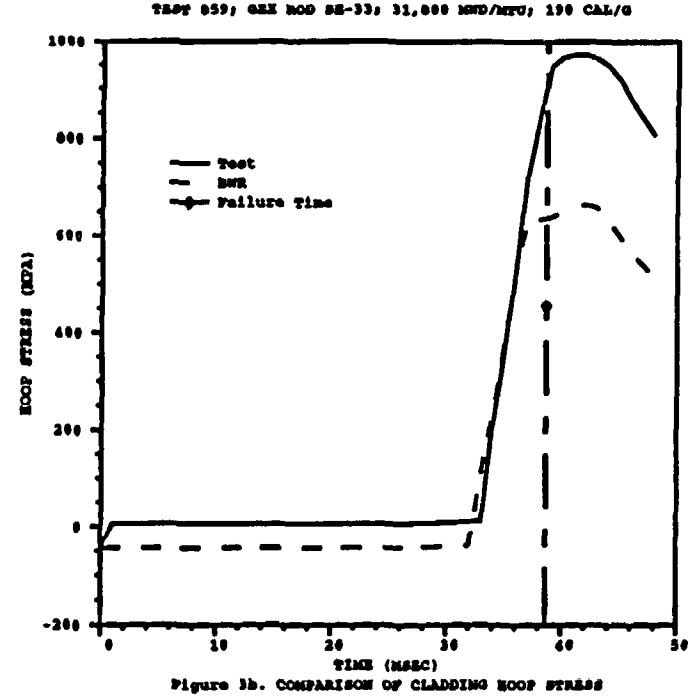

Figure 3b. COMPARISON OF CLADDING HOOP STRESS

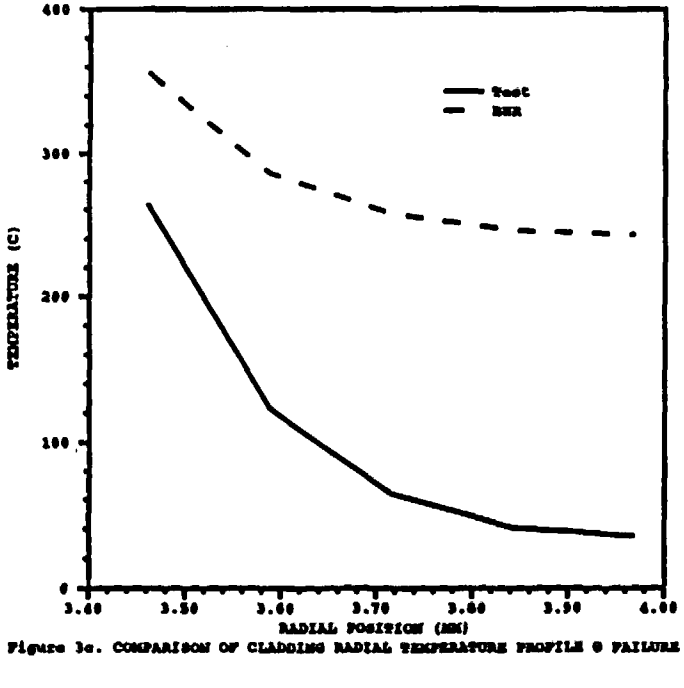

Figure 3c. COMPARISON OF CLADDING RADIAL TEMPERATURE PROFILE @ FAILURE TIME

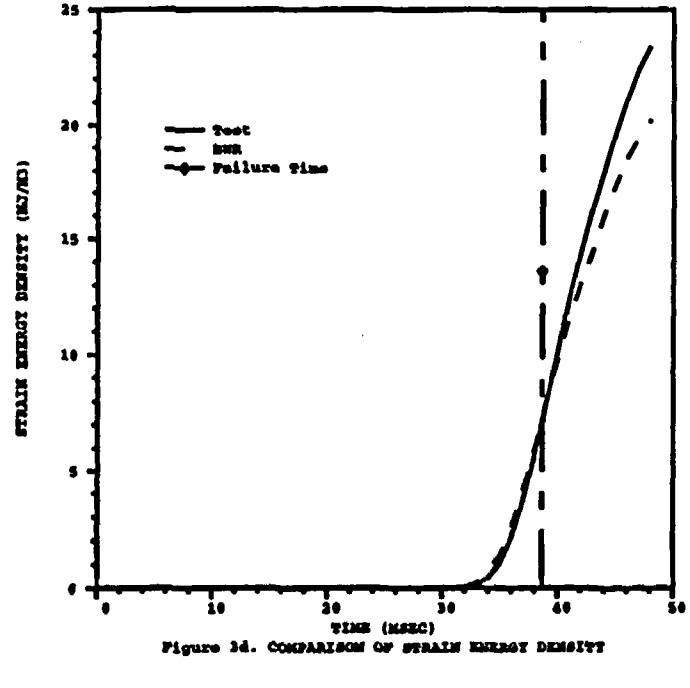

Figure 3d. COMPARISON OF STRAIN ENERGY DENSITY

POWER EXCURSION ANALYSIS FOR BWRs AT HIGH BURNUP[1]

David J. Diamond, Lev Neymotin, and Peter Kohut
Brookhaven National Laboratory
Department of Advanced Technology
Upton, NY 11973-5000

ABSTRACT

A study has been undertaken to determine the fuel enthalpy during a rod drop accident and during two thermal-hydraulic transients. The objective was to understand the consequences to high burnup fuel and the sources of uncertainty in the calculations. The analysis was done with RAMONA-4B, a computer code that models the neutron kinetics throughout the core along with the thermal-hydraulics in the core, vessel, and steamline. The results showed that the maximum fuel enthalpy in high burnup fuel will be affected by core design, initial conditions, and modeling assumptions. The important parameters in each of these categories are discussed in the paper.

SUMMARY

This study was undertaken for the U. S. Nuclear Regulatory Commission to determine the fuel enthalpy in high burnup fuel during design-basis events which cause power excursions. Analysis was done for a rod drop accident (RDA) and transients initiated by main steam isolation valve (MSIV) closure and recirculation flow controller failure. The calculations were done with the RAMONA-4B code which models the core with 3-dimensional neutron kinetics and multiple parallel coolant channels. The code used a model for a BWR/4 with fuel bundles having burnups up to 30 GWd/t, and for the RDA, the calculations were repeated with a model with bundle burnups to 60 GWd/t.

The RDA calculations were done assuming initial conditions at zero power with the coolant 70°C subcooled. The control rod pattern was at 50 percent control density, and the dropped rod had a static worth of 950 pcm. The RDA caused a power excursion that was initially terminated by fuel temperature (Doppler) feedback. The power remained at relatively high levels until void feedback and reactor trip reduced the reactivity sufficiently.

The maximum increase in fuel enthalpy in the core was less than 70 cal/g for the medium burnup core which is low relative to existing acceptance criteria for this event. The enthalpy rise was determined not only by the dropped rod worth and magnitude of the

[1]This work was performed under the auspices of the U. S. Nuclear Regulatory Commission.

feedback but also by the timing of the feedback. With large subcooling, the generation of void feedback is delayed and the fuel enthalpy continues to rise after the initial increase in enthalpy due to the power pulse.

The maximum increase in fuel enthalpy was calculated for the bundles surrounding the dropped rod and then plotted versus the burnup of the node in which the maximum occurred. The results of the calculations were consistent with the expectation that the peak fuel enthalpy in any bundle would be a complicated function of the dropped control rod worth, the distance of the bundle from the dropped rod, and the burnup at that location. This result was found to be the case for both the medium and high burnup cores for which the RDA was calculated.

There are several sources of uncertainty in calculations with high burnup fuel. One source is the "rim" effect which is the extra large peaking of the power distribution at the surface of the pellet. This increases the uncertainty in reactor physics and heat conduction models that assume that the energy deposition has a less peaked spatial distribution. Two other sources of uncertainty are the result of the delayed neutron fraction decreasing with burnup and the positive moderator temperature feedback increasing with burnup. Since these effects tend to increase the severity of the event, an RDA calculation for high burnup fuel will underpredict the fuel enthalpy if the effects are not properly taken into account. Other sources of uncertainty that are important come from the initial conditions chosen for the RDA. This includes the initial control rod pattern as well as the initial thermal-hydraulic conditions. The peaking factor that is used to calculate fuel rod enthalpy from bundle average enthalpy also is uncertain and is underpredicted when it is obtained from single bundle calculations.

The two thermal-hydraulic events calculated in the study were selected by reviewing all events calculated for a Safety Analysis Report. Overpressurization events and the failure of the recirculation flow controller failure were determined to potentially lead to the highest fuel enthalpy increase. The calculations of an MSIV closure and a recirculation flow controller failure showed that the enthalpy increase is small and takes place over a long time interval relative to the case of an RDA.

INTRODUCTION

Reactivity-initiated accidents and certain design-basis transients lead to power excursions which are considered acceptable if they meet specified acceptance criteria. For rapid power excursions, these criteria are based on the energy deposition in the fuel pellet which is equal to the fuel enthalpy assuming adiabatic conditions. In recent years, experiments have been performed to examine the behavior of high burnup fuel subjected to power pulses. Some fuel has failed at energy depositions that are low relative to the acceptance criteria. Furthermore, other recent studies of high burnup fuel show that property changes, especially in the cladding and at the surface of the pellet, could make the fuel more vulnerable to power pulses. These activities have called into question the current acceptance criteria, and new studies to address this issue have been undertaken by the light water reactor community throughout the world.

The U.S. Nuclear Regulatory Commission (NRC) has expressed its concern regarding the above in two Information Notices that have been issued: (NRC, 1994) and (NRC, 1995). In addition, the NRC sponsored a research program to improve their understanding of the situation and to see if regulatory action is needed. This program includes several studies related to fuel behavior and the study discussed herein on the analysis of power excursions under transient/accident conditions.

ANALYSIS OF THE BWR ROD DROP ACCIDENT

Description of RAMONA-4B

RAMONA-4B (Wulff, 1984) is a systems transient code for boiling water reactors. The code uses a 3-dimensional neutron kinetics model coupled with a multichannel, 2-phase flow model of the thermal-hydraulics in the reactor vessel. The code is designed to analyze a wide spectrum of BWR core and system transients. The 3-dimensional neutron kinetics makes the code well-suited for predicting transients and accidents where the spatial core power variations are expected to be significant.

The reactor core is modeled with multiple parallel coolant channels and a bypass channel. Each coolant (i.e., thermal-hydraulic) channel is interfaced with one or more fuel bundles. The reactor power, including decay heat, is calculated in 3-dimensional geometry. The fission power calculation takes into account control rod movement (including accidental rod drop and reactor trip) and the feedback throughout the core due to changes in the fuel and coolant temperatures and steam void fraction. Energy deposited directly into the coolant and bypass channels is taken into account. Thermal conduction through the fuel pellet, gas gap, and fuel cladding is modeled to obtain the heat transfer from the fuel to the coolant.

The neutron kinetics model of RAMONA-4B is based on 2-group diffusion theory with six delayed neutron precursor groups. Simplifications are made in treating the thermal neutron flux to reduce the formulation to a 1½ group, coarse mesh diffusion model in a 3-dimensional rectangular coordinate system. Neutronic boundary conditions are specified at the axial and radial core periphery.

The thermal-hydraulic calculation in RAMONA-4B is based on a 4-equation, nonequilibrium, drift-flux model. The four balance equations are conservation of: (1) vapor mass, (2) mixture mass, (3) mixture momentum, and (4) mixture energy. The thermal-hydraulics modeling extends outside of the core to the vessel, steamline, and recirculation loop.

BWR Reactor Model

A BWR/4 reactor core was modeled with RAMONA-4B using half-core mirror symmetry. The model included 382 neutronic channels, where each channel represented a single fuel bundle. The core model included 100 control rods. The number of calculational nodes in the vertical direction was 24.

The thermal-hydraulics of the half-core region was modeled using 160 thermal-hydraulic channels associated with fuel bundles and one bypass channel representing the region

between the bundles. The majority of the thermal-hydraulic channels were "shared" by several neutronic channels. The thermal energy released in those several neutronic channels was collectively deposited into the liquid flowing in that particular thermal-hydraulic channel. Each of the neutronic channels in three rows of bundles adjacent to the core's axis of symmetry had a dedicated thermal-hydraulic channel in order to most accurately represent the thermal-hydraulic reactivity feedback effects (void fraction and moderator and fuel temperature) following a control rod drop.

Two cores were modeled. One model was for a medium burnup core and represented fuel bundles with burnups up to a maximum of approximately 30 GWd/t. The cross sections for this core had been generated using the CASMO code (Ahlin, 1978) for a previous study.

The other model was meant to represent the situation with bundle average burnups up to 60 GWd/t (and, hence, fuel rod burnups of up to approximately 65 GWd/t). Since no data were available to the authors for actual or planned cores with this burnup, a method was used which allowed for the medium burnup data to be extrapolated to produce the high burnup core. New cross sections were generated using the CPM code (Ahlin, 1975). This core model is only an approximation to an actual core. However, it provides sufficient information to test certain hypotheses and add to our understanding of high burnup cores.

Initial Conditions for RDA Analysis

The calculation of rod drop accidents was done for both the medium and high burnup core models. Table 1 contains some of the neutronic and thermal-hydraulic parameters used to describe initial conditions, plant response, and modeling in RAMONA-4B for these calculations.

The initial control rod pattern with 50 percent control density, shown in Figure 1, was chosen for several reasons. The most important was that in a study of limited scope, it would be too difficult to search through all of the possible patterns to obtain a pattern with the highest worth dropped control rod or the worst fuel enthalpy increase. BWR reactors use systems that lead to patterns such as those in the banked position withdrawal sequence (Paone, 1977). Not only would one have to go through all the patterns possible using this system but also patterns possible if a single failure criterion was applied. With the 50 percent control density, control rod worths of up to 950 pcm were calculated along the axis of symmetry. This highest worth corresponds to rod worths obtained by other analysts using the banked position withdrawal sequence; and, therefore, it was justifiable to use for the rod drop analysis.

The initial thermal-hydraulic conditions in the reactor corresponded to cold startup. The power was 10^{-6} of full power, and the core coolant temperature was 30°C. This represented 70°C subcooling at atmospheric pressure which was assumed to be the system pressure. This delays the onset of steam generation caused by the RDA and, therefore, the addition of negative void reactivity feedback which tends to mitigate the accident. The single-phase coolant decreases the heat transfer to the coolant relative to the case with 2-phase flow. This has the effect of keeping the fuel temperature (and fuel enthalpy) higher; and, as with the void reactivity, this is in the direction so as to make the results more severe, i.e., more limiting. This higher fuel temperature increases the fuel

Table 1 Reactor Model Parameters for Medium and High Burnup RDA Cases

Parameter/Condition	Value/Description	Comment
Fuel bundle maximum burnup	30/60 GWd/t	For medium/high burnup calculations
Reactor power	3.29 kW ("zero" power)	10^{-6} of rated power
Control rod insertion pattern	Checkerboard; 50% control rod density	See Figure 1
Fraction of energy deposited directly into coolant	0.04	Total for the in-channel and bypass liquid
Delayed neutron fraction	0.006/0.005	For medium/high burnup calculations
Xenon inventory	Fully depleted	
Reactor trip setpoint	15% of rated power with 0.2 s delay	
Scram insertion speed	1.2 m/s (3.9 ft/s)	
Control rod drop speed	0.94 m/s (3.1 ft/s)	
System pressure	0.1 MPa	Non-condensible atmosphere
Liquid temperature	30°C	70°C subcooled
Core flow rate	3260 kg/s	25% of rated flow

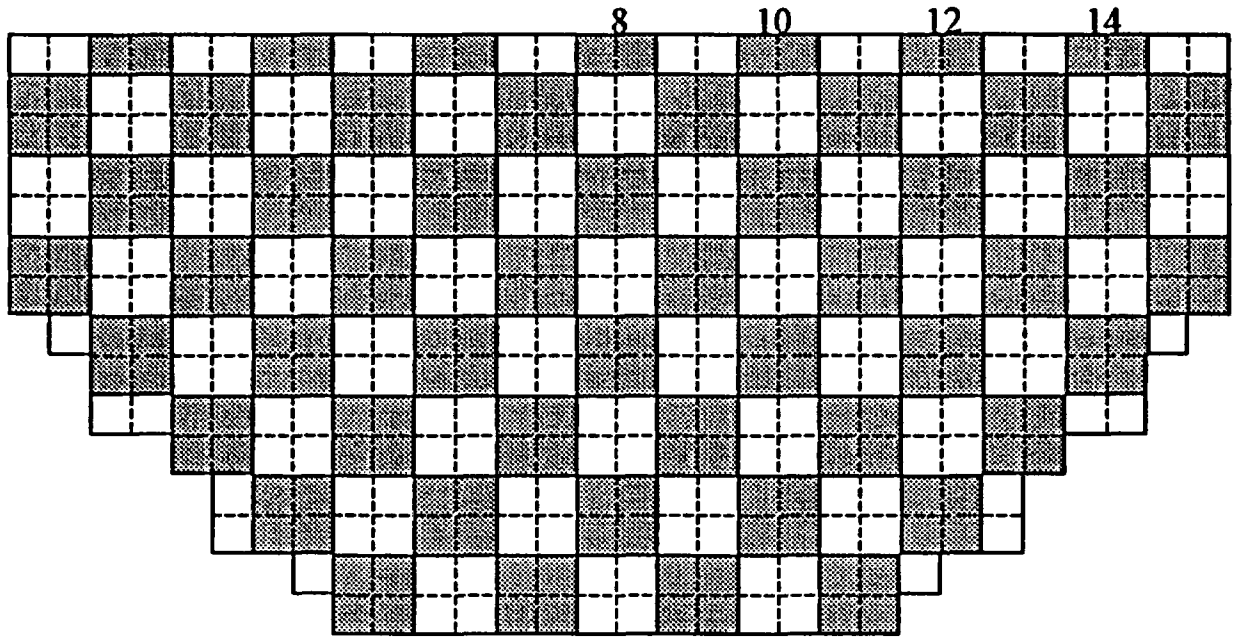

Unshaded core cells: control blade withdrawn
Shaded core cells: control blade inserted

Figure 1 Initial Control Rod Pattern for RDA Analysis

temperature reactivity feedback which limits the severity of the accident, but this is a second-order effect. The high subcooling at low initial temperature means that coolant/moderator temperature reactivity feedback can be important. For a BWR at cold conditions, the feedback is positive and, therefore, can exacerbate the power excursion.

In most BWRs, the reactor becomes critical when only approximately one-fourth of the control rods are withdrawn. Hence, cold conditions would correspond to higher control rod densities than the 50 percent used in this study. At 50 percent control density, higher temperatures and pressures are expected as the power would have increased from its initial level at the cold condition. Best-estimate calculations would have to take into account the change in thermal-hydraulic conditions with changing control rod patterns. The thermal-hydraulic conditions control the positive moderator feedback, the heat transfer to the coolant, and the onset of negative void feedback.

The initial conditions for the medium burnup core results in a (high) axial peaking factor of 3.5 at the top of the core-typical of shutdown conditions in a BWR. This axial peaking tends to increase the rate of reactivity insertion when the rod drops out of the core. This means that the power increases rapidly while the control rod is still in the top half of the core.

Results for a Medium Burnup Core

The accident was initiated at time zero with CR #14 (see Figure 1) dropping at a speed of 0.94 m/s (3.1 ft/s). The prompt power excursion started at about one second, as can be seen in Figure 2, which shows the power during the transient on a logarithmic scale relative to nominal, or rated, power. The power increases more than six decades which is typical for this type of RDA.

The figure also shows the position of the control rod which is initially completely inserted. As can be seen, when the tip of the control rod traveled only three to four feet through the core, sufficient reactivity had been inserted to cause the power excursion which, in turn, was terminated by fuel temperature feedback (primarily due to the Doppler effect). This means that when realistic control patterns are considered in setting up conditions for the RDA, it is only necessary that the control rod drive mechanism be withdrawn halfway out of the core in order to set the stage for the assumption that the corresponding blade has been decoupled and has stuck so that it can later drop to the position of the drive mechanism.

The reactor power reached a peak value of approximately 2.4 of nominal power at about 1.3 seconds. At that time, the negative Doppler reactivity feedback is large enough so that the power excursion is terminated. The history of the different reactivity feedback components is shown in Figure 3 which also shows the power excursion on a linear scale. This figure shows that the accident can be separated into four major phases. In the first phase, reactivity is being inserted due to withdrawal of the dropped control rod. The second phase starts when the power surge is reversed due to fuel temperature (Doppler) reactivity. The third phase covers the period from the initiation of boiling in the core and its associated negative reactivity. The fourth phase occurs when the void feedback and scram become effective enough to completely shut down the core.

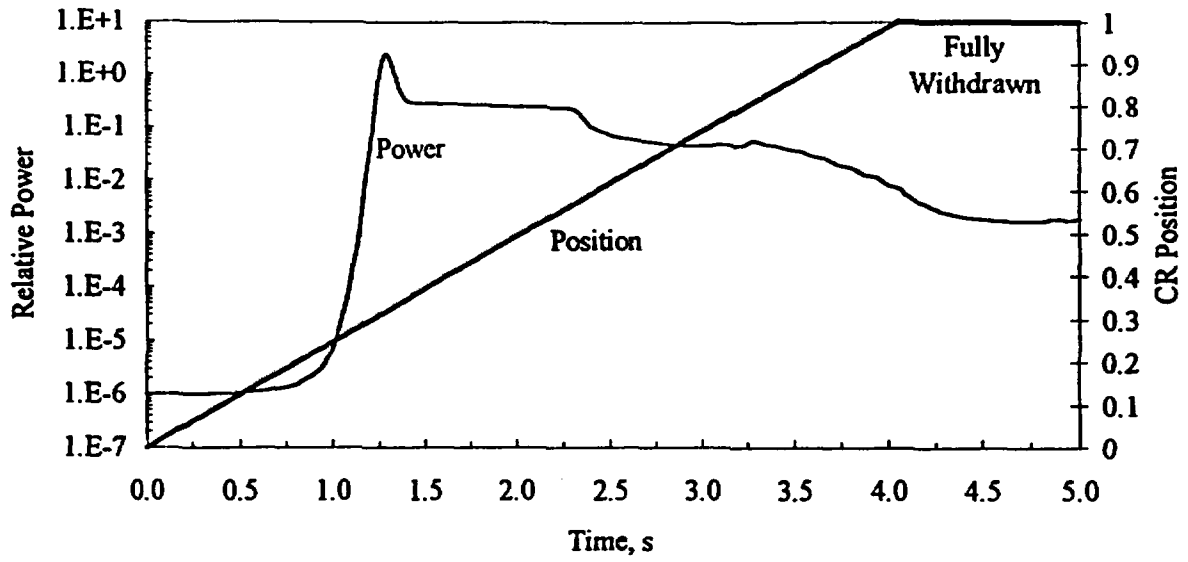

Figure 2 Power and Rod Position During RDA (Medium Burnup Case)

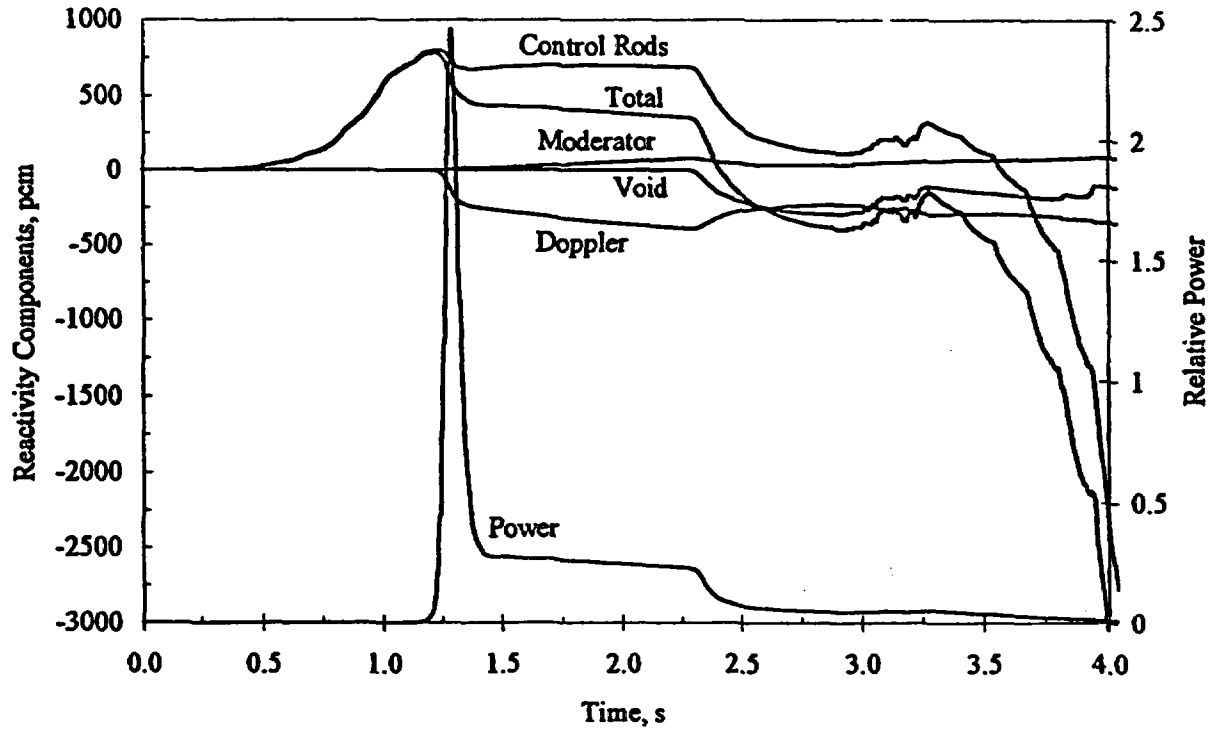

Figure 3 Reactivity Components During RDA (Medium Burnup Case)

The plot of reactivity effects shows that the control rod worth germane to this event is approximately 750 pcm. This is 80 percent of the total static worth of the rod and primarily is the result of the fact that the rod does not withdraw all the way before the event is terminated. The figure also shows the positive reactivity feedback due to moderator heatup.

The axial power distribution also changes during the transient, but because it is peaked at the top of the core initially and the rod is dropping from the top of the core, the axial node with the peak power remains at the top (node 21 where node 24 is at the top of the core).

Although core-average thermal-hydraulic parameters do not change significantly, the localized values change dramatically. The coolant temperature rises to saturation and then boiling begins in the bundles surrounding the dropped rod. This is primarily the result of direct energy deposition; although after approximately one second, heat transfer across the cladding also becomes important. At the incipience of boiling, RAMONA-4B predicted flow oscillations and reversal in the hot channels. This, in turn, led to critical heat flux in a number of channels.

Boiling introduces negative reactivity and, therefore, could be important in mitigating the total enthalpy increase. In other situations, with little or no subcooling, boiling could begin very soon into the transient and reduce the power excursion and the immediate enthalpy increase. In these situations, there is a burden on the accuracy of the thermal-hydraulics model being used. Although it is clear that a certain amount of energy deposition in the coolant leads to boiling, the timing could be important, and current void generation models are based on experiments that do not mimic the dynamic conditions found during a RDA.

The results of most interest in this study are for fuel enthalpy (defined as the pellet radial average at any location in the core) as that is the parameter which is currently used to determine the acceptance limit for the RDA (280 cal/g in the U.S.) and the condition for fuel failure (170 cal/g in the U.S. for BWRs at low or zero power) for the purpose of calculating the radiological response. In the past, only the peak fuel enthalpy throughout the core has been of interest in licensing calculations, i.e., the maximum in both space and time. However, in the present study, it was of interest to understand the peak during the event as a function of the burnup of the fuel and that requires knowing the peak enthalpy in all the nodes in the region around the dropped rod. In the following, bundle-average fuel enthalpy is considered recognizing that if the results could be translated to an individual rod within a bundle, the fuel enthalpy would be higher. In order to know how much higher, one would have to do detailed calculations for the region surrounding the dropped rod. The hottest rod in a steady state might have a power 10-30 percent above the bundle average, but in the transient situation, the peaking could be considerably higher.

Figure 4 shows the maximum fuel bundle enthalpy in three neutronic channels (fuel bundles) as a function of time. The maximum in time occurs in Channel 27, which is one of the bundles directly adjacent to the dropped control rod (CR #14 in Figure 1). Channel 56 is diagonally adjacent to Channel 27, and Channel 89 is one pitch removed from Channel 27. The predicted enthalpies are for an interval of 15.9 cm (6.3 in) corresponding to axial node 21which is the node with maximum fission power. The legend

shows the bundle burnup at the node in the bundle for which the enthalpy is a maximum. Reactor power history is also shown on the figure.

There are three distinct phases in the enthalpy plots: (1) prompt heatup due to the fission power excursion, (2) continuing fission power heatup, and (3) shutdown cool-off. Observation of the enthalpy curves indicates that in this particular calculation, the amount of prompt heatup is roughly equal to the fission power heatup. This results from the initial conditions, mainly from the high initial moderator subcooling which delays bulk boiling in the core--an important factor responsible for shutting down the fission reaction by introducing large negative void reactivity. A lower initial coolant subcooling would result in a lower maximum fuel enthalpy reached during the accident. Note that the separation of the fuel enthalpy increase into the first two phases may become particularly important if studies of fuel behavior in the future lead to acceptance criteria that are based on both the initial fuel enthalpy rise and the ultimate value.

The peak fuel enthalpy for this event (see Figure 4) is less than 70 cal/g which is considerably below the current values of interest from a licensing point of view. However, for this study, it was of interest to consider the fuel enthalpy as a function of burnup for a given RDA. Figure 5 shows enthalpy versus burnup not only for the three bundles used to generate Figure 4 but rather for all 16 bundles (identified by number on the graph) of most interest surrounding the position of the dropped rod. The figure shows the orientation of these bundles relative to the dropped rod position of CR #14 which is between bundles 27 and 28. The crosses indicate control rods initially inserted.

These results do not indicate a simple correlation between fuel enthalpy and burnup. Rather, they suggest that for the given rod worth, the peak fuel enthalpy in a bundle is a complex function of factors, such as the distance of the bundle from the dropped rod and the burnup of the fuel. In other cases for different control rod worths, the enthalpy in a given bundle could be higher or lower depending on the specific circumstances.

This conclusion is probably valid in spite of the fact that there are several other factors influencing Figure 5--namely, that (1) bundles 30 and 60 are on the core periphery and, therefore, the power surge is mitigated by the neutron leakage into the reflector and (2) the bundles with burnups of about 5 GWd/t have reactivities impacted by the burnout of gadolinium and, therefore, cannot be expected to have the same burnup dependence as bundles with higher burnups where gadolinium is no longer an important factor.

Results for a Pseudo High Burnup Core

The pseudo high burnup core model was used to calculate the effect of dropping CR #14 from a control rod pattern corresponding to 50 percent control rod density. The power versus time is shown in Figure 6 on a logarithmic scale. The behavior is similar to that for the medium burnup case except that the peak power is higher. Although the fuel has a higher burnup in this case, the reactivity is not necessarily lower. More reactivity is designed into the fuel so that the reactor can continue to produce power at the higher burnup. Therefore, it is not surprising that results for the two burnup cases are similar.

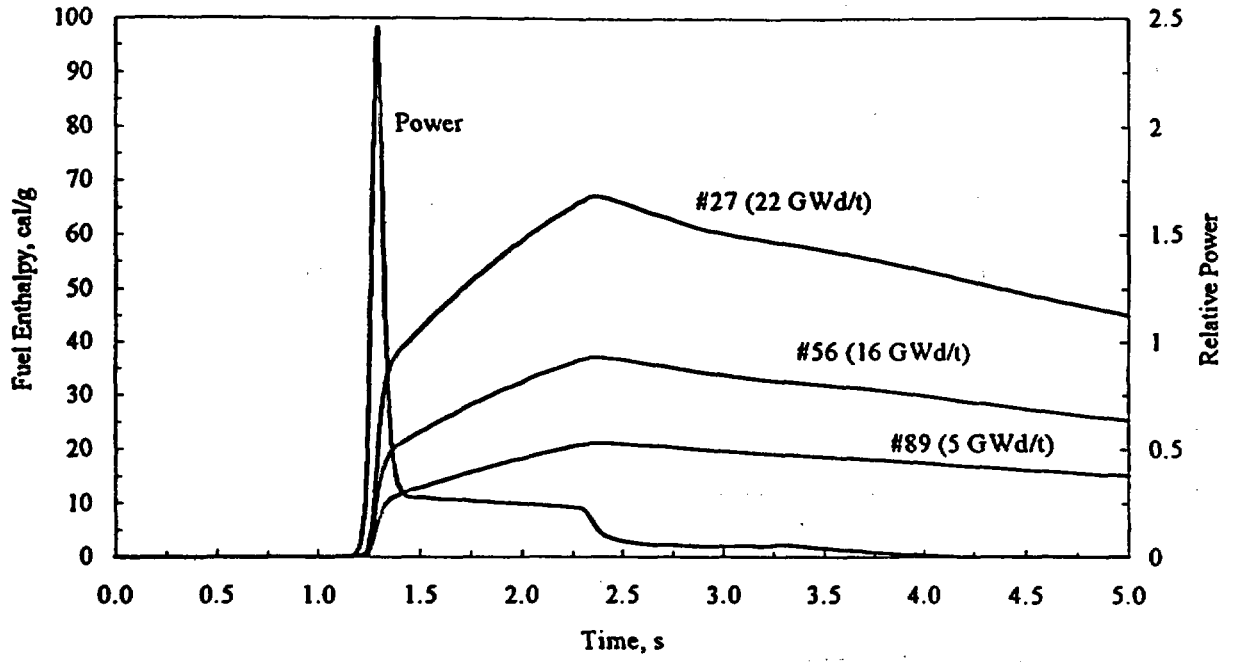

Figure 4 Maximum Fuel Bundle Enthalpy and Total Power During RDA (Medium Burnup Case)

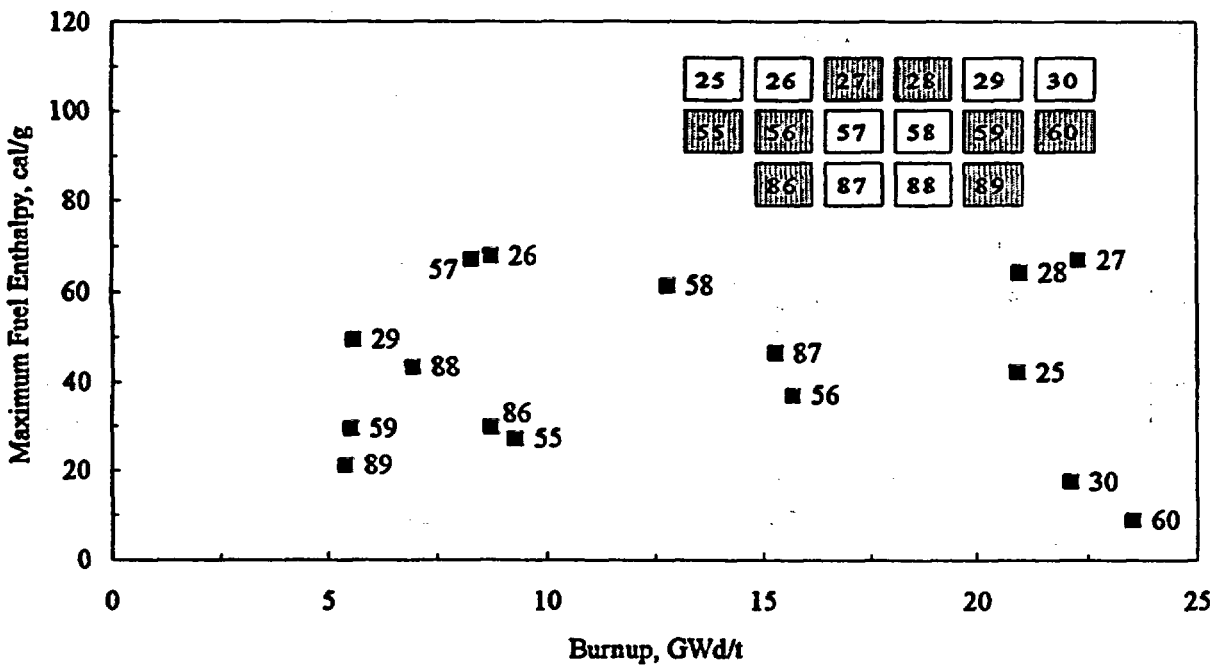

Figure 5 Maximum Fuel Bundle Enthalpy vs. Burnup (Medium Burnup Case)

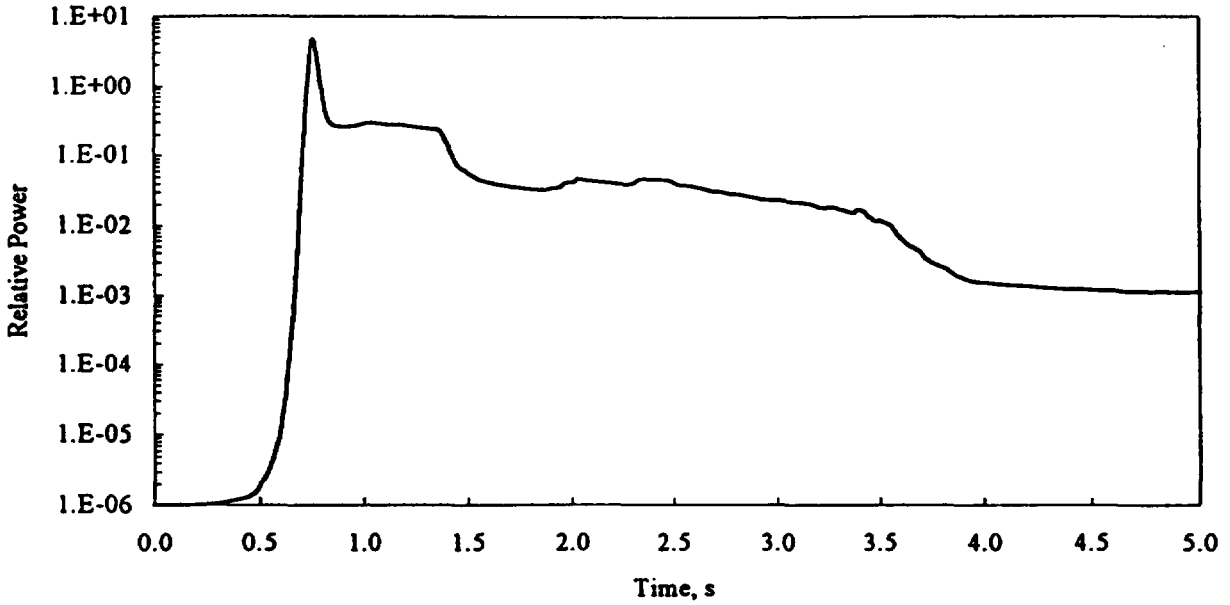

Figure 6 Power During RDA (Pseudo High Burnup Case)

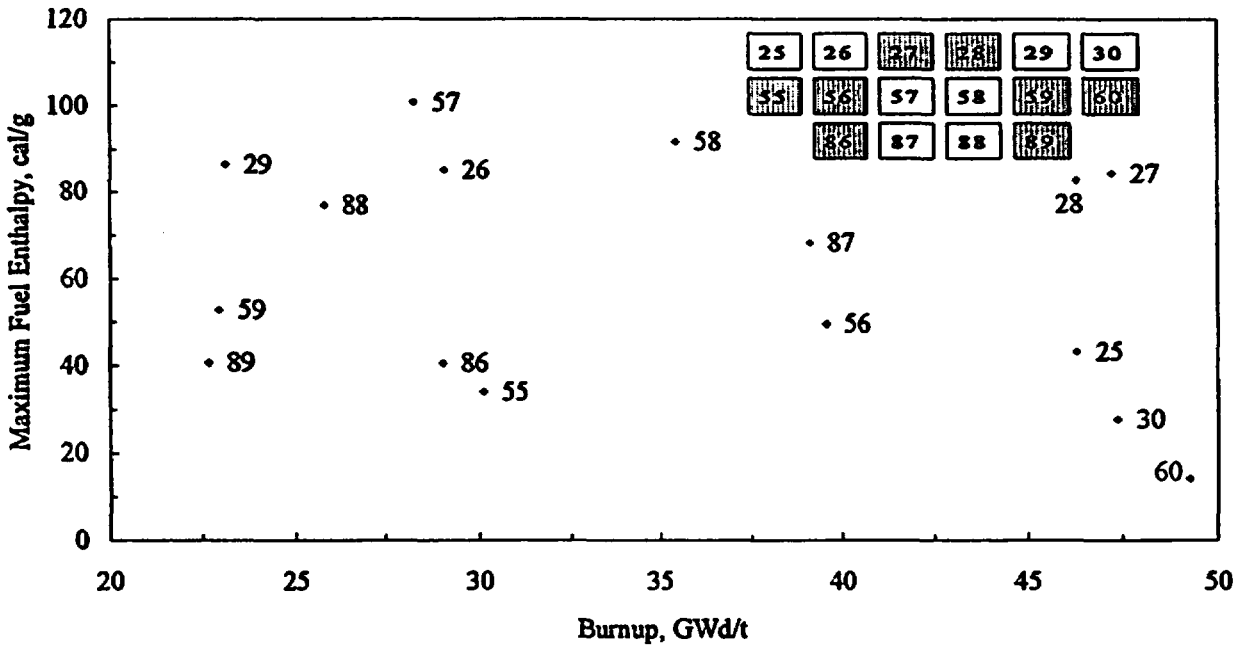

Figure 7 Maximum Fuel Bundle Enthalpy vs. Burnup (Pseudo High Burnup Case)

The results for maximum fuel enthalpy versus burnup are shown in Figure 7 for the bundles surrounding the position of the dropped rod. Again, there is no clear correlation between burnup and enthalpy, and the conclusions discussed above seem to apply here as well, i.e., that the enthalpy in any node depends on control rod worth, distance from the rod, and also on burnup. In this figure and in Figure 5 for the medium burnup core, only the axial node with the peak enthalpy has been considered for a given bundle. Since the bundle burnup will be higher at nodes that are closer to the center of the core, if these additional nodes were added to the plot, they would show points at higher burnup and lower fuel enthalpy relative to each of the points on the present plot. This would tend to create more points on the graph to the right and down from existing points. However, the nodes further away from the center (e.g., nodes 23 and 24) would have lower enthalpy and lower burnup adding points to the left and down from the existing points. These additional axial points would, therefore, not be expected to reveal any trends and would not negate the possibility of relatively high enthalpy in a high burnup node if it were close to a high worth dropped control rod.

Sources of Uncertainty in RDA Analysis

There are two general sources of uncertainty: (1) the methodology and (2) the assumptions used to define the reactor state. The methodology consists of the computer models and the values of the neutronic and thermal-hydraulic parameters that are used in those models. The validation of computer codes for application to the rod drop accident has always been a difficult matter. Since there have never been any rod drop accidents in a BWR, no data exists to directly assess the uncertainty in the calculated fuel enthalpy during a rod drop accident. Instead, the approach in the past has been to generally validate the computer codes and then to use a conservative approach to determine the margin to the acceptance limits for the rod drop accident. The conservative approach biases the assumptions used to define the reactor state so that the calculated peak fuel enthalpy is maximized.

Although this has been an adequate practice in the past, it will be important in the future to provide an estimate of uncertainty if either the margin between expected fuel failure and calculated fuel enthalpy becomes much smaller than is currently the case or if calculations are done using a best-estimate approach rather than a conservative approach. It will then be important to know the sources of important uncertainties within the models and what impact these have on the uncertainty in fuel enthalpy in a given bundle.

One source of uncertainty is due to the "rim" effect in high burnup fuel. In general, the power distribution through a pellet is peaked at the surface due to self-shielding. This causes the plutonium concentration to grow at the surface. This effect accelerates with time so that the power and the plutonium distributions become highly peaked in a small region at the rim [see, for example, (Lassmann, 1994)]. Reactor physics models that generate cross sections make assumptions about the temperature and power distributions across the pellet. With the rim effect, these assumptions may not be as valid, and the uncertainty in results may increase. In addition, the uncertainty may increase due to the need to include more actinides in the models.

The change in composition with burnup influences the thermal properties of the pellet. The rim effect introduces a spatial distribution of properties that may become important. Furthermore, the uncertainty in calculations may increase with heat conduction models that do not account for the peaked spatial distribution of energy deposition in the pellet.

Two physics properties that may become more important with high burnup are the effect of the delayed neutron fraction (β) and moderator temperature feedback. The power excursion during an RDA is made worse when the delayed neutron fraction becomes smaller. The delayed neutron fraction decreases with burnup, and the ideal model would allow for the spatial distribution of β to account for the burnup throughout the core.

The moderator temperature feedback is positive when the moderator is relatively cold. The effect is made worse if there is significant subcooling. Again, the effect becomes stronger with burnup, i.e., it is more important to model the effect for high burnup cores. This effect was somewhat quantified by redoing the calculation of the RDA for the medium burnup core with no moderator temperature feedback. The elimination of moderator temperature feedback had no significant effect on the initial power pulse and fuel enthalpy increase, but it did decrease the maximum enthalpy by approximately 5 cal/g. Since the moderator temperature reactivity coefficient is linear in the burnup range from 22 GWd/t (the burnup of the node with maximum enthalpy) to a high burnup value of 66 GWd/t, it is reasonable to expect that the effect may be on the order of three times as large or 15 cal/g for high burnup fuel. If the amount of subcooling is less than the value of 70°C used in this study, then the effect is reduced.

Several other sources of uncertainty have been discussed above in the context of the assumptions used to model the initial conditions. The assumed initial control rod pattern (and the core design) determines the rod worth. The assumed initial thermal-hydraulic conditions determine the moderator feedback and the timing of negative void feedback. In a best-estimate calculation, it is necessary to take into account the withdrawal sequence being used at a particular plant, the possibility of an error in that withdrawal, the presence of out-of-service rods, and the thermal-hydraulic conditions which correspond to a particular time during the withdrawal sequence. It is difficult to find a single worst initial condition because the highest worth rod may not lead to the most limiting fuel enthalpy if the acceptance criterion is based on burnup. Nevertheless, it should be possible to identify the leading contenders for worst initial condition so that only a few of the hundreds of theoretically possible accident situations would have to be calculated.

Another source of uncertainty is the bundle power peaking factor which is used to calculate maximum fuel rod enthalpy given the maximum bundle-average fuel enthalpy at a particular axial position. It is necessary to use this factor because most transient analysis is done with computer codes that model the bundle as an homogenized region. The peaking factor is an approximate means of accounting for the power distribution in the bundle and is straightforward to use to calculate the maximum fuel enthalpy in the bundle. Typically, this peaking factor is taken from a single-bundle calculation which assumes an infinite array of uncontrolled bundles. This does not account for the actual environment of the bundle which might sustain a large power gradient due to the particular control rod pattern. In order to account for the local power peaking more accurately, it is possible to either use a transient calculation with a model for fuel rod power reconstruction, or a

supplemental steady-state calculation of rod-by-rod power that accounts for the actual reactor control rod configuration during the RDA.

ANALYSIS OF THERMAL-HYDRAULIC TRANSIENTS

Calculations were carried out with the medium burnup model for a transient initiated by closure of the main steam isolation valves (MSIVs). The transient started from full power with all rods withdrawn. The MSIVs took four seconds to close. The event was calculated for the first five seconds following the beginning of MSIV closure. By the end of this period, the reactor was scrammed and was cooling down.

The MSIV closure causes pressure to increase and reach the level of the safety/relief valve setpoints, thus reversing the system pressure surge. The pressure rise is responsible for a decrease in void fraction and an increase in fission power. The void fraction keeps decreasing even after the pressure surge is over because of a decrease in thermal power. The control rods start to move into the core at approximately 1.1 seconds, and the recirculation pump trips on a high system pressure signal at about 3.4 seconds. The transient is driven by two competing feedbacks: void and scram. The moderator and fuel temperature (Doppler) effects are of minor importance in this transient.

Figure 8 shows the calculated history of maximum fuel enthalpy in the core. The peak increase over the duration of the transient is approximately 13 cal/g. The graph also shows the maximum and average fuel temperature during the transient.

The failure of the recirculation flow controller is the transient with the potential for causing the highest fuel enthalpy increase. This transient is caused by an increase in flow rate leading to the insertion of positive void reactivity when the void fraction decreases. In order to have a large increase in flow rate, it is necessary to start this transient from a flow rate considerably below nominal conditions. The starting point was, therefore, at a power 68 percent of nominal and a flow 50 percent of nominal. All control rods were out of the core simulating moving down a line of constant control rod density on the power-flow map from the operating condition corresponding to full power. Although there are various procedures defining the reactor trip setpoint on high neutron flux depending on the flow rate, the setpoint in the present calculation was a conservative 120 percent of rated power.

The core inlet flow history emulated the transient conditions found in a BWR/4 Safety Analysis Report. One of the two recirculation pumps was ramped to rated level from the initial conditions. At the end of the transient (2 s), the core inlet flow rate was approximately 70 percent of nominal.

As the core inlet flow increased, the core void fraction dropped leading to positive void reactivity insertion. At 1.35 seconds, negative reactivity due to scram, together with the negative fuel temperature reactivity, starts to reverse the power surge. Figure 9 shows that the maximum fuel enthalpy during this transient starts at 47.5 cal/g and increases approximately 3 cal/g. However, the initial enthalpy at the location where it is a maximum

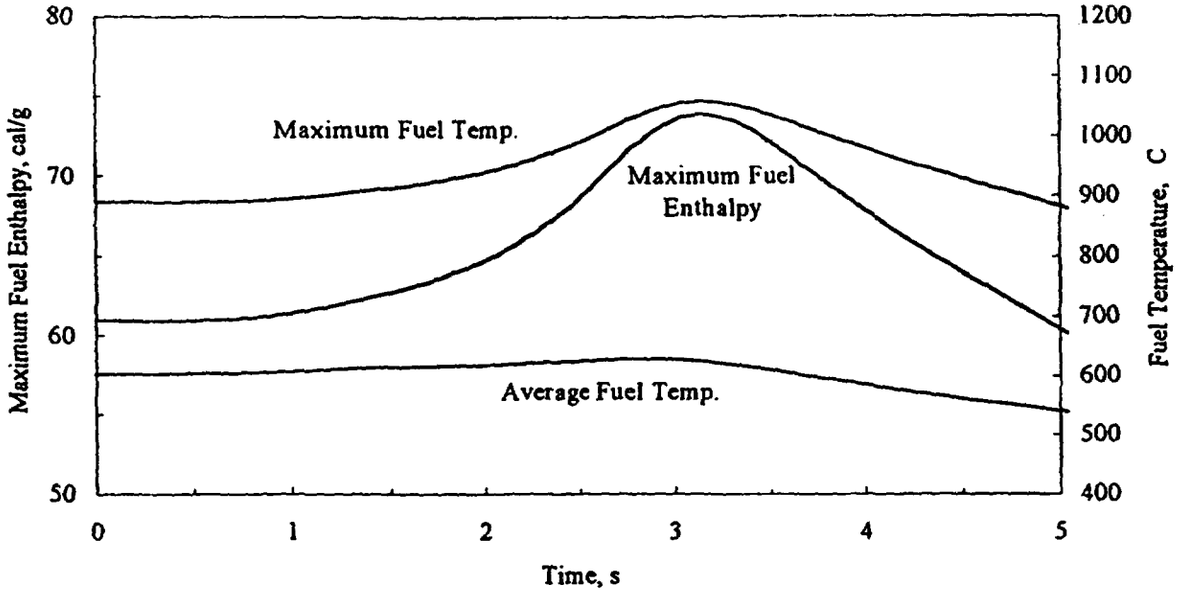

Figure 8 Fuel Enthalpy and Temperature During MSIV Closure Event

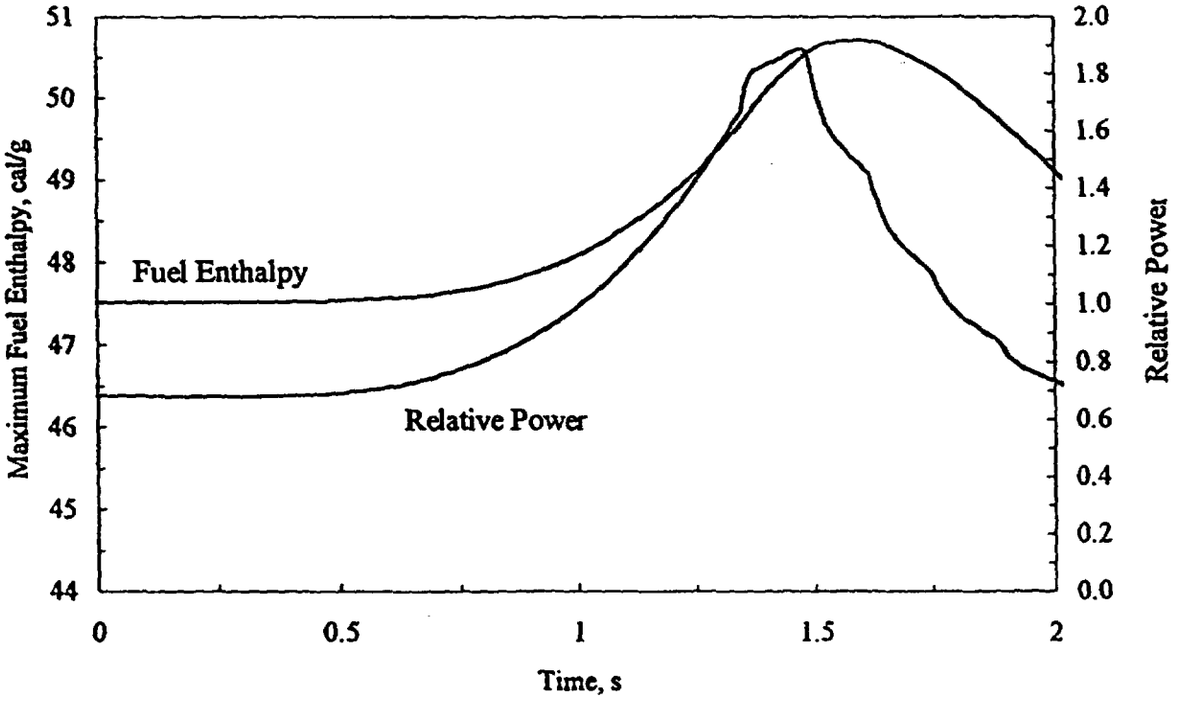

Figure 9 Power and Fuel Enthalpy During Recirculation Flow Transient

during the transient was approximately 20 percent less than the maximum. Hence, the increase in fuel enthalpy during this event is approximately 12 cal/g, which is comparable to that found for the overpressurization transient considered above.

REFERENCES

Ahlin, A. and M. Edenius, "The Collision Probability Module, EPRI-CPM," Advanced Recycle Methodology Program System Documentation, Part II, Chapter 6, Electric Power Research Institute, November 1975.

Ahlin, A., M. Edenius, and H. Häggblom, "CASMO: A Fuel Assembly Burnup Program," AE-RF-76-4158 (Rev Ed), Studsvik Energiteknik AB, June 1978.

Lassmann, K., et al., "The Radial Distribution of Plutonium in High Burnup UO_2 Fuels," *J. of Nuclear Materials, 208,* p. 223, 1994.

Paone, C. J., "Banked Position Withdrawal Sequence," NEDO-21231, General Electric Co., January 1977.

U. S. Nuclear Regulatory Commission, "Reactivity Insertion Transient and Accident Limits for High Burnup Fuel," NRC Information Notice 94-64, August 31, 1994.

U. S. Nuclear Regulatory Commission, "Reactivity Insertion Transient and Accident Limits for High Burnup Fuel," NRC Information Notice 94-64, Supplement 1, April 6, 1995.

Wulff, W., et al., "A Description and Assessment of RAMONA-3B MOD.0 Cycle 4: A Computer Code With Three-Dimensional Neutron Kinetics for BWR System Transients," NUREG/CR-3664, Brookhaven National Laboratory, January 1984.

REVIEW OF HALDEN REACTOR PROJECT HIGH BURNUP FUEL DATA THAT CAN BE USED IN SAFETY ANALYSES

W. Wiesenack

Institutt for Energiteknikk

OECD Halden Reactor Project, Norway

23rd Water Reactor Safety Information Meeting

Bethesda, Maryland, USA

23 - 25 October, 1995

ABSTRACT

The fuels and materials testing programmes carried out at the OECD Halden Reactor Project are aimed at providing data in support of a mechanistic understanding of phenomena, especially as related to high burnup fuel. The investigations are focused on identifying long term property changes, and irradiation techniques and instrumentation have been developed over the years which enable to assess fuel behaviour and properties in-pile.

The fuel-cladding gap has an influence on both thermal and mechanical behaviour. Improved gap conductance due to gap closure at high exposure is observed even in the case of a strong contamination with released fission gas. On the other hand, pellet-cladding mechanical interaction, which is measured with cladding elongation detectors and diameter gauges, is re-established after a phase with less interaction and is increasing. These developments are exemplified with data showing changes of fuel temperature, hydraulic diameter and cladding elongation with burnup.

Fuel swelling and cladding primary and secondary creep have been successfully measured in-pile. They provide data for, e.g., the possible cladding lift-off to be accounted for at high burnup.

Fuel conductivity degradation is observed as a gradual temperature increase with burnup. This affects stored heat, fission gas release and temperature dependent fuel behaviour in general.

The Halden Project's data base on fission gas release shows that the phenomenon is associated with an accumulation of gas atoms at the grain boundaries to a critical concentration before appreciable release occurs. This is accompanied by an increase of the surface-to-volume ratio measured in-pile in gas flow experiments. A typical observation at high burnup is also that a burst release of fission gas may occur during a power decrease.

Gas flow and pressure equilibration experiments have shown that axial communication is severely restricted at high burnup. Therefore gas in fuel cracks and the gap cannot easily escape to the plena, and fill gas flow from the plena to a ballooning spot may be impeded.

1. INTRODUCTION

Safe and economic nuclear power generation requires a fundamental knowledge of fuel behaviour in different situations. The research programmes carried out at the OECD Halden Reactor Project have for more than thirty years addressed areas of particular interest to the nuclear community and provided significant contributions to the understanding of LWR fuel behaviour. From the beginning, fuel performance and reliability investigations were supported by the development and perfection of in-core rod instruments. The measurement capabilities are expanded through development of experimental rig and loop systems where reactor fuel and material can be tested under light water reactor conditions, including prototypic PWR and BWR water chemistries.

Fuels testing at the Halden Project has for a number of years focused on implications of extended burnup operation schemes aimed at an improved fuel cycle economy. The experimental programmes are therefore set up to identify long term property changes with an impact on performance and safety. The data generated in the Halden Project fuels testing programmes originate from in-pile sensors which allow to assess

- fuel centre temperature and thermal property changes as function of burnup;
- fission gas release as function of power, operational mode and burnup;
- fuel swelling as affected by solid and gaseous fission products;
- pellet - cladding interaction manifested by axial and diametral deformations.

Investigations of fuel performance parameters, especially at high burnup, have to deal with a number of experimental problems, i.e. the time required for burnup accumulation, the demand on instrumentation to function reliably for the long time of in-core service, and the need for a separation of an increasing number of phenomena. The Halden Project has developed and applied techniques which make it possible to obtain reliable data for all relevant burnups, from beginning-of-life to ultra high exposure reaching 100 MWd/kgUO_2. Among these are rod designs simulating high burnup effects such as closed gap and fill gas contamination with fission gas, accelerated burnup accumulation, and the re-instrumentation of pre-irradiated fuel segments [1, 2].

The irradiation of instrumented fuel rods can be carried out in specialised rigs according to test objectives, e.g. long term base irradiation, diameter measurements or ramps and overpower testing. The *gas flow* rig allows the exchange of fuel rod fill gas during operation which makes it possible to determine gas communication properties as well as the gap thermal resistance and its influence on fuel temperatures. It is also possible to analyse swept out fission products for assessment of structural changes and fission gas release. This is an important experimental technique for the high burnup programmes currently being executed.

The paper presents in-core data and findings on effects which relate to behaviour of high burnup fuel. The results, which encompass both thermal and mechanical data from the Halden Project's experimental programme, can be used for fuel behaviour model development and verification and safety analyses.

2. PELLET - CLADDING GAP

Standard fuel designs employ a gap between pellet and cladding of about 2% of the pellet diameter (150 - 250 μm) to accommodate thermal expansion and fuel swelling. A good knowledge of gap size and its change with burnup is essential for prediction of both thermal and mechanical behaviour. An underestimation of gap conductance at high burnup will lead to overprediction of fuel temperatures (stored energy) and fission gas release and may thus severely impact safety assessments.

Gap closure due to fuel swelling

The closing of the gap with burnup can be observed in many ways. A particular technique is the determination of the "hydraulic diameter" from the flow of gas (0.5 - 1.0 l/min) through the gap, driven by a pressure difference of 20 - 60 bar. Fig. 1 shows the development with burnup averaged for three rods of identical design (200 μm as fabricated diametral gap). After an initial drop, the decrease follows solid fission products fuel swelling. At high burnup, the gap seems to approach a minimum value, indicating that pellet-cladding contact restricts a further diameter increase; rather, the fuel may comply with closing cracks and creep. The gap at power is closed at about 30 kW/m at a burnup of 50 MWd/kg UO_2.

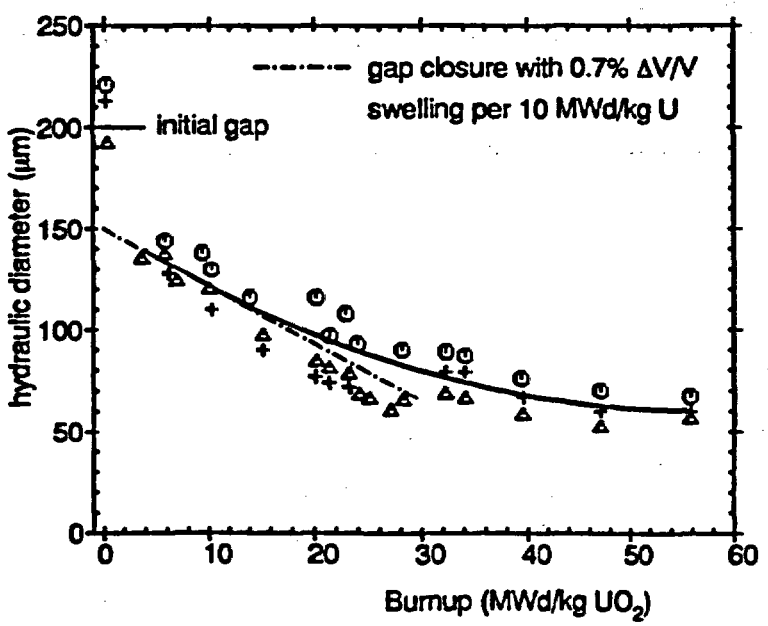

Fig. 1

Gap closure determined with hydraulic diameter measurements. After an initial decrease due to pellet fragment relocation, the gap closes with fuel swelling.

Influence on thermal behaviour and change with burnup

The determination of gap conductance at high burnup is affected with uncertainties which accumulate throughout irradiation. The problem can be alleviated by using - for experimental purposes - rod designs with small gaps (simulated gap closure) and Xe fill gas (simulated fission gas release). This has been applied in a large number of fuel tests at the Halden Project. A summary of the influence of gap size and fill gas type on fuel centre temperature determined in this way is shown in Fig. 2. The data represent the starting conditions where the gap size is not yet changed and uncertain due to fuel densification. As-fabricated diametral gaps ranged from 50 to 230 μm for Xe filled rods and 50 to 400 μm for He filled rods.

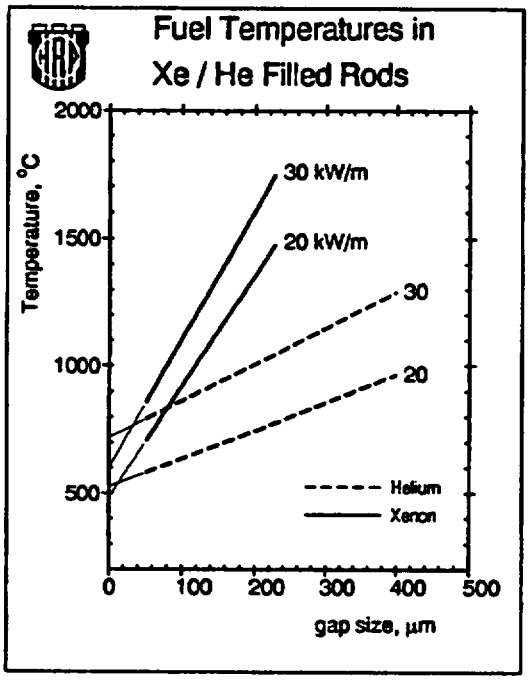

Fig. 2: Typical fuel centre temperatures in He/Xe filled rods. Differences disappear with tightly closed gap.

It is of interest to note that the temperature difference between helium and xenon filled rods disappears at small initial gaps which are strongly closed at power. This implies that gap conductance is dominated by solid-solid contact conductance in this situation. Consequently, a gap conductance model should not retain a minimum separation between pellet and cladding due to roughness and waviness in the case of very hard contact. A similar conclusion was reached in [3, 4]. Also results recently obtained with high burnup fuel confirm this point.

The improved gap conductance as a consequence of gap closure due to fuel swelling can also be observed in-pile as function of burnup. An example is given in Fig. 3, again for a Xe filled rod where improved gap conductance supersedes fuel conductivity degradation, resulting in an overall temperature decrease after the initial densification phase.

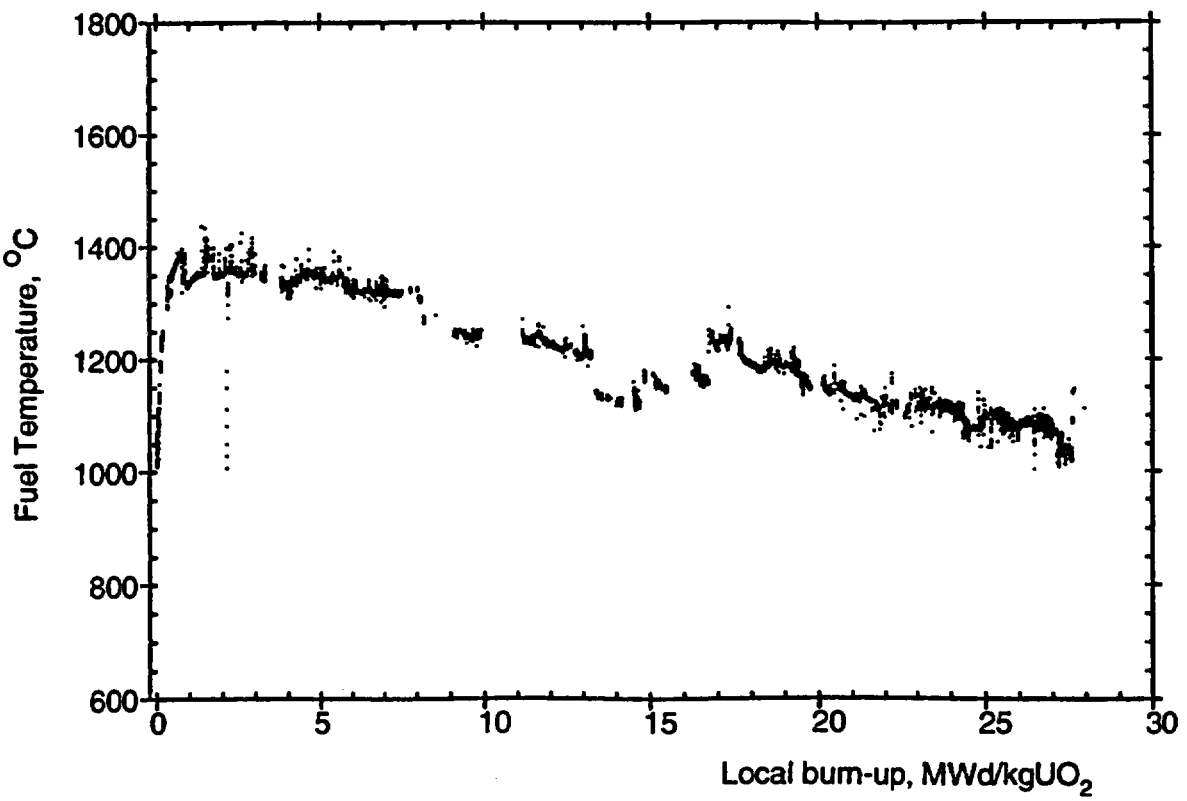

Fig. 3: Fuel centre temperatures at 25 kW/m in a Xe filled rod with 100 µm as fabricated gap. The gap conductance improvement due to gap closure outweighs fuel conductivity degradation.

Mechanical interaction

Pellet-clad mechanical interaction (PCMI) can be measured in-pile in two ways: with a diameter gauge moving along the length of a rod, and with a cladding elongation detector. Since axial elongation can be measured more easily and frequently than diametral deformation, the data should not be neglected. However, the difficulties of modelling axial PCMI are recognised; they are probably the main reason why only few codes try to include the effect in a non-simplistic way.

Cladding elongation can also provide information on diametral deformation. The close relation between hoop strain and axial strain, both in terms of magnitude and relaxation behaviour, has been shown with Halden Project data comparing elongation and diameter changes obtained in-pile for the same rod [5].

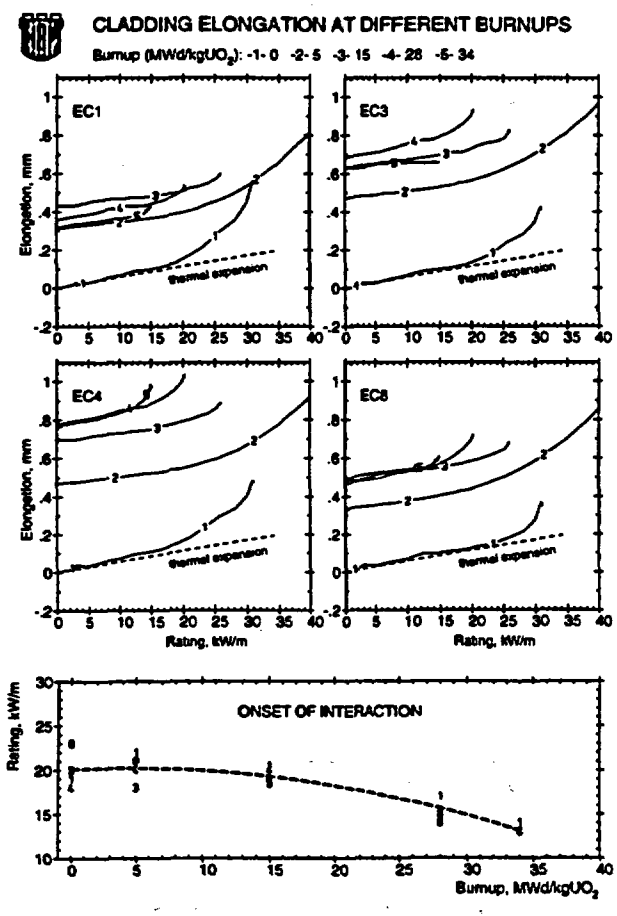

Fig. 4:
Cladding elongation of BWR fuel rods and change of interaction onset with burnup

The development of axial interaction with burnup for four similar rods (active length 768mm, pellet diameter 12.59mm, diametral gap 170μm) is shown in Fig. 4. It is a common experience that axial interaction during the first rise to power is strong and decreases during the following cycles. This can be attributed to random eccentric stacking of the pellets which are pushed to more central positions in contact with the cladding [6]. It should be noted that thermal expansion is not sufficient to close the gap at start-up (not even with fuel swelling at end of life, 34 MWd/kgUO_2), thus conventional models based on concentric geometry would not calculate any interaction, obviously at variance with the experimental evidence.

It is apparent that the onset of interaction (defined as point of deviation from free thermal expansion) moves to lower power with increasing burnup. There is also a change in curve shape to a more abrupt transition from free thermal expansion to expansion following fuel elongation. However, the interaction remained small in the examples because power in general did not exceed previously reached levels. As already discussed with the hydraulic diameter measurements, a kind of balance between fuel swelling and creep caused by contact forces seemed to have evolved. Since there is no gap left between fuel and cladding at power, a transient will lead to cladding load from the beginning.

3. DEGRADATION OF UO_2 THERMAL CONDUCTIVITY

Most fuel properties and phenomena are temperature dependent. An accurate description of the temperature distribution in a fuel rod is therefore required before other effects can be quantitatively defined. Conductivity degradation of UO_2 has been manifested both with simulated and in-reactor burnup [2, 7, 8, 9] and is now generally accepted as an important phenomenon to be considered in modelling of high burnup fuel behaviour. There is a general consensus that the effect is due to increased phonon scattering caused by the accumulation of fission products. The Halden Project's fuel testing programme contains a number of experiments where temperature measurements allow the conductivity degradation to be inferred. In general, increasing temperatures are observed in such tests, but the effect may be partly covered by improved gap conductance due to fuel swelling and gap closure (ref. Fig. 3). The temperature evolution in a dedicated test irradiated to very high burnup is shown in Fig. 5. The evaluation of this and other experiments points to a

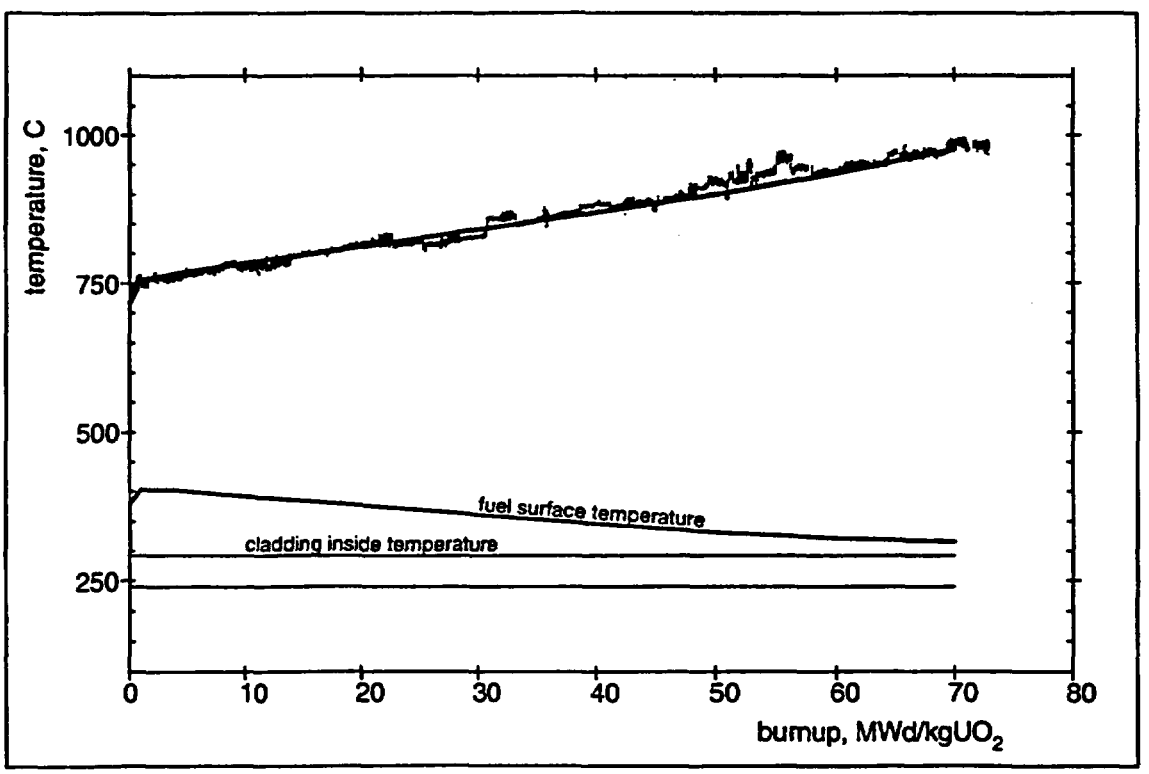

Fig. 5: Measured temperature increase due to fuel thermal conductivity degradation.

degradation factor of about b=3 (K·m/kW per MWd/kgUO_2) in the UO_2 conductivity term $\lambda_{phonon} = (a + b \cdot burnup + c \cdot T)^{-1}$. It should be noted that the constant "b" also accounts for other irradiation dependent effects which may have an influence on conductivity, i.e.microcracking, Frenkel defects and the formation of small fission gas bubbles. The constant "b" is therefore larger than obtained from out-of-pile tests with simulated burnup adding only solid fission products.

Together with gap conductance, the UO_2 thermal conductivity has an influence on the stored energy, the initial enthalpy of a hot-full-power RIA and the heat flow to the coolant after the energy deposition. Under normal (non-dryout) cooling conditions, the time constant of heat removal from the fuel can be obtained from the temperature decay following a reactor scram. An example is shown in Fig. 6 for a BWR type rod at three different burnups. An increase of the time constant due to conductivity degradation (no fission gas release) is apparent.

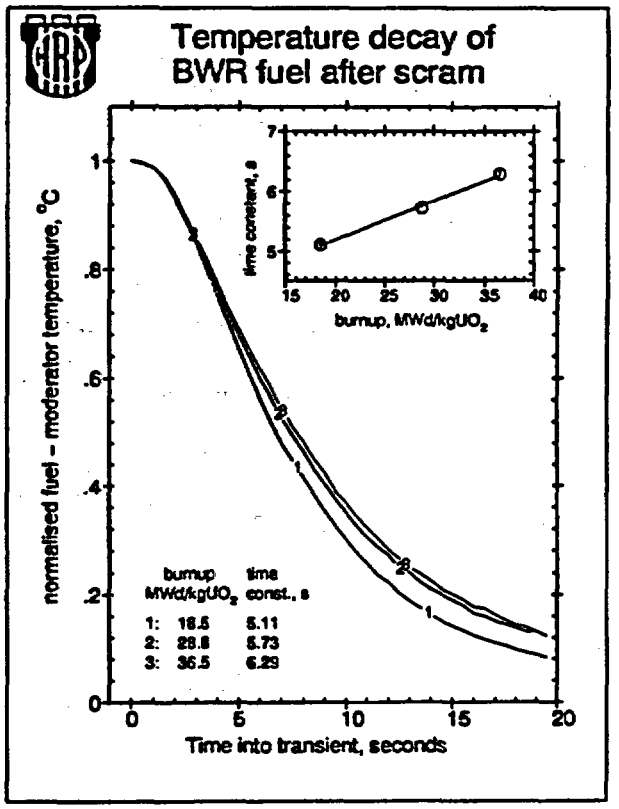

Fig. 6: Temperature decrease in BWR fuel after scrams at different burnups

4. FISSION GAS RELEASE

The release of fission gas from UO_2 fuel continues to be a subject of considerable interest. At high burnup, the release may lead to rod overpressure and become a life-limiting factor. The influence on fuel temperatures and stored energy via gap conductance has direct consequences for the assessment of core reliability and safety during normal operation and transients.

A possible enhancement of fission gas release with burnup has been reported in several publications [10, 11], but evidence for behaviour more "as expected" to burnups up to 50 MWd/kg UO_2 has also been presented [2, 12]. An enhancement can be associated with two effects: the formation of a porous rim with increasing athermal release, and higher fuel temperatures due to poorer conductivity of the rim as well as a general UO_2 conductivity degradation.

Fission gas release model

Fission gas release has been investigated extensively at the Halden Project using rods instrumented with pressure transducers and fuel centre thermocouples. A well known result from theses studies is the discovery of a temperature threshold for the onset of appreciable release (> 1%), [13]. The original empirical correlation covered burnups to 30 MWd/kg UO_2 and could later be explained with the formation of bubbles on the grain boundaries (e.g. [14]) and their interlinkage to a tunnel network providing a release path

to the open surface (the structural change is apparent as an increase of the fuel surface-to-volume ratio measured in gas flow experiments [7]). Using a Booth diffusion model together with a storage of gas at the grain boundaries up to a concentration limit of $5x10^{15}$/ cm^2 before release occurs, the empirical threshold could be well reproduced (for details of the model see [15]).

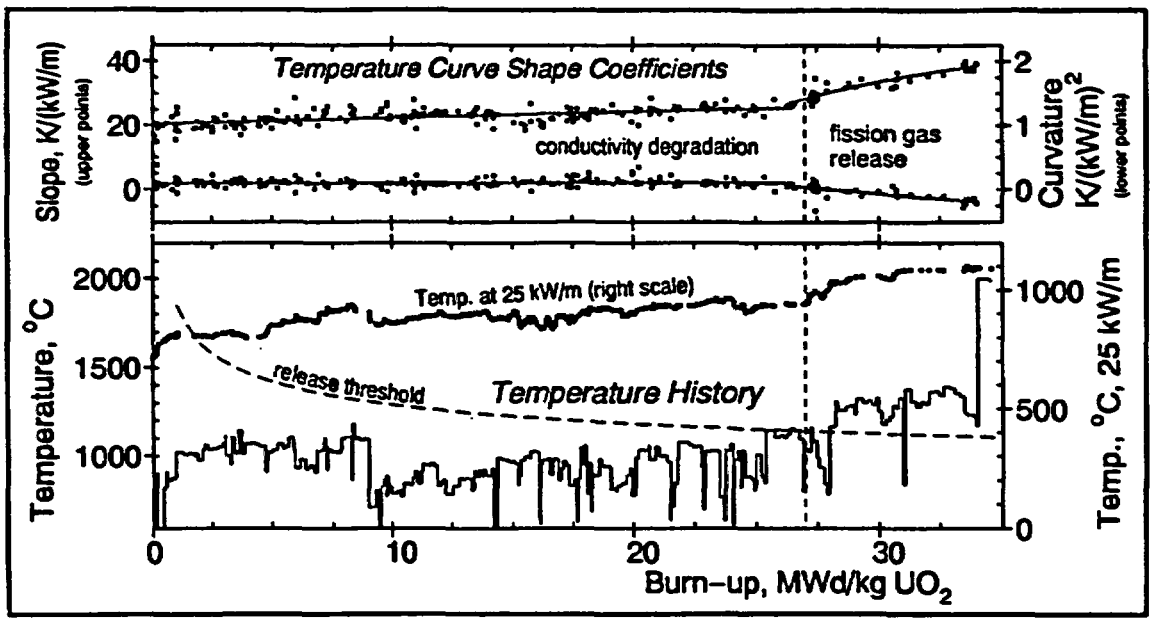

Fig. 7: Fission gas release after exceeding the release threshold temperature. Temperatures increase due to changed gap conductance.

The release threshold rule is quite accurate; see example shown in Fig. 7. The fuel rod was of short length (14 cm) with a thermocouple inserted such that a good knowledge of fuel temperature was available for the entire length. Release onset can be seen with its effect on temperature at around 27 MWd/kg UO_2 when the threshold was reached or exceeded for the first time. The temperature data reflect the gap contamination with fission gas in two respects: a) a temperature increase as seen from the curve of data normalised to a constant power of 25 kW/m, and b) a change of the shape of temperature-versus-power curves from slightly positive to negative curvature which is a characteristic difference between He and Xe filled rods. (This can also be used to distinguish between temperature increase due to conductivity degradation and due to fission gas release. The increase up to 27 MWd/kg UO_2 can be explained with the degradation coefficient indicated above.)

Release enhancement

The release model takes into account known effects with an influence on fuel temperatures such as conductivity degradation and gap closure, either by directly using measured temperatures or by applying best estimate correlations from the Halden Project's experimental programme. A release enhancement may therefore be defined as due to effects not accounted for by the model and apparent as a definite deviation from predictions.

The model described above has been applied to many experiments from the Halden reactor and gives good agreement with measurements especially when temperatures are known

(the fuel temperature is otherwise a major source of uncertainty due to the exponential dependence of the diffusion coefficient). An example is shown in Fig. 8; it can be seen that fission gas release as inferred from pressure measurements is well followed by the model to a burnup of 56 MWd/kg UO_2. During the last part of irradiation, a deviation becomes apparent which may be due to an effect not accounted for by the model. Although a pronounced rim development does not occur in the Halden reactor, it should be noted that the peak burnup (axial, radial) measured in MWd/kgU has reached about 70 at the point of deviation. This number is now regarded as the lower limit for rim structure formation.

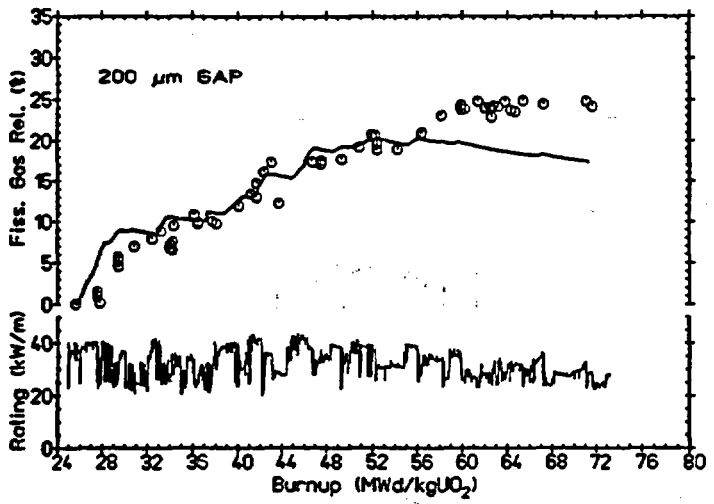

Fig. 8:
Fission gas release as measured with in-core pressure transducer and predicted by the model. The deviation at high burnup may be due to a release enhancement effect not accounted for by the model.

Another application of the release model is shown in Fig. 9. Fission gas release (about 2%) is calculated for a period with high temperatures early in life, followed by little further release as also shown by the pressure measurements. A definite change of slope of the pressure versus burnup curve occurs at about 58 MWd/kg UO_2. The release continues despite decreasing temperatures during the last part of irradiation.

The total release as deduced from the pressure change is still small in this case (about 4%), and an appreciable amount of fission gas must be stored on the grain boundaries. Especially at lower temperatures, the gas atoms will remain segregated and lead to a grain boundary embrittlement. It can be expected that this has a bearing on transient fuel behaviour. The same may be true for not yet interlinked bubbles on the grain boundaries.

Burst release during power decrease

Steps of pressure increase coinciding with reactor shut-downs can be noted in the high burnup part of Fig. 10, see indication at 65 MWd/kgUO_2. This is detailed in Fig. 10 where pressure is shown as function of rod power for a period of start-up, 12 days at power and shut-down. The entire pressure increase occurs during power decrease and is finished at 10 kW/m. This behaviour has also been observed in other experiments and is associated with the propensity of the fuel to release fission gas together with a small residual gap due to fuel swelling and/or thermal expansion. Both effects increase with increasing burnup.

It can be assumed that the gas was released to the interlinkage network of gain boundary bubbles during the steady state period, but could not escape to the gap and the plenum. With decreasing power, old and new cracks open and allow the gas to escape. This accumulation of fission gas already at high pressure may have an influence on transient behaviour (increased mechanical load) when a transient starts from high power.

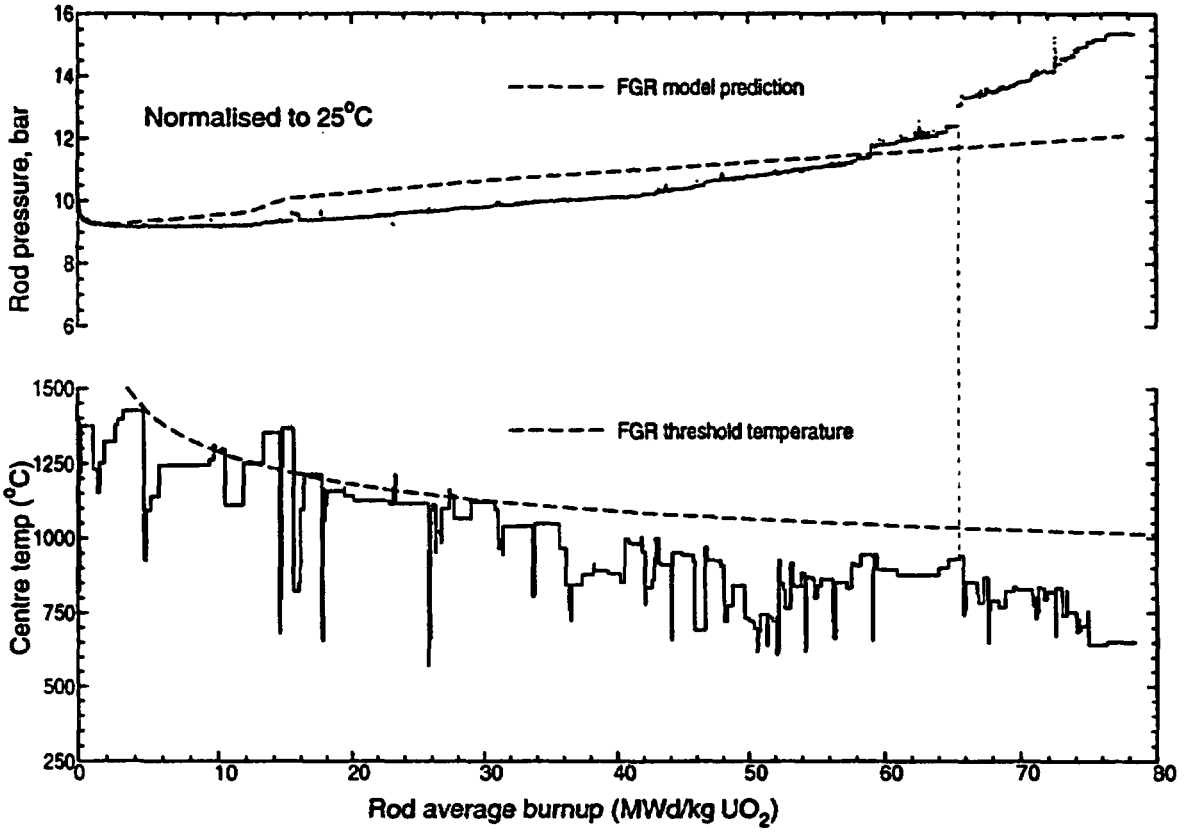

Fig. 9: Pressure increase due to fuel swelling and fission gas release in a rod irradiated to high burnup. Model predictions deviate more pronounced for exposure >58 MWd/kgUO$_2$.

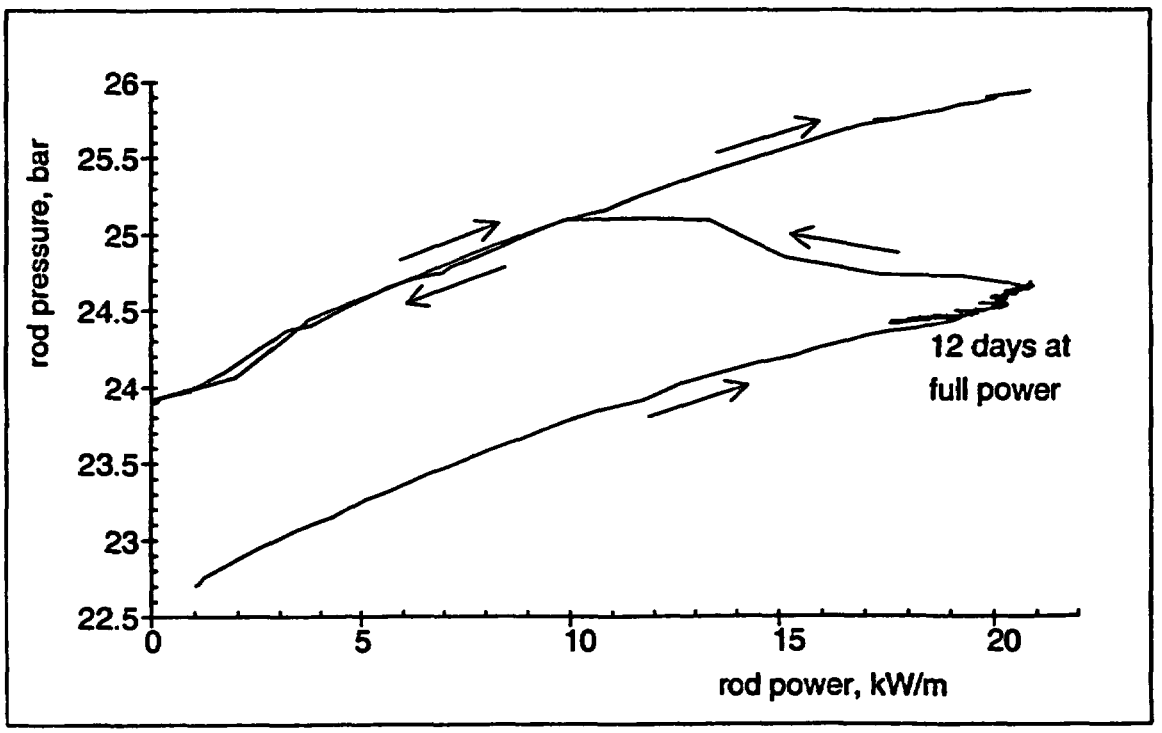

Fig. 10: Burst release of trapped fission gas during power decrease at 65 MWd/kgUO$_2$.

5. CLADDING CREEP REVERSAL (ROD OVERPRESSURE)

Fission gas release at high burnup may result in the rod pressure exceeding the coolant pressure. A creep-out of the cladding may then open the fuel-cladding gap and lead to increasing fuel temperatures and further, increased fission gas release. In order to assess the consequences to fuel integrity, the creep characteristics of cladding material must be known.

Cladding creep data at high fluence in the presence of neutron flux were produced in the Halden reactor under representative LWR conditions in a diameter measurement rig. A gas line connected to the cladding tube enabled to change the rod inner pressure. In this way, several stress reversals were produced, and the cladding creep was measured in-pile by a diameter gauge with a relative precision of ±2 μm. The test matrix encompassed both BWR and PWR tubes.

Unlike PIE which only provides a single point, the results obtained show in a unique manner the development from primary to secondary creep. A typical reaction to stress reversal is shown in Fig. 11. BWR cladding material pre-irradiated to a fast neutron fluence of $6x10^{21}$ n/cm^2 (> 1 MeV) was used in this case. These data are used by Halden Project participants for modelling the creep-out behaviour at high burnup as consequence of rod overpressure. A complementary test, in which a pre-irradiated PWR rod equipped with a fuel centreline thermocouple will be subjected to rod overpressure, is in preparation for execution in 1996. The objective is to determine the pressure beyond which fuel temperature will increase as a consequence of clad creep-out.

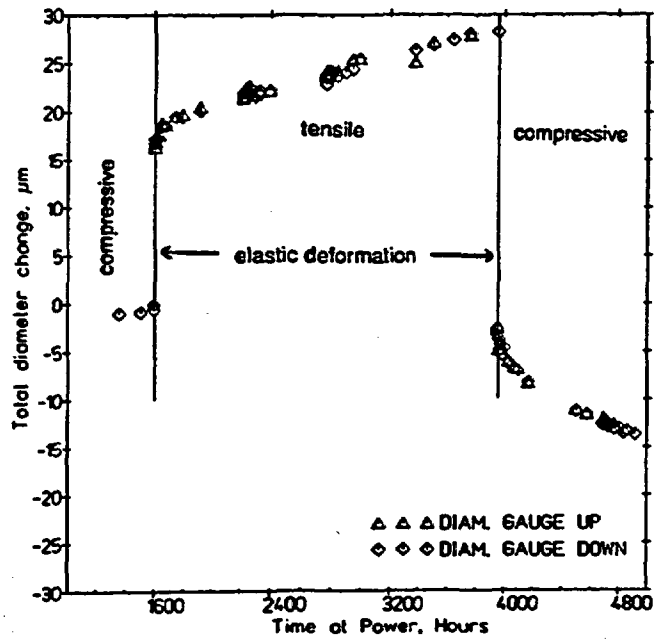

Fig. 11: Measured in-pile diameter increase for a BWR cladding tube subjected to stress reversal.

6. GAS TRANSPORT THROUGH THE GAP

The data on hydraulic diameter measurements, cladding elongation and fission gas release presented in the previous sections have given evidence for a closed gap at high burnup. Gas transport through the gap is severely restricted in this case. Pressure equilibration experiments have shown that flow driven by a pressure difference of 30 bar may be as low as 60 cm^3/h, decreasing approximately with ΔP^2. An example is shown in Fig. 12. This information is relevant for assessment of situations where gas transport (diffusion or driven by a pressure difference) plays a role, e.g. mixing of released fission gas with the gas in the plenum, ballooning during a LOCA, secondary fuel failure degradation and, possibly during RIA, the pressure exerted by gas heated up in the rim.

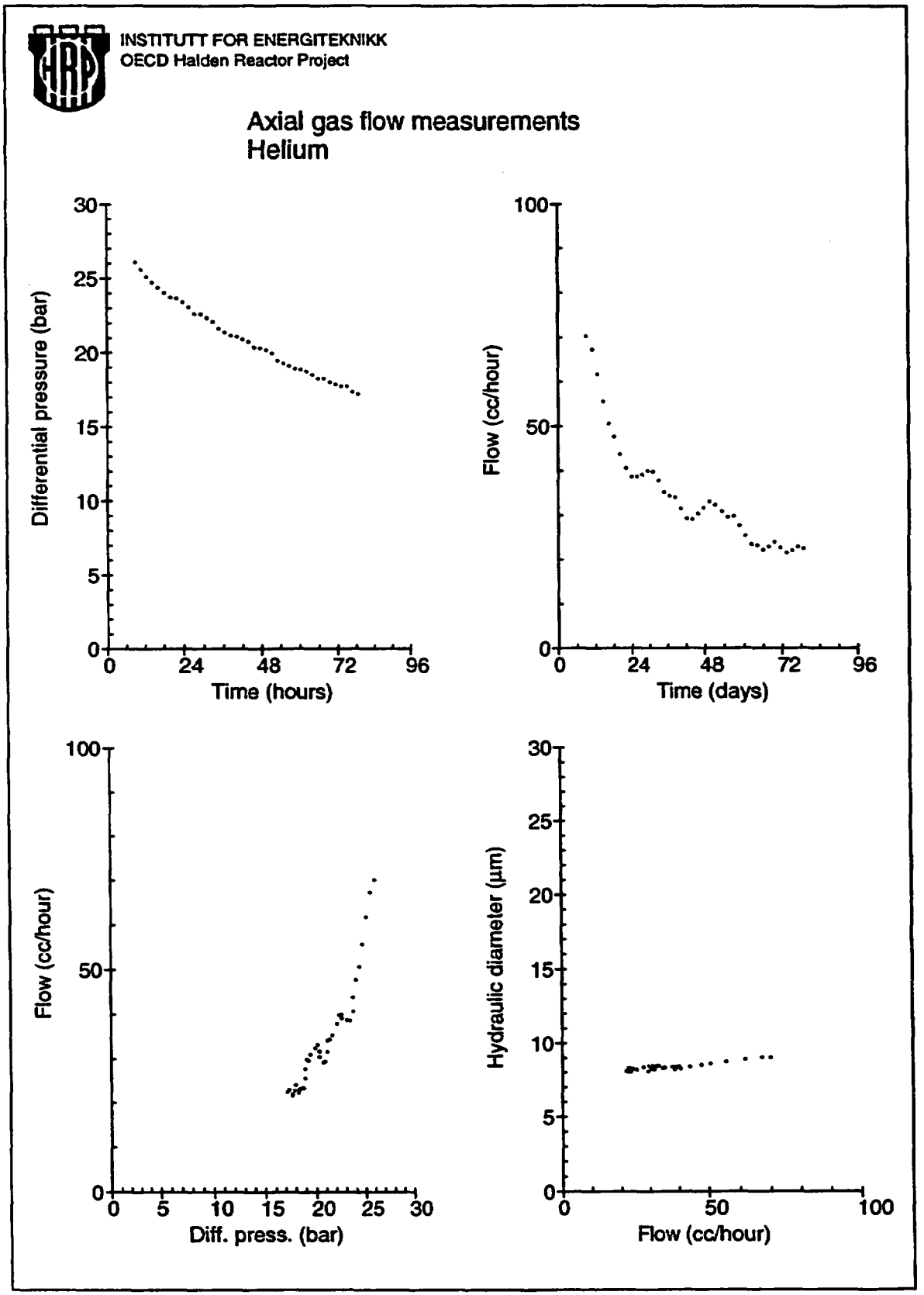

Fig. 12: Gas flow through a fuel rod with closed gap at hot conditions.

7. REFERENCES

[1] *O. Aarrestad:* Fuel Rod Instrumentation; IAEA meeting on "In-core Instrumentation and In-situ Measurements in Connection with Fuel Behaviour", Petten, NL, 1992

[2] *W. Wiesenack:* Experimental techniques and results related to high burnup investigations at the OECD Halden Reactor Project; IAEA Technical Committee Meeting on fission gas release and fuel-rod chemistry related to extended burnup (IAEA-TECDOC-697), Pembroke, Canada, 1992

[3] *D. A. Wesley, M. M. Yovanovich:* A new gaseous gap conductance relationship; Nuclear Technology vol. 72, 1986

[4] *F. Sontheimer, R. Eberle:* Evaluation of IFA-562.1 roughness rig data to improve modelling of pellet-to-clad heat conductance in tight gap/high fission gas release situations; EHPGM Storefjell, 1993

[5] *K. O. Vilpponen:* In-pile measurements of pellet cladding interaction and relaxation; IAEA specialists meeting on "Fuel Element Performance Computer Modelling", Blackpool, 1980

[6] *W. Wiesenack:* Zur Behandlung der axialen Wechselwirkung zwischen Brennstoff und Hülle in einem integralen Stabprogramm unter Berücksichtigung verschiedener Randbedingungen; Jahrestagung Kerntechnik, Berlin 1983

[7] *E. Kolstad, C. Vitanza:* Fuel rod and core materials investigations related to LWR extended burnup operation; Journal of Nuclear Materials 188 (1992), pp 104-112

[8] *P. G. Lucuta, R. A. Verrall, H. Matzke, I. J. Hastings:* Thermal conductivity and gas release from SIMFUEL; IAEA Technical Committee Meeting on fission gas release and fuel-rod chemistry related to extended burnup (IAEA-TECDOC-697), Pembroke, Canada, 1992

[9] *W. Wiesenack:* Data for FUMEX: Results from fuel behaviour studies at the OECD Halden Reactor Project for model validation and development; IAEA technical committee meeting on water reactor fuel element modelling at high burnup and its experimental support, Windermere, UK, September 1994

[10] *R. Manzel, R. Eberle:* Fission gas release at high burnup and the influence of the pellet rim; International topical meeting on LWR fuel performance, Avignon, France, 1991.

[11] *C. Forat et al.:* Fission gas release enhancement at extended burnup: experimental evidence from French PWR irradiation; IAEA Technical Committee Meeting on fission gas release and fuel-rod chemistry related to extended burnup (IAEA-TECDOC-697), Pembroke, 1992

[12] *P. Knudsen, C. Bagger, M. Mogensen, H. Toftegaard:* Fission gas release and fuel temperature during power transients in water reactor fuel at extended burnup; ibid

[13] *C. Vitanza, E. Kolstad, U. Graziani:* Fission gas release from UO_2 fuel at high burnup; ANS topical meeting on light water reactor fuel performance, Portland 1979

[14] *F. Sontheimer, R. Manzel, H. Stehle;* Journal of Nuclear Materials, 160 (1984).

[15] *C. Vitanza:* Fuel performance at high burnup; International KTG/ENS Topical Meeting on Nuclear Fuel, Würzburg/Germany, March 1995

New High Burnup Fuel Models for NRC's Licensing Audit Code, FRAPCON

D.D. Lanning, C.E. Beyer, and C.L. Painter

Pacific Northwest Laboratory
Richland, Washington

1.0 INTRODUCTION

Fuel behavior models have recently been updated within the U.S. Nuclear Regulatory Commission steady-state FRAPCON code used for auditing of fuel vendor/utility codes and analyses. These modeling updates have concentrated on providing a best estimate prediction of steady-state fuel behavior up to the maximum burnup levels of current data (60 to 65 GWd/MTU rod-average). A decade has passed since these models were last updated. Currently, some U.S. utilities and fuel vendors are requesting approval for rod-average burnups greater than 60 GWd/MTU; however, until these recent updates the NRC did not have valid fuel performance models at these higher burnup levels.

Pacific Northwest Laboratory (PNL) has reviewed 15 separate effects models within the FRAPCON fuel performance code (References 1 and 2) and identified nine models that needed updating for improved prediction of fuel behavior at high burnup levels. The six separate effects models not updated were the cladding thermal properties, cladding thermal expansion, cladding creepdown, fuel specific heat, fuel thermal expansion and open gap conductance. Comparison of these models to the currently available data indicates that these models still adequately predict the data within data uncertainties. The nine models identified as needing improvement for predicting high-burnup behavior are fission gas release (FGR), fuel thermal conductivity (accounting for both high burnup effects and burnable poison additions), fuel swelling, fuel relocation, radial power distribution, fuel-cladding contact gap conductance, cladding corrosion, cladding mechanical properties and cladding axial growth. Each of the updated models will be described in the following sections and the model predictions will be compared to currently available high burnup data.

FISSION GAS RELEASE MODEL

The original FRAPCON code (References 1 and 2) had six FGR models. All of these models have been removed except the ANS 5.4 model (Reference 3) because they under predicted high burnup FGR data. The ANS 5.4 model was retained for two reasons: 1) it provides a reasonably good prediction of high burnup steady-state FGR data and 2) it is an industry standard for steady-state FGR predictions. However, the ANS 5.4 model does have two limitations: 1) it is based on simple diffusion (does not account for gas resolution or grain boundary gas storage), and 2) it under predicts FGR for fuel subjected to power ramps. The under prediction of FGR during ramping occurs because the

diffusion constant in the ANS 5.4 model is too low to allow any significant diffusion for power ramps lasting 12 to 48 hours.

A modified version of the Forsberg-Massih FGR model (Reference 5) has been developed to supplement the ANS 5.4 model because it allows for diffusion from a spherical grain like the original Booth model but also allows for storage of the gas on the grain boundaries as bubbles and resolution of the bubbles back into the matrix. This model does not allow FGR to occur until the grain boundary becomes saturated with bubbles, i.e., a particular gas concentration needs to be achieved at the grain boundary. Several modifications were necessary to the original Forberg-Massih model because it under predicted the high burnup steady-state and power ramp FGR data. In order to get a good prediction of both high burnup steady-state and power ramp FGR data (References 6, 7, 8, 9, 10, 11, 12, 13, 14 and 15) the following modifications were made to the original Forsberg-Massih model:

1) Only the mid-temperature form of the Forsberg-Massih diffusion constant is used and the activation energy is increased by a factor of 1.27.

2) The pre-exponential constant of the diffusion coefficient is increased by a factor of 10 and the diffusion coefficient is multiplied by a burnup enhancement factor of $100^{(BURN-25)/15}$, where BURN = GWd/MTU. A maximum value of 2×10^4 is allowed for this factor.

3) The partitioning of the gas arriving at the grain boundary, into that which remains at the boundary and that which is resolved back into the matrix, is simplified using the following equations at the end of each time step.

$$\Delta G_{gb} = \left[\frac{F}{1+F}\right] * \Delta G_{db} = \text{gas on grain boundary} \qquad (1)$$

$$\Delta G_r = \frac{\Delta G_{db}}{1+F} = \text{gas resolved back into fuel matrix} \qquad (2)$$

Where: F = resolution parameter
ΔG_{db} = amount of gas that diffuses to grain boundary during time step

This simple relationship allows the resolution, F, to be more easily estimated in the fit to the FGR data and also get an acceptable partition between resolved and grain boundary gas.

The changes to the Forsberg-Massih model increased the diffusion coefficient to allow the predicted FGR to reach an equilibrium rate faster when fuel temperatures increase in order to agree with the FGR power ramp data. This also required an increase in the resolution parameter to retard the predicted FGR for fuel at steady-state operating temperatures. The burnup enhancement factor on the diffusion coefficient was necessary in order to get good predictions of both low and high burnup FGR data.

The activation energy, pre-exponential burnup enhancement factor, and the resolution parameters were estimated from a non-linear regression fit of the basic Forsberg-Massih formulation to both steady-state and power ramp FGR data. Non-linear regression techniques allow regression coefficients to be estimated from highly nonlinear models such as the Forsberg-Massih model based on finding those combinations of coefficients that result in the minimum of the sum-of-squares residuals, i.e., best fit to the data.

Comparisons of the predictions from the modified model to low and high burnup FGR steady-state data and power ramp data are presented in Figures 1 and 2. The measured and predicted values of FGR are shown to be reasonably close in Figure 1. An analysis of the residuals (difference between prediction and data) presented in Figure 2 demonstrates that there is no bias between the model predictions and data as a function of burnup. The model predictions of the power ramp data have more variability (a standard deviation of 8% FGR) than the predictions of the steady-state data (a standard deviation of <5% FGR).

FUEL THERMAL CONDUCTIVITY

The original FRAPCON model for fuel thermal conductivity has been modified to include both degradation due to burnup and gadolinia effects. Both of these effects similarly alter the basic atom structure of the UO_2 and, therefore, similarly alter the phonon heat transfer term of the FRAPCON model.

The original model under predicted fuel temperatures at high burnups because of no thermal conductivity degradation at high burnups. The burnup degradation is due to the buildup of fission products with burnup that distorts the UO_2 atomic structure thus retarding phonon heat transfer. The effect is relatively small at low burnups and high fuel temperatures (> 1300°C) and was not easily determined until recent in-reactor experiments have measured fuel centerline data at burnups greater than 35 GWd/MTU (References 16 and 17). These experiments have demonstrated that the measured temperature difference between the fuel centerline and coolant is increasing slowly with burnup at a constant linear heat generation rate (LHGR) by about 8% per 10 GWd/MTU at low temperatures (< 900°C). This estimate has a standard deviation of approximately 1.2% per 10 GWd/MTU (absolute).

Thermal conductivity measurements have also been performed on fuel with simulated fission products (mixture of 11 rare earth oxides in the Urania

matrix) to simulated burnups of 0, 3, and 8 atom percent (Reference 18). Lucuta (Reference 18) also proposed a burnup dependent phonon heat transfer term based on his thermal conductivity measurements that results in a thermal conductivity reduction of approximately 6% per 10 GWd/MTU at low temperatures (< 900°C). Lucuta's uncertainty in his out-of-reactor measurements resulted in a standard deviation of approximately 0.4% per 10 GWd/MTU (absolute). If measurement uncertainties are included, the out-of-reactor and in-reactor values for thermal conductivity degradation of 6 and 8% per 10 GWd/MTU respectively are relatively close. The Lucuta burnup dependent phonon term has been selected for use with the FRAPCON thermal conductivity equation because it is easily incorporated in the FRAPCON formulation as demonstrated below in Equation 3. The burnup and temperature dependence predicted by this model is shown in Figure 3.

The use of burnable poisons (principally gadolinia, Gd_2O_3) in UO_2 has increased significantly in LWR cores with the increase in fuel burnups. The addition of gadolinia to the fuel has a similar degrading effect on phonon heat transfer as do the fission products. Massih, et al. (Reference 19) have developed a gadolinia dependent phonon term similar to the burnup dependent phonon term proposed by Lucuta that is also easily incorporated into the FRAPCON thermal conductivity equation as shown below (the burnup and gadolinia terms are underlined):

$$K_{Fuel} = \frac{C_v}{D_v * (A + B * TEMP + \underbrace{0.016 * C_v * P * b}_{Lucuta\ et\ al.} + \underbrace{0.01159 * C_v * P * g}_{Massih\ et\ al.})} * P + C_e \qquad (3)$$

Where:

K_{Fuel}	=	Fuel thermal conductivity
C_v	=	Phonon contribution to specific heat
P	=	Porosity correcting for thermal expansion
D_v	=	Correction for thermal expansion
A	=	0.339
B	=	6.867E-2
TEMP	=	Modified temperature, K
b	=	Burnup in atom % (of initial heavy metal atoms)
g	=	Gadolinia content, wt. %
C_e	=	Electronic term

This revised model has been compared to other models and thermal conductivity measurements on samples having gadolinia contents ranging from 0 to 10 wt% from three different sources (References 20, 21 and 22) and shows reasonably good prediction above 300°C as demonstrated in Figure 4 for 8.5 wt% gadolinia.

FUEL SWELLING

The original FRAPCON fuel swelling model included a solid fission product component and a significant gaseous swelling component when fuel temperatures exceeded 1250°C.

Solid fission product swelling is due to the buildup of rare earth fission products in the fuel with progressive burnup decreasing the fuel density and increasing the fuel volume. The current swelling rate ($\Delta V/V$ per unit burnup) in FRAPCON is 0.67% $\Delta V/V$ per 10 GWd/MTU. Fuel density measurements have been made from commercially irradiated fuel with pellet burnups ranging from 20 to 70 GWd/MTU and these data (References 23, 24, 25, and 26) are represented in Figure 5 in terms of fuel volume change. A linear regression analysis of these data provides a constant swelling rate of 0.77% $\Delta V/V$ per 10 GWd/MTU (solid line in Figure 5). This revised solid fission product swelling rate has been included in FRAPCON.

The original gaseous swelling component in FRAPCON was based on swelling from unrestrained fuel that is atypical of the constrained nature of commercial light-water reactor (LWR) fuel. Experimental irradiations of boiling-water reactor (BWR) type fuel rod designs near peak LWR fuel operating conditions have shown that gaseous swelling is not significant. This is best illustrated in Figure 6 where fuel swelling is predicted as a function of burnup for Rod 1 of IFA-432 from the Halden reactor using the original solid and gaseous swelling model in FRAPCON and compared to the measured fuel swelling in this rod (Reference 27). As illustrated the original FRAPCON model significantly over predicted swelling on this rod because significant portions of the fuel were at temperatures greater than 1250°C that activated the gaseous swelling model. The revised FRAPCON swelling model adequately predicts the swelling in this rod. Comparisons of the original FRAPCON model to swelling data from four other experimental rods with fuel temperatures greater than 1250°C have also shown similar over predictions in gaseous swelling. Therefore, the gaseous swelling model in FRAPCON has been removed.

FUEL RELOCATION AND CRACKING

The original FRAPCON code had several different fuel relocation and cracking models associated with each of the mechanical models in the code: FRACAS-1 (non-deformable pellet) and FRACAS-2 (deformable pellet). The FRACAS-1 model in the currently revised FRAPCON uses only one fuel relocation model (Reference 28) that: a) is a function of burnup and LHGR as illustrated in Figure 7, and b) assumes solid-pellet thermal conductivity. Solid-pellet thermal conductivity is used for two reasons: 1) it maximizes fuel stored energy for the LOCA calculation, and 2) the crack patterns in the fuel, particularly early-in-life, are primarily radially orientated and do not retard the heat flow. The FRACAS-1 model will principally be used for best-estimate thermal and fission gas release calculations.

The FRACAS-2 model will continue to use the existing fuel relocation and fuel cracking models. The FRACAS-2 model will be used to predict best-estimate mechanical behavior of fuel rods experiencing load follow or power ramping conditions.

RADIAL POWER

The original FRAPCON code used the RADAR model (Reference 29) for predicting fuel radial power distribution as a function of fuel burnup. This model provided a reasonably good prediction of the plutonium buildup at the fuel surface due to U^{238} resonance neutron captures and radial power distribution when fuel burnups were less than 40 GWd/MTU. However, as fuel burnup increases, RADAR under predicts the plutonium buildup and resulting power peaking at the fuel surface.

The TUBRNP model by K. Lassmann (Reference 30) improves the original RADAR model by modifying the parameters for the plutonium distribution function and accounting for the plutonium isotopes and their cross sections explicitly. This model results in a more edge-peaked radial power profile for high burnup fuel, as illustrated in Figure 8. This model also compares well with detailed neutronics calculations at 50 GWd/MTU performed by Matsamura and Kameyama (Reference 31) as illustrated in Reference 30 and presented here as Figure 9, and with detailed electron microprobe (EPMA) scans for neodymium (fission product concentration used as a measure of fuel burnup).

FUEL-CLADDING CONTACT GAP CONDUCTANCE

The original FRAPCON code calculated gap conductance when the fuel-to-cladding gap is closed using a modification of the Mikic-Todreas model (Reference 32) as proposed in Reference 33. This model under predicts fuel-cladding contact conductance.

The NRC sponsored a research program (Reference 34) to examine fuel-cladding contact conductance on typical UO_2-Zircaloy compacts with various surface and contact pressures typical for LWR fuel rods. Experimentally measured contact conductances from UO_2 and Zircaloy samples representative of LWR fuel surface conditions are provided in Figure 10 (Reference 34). The upper bound conductance data (solid triangles) are from UO_2 samples with a relatively smooth surface while the lower bound conductance data (open squares) are from fuel samples with a relatively wavy (coarse) surface, representing the possible variability in fuel surface conditions. A comparison of the original FRAPCON contact conductance model predictions compared to these data (Figure 10) shows an under prediction of even the lower bound data when contact pressures exceed 7 MPa. This model has been modified to increase the contact conductance by a factor of 2 when interface pressures exceed 7 Mpa. The solid line in Figure 10 represents the recent modification to the FRAPCON model and shows a slight over prediction of the lower bound data. This new modified

model may still result in a small degree of conservatism in contact conductance for some fuel but the impact on fuel temperatures will be small.

PWR CLADDING CORROSION

The original FRAPCON PWR cladding corrosion model significantly under predicted corrosion when fuel burnups exceeded 30 GWd/MTU. A corrosion model proposed by Garzarolli et al (Reference 35) has been incorporated into FRAPCON because it provided the best prediction among other published models reviewed in this project when compared to a variety of high burnup corrosion data from different PWRs as demonstrated in Figure 11. The model also compares well to corrosion data measured along the axial length of a high burnup rod (Figure 12) whereas the original FRAPCON model significantly under predicts corrosion in this same rod. The Garzarolli corrosion model includes a pre-transition oxidation and a flux enhanced post-transition oxidation dependence. The cladding interface temperature is calculated for each time step using an assumed thermal conductivity for the Zircaloy-oxide and the oxide thickness.

Cladding corrosion also results in the retention of some hydrogen in the cladding from the reaction

$$Zr + 2H_2O = ZrO_2 + 2H_2.$$

The retained hydrogen precipitates out as zirconium hydride platelets when the hydrogen level exceeds the solubility limit in Zircaloy (about 80 ppm at operating temperatures). Hydriding strengthens the cladding but it also decreases cladding ductility and, therefore, is important in determining cladding mechanical properties. Hydrogen pickup fraction as a function of oxide thickness from three different reactors (References 23, 24, 25, and 26) demonstrates that the fraction is relatively constant at approximately 0.15 even though the data scatters between 0.12 and 0.22 (Figure 13).

CLADDING MECHANICAL PROPERTIES

The original Zircaloy cladding yield and tensile strength models in FRAPCON over predict recent measured data from tensile test specimens of high burnup cladding (fast fluence between 5 to 12 x 10^{25} n/m^2)(Figures 14 and 15). The cladding test specimens also had oxide thicknesses between 4 to 100 μm and hydrogen levels between 10 and 720 ppm. The tensile tests were typically performed at a strain rate of 8 x 10^{-5}/sec and temperatures between 300° and 400°C.

Fast neutron fluence and waterside corrosion both lead to changes in the mechanical properties of Zircaloy cladding with increasing burnup. The fast neutron fluence increases yield and tensile strength, and decreases cladding ductility due to intrinsic cladding damage (displacement of atoms). The fluence effect on ductility appears to saturate when a fluence of 4 x 10^{25} n/m^2

is accumulated (i.e., at local burnups exceeding approximately 20 GWd/MTU). The effects of waterside corrosion and the concomitant accumulation of hydrides in the cladding appear to dominate further changes in mechanical properties when the excess hydrogen concentration (i.e., the hydrogen in excess of the solubility limit at operating temperature) exceeds approximately 200 ppm. This typically occurs at local burnups in excess of 40 GWd/MTU. The original FRAPCON mechanical property models do not account for the effects of hydrides at high burnups.

The FRAPCON mechanical models were modified to account for the effects of hydriding at high burnups. Comparisons of the revised yield and tensile strength models to measured tensile data (References 7, 23, 24, 25, and 26) are shown in Figures 16 and 17, respectively.

A comparison of the revised uniform strain model to measured data is shown in Figure 18. The decrease in uniform strain due to excess hydrogen is illustrated in Figure 19. This data suggests that the decrease in cladding uniform strain capability to less than 1% uniform strain may result in decreased failure thresholds for power ramped rods when excess hydrogen levels exceed 400 ppm.

CLADDING AXIAL GROWTH

The original FRAPCON model has been found to under predict axial growth of high burnup PWR fuel cladding. The axial growth model proposed by Franklin (36) has been adopted and compares well with PWR fuel cladding data (Figure 20 and also compares well with BWR data when the growth rate is decreased by 0.5 (Figure 21). Therefore, the original Franklin axial growth model was modified for BWR applications by decreasing the growth rate by 0.5. The PWR axial fuel cladding data comes from five different reactors (References 6, 24, 25, 37, and 38) and rod-average fast fluences up to $9 \times 10^{25}/m^2$. The BWR data comes from two BWR reactors (References 12 and 39) and fast fluences up to 10×10^{25} n/m^2.

2.0 SUMMARY

Nine separate effects fuel performance models in FRAPCON have been updated. These updated models have compared well to data from rods having rod-average fuel burnups up to 62 GWd/MTU (peak pellet burnups up to 70 GWd/MTU) and fluences up to 12×10^{25} n/m^2 . These models have recently been incorporated into FRAPCON and the code is currently being assessed against integral thermal and fission gas release data.

3.0 REFERENCES

1. Berna, G. A., et al. December 1980. FRAPCON-2: A computer Code for the Calculation of Steady-State Thermal-Mechanical Behavior of Oxide Fuel Rods. NUREG/CR-1845, Idaho National Engineering Laboratory, Idaho Falls, Idaho.

2. Berna, G. A., D. D. Lanning, and W. N. Rausch. June 1981. FRAPCON-2 Developmental Assessment. NUREG/CR-1949 (PNL-3849), Pacific Northwest Laboratory, Richland, Washington.

3. ANSI/ANS 5.4-1982. "Method for Calculating the Fractional Release of Volatile Fission Products From Oxide Fuel," American Nuclear Society.

4. A. H. Booth. 1957. A Method of Calculating Fission Gas Diffusion From UO_2 Fuel and Its Application to the X-2-f Loop Test, AECL No. 496, Chalk River, Ontario, Canada.

5. Forsberg, K. and A.R. Massih. 1985. "Diffusion Theory of Fission Gas Migration in Irradiated Nuclear Fuel UO_2," Journal of Nuclear Materials Vol. 135, pp. 140-148.

6. Balfour, M. G., W. C. Chubb, and R. F. Boyle. November 1982. BR-3 High Burnup Fuel Rod Hot Cell Program, Volume 1: Final Report. DOE/ET/34073-1, WCAP-10283, Volume 1, Westinghouse Electric Corp., Pittsburgh, Pennsylvania.

7. Balfour, M. G., E. Roberts, E. Dequidt, and P. Blanc. September 1982. Zorita Research and Development Program: Volume 1, Final Report. WCAP-10180, Volume 1, Westinghouse Electric Corp., Pittsburgh, Pennsylvania.

8. De Meulemeester, E., et al. 1973. "Review of Work Carried out by BEGONUCLEAIRE and CEA on the Improvement and Verification of the Computer Code With the Aid of In-Pile Experimental Results," BNFL Conference on Nuclear Fuel Performance. Oct. 15-19, 1973.

9. Ainscough, J. A. 1971. An Assessment of the IFA-116 and IFA-117 Irradiations From Data Obtained From the In-Reactor Instrumentation, HPR-129. Halden Reactor Project, Halden, Norway.

10. Beyer, C. E. And C. R. Hann. 1974. Prediction of Fission Gas Release From UO_2 Fuel. BNWL-1875 Pacific Northwest Laboratory, Richland, Washington.

11. Bagger, C., H. Carlson, and P. Knudsen. December 1978. Details of Design, Irradiation and Fission Gas Release for the Danish UO_2ZR Irradiation Test 022. RISO-M-2152, Riso National Laboratory, Denmark.

12. Barner, J. O., et al. 1990. High Burnup Effects Program Summary Report. DOE/NE/3406-1. Battelle, Pacific Northwest Laboratories, Richland, Washington.

13. Djurle, S., 1985. Final Report of the Super-Ramp Project. DOE/ET/34032-1.

14. Lysell, G., and S. Birath. 1979. The Studsvik Inter-Ramp Project Hot Cell PIE Final Report. STIR-51.

15. Knudsen, P., et al. 1983. Riso Fission Gas Release Project Final Report. DOE/ET/340331-1.

16. Kolstad, E., 1992. "Fuel Rod and Core Materials Investigations Related to LWR Extended Burnup Operation," Journal of Nuclear Materials. Vol. 188, pp. 104-113.

17. Kolstad, E., et al. 1991. "High Burnup Fuel Behavior Studies by In-Pile Measurements," ANS/ENS International Topical Meeting on LWR Fuel Performance. Avignon, France, pp. 838-849.

18. Lucuta, P. G., et al. 1992. "Thermal Conductivity of SIMFUEL," Journal of Nuclear Materials. Vol. 188, pp. 198-204.

19. Massih, A. R., et al. 1992. "Modeling of $(U,Gd)O_2$ Fuel Behavior in Boiling Water Reactors," in Proceedings of Symposium on Nuclear Materials for Fission Reactors of the 1991 E-MRS Fall Conference; Journal of Nuclear Materials. Vol. 199, pp. 319-330.

20. Hirai, M.V., and S. Ishimoto. 1991. "Thermal Diffusivities and Thermal Conductivities of UO_2-Gd_2O_3," Journal of Nuclear Science and Technology. Vol. 28, pp. 995-1000.

21. Fukushima, S., et al. 1982. "The Effect of Gadolinium Content on the Thermal Conductivity of Near-Stoichiometric $(U,Gd)O_2$ Solid Solutions," Journal of Nuclear Materials. Vol. 105, pp. 201-210.

22. Newman, L.W., et al. 1984. Thermal and Physical Properties of Urania-Gadolinia Fuel. DOE/ET/34212-43, BAW-1759.

23. Garde, A. M. 1986. Hot Cell Examination of Extended Burnup Fuel From Fort Calhoun. DOE/ET/34030-11.

24. Dideon, C. G. 1983. Fuel Performance Under Extended Burnup for the B&W 15 x 15 Design. DOE/ET/34212.

25. Newman, L. W. 1986. The Hot Cell Examination of Oconee 1 Fuel Rods After Five Cycles of Irradiation. DOE/ET/34212-50.

26. Smith, G. P. 1994. The Evaluation and Demonstration Methods for Improved Nuclear Fuel Utilization. DOE/ET/34013-15.

27. Lanning, D. D., and E. R. Bradley. 1984. Irradiation History and Interim Post-Irradiation Data for IFA-432. NUREG/CR-3071. Pacific Northwest Laboratoy, Richland, Washington.

28. Cunningham, M. E., and C. E. Beyer. 1984. GT2R2: An Updated Version of GAPCON-THERMAL-2. NUREG/CR-3907 (PNL 5178) Pacific Northwest Laboratory, Richland, Washington.

29. Palmer, I. D., et al. 1982. "A Model for Predicting the Radial Power Profile in a Fuel Pin," Presented at the IAEA Specialist's Meeting on Water Reactor Fuel Element Performance Computer Modeling, Preston U.K., Applied Science 1983, p. 321

30. Lassmann, K., et al. 1994. "The Radial Distribution of Plutonium in High Burnup UO_2 Fuels," Journal of Nuclear Materials. Vol. 208, pp. 223-231.

31. Matsamura, T. V., and T. Kameyama. 1988. "Burnup and Plutonium Distribution Near the Surface of High Burnup Fuel," Proceedings of IAEA Technical Committee Meeting on Water Reactor Fuel Element Computer Modeling in Steady State, Transient, and Accident Conditions, Preston UK, September 1988.

32. Todreas, N. V., and G. Jacobs. 1983. "Thermal Contact Conductance of Reactor Fuel Elements," Nuclear Science and Engineering. Vol. 50, p. 283.

33. C. E. Beyer, et al. 1975. GAPCON-THERMAL-2: A Computer Program for Calculating the Thermal Behavior of an Oxide Fuel Rod. BNWL-1898, Pacific Northwest Laboratory, Richland, Washington.

34. Garnier, J. E., and S. Begej. 1979. Ex-Reactor Determination of Thermal Gap and Contact Conductance Between Uranium Dioxide: Zircaloy-4 Interfaces; Stage I: Low Gas Pressure. NUREG/CR-0330 (PNL-2696), Pacific Northwest Laboratory, Richland, Washington.

35. Garzarolli, F., et al. 1980. Review of PWR Fuel Rod Waterside Corrosion Behavior. EPRI-NP-1472, Electric Power Research Institute, Palo Alto, California.

36. Franklin, D. G. 1982. "Zircaloy Cladding Deformation During Power Reactor Irradiation," in Proceedings of the Fifth International Symposium on Zirconium in the Nuclear Industry. ASTM-STP-754, pp. 235-267.

37. Smalley, W. R. 1974. Evaluation of Saxton Core III Fuel Material Performance. WCAP-3385-57.

38. Smith, G. P. 1986. The Non-Destructive Examination of Fuel Assemblies With Standard and Advanced Design After Three Cycles of Irradiation. DOE/ET/34013-12.

39. J. S. West, et al. 1983. EOC9-Final Fuel Bundle Examination at Monticello Nuclear Generating Station. DOE/ET/34031-16.

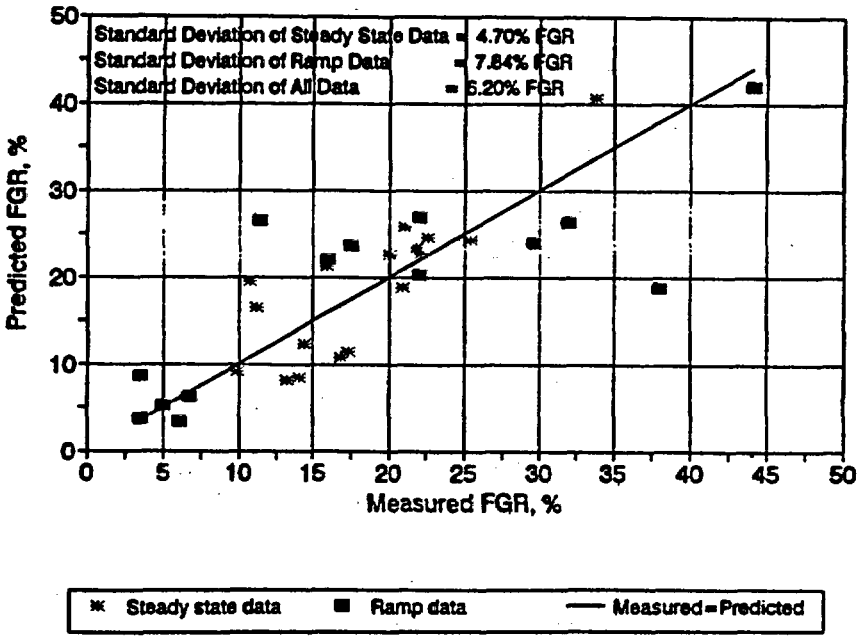

FIGURE 1. Comparison of Modified Forsberg-Nassih Model to High Burnup Steady-State and Power Ramp FGR Data

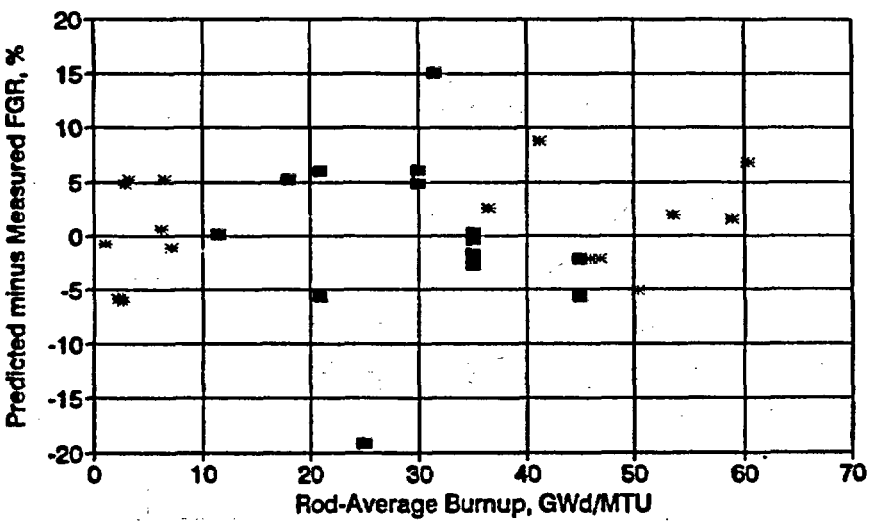

FIGURE 2. Residuals (Modified Forsberg-Nassih Model Predictions Minus Measured FGR Data) Show No Bias Versus Rod Average Burnup

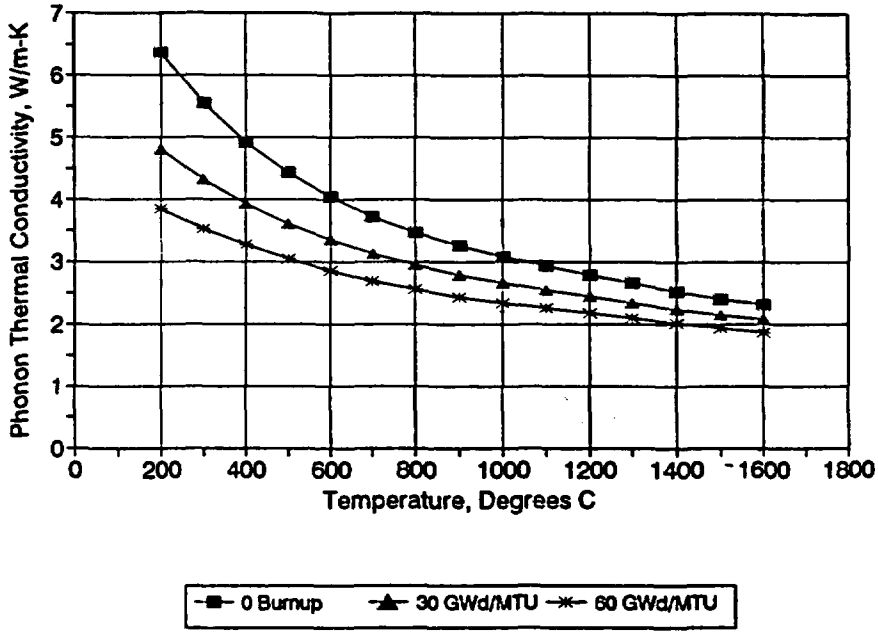

FIGURE 3. The Burnup and Temperature Dependence of Revised FRAPCON Thermal Conductivity Using Lucuta's (Reference 18) Phonon Term for Burnup Degradation

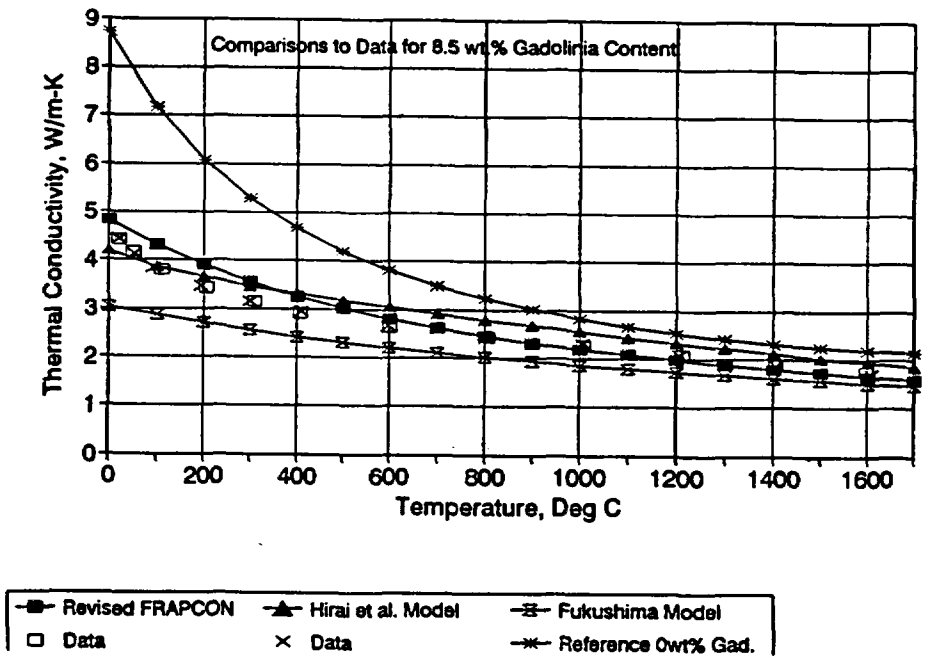

FIGURE 4. Comparison of the Revised FRAPCON Thermal Conductivity Prediction to Conductivity Data and Other Correlations From 8.5 Wt% Gadolinia-Urania Fuel at 95% TD

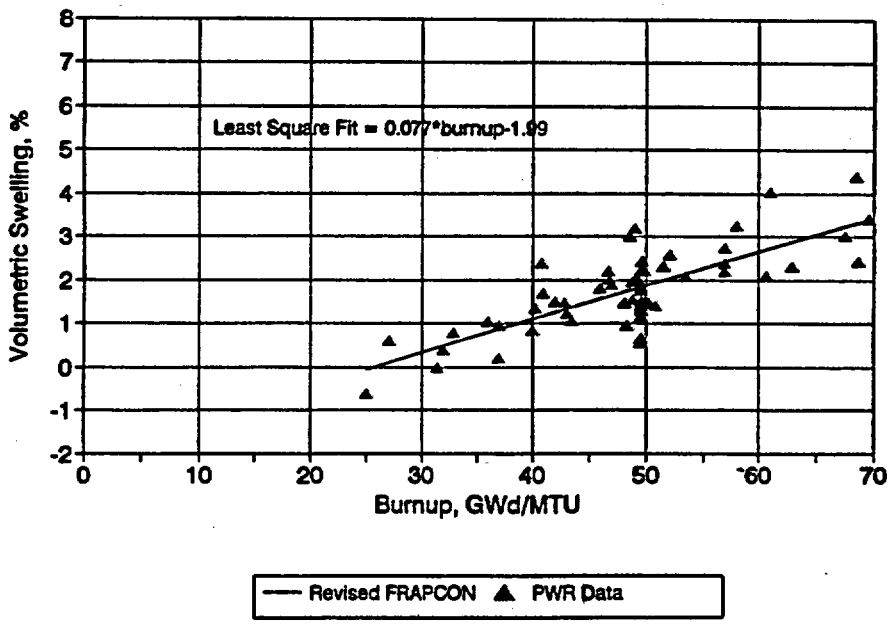

FIGURE 5. Revised FRAPCON Solid Swelling Model Based on Linear Fit to Swelling Data

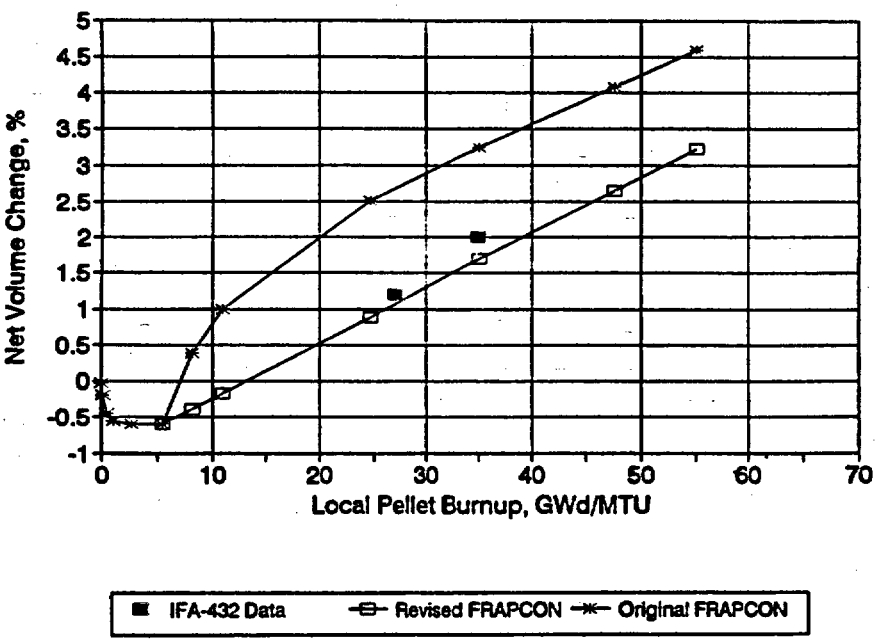

FIGURE 6. Comparison of the Original and Revised FRAPCON Swelling Models to Data From Rod 1 of IFA-432 (Reference 27)

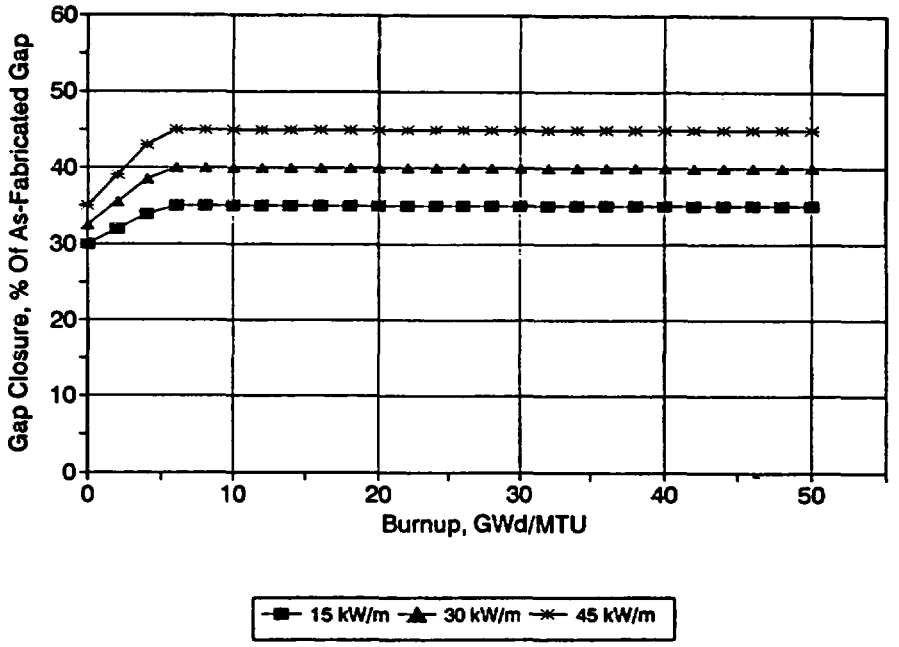

FIGURE 7. Power and Burnup Dependence of the Revised FRAPCON Relocation Model

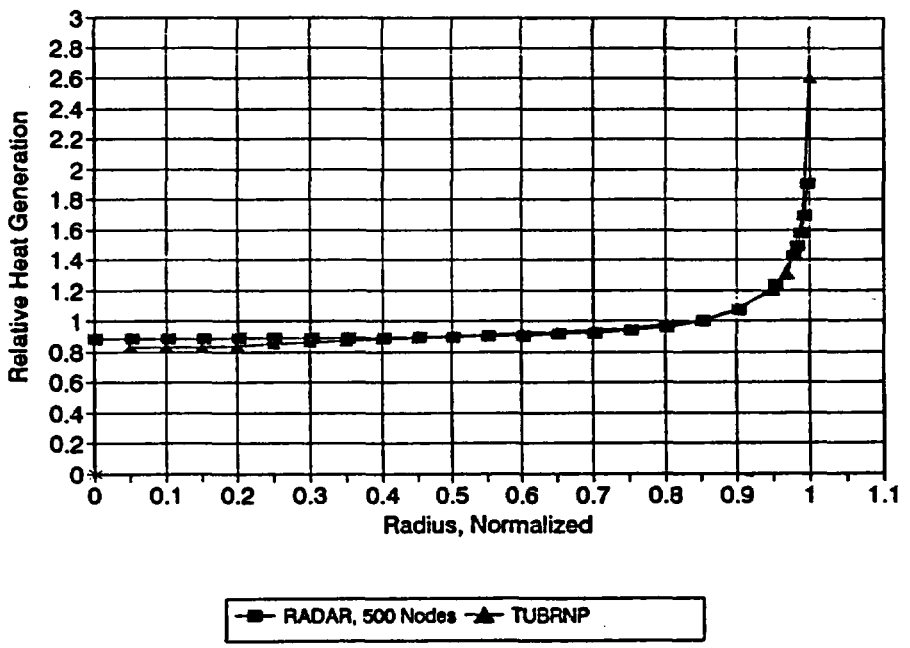

FIGURE 8. Radial Power Distribution From TUBRNP (Reference 30).are More Peaked at Pellet Edge Than Those Predicted by RADAR (Reference 29)

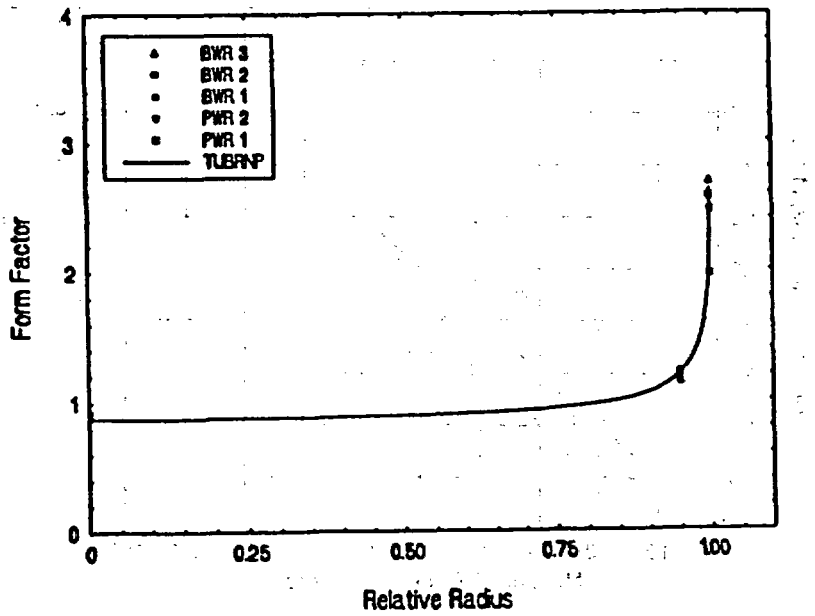

FIGURE 9. Comparison of TUBRNP and Detailed Physics (Reference 31) Radial Power Distributions for Five Reactors at 50 Gwd/MTU and Enrichment of 5%(From Reference 30)

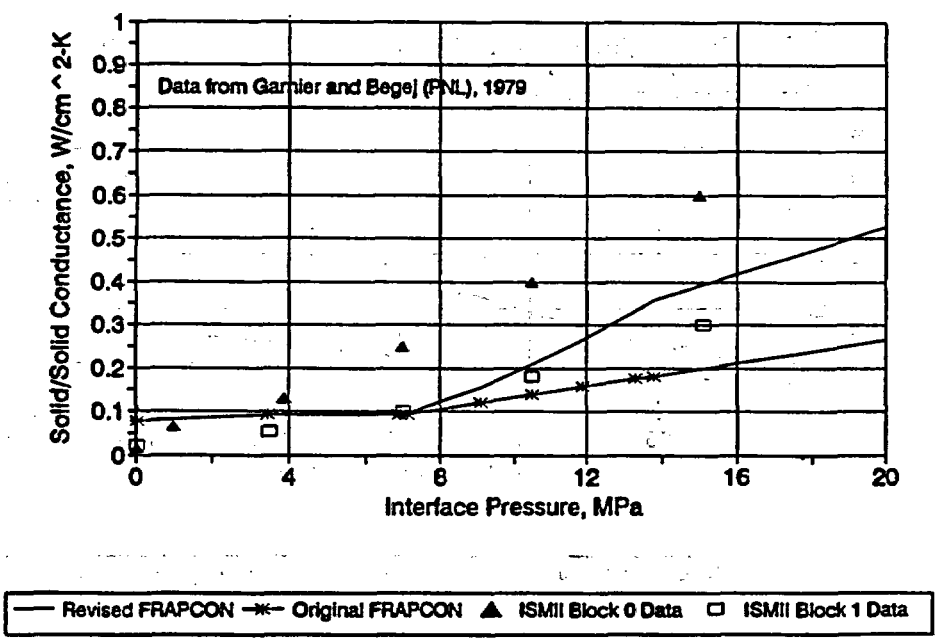

FIGURE 10. Comparison of the Original and Revised FRAPCON Predictions to Contact Conductance Data From (Reference 34) for Varying Interface Pressures

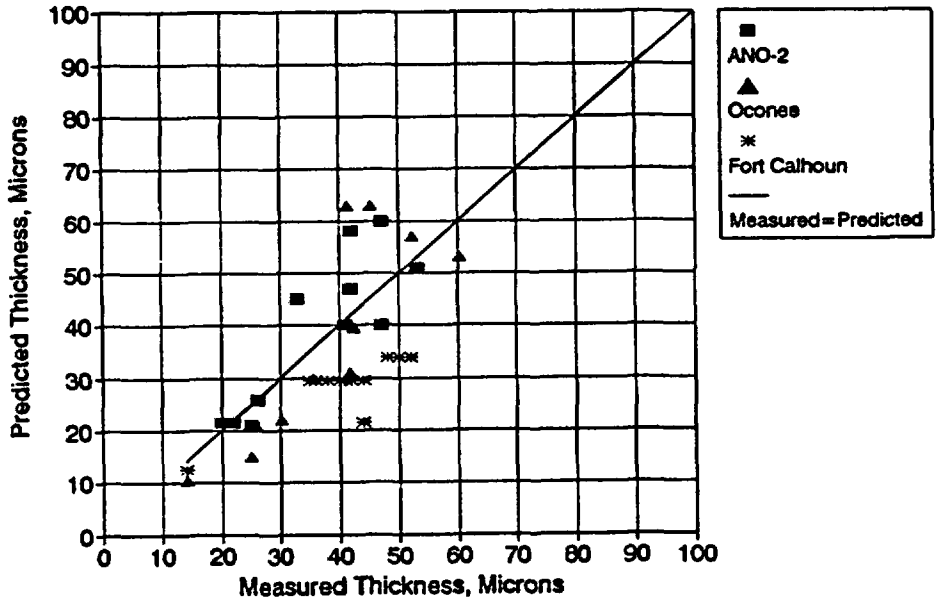

FIGURE 11. Comparison of Garzarolli Model (Reference 35) Predictions to Corrosion Data From High Burnup Fuel Rods

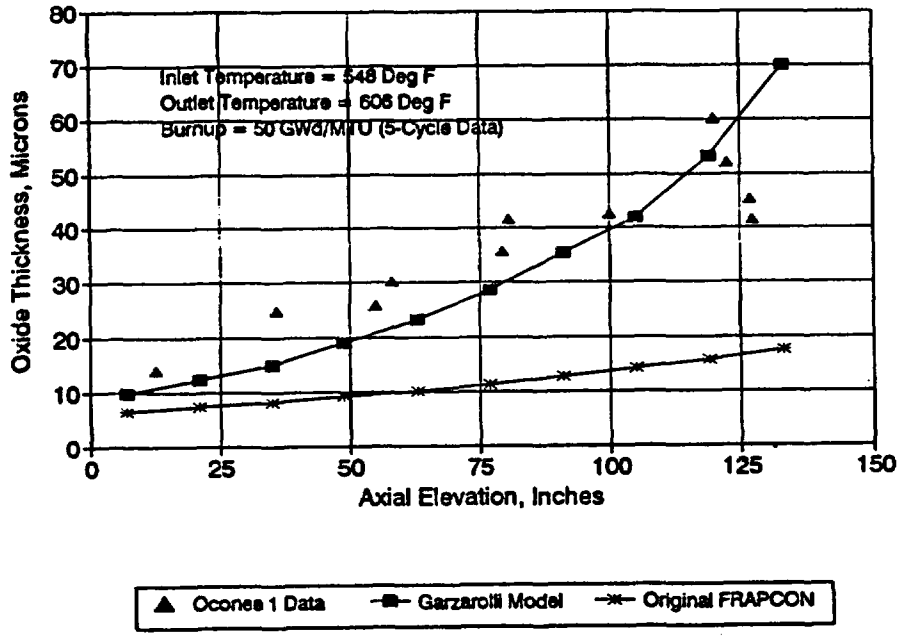

FIGURE 12. Comparison of Original and Garzarolli Corrosion Model (Reference 35) Predictions to Axial Corrosion Data From an Oconee-1 Cycle 5 Fuel Rod (Reference 25)

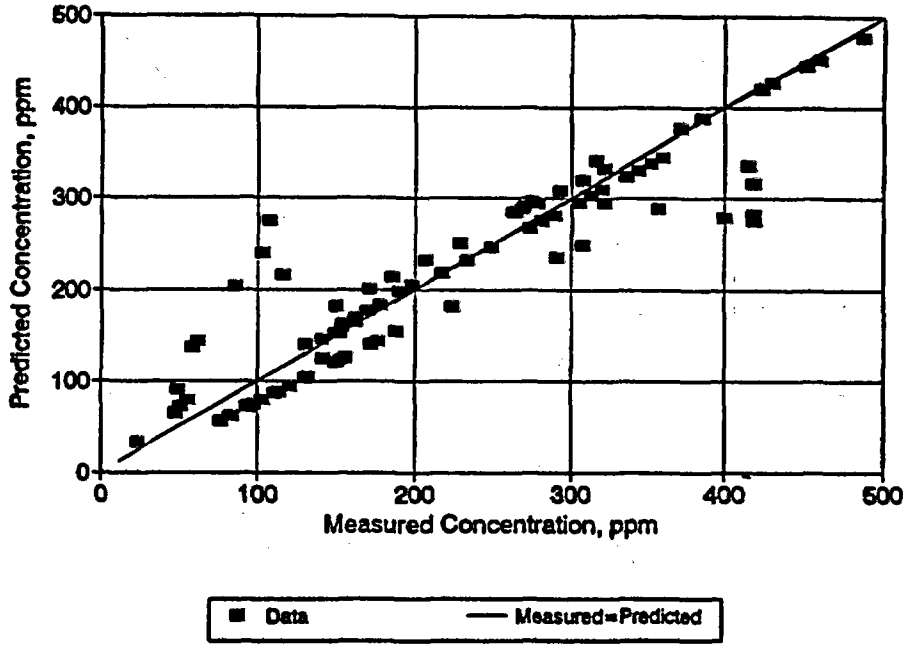

FIGURE 13. Comparison of Predicted Hydrogen Concentration Using New 0.15 Pickup Fraction to Data From High Burnup BWR Fuel Cladding

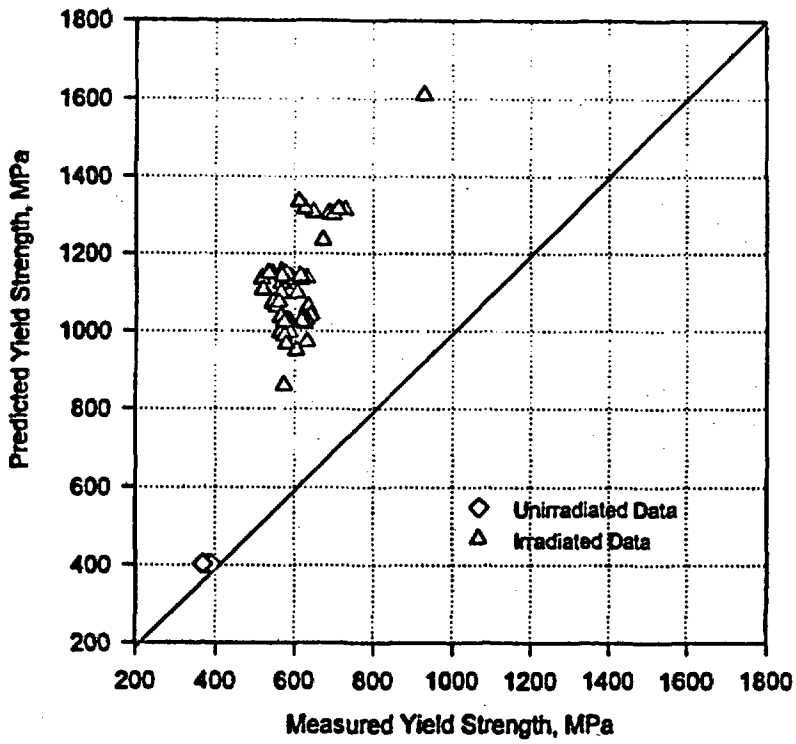

FIGURE 14. Comparison of Original Yield Strength Model to Tensile Data From Unirradiated and High Burnup Fuel Cladding

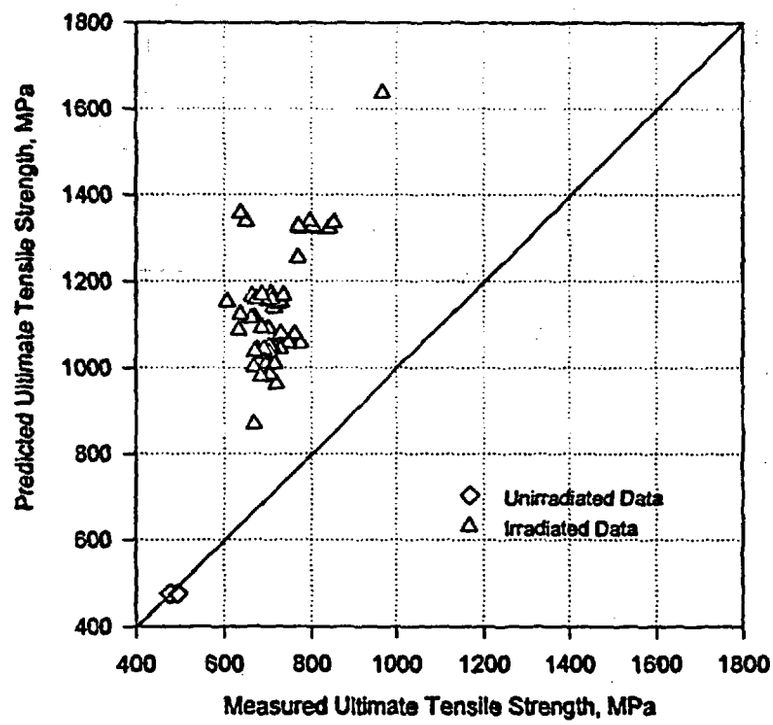

FIGURE 15. Comparison of Original FRAPCON Tensile Strength Model to Tensile Data From Unirradiated and High Burnup Fuel Cladding

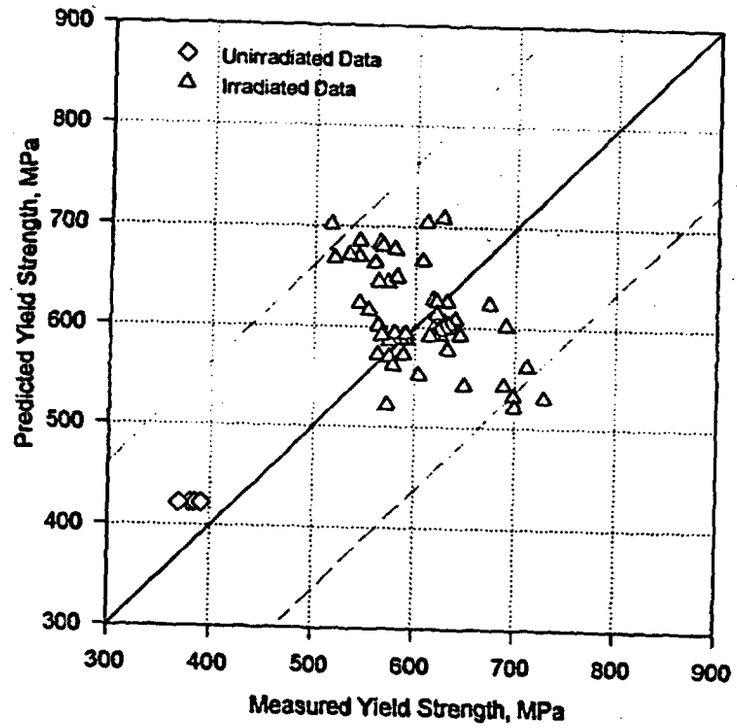

FIGURE 16. Comparison of Revised Yield Strength Model to Tensile Data From Unirradiated and High Burnup Fuel Cladding

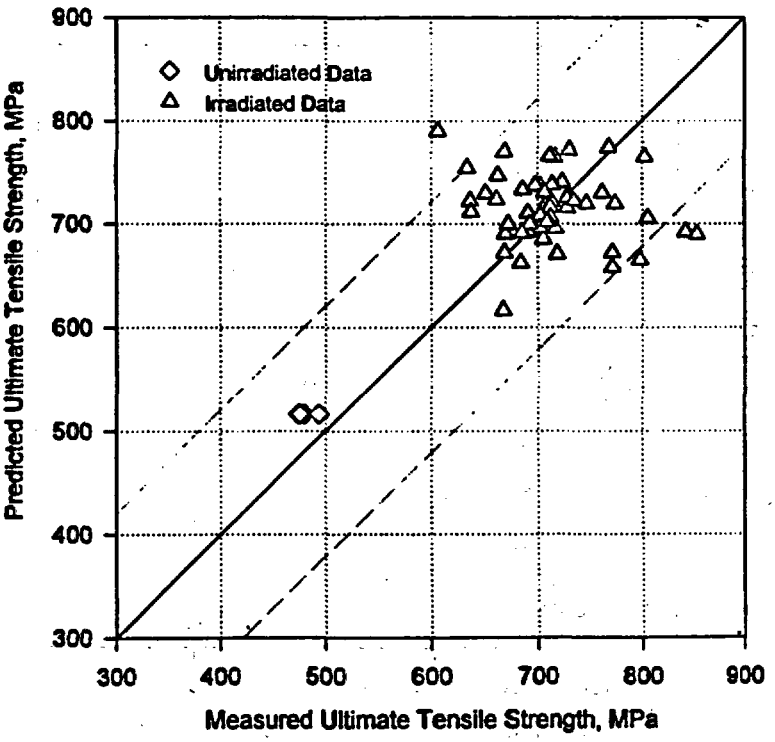

FIGURE 17. Comparison of Revised Tensile Strength Model to Tensile Data From Unirradiated and High Burnup Fuel Cladding

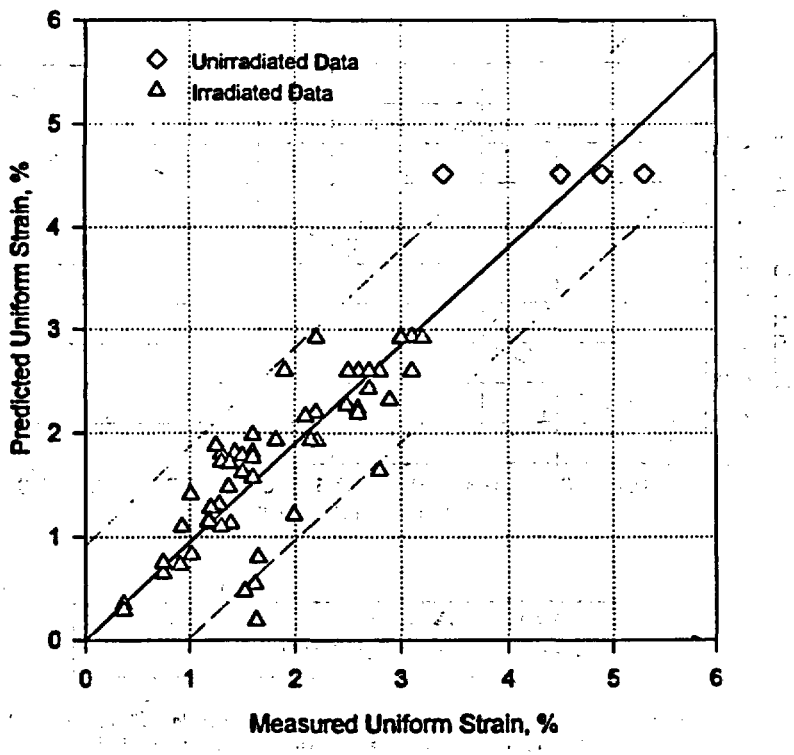

FIGURE 18. Comparison of Revised Uniform Strain Model to Tensile Data From Unirradiated and High Burnup Fuel Cladding

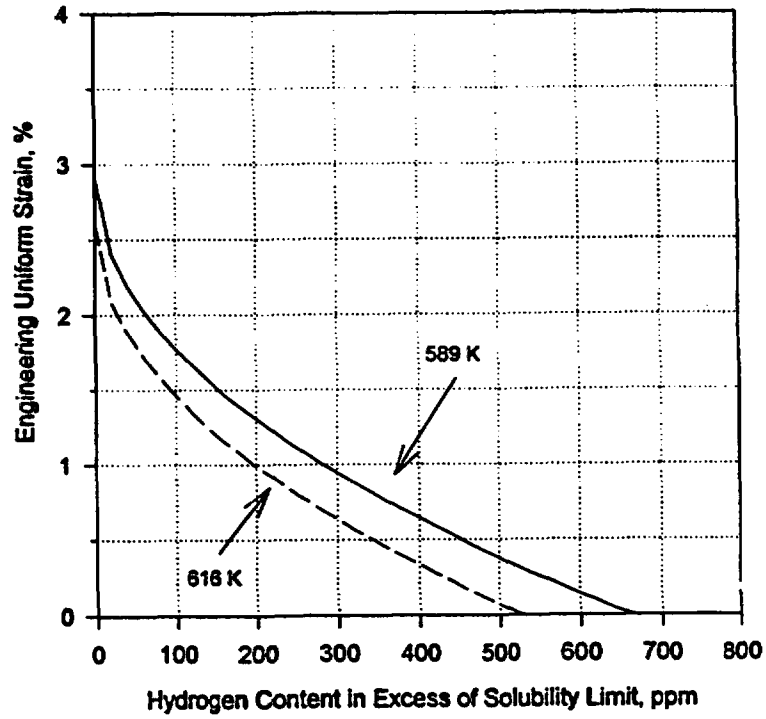

FIGURE 19. Revised FRAPCON Model Prediction of Uniform Strain as a Function of Excess Hydrogen and Temperature at a Fast Fluence of 11 x 10^{25} n/m^2

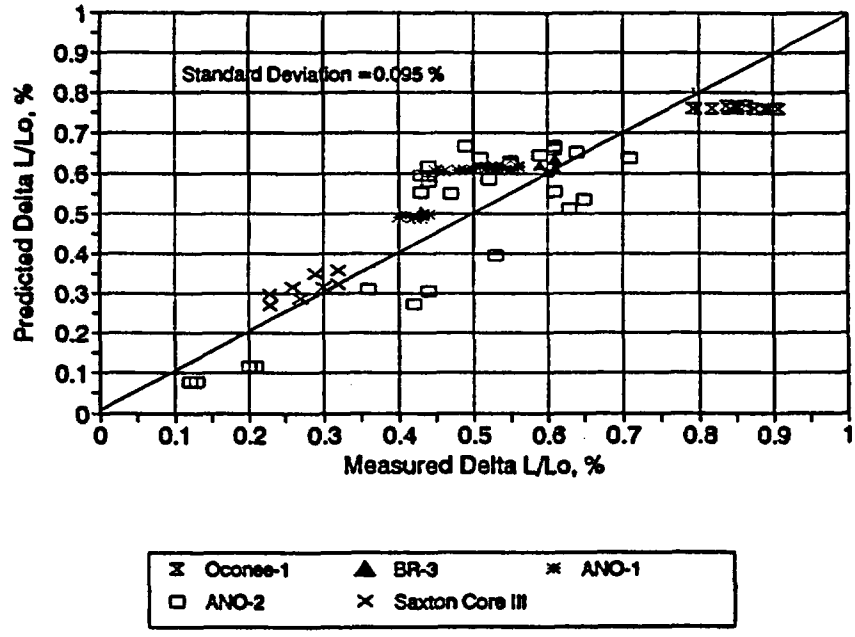

FIGURE 20. Comparison of Franklin Axial Growth Model (Reference 35) Predictions to PWR Data With Rod Average Fast Fluences up to 9 x 10^{25} n/m^2

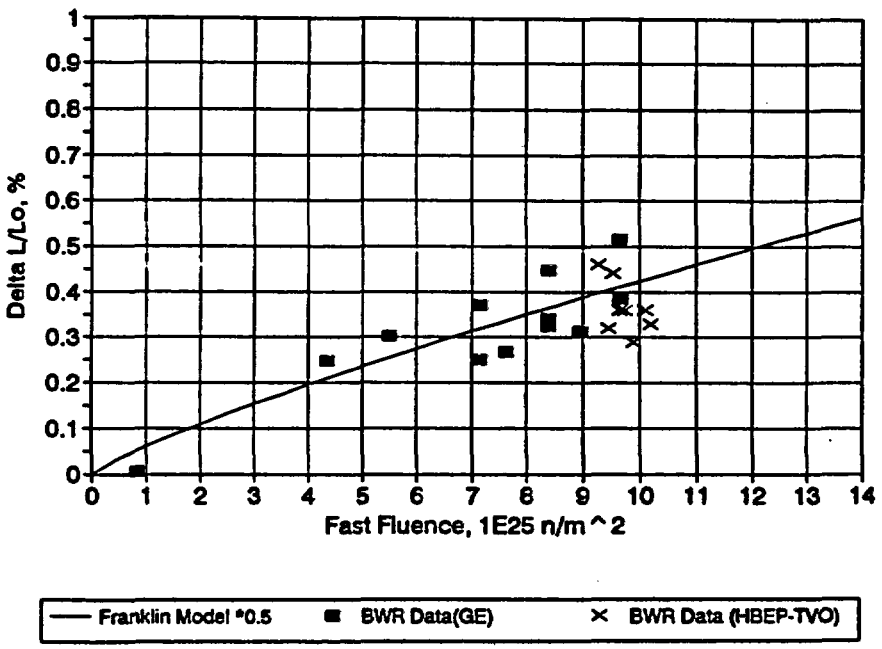

FIGURE 21. Comparison of Modified Franklin Axial Growth Model to High Burnup BWR Data

GIRAFFE TEST RESULTS SUMMARY

Seiichi Yokobori, Kenji Arai and Hirohide Oikawa
Nuclear Engineering Laboratory, Toshiba Corporation
Kawasaki, Japan

ABSTRACT

A passive system can provide engineered safety features enhancing safety system reliability and plant simplicity. Toshiba has conducted the test program to demonstrate the feasibility of the SBWR passive safety system using a full-height, integral system test facility GIRAFFE. The test facility GIRAFFE models the SBWR in full height to correctly present the gravity driving head forces with a 1/400 volume scale. The GIRAFFE test program includes the certification tests of the passive containment cooling system (PCCS) to remove the post-accident decay heat and the gravity driven cooling system (GDCS) to replenish the reactor coolant inventory during a LOCA. The test results have confirmed the PCCS and GDCS design and in addition, have demonstrated the operation of the PCCS with the presence of a lighter-than-steam noncondensable as well as with the presence of a heavier-than-steam noncondensable.

The GIRAFFE test program has also provided the database to qualify a best estimate thermal-hydraulic computer code TRAC. The post test analysis results have shown that TRAC can accurately predict the PCCS heat removal performance and the containment pressure response to a LOCA.

This paper summarizes the GIRAFFE test results to investigate post-LOCA PCCS heat removal performance and post-test analysis using TRAC.

1. INTRODUCTION

A passive safety system is an approach to improve plant safety for advanced nuclear reactors. The passive containment cooling system (PCCS) is adopted in the Simplified Boiling Water Reactor (SBWR) design[1], its purpose being to remove the decay heat following a loss of coolant accident (LOCA) without any electric power supply. The PCCS is automatically placed in operation when the containment pressure rises due to mass and energy input through a break pipe and it does not require even a valve operation to start the heat removal function. Consequently the PCCS offers high reliability of functioning, due to no valve operation being required. In addition, the PCCS is expected to suppress the containment pressure in case of a severe accident as well as in a LOCA, and prevent containment failure, without venting gases in the containment to the atmosphere.

Toshiba has taken the lead in the thermal-hydraulic research of the PCCS and has carried out an experimental program as well as analytical work to develop the PCCS. Based on these experimental and analytical studies, the mechanism of the passive heat removal has been clarified and the PCCS heat removal performance following a LOCA has been assessed. In addition, the test results have demonstrated the operation of the PCCS with the presence of a lighter-than-steam noncondensable.

2. PASSIVE SAFETY SYSTEM DESIGN SUMMARY

The SBWR passive safety system consists of depressurization valves (DPVs), the gravity driven cooling system (GDCS), the equalizing line (EQL) and the PCCS, as shown in Fig. 1. The GDCS injects the emergency core cooling water into the reactor pressure vessel (RPV) by gravity, in the case of a LOCA, and the DPVs promote the GDCS injection by depressurizing the reactor vessel. Long-term reactor core coverage, following a LOCA, is achieved by the EQL, which allows the flow of suppression pool (SP) water into the RPV.

The decay heat removal following a reactor isolation or a LOCA is achieved by the isolation condenser (IC) and/or the PCCS. The PCCS consists of a steam supply line, a vertical tube single path heat exchanger in a large water pool, a condensate drain line and a noncondensable vent line (PCC vent line). During a LOCA, high pressure steam flows from the RPV to the drywell (D/W) and causes a pressure rise in the D/W. The resultant pressure difference between the D/W and the suppression chamber (S/C) drives the steam-noncondensable mixture in the D/W into the PCCS heat exchanger through the steam supply line. The condensate drains to the GDCS pool through the condensate drain line by the gravitation force, and the noncondensable is vented to the S/C through the PCC vent line. No power-actuated active devices are required for the PCCS to function.

The large water pool is located outside the drywell and serves as a heat sink for reactor decay heat. The water pool retains a sufficient amount of water to remove the decay heat from the reactor shutdown for three days, 'the 3-day walk-away period'.

3. PROGRAM OVERVIEW

Table 1 shows the timetable of the GIRAFFE test program performed in Toshiba. The program has focused on the thermal-hydraulic area for demonstrating the feasibility of the passive safety system and the tests have covered the major phenomena encountered during the period from late blowdown phase (prior to GDCS injection) to PCCS dominant phase.

A full-height, integral system test facility, "GIRAFFE" (Gravity-Driven Integral Full-Height Test for Passive Heat Removal) has been constructed to investigate the basic heat removal performance of the PCC heat exchanger and various thermal-hydraulic phenomena in the pressure containment vessel following a LOCA. GIRAFFE models the SBWR in full-height to correctly represent the gravity head driving forces. The GIRAFFE testing program includes two types of separate effect tests (basic heat transfer test and noncondensable gas venting test) and the system response tests which focus mainly on the post-accident PCCS heat removal performance and on the post-LOCA GDCS performance.

From the thermal hydraulic viewpoint, a key phenomenon to determine the PCCS heat removal performance is steam condensation in the presence of a noncondensable in the PCC heat exchanger. In the first instance, separate effect heat transfer tests have been conducted in GIRAFFE to investigate the degradation of the steam condensation heat transfer caused by the noncondensable. The test results showed that the heat transfer degradation in the PCC heat exchanger tubes is slightly milder than the Sparrow's analysis for forced convection condensation.

The basic characteristics of noncondensable gas venting to the suppression chamber were demonstrated following the separate effect heat transfer tests. Tests have also been conducted which include changing the PCC vent line submergence.

The noncondensable mass and distribution in the containment volume following a LOCA determines the amount of noncondensable absorbed into the PCC heat exchanger. The noncondensable mass and distribution in the containment space is affected by break location, emergency coolant injection (for instance, the GDCS injection), or leakage between the drywell and the suppression chamber. DBA (design basis accident) LOCA scenarios were simulated to investigate the IC and the PCCS performance following a LOCA in the PCCS system response test Phase 2. The effect of the break pipe location on the PCCS performance have been also investigated. From these system response test results, it has been clarified that the PCCS is capable of suppressing the containment pressure below the design limit in DBA break cases, although the PCCS heat removal

performance changes depending on the break locations. The effect of the GDCS or the suppression pool water injection via EQL into the reactor pressure vessel and the leakage effect on the PCCS heat removal performance, mentioned above, were also examined.

In the PCCS system response tests Phase 3, lighter-than-steam gas effect on the post-accident PCCS performance has been investigated. Helium gas was used to simulate hydrogen gas which can be generated by radiolysis or metal-water reaction during a severe accident. The test results have demonstrated the operation of the PCCS in the presence of helium gas as well as in the presence of a heavier-than-steam noncondensable although the characteristics of helium gas accumulation in the PCC tube is completely different from that of nitrogen gas. It is considered from the test results that the PCCS can suppress the containment pressure even in a severe accident and prevent containment failure without venting gases to the environment.

The GDCS performance demonstration tests have been also conducted addressing potential systems interaction effect during the late blowdown and early GDCS phase of a LOCA. The tests simulated a DBA (a GDCS drain line break or a RPV bottom drain line break) for the GDCS design. From the test results it is seen that the GDCS coolant injection is smoothly accomplished and the core region is covered by two-phase mixture during the entire transient. No adverse systems interaction were discovered in the tests.

Thus the GIRAFFE test program has demonstrated the post-accident passive safety systems performance, which are, the GDCS performance to replenish the RPV coolant inventory, and the PCCS performance to remove the long-term decay heat following a LOCA and possibly even in a severe accident.

The program has also provided the database to establish the analysis model to evaluate the PCCS heat removal performance. Based on the GIRAFFE basic heat transfer test results, the steam condensation heat transfer models in the presence of noncondensable in the PCCS heat exchanger and in the containment air space have been incorporated into TRAC. The applicability of the TRAC model to a PCCS performance analysis has been qualified against the PCC system response tests conducted in GIRAFFE. The post-test analysis results show that TRAC can accurately predict the PCCS heat removal performance and the containment pressure response following a LOCA.

4. GIRAFFE TEST PROGRAM

4.1 GIRAFFE Test Facility(2)

The front view and the schematic diagram of GIRAFFE are shown in photo 1. GIRAFFE consists of separate component vessels for the PCCS pool, RPV, S/C, D/W and GDCS pool. The design criterion for the GIRAFFE test facility was to make the long term PCV pressure transient be identical to a reference passive plant, SBWR, in real time. Since for the long post-LOCA transients most flow paths are driven primarily by

gravitational forces, GIRAFFE has been constructed on a 1:1 height scale to the SBWR design. The scale of the test facility is 1/400 in volume and the height is 30 m.

The passive containment cooler (PCC) unit consists of a steam box, heat transfer tubes and a water box, as shown in Fig. 2. PCC has three heat transfer tubes, which have dimensions of 0.051m outer diameter, 0.046m inner diameter, and 2.4 m length for all tests conducted in the PCCS system response test Phase 2 and 1.8 m for lighter-than-steam gas tests and systems interaction tests, corresponding to 1/400 scaled volume. Dimensions of the heat transfer tube, the clearance between adjacent tubes and the secondary side flow cross-sectional area per tube are in full-scale of the original SBWR design. In the PCCS pool a chimney contains the PCC, which separates the boiling region around the PCC from the subcooled water outside. The pool water circulates along the chimney and boils off to the atmosphere. The effective water volume is the 1/400 scaled SBWR volume which is sufficient to remove decay heat for three days by the evaporation of water.

To reduce the heat loss from the vessels, electrical heaters are wrapped around the S/C, GDCS pool and the D/W walls. Flange portions are fully insulated. The remaining heat loss from the vessels is mainly from RPV and is compensated by increasing the heater power of the channel in the RPV.

4.2 Basic Heat Transfer Test [2]

The heat removal degradation due to nitrogen, inside the PCCS heat exchanger tube under the forced convective flow conditions, was measured as the first step of the test program. Table 2 summarizes the test conditions. These conditions have been determined from the TRAC analysis result for the SBWR and correspond to the long-term post-LOCA conditions [10].

As the reference case, pure steam condensation behavior in the heat exchanger was steadily measured, which was found to be close to the laminar condensation on a vertical plate with negligible shear at liquid-steam interface and included the wave effect at the liquid film surface. Figure 3 shows the steam condensation degradation obtained in the GIRAFFE test as a function of the nitrogen partial pressure fraction, compared with Sparrow's analysis [11]. The overall degradation coefficient indicates the amount of degradation of the condensate drainage flow rate when compared to the rate for a case with pure steam. The local degradation coefficient represents the amount of degradation of the heat flux measured at a location 0.05m downstream of the heat exchanger tube inlet. Sparrow's analysis results show the steam condensation degradation for both stagnant and convective air conditions on a horizontal plate at 0.1 MPa with wall subcooling 11K.

The GIRAFFE degradation coefficients were much milder than Sparrow's analysis result for the stagnant condition due to the steam flow effect. It should be noted that the extent of degradation obtained in the GIRAFFE test was similar to Sparrow's

analysis result for the convective condition and was slightly milder. This was probably due to the higher pressure in the GIRAFFE test than that in Sparrow's analysis.

The overall degradation coefficient shows considerably good agreement with the local value because most of the steam was condensed within the upper portion of the tube where the gas mixture flow was not fully developed. The larger difference between the local and overall degradation coefficient which was observed for higher nitrogen partial pressure was due to the difference in the effective heat transfer area.

4.3 Nitrogen Venting Test [3]

The mechanism of nitrogen transfer from the D/W to the S/C, which includes the venting behavior from PCC unit to S/C was investigated. Initial test conditions are summarized in Table 3, which corresponds to the typical long-term post-LOCA condition in the SBWR. GDCS injection was not included in this test. In the pre-test procedure, each component vessel was isolated by closing the connecting valves and the initial conditions were established. Following the pre-test procedure, the connecting valves were opened and the PCV long-term post-LOCA behavior was simulated. The RPV heater power simulating the reactor decay heat was held constant in this test in order to simplify the situation. Figure 4 shows the submergence of the PCC vent line and main LOCA vent in the S/C.

The major parameters measured in the test are shown in Figs. 5 through 8. Since the vapor temperature is the saturation steam temperature, a low vapor temperature indicates a high nitrogen concentration.

When the test started, steam came from the RPV to the D/W, which was produced by the RPV heater power, and the D/W pressure rose. The steam mixed with the nitrogen in the D/W and the steam-nitrogen mixture entered the PCC unit, which was indicated by a sudden decrease in the PCC tube inner surface temperature as shown at point A in Fig. 5. As the D/W pressure increased (point B in Fig. 6), the water level in the PCC vent line was falling (point C in Fig. 7). After 800 seconds, the pressure difference between the D/W and the S/C became large enough to clear the PCC vent line and vent the nitrogen to the S/C. In the nitrogen venting period, the nitrogen in the D/W was gradually transferred to the S/C via the PCCS, as indicated by the sudden temperature rise measured in the D/W (points A, B and C in Fig. 8). Most nitrogen in the D/W was transferred by 7,500 seconds and nearly pure steam was provided afterward to the PCC unit, which is suggested by the temperature rise in the PCC tube inner surface temperature (Fig. 5). The PCC heat removal performance, therefore, improved and the D/W pressure decreased. Thus, the test results clearly explain the characteristics of the PCCS nitrogen venting to the S/C.

4.4 PCCS System Response Test Phase 2 [5, 7, 8, 13]

Following the separate effect tests, integral system tests have been performed to investigate the PCCS heat removal performance following a LOCA and to provide the database for the analytical model verification. In this paper, a main steam line break (MSLB) simulation test, a RPV bottom drain line break (DLB) simulation test and a GDCS drain line break (GDCSLB) simulation test have been described. Table 4 summarizes the initial conditions for these tests, corresponding to one-hour after the LOCAs, which were determined from TRAC analysis for SBWR[4, 6]. The RPV heater power was controlled to fit the May-Witt decay heat curve. The tests ran for approximately 8 hours.

a) Main steam line break (MSLB) test

Figures 9 through 12 show the major system parameter transients. The D/W pressure increased and took its maximum at about 14,000 seconds and then decreased gradually. The maximum pressure was about 0.26 MPa, which was well below the design pressure (0.48 MPa).

Before about 10,000 seconds, the PCC vent water level was cleared, and the noncondensable gas in the D/W had been transferred to the S/C via the PCC vent line, as shown in Fig. 10. Due to the continuous GDCS injection to the RPV, the RPV water level increased and reached the DPV elevation. Consequently the RPV water spilled to the D/W via the DPV. The spilled water caused mixing in the D/W, since the noncondensable gas distribution in the D/W tends to be uniform, and the additional mixing increased the noncondensable transfer from the D/W to the PCC and S/C.

The noncondensable behavior, stated above, is demonstrated by Figs. 11 and 12. Before roughly 10,000 seconds, most of the noncondensable in the D/W was transferred and the axial vapor temperature distribution in the D/W tended to become a uniform distribution, as shown in Fig. 12. The vapor temperature shown in Fig. 11 also indicates the noncondensable accumulation in the bottom region of the tubes before 10,000 seconds.

The GDCS injection terminated at about 9,000 seconds and it caused a temporary increase in D/W pressure rise since the vapor generation in the RPV increased. The PCCS absorbed almost pure steam afterward as shown in Fig. 11, and therefore the PCCS heat removal rate improved. This resulted in the gradual depressurization in the D/W.

b) RPV bottom drain line break (DLB) test

The PCV pressure transient and the vapor temperature transient in the D/W are shown in Figs. 13 and 14. The overall pressure transient behavior is similar to that in the MSLB test since the major phenomena observed in the MSLB also occurs in the DLB. That is, the noncondensable transfer by steam flow and the mixing effect of the DPV

spill-over flow, the temporary D/W pressure rise caused by the GDCS termination and the gradual nitrogen gas accumulation in the annulus and bottom D/W. The initial nitrogen inventory in the D/W is, however, slightly less than that in the MSLB and therefore the peak D/W pressure is also smaller. The peak D/W pressure is about 0.24 MPa, which is within the design limit by a sufficient margin as in the case of the MSLB test.

c) GDCS line break (GDCSLB) test

Figures 15 and 16 illustrate the pressure transient and the vapor temperature in the D/W. In the GDCS line break case, the GDCS termination occurred earlier in the transient and there is no spill-over flow via the DPV. Hence, in the GDCSLB case, the pressure transient becomes flat and the pressure rise is milder, compared with the MSLB case. The peak D/W pressure of 0.24 MPa occurred at about 11,000 seconds. It is considered that nitrogen in the D/W is transferred to the S/C by the steam flow via the DPV and the steam flow generated by the break flow. It appears, however, from the temperature transient measured in the annulus D/W that the upward steam flow generated by the break flow may be so small that most nitrogen in the annulus D/W is not transferred to the S/C since the temperature suggested the accumulation of nitrogen in the annulus D/W.

d) Other cases

In the GIRAFFE test program, some potential issues, which may degrade the PCCS heat removal rate, have been investigated. In the later stage of LOCA blowdown phase, temperature stratification is formed in the S/P. The PCCS vents uncondensed steam to the hot temperature stratification layer in the S/P, while the PCCS heat removal rate is not large enough to condense all the steam to the PCC units. This may promote the temperature stratification and raise the S/C pressure.

If the leakage between D/W and S/C is considered, steam-noncondensable mixture in D/W directly flows into S/C. The steam through the leakage can raise the S/C pressure without being condensed by the PCCS and the S/P water. The leakage flow affects the noncondensable distribution in the PCV and the PCCS heat removal performance.

These issues have been fully investigated in the GIRAFFE tests and presented in references (7, 8). It has been shown that the peak PCV pressure is suppressed well below the design pressure even if these issues are taken into account.

From these test results, it can be concluded that the PCCS can suppress the containment pressure well below the design pressure regardless of the break pipe and some potential issues which affect the PCCS heat removal performance.

4.5 PCCS System Response Test Phase 3 with Lighter-than-steam Gas [14]

Even in a severe accident case, the PCCS is expected to suppress the containment pressure and prevent gas venting from the containment to the environment. As the first step to demonstrate the PCCS heat removal performance during a severe accident, the effect of a lighter-than-steam gas on the PCCS performance has been investigated in the PCCS system response test Phase 3. Helium gas was used to simulate hydrogen gas which can be generated by radiolysis or metal-water reaction in a severe accident.

The initial condition of the test was the same as that in the MSLB shown in Table 4, except that the noncondensable initially filled in the D/W was replaced by helium gas. Comparing with the MSLB test result using nitrogen gas, the effect of the helium gas can be understood. The test ran for approximately 30 hours.

The PCV pressure response is shown in Fig. 17. Although the pressure transient before GDCS termination (about 9000 seconds) and the peak D/W pressure are very similar to those obtained in the MSLB test with nitrogen gas, the pressure becomes flat after the GDCS termination while the pressure in the nitrogen case decreases after the timing. After the GDCS injection stops and there is no more mixing effect of the spilled water, nitrogen gas in the lower portion of D/W shows the tendency to accumulate as pointed out in the nitrogen case (see Figs 11 and 12). The PCC therefore absorbs almost pure steam from the D/W afterward. On the other hand, in the helium gas case, the annulus and lower D/W region continuously supplies the helium to the PCCS for the entire test duration as shown in Fig. 18. It is considered that the difference in the gas behavior is caused by the difference in the gas density.

The bulk vapor temperature in the PCC tube in the helium gas case is completely different from that in the nitrogen gas case, as illustrated by the comparison between Fig. 11 and Fig. 19. Due to the continuous gas supply to the PCC tube, the gas accumulation (vapor temperature decrease from the saturation temperature) is observed even after the GDCS termination. In addition, the helium gas tends to accumulate in the upper portion of the tube preferably in the long-term quasi-steady state condition.

In spite of these differences in the noncondensable behavior, the D/W peak pressure in the helium case is very similar to that in the nitrogen case. In the helium gas case, the gas in the PCC tube is vented intermittently to the S/C through the PCC vent line as shown in Fig. 20. Hence, the D/W pressure is kept almost constant in the long-term transient. In other words, the accumulation of the noncondensable in the helium gas case is determined such that the PCC heat removal rate matches the heat input

From the test result, it is considered that the PCCS can be a effective system even in a severe accident to remove the decay heat and maintain the integrity of the containment vessel. It is indispensable, however, to take the effect of both hydrogen and aerosol into account in order to demonstrate the feasibility.

5. GIRAFFE POST-TEST ANALYSIS (15)

The PCCS heat removal performance is affected by thermal-hydraulic behavior in the PCV, especially the noncondensable behavior, following a LOCA. The PCCS performance analysis model, therefore, needs to be qualified against system response tests with wide break spectra, which simulate accident scenarios in the whole containment system. In this section, the TRAC post-test analyses for the major GIRAFFE tests stated in section 4.4 are summarized.

In the TRAC post-test analysis, the GIRAFFE main component vessels, RPV, S/C, D/W, GDCS pool and PCCS pool are modeled using a 3-dimensional component, VESSEL component having three radial rings, one azimuthal sector and twelve axial levels and a one-dimensional component as shown in Fig. 21. The RPV occupies Levels 1 through 7 in Ring 1. The S/C is modeled with eight fluid cells, Levels 1 through 4 in Rings 2 and 3. The upper portion of D/W is simulated with the VESSEL cells, Levels 6 and 7 in Ring 3, and the middle and bottom region of the D/W (annulus D/W) is modeled with a one-dimensional component, PIPE component. Levels 8 through 12 in Rings 1 and 2 represent the PCCS pool and the chimney wall which separates the boiling region around the PCC from the subcooled water outside exists between Rings 1 and 2. This modeling makes it possible to simulate the natural circulation along the chimney. The GDCS pool is modeled with Levels 8 through 12 in Ring 3. The level tracking model is applied in all these component vessels to simulate the water level transients in these vessels. The PCC unit, the related piping and the other piping connecting the main vessels are modeled using one-dimensional components. The channel, the chimney region above the channel and the guide tube-bypass regions in the RPV are also modeled.

Heat loss from each component vessel to the ambient is modeled by specifying an outside wall heat transfer coefficient determined from the GIRAFFE system heat loss data. The measured values of the piping flow resistance are input to the analytical model. The circulation flow in the S/P is limited by specifying the flow resistance in the S/P to simulate the temperature stratification in the S/P.

Regarding the steam condensation heat transfer model in the presence of the noncondensable, two models have been applied depending on the vapor velocity. Inside the PCCS heat exchanger, Uehara correlation(12) has been applied to calculate the pure steam condensation heat transfer coefficient and the GIRAFFE data shown in section 4.2 has been used for the degradation coefficient. Uehara correlation is an empirical correlation which includes the effect of wavy pattern at the liquid film surface between laminar and turbulent regions. At the D/W inside wall, Nusselt film condensation model and Sparrow's stagnant model have been used, since the vapor velocity in the D/W vessel is very small compared with that in the PCCS heat exchanger.

Figures 22 and 23 show the TRAC prediction for the D/W and the S/C pressure responses to the MSLB, and D/W vapor temperature transient which should be compared

with Figs. 9 and 12. The TRAC calculation showed a good agreement for the overall pressure response and the D/W temperature transient. The pressure rise before 2,000 seconds which is mainly caused by the break flow and the DPV flow was well predicted. Between 2,000 and 10,000 seconds, TRAC predicted the pressurization in the PCV, which was due to the nitrogen transfer from the D/W to the S/C caused by the spilled water via the DPV, which is indicated by the temperature rise in the annulus D/W during the period. The temporary pressure rise around 10,000 seconds caused by the GDCS flow termination was also predicted. Although the depressurization rate in the D/W after 13,000 seconds was slightly underestimated, the peak D/W pressure agreed well with the GIRAFFE result. The S/C pressure was maintained constant after 13,000 seconds, also as in the GIRAFFE test. From the comparison, it was shown that the TRAC model can predict the major phenomena in the PCV and the PCCS heat removal performance in the MSLB.

The D/W and S/C pressure responses to the DLB and the GDCSLB are shown in Figs. 24 and 25, which should be compared with Figs. 13 and 15. It can be said that the overall transient are well predicted. From these results, it can be concluded that the TRAC model can accurately predict the major phenomena occurring in the PCV, and the PCCS heat removal rate following the LOCAs.

6. CONCLUSIONS

The passive containment cooling system provides engineered safety features which enhance system reliability and plant simplicity. The GIRAFFE testing program results have demonstrated that the PCCS has the capability to remove sufficient heat to suppress the post-LOCA containment pressure well below the design limit. In addition, it is shown that the PCCS can work even in the presence of the lighter-than-steam gas. This suggests the capability to maintain the integrity of the containment vessel even in a severe accident by the PCCS without releasing the gas to the environment.

The GIRAFFE program has provided the data base to qualify the TRAC model to predict the PCCS performance. The post test analysis has shown that the TRAC model can accurately predict the major post-LOCA phenomena occurring in the containment and the PCCS performance.

REFERENCES

1. Rao, A. S., et al., "Simplified Boiling Water Reactor Design," *Proceedings, The 1st JSME/ASME Joint International Conference on Nuclear Engineering (ICONE-1)*, Tokyo, pp. 295, 1991.
2. H. Nagasaka, et al., "Heat Removal Test of Isolation Condenser Applied as a Passive Containment Cooling System," ibid., b-1, pp.257.
3. S. Yokobori, et al., "System Response Tests of Isolation Condenser Applied as a Passive Containment Cooling System," ibid., b-2, pp. 265.
4. K. Arai, et al., "Analytical Study on Drywell Cooler Heat Removal Performance as a Passive Containment Cooling System," ibid., b-4, pp. 281.
5. S. Yokobori, et al., "System Response Test of PCCS Performance focused on the Equalizing Line Actuation," *Proceedings, International Conference on Design and Safety of Advanced Nuclear Power Plants (ANP'92)*, Tokyo, Vol. III., 1992.
6. K. Arai, et al., "Effects of Break Location on Passive Containment Cooling System Heat Removal Performance," ibid., Vol. III.
7. H. Nagasaka, et al., "System Response Test Focusing on the Thermal Stratification Effect in Suppression Pool," *Proc. of the 2nd JSME/ASME Joint Int. Conference on Nucl. Eng. (ICONE-2)*, San Francisco, pp.319, 1993.
8. S. Yokobori, et al., "System Response Test of PCCS Performance Considering Drywell-Wetwell Leakage," ibid., pp.683.
9. K. Arai, et al., "TRAC Analysis of Passive Containment Cooling System Performance," ibid., pp.143.
10. J. Otonari, et al., "Evaluation of Passive Containment Cooling System Performance for Simplified BWR," *Proc. of ANS Winter Meeting*, November, 1989, p.471.
11. E.M. Sparrow, et al., "Forced Convection Condensation in the presence of Non-condensables and Interfacial Resistance," Int. J. Heat Mass Transfer, pp. 1829, 10,1967.
12. H. Uehara, et al., 1991, "Gravity Controlled Film Condensation on a Vertical Plate (Empirical Equations for Harmonic Wavy and Turbulent Flow)," *Proceedings, 28th National Heat Transfer Symposium of Japan*, Vol. III, pp. 883.
13 S.Yokobori et al., "System Response Tests of Passive Containment Cooling System (PCCS) Heat Removal Performance Against Major Three Break Scenarios," *Proc. of the 3rd JSME/ASME Joint Int. Conference on Nucl. Eng. (ICONE-3)*, Kyoto, pp.1041, 1995.
14 S.Yokobori et al., "System Response Tests of PCCS Performance with Light Noncondensable Gas Considering Severe Accident Conditions," ibid., pp.1047, 1995.
15 K. Arai, "TRAC Qualification for Passive Containment Cooling System Performance Prediction against the GIRAFFE Tests" ibid., pp.1035, 1995.

ABBREVIATION

DPV	Depressurization Valve
D/W	Drywell
EQL	Equalizing Line
GIRAFFE	Gravity-Driven Integral Full-Height Test for Passive Heat Removal
GDCS	Gravity Driven Cooling System
IC	Isolation Condenser (IC)
LOCA	Loss of Coolant Accident
PCC	Passive Containment Cooler
PCCS	Passive Containment Cooling System
PCV	Primary Containment Vessel
RPV	Reactor Pressure Vessel
SBWR	Simplified Boiling Water Reactor
S/C	Suppression Chamber
S/P	Suppression Pool
V/B	Vacuum Breaker

Table 1 GIRAFFE Test Program

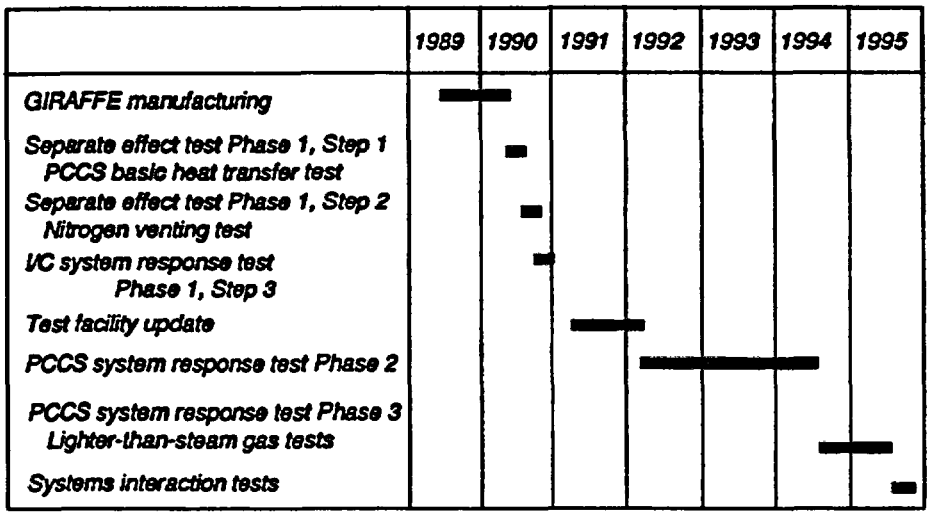

Table 2 Test Conditions for Basic Heat Transfer Tests (Phase 1, Step 1)

Total pressure	0.2 - 0.4 MPa
Nitrogen inlet partial pressure fraction (PN2/PTotal)	0.0 - 0.10
Steam inlet flow rate	0.02 - 0.04 Kg/sec

Table 3 Initial Test Conditions for Nitrogen Venting Test (Phase 1, Step 2)

D/W total pressure	0.314 MPa
D/W nitrogen partial pressure	0.016 MPa
D/W gas temperature	406 K
S/C total pressure	0.301 MPa
S/C nitrogen partial pressure	0.278 MPa
S/C temperature	336 K
S/C water level	5.55m
RPV pressure	0.314 MPa
RPV temperature	407 K
PCCS pool temperature	373 K

Table 4 Initial Test Conditions for MSLB, DLB and GDCSLB Tests
(Phase 2 Tests)

	MSLB	GDCSLB	DLB
D/W total pressure (MPa)	0.192	0.186	0.197
D/W nitrogen partial pressure fraction	0.281	0.210	0.091
D/W gas temperature (K)	381	383	389
D/W water level (m)	0.0	0.24	0.32
S/C total pressure (MPa)	0.174	0.187	0.199
S/C nitrogen partial pressure (MPa)	0.164	0.177	0.190
S/C temperature (K)	326	325	324
S/C water level (m)	5.5	5.5	5.5
RPV pressure (MPa)	0.193	0.186	0.197
RPV temperature (K)	392	390	393
GDCS pool water level (m)	2.8	1.0	2.2
GDCS pool temperature (K)	350	344	348
PCCS pool temperature (K)	373	373	373

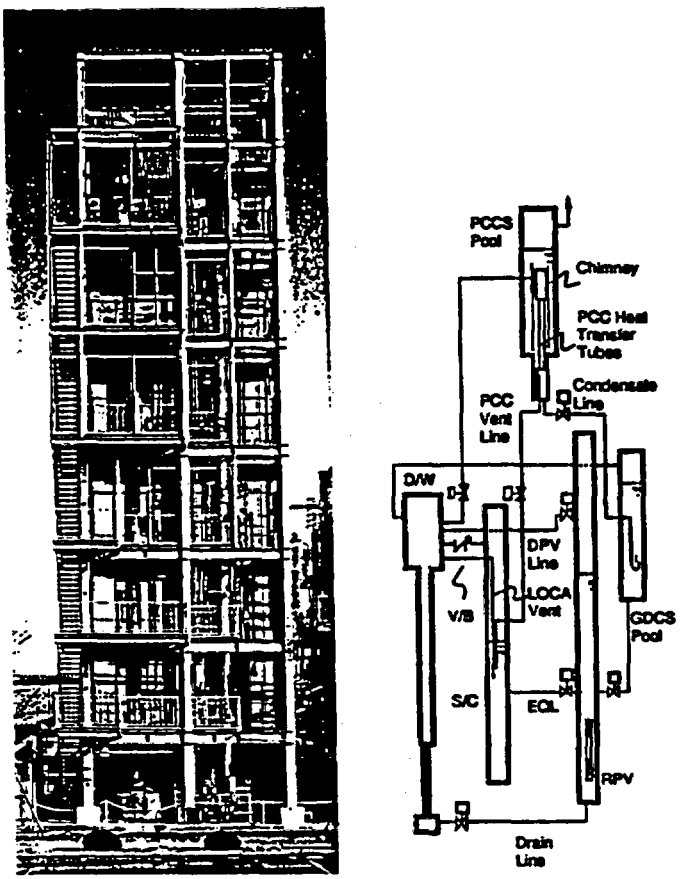

Photo 1 GIRAFFE Loop Schematics

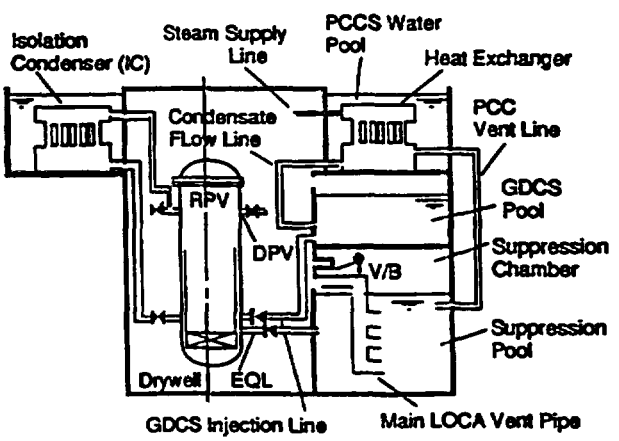

Fig. 1 Schematic Diagram of SBWR Safety System

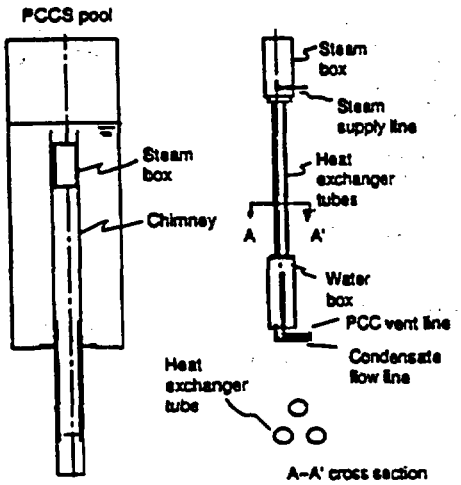

Fig. 2 Passive Containment Cooler Unit and PCCS Pool

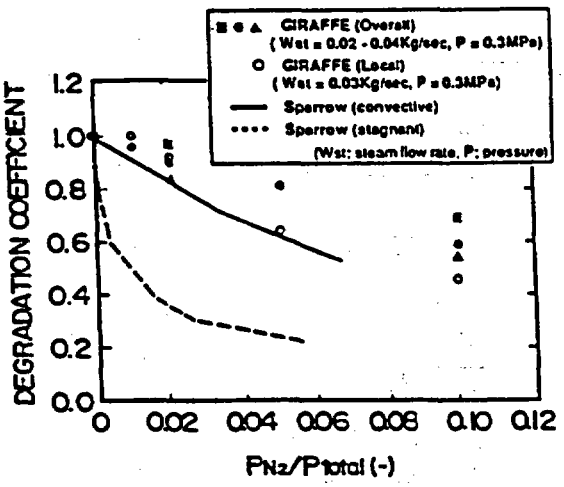

Fig. 3 Steam Condensation Degradation Coefficients

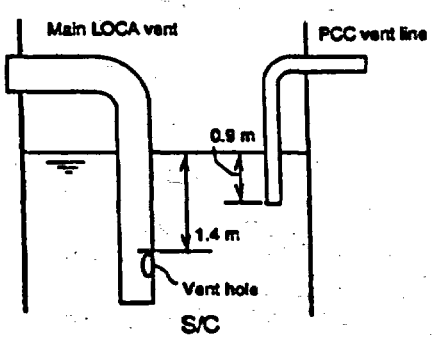

Fig. 4 Submergence of PCC Vent and Main LOCA Vent Pipes

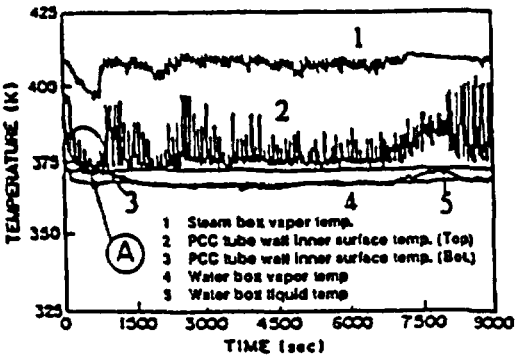

Fig.5 PCC Wall Inner Surface Temperature

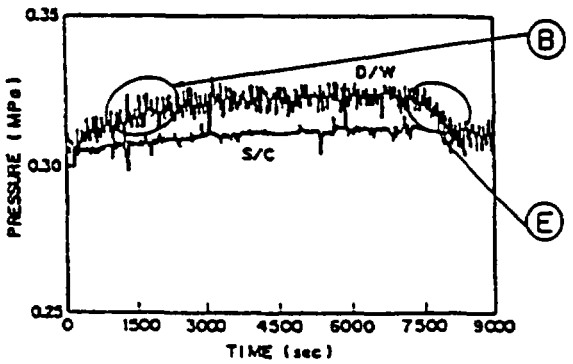

Fig.6 D/W and S/C Pressures

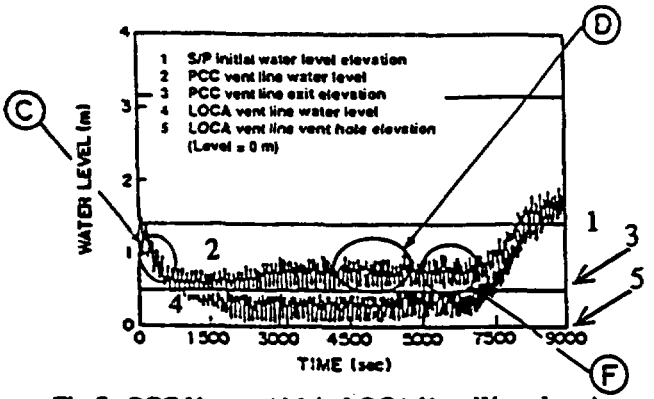

Fig.7 PCC Vent and Main LOCA Vent Water Levels

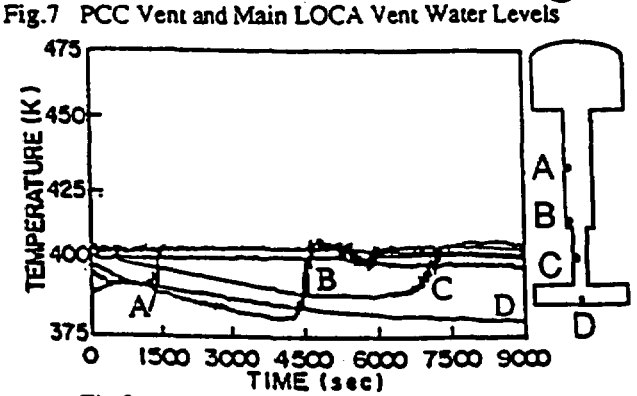

Fig.8 Annulus D/W Vapor Temperature

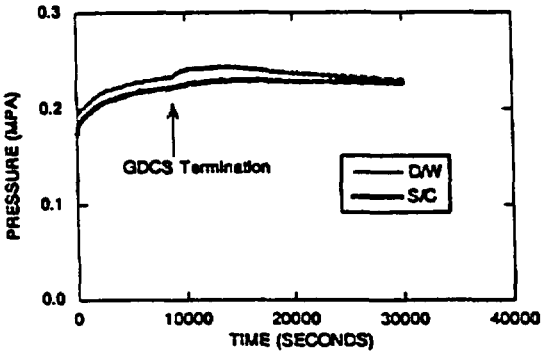

Fig. 9 PCV Pressure Response to MSLB

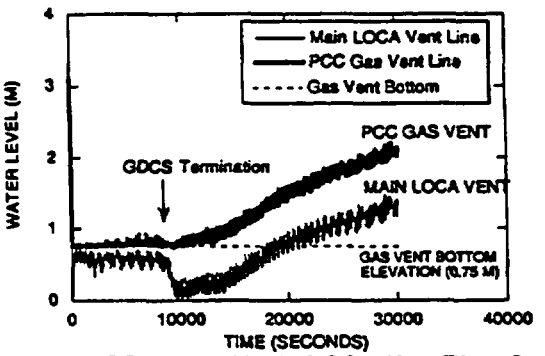

Fig. 10 PCC Vent and Main LOCA Vent Water Levels (Elevation of LOCA Vent Hole = 0.0 m)

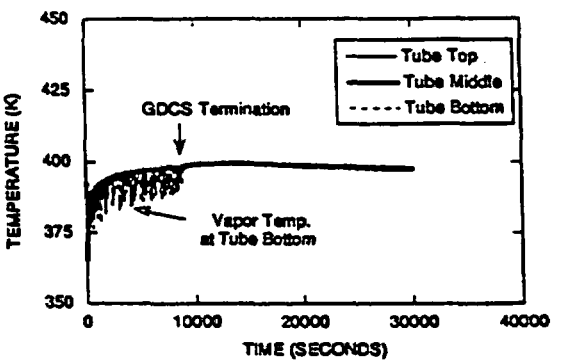

Fig. 11 PCC Tube Vapor Temperature

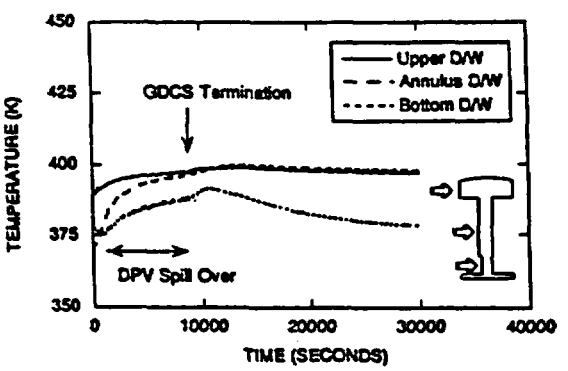

Fig. 12 D/W Vapor Temperature

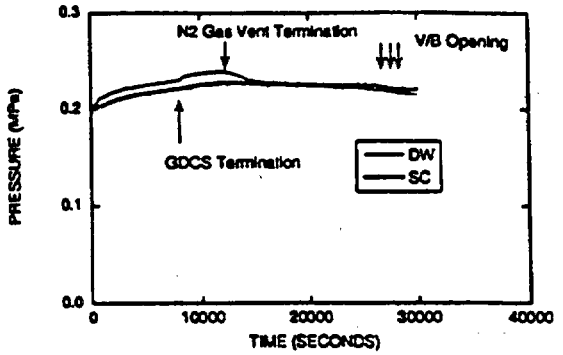

Fig. 13 PCV pressure response to DLB

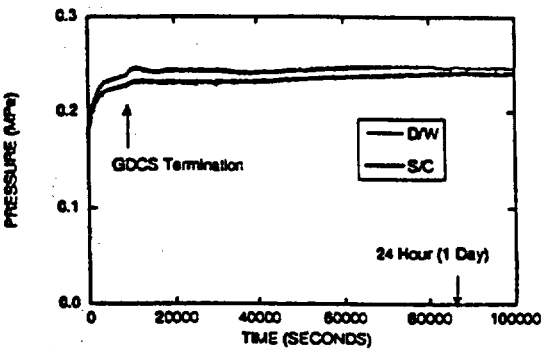

Fig. 17 PCV Pressure Response in Helium Case

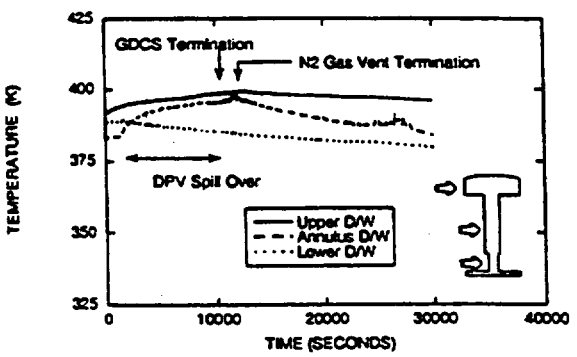

Fig. 14 DW Vapor Temperature (DLB)

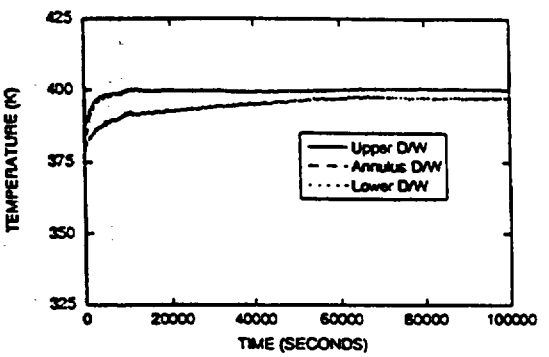

Fig. 18 D/W Vapor Temperature in Helium Case

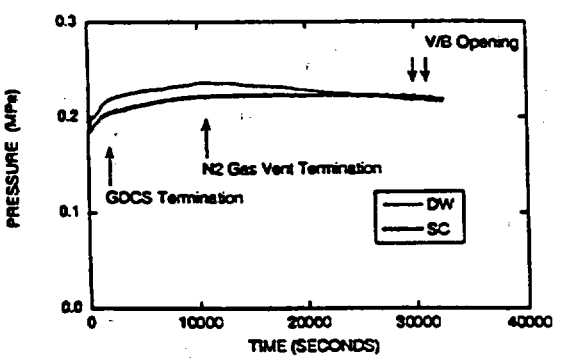

Fig. 15 PCV Pressure Response to GDCSLB

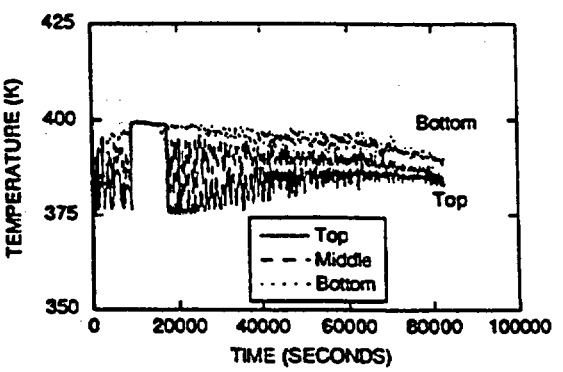

Fig. 19 PCC Bulk Temperature in Helium Case

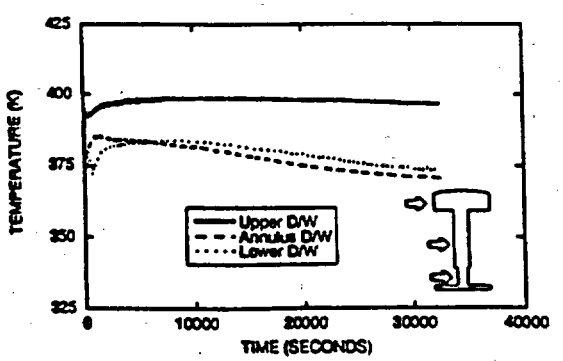

Fig. 16 DW Vapor Temperature (GDCSLB)

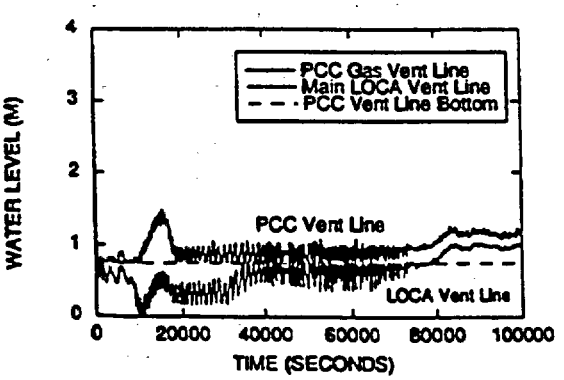

Fig. 20 PCC Vent & LOCA Vent Water Level (Bottom of LOCA Vent = 0.0 m)

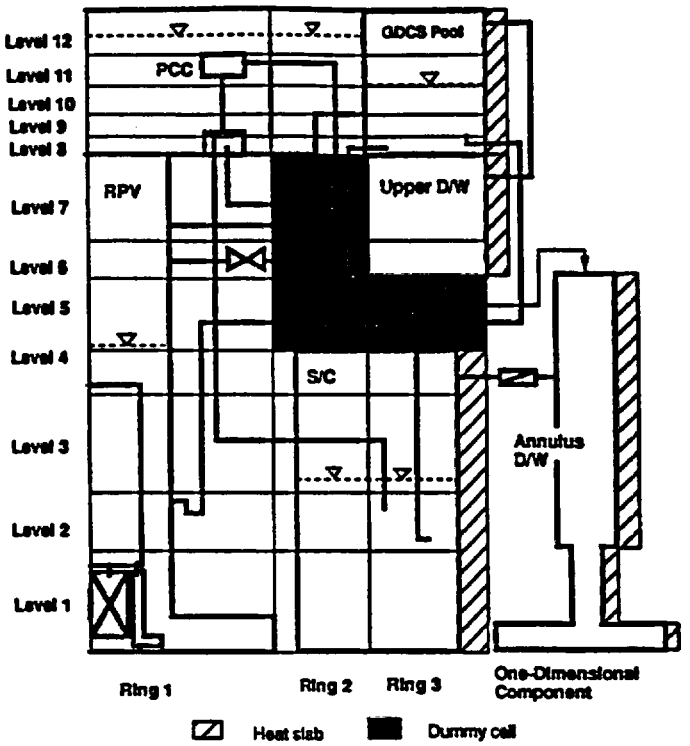

Fig. 21 TRAC Nodalization for GIRAFFE Analysis

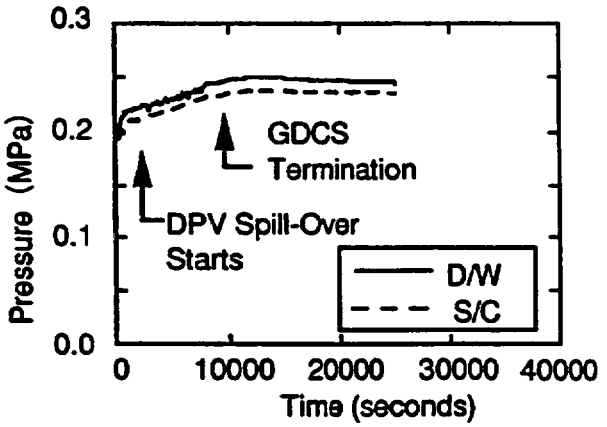

Fig. 22 TRAC Prediction of Pressure Response (MSLB Case)

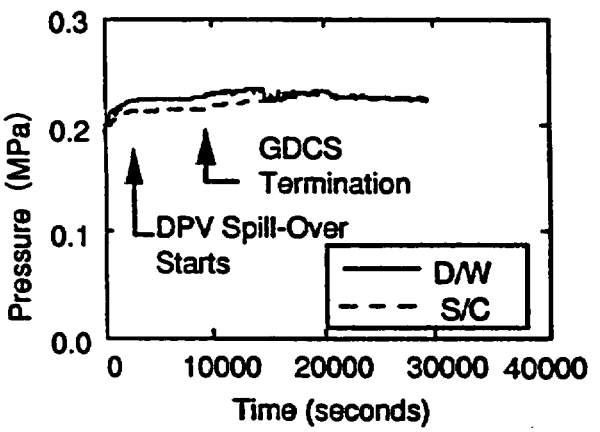

Fig. 24 TRAC Prediction of Pressure Response (DLB Case)

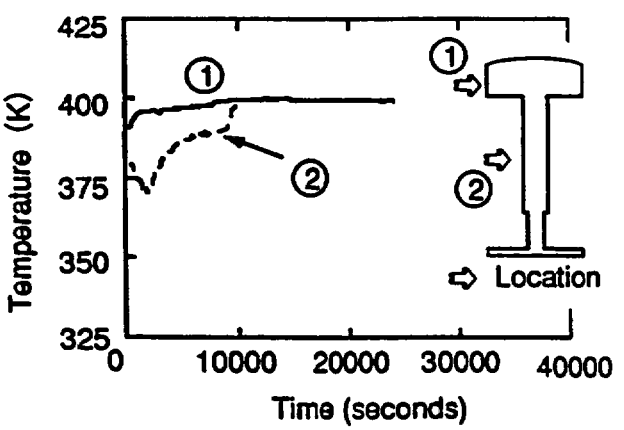

Fig. 23 Vapor Temperature in D/W (TRAC) (MSLB Case)

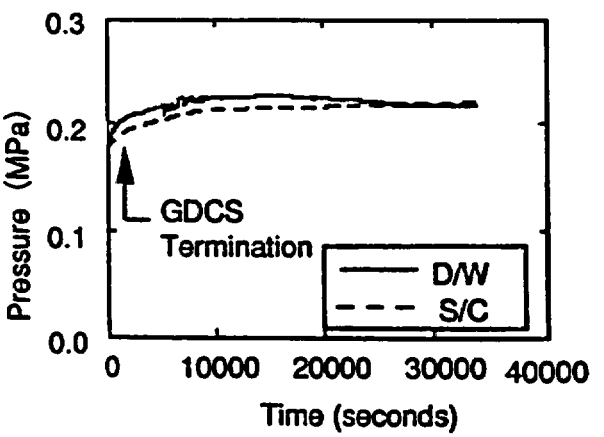

Fig. 25 TRAC Prediction of Pressure Response (GDCSLB Case)

RESULTS FROM THE NRC AP600 TESTING PROGRAM AT THE OREGON STATE UNIVERSITY APEX FACILITY

Jose N. Reyes, Jr.
Department of Nuclear Engineering
Oregon State University
Radiation Center C116
Corvallis, Oregon, USA 97331-5902

David E. Bessette
Reactor and Plant Systems Branch
Division of Systems Research
Office of Nuclear Regulatory Research
U.S. Nuclear Regulatory Commission
Washington, D.C., USA 20555

Marino DiMarzo
Department of Mechanical Engineering
University of Maryland
College Park, Maryland, USA 20742

ABSTRACT

The Department of Nuclear Engineering at Oregon State University (OSU) is performing a series of confirmatory tests for the U.S. Nuclear Regulatory Commission. These tests are being conducted in the Advanced Plant Experiment (APEX) facility which is a 1/4 length scale and 1/192 volume scale integral system simulation of the Westinghouse Advanced Passive 600 MWe (AP600) plant. The purpose of the testing program is to examine AP600 passive safety system performance, particularly during long term cooling. Thus far, OSU has successfully performed ten integral system tests for the NRC. This paper presents a description of the APEX facility and summarizes the important results of the NRC test program at OSU.

1. INTRODUCTION

The AP600 is an advanced reactor design, developed by Westinghouse, which relies on passive systems for safety injection and long term cooling of the core. Title 10 Part 50.46 of the Code of Federal Regulations requires that the computer codes used to evaluate the performance of these new passive safety systems be benchmarked against applicable experimental data. To this end, the Department of Energy (DOE) and Westinghouse Electric Corporation cooperated on the construction of an integral test facility that models the AP600 design. The facility, called the *Advanced Plant Experiment (APEX)*, was build at Oregon State University (OSU).

Westinghouse performed a series of experiments in APEX as part of its experimental program in support of AP600 design certification. The NRC subsequently contracted with OSU to run a series of experiments following the completion by Westinghouse of its experimental program.

The facility is designed around a basic concept: study the passive safety features of the AP600 under natural circulation and depressurization conditions. The facility scaling objectives were to: identify important processes; establish the priorities for preserving important processes; obtain the similarity groups that should be preserved between the facility and the full-scale prototype for these processes; establish the priorities for preserving the similarity groups to assure that important processes have been identified and addressed; provide specifications for test facility designs; and quantify the biases due to distortions. The facility design and testing program takes account of the following:

- A spectrum of transients are possible, i.e.. small break LOCAs in various locations (e.g. P cold leg, C cold leg, hot leg, PBL line DVI line) orientations (top, side, bottom), SGTR(s), large breaks, secondary side breaks, transients, etc.;

- The AP600 system has multiple loops capable of competing flow and interactions i.e. PRHR loop, two CMT loops, two primary loops, ADS 1-3 loop, two ADS4 loops;

- The AP600 system has multiple components acting as mass and energy sources and sinks. Mass sources include CMTs, accumulators, IRWST, sump, non-safety systems while mass sinks include the break, ADS 1-3, ADS4a and ADS4b. Energy sources: core, structures, steam generators. Energy sinks consist of the break, ADS 1-3, ADS4s, steam generators, CMTs, and the PRHR.

In general, the purpose of the NRC test program is to assess the margin of safety afforded by the AP600 design and to benchmark the NRC assessment code RELAP5/MOD3. This paper presents a description of the APEX facility and the key results obtained thus far from the NRC test program at OSU.

2. APEX FACILITY DESCRIPTION

The facility scaling basis is described in Reference 1. This report describes the comprehensive scaling methodology used to design a scaled test facility representative of the AP600 at 1:4 height and 1:192 volume scale. The report provides a ranking of the important AP600 phenomena, the dimensionless groups that should be preserved in the test facility and the critical geometric attributes of the scaled facility. Most facility dimensions follow from three basic decisions: (1) 1:4 height; (2) 1:6.9 diameter scale; and (3) pressure scale (400 psi). For gravity driven systems, a 1:2 time scale is the natural consequence of selecting a 1:4 height scale. This time scale was preserved for all of the important transport processes.

APEX accurately models the details of the AP600 geometry including the primary system, the passive safety systems, and parts of the non-safety grade CVCS and RNS. The interconnecting pipe routings are also duplicated in the model. Reference 2 provides a detailed description of APEX.

2.1 Primary System

The APEX primary system includes the following components:

- A *RPV* that models the upper and lower reactor internals, the core barrel, the downcomer, and the core. Connections for the hot and cold legs and DVI lines are provided. The RPV houses 48 electric heater rods each having a 1 inch (2.54 cm) diameter and a heated length of 36 inches (91.44 cm). The maximum core power is 600 kW.

- *Reactor coolant loop piping* that models two primary loops, each consisting of one hot leg and two cold legs. Break spool pieces have been installed on the hot and cold legs, the DVI line, and the CMT-PBL to simulate pipe breaks. The discharge from these valves vent to the BAMS to separate and measure break flow rates.

- Two *SGs*, one on each loop, each having tube and shell dimensions scaled to simulate a Westinghouse Delta-75 SG.

- Four *RCPs*, two attached to the lower channel head of each SG.

- A *Pressurizer* with internal heaters capable of controlling pressure and minimizing pressure spikes in the RCS.

2.2 Passive Safety System

The APEX facility includes the following passive safety systems:

- Two *CMTs* each having a pressure balance line that connects the CMT head to the cold leg. Each CMT also has an injection line that permits draining of the CMT into one of two DVI lines connected to the reactor downcomer. Check valves and isolation valves have been included.

- An *ADS* system that includes three valves off the top of the pressurizer. The flow from ADS 1-3 is directed to a sparger that vents directly into the IRWST. The ADS 1-3 flow nozzles are sized to represent two-trains of ADS 1-3 in the AP600. Fourth stage ADS is modeled by a single valve located off the top of each hot leg. The ADS 4 flow nozzles are sized to model two trains of ADS 4 on each hot leg in the AP600. Failure of the ADS 1-4 valves can be simulated by installing different flow nozzles.

- Two *Accumulators* pressurized with nitrogen to provide safety injection during depressurization events. Each accumulators has an injection line that connects to one of two DVI lines. Check valves and isolation valves have been included.

- An *IRWST* having two injection lines that connect to each DVI line. The IRWST is capable of being pressurized to 80 psia to simulate containment backpressure. Return lines to the DVI lines are provided to represent containment sump recirculation lines.

- A *PRHR* heat exchanger located inside the IRWST. The PRHR is driven by natural circulation. It draws liquid from one hot leg, rejects heat to the IRWST liquid, and returns cooled liquid into the lower channel head of one SG.

Figures 1 and 2 present schematics of the APEX Test Facility.

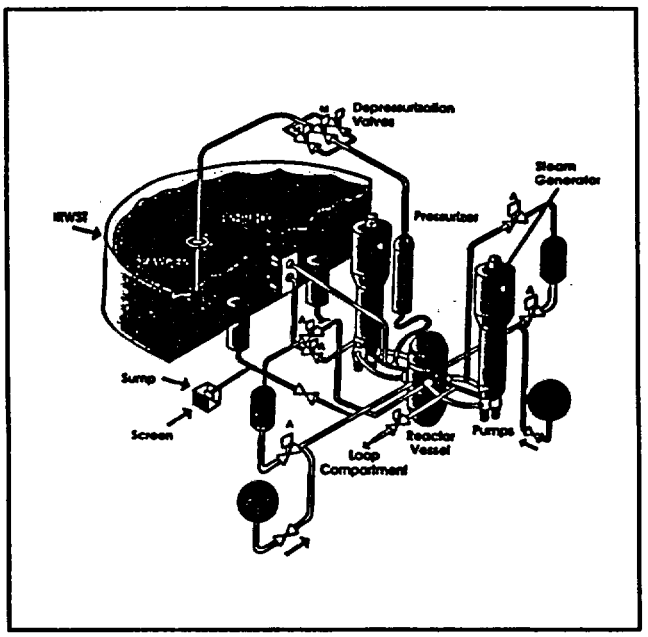

Figure 1. Layout of the APEX Test Facility

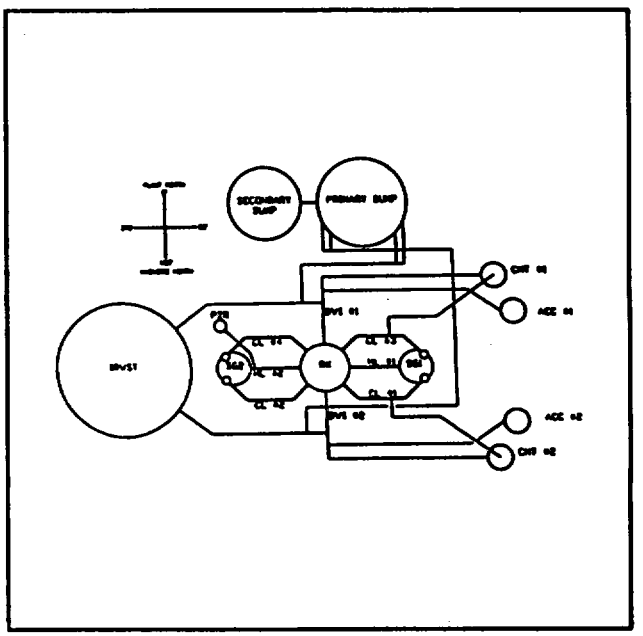

Figure 2. Line Diagram of APEX Test Facility

2.3 Break and ADS Measurement System

The BAMS is used to measure two-phase flows from breaks and the ADS measurement system. The two-phase flow is directed to a separator where the flow is separated into liquid and vapor. The liquid flow is measured and directed to the appropriate tank (IRWST or Primary Sump). The vapor flow is measured and vented from the test facility. Vapor flow from ADS 1-3 is directed into the IRWST. Electrical strip heaters are used to maintain boundary conditions at approximately 200°F. The system is capable of being pressurized to 80 psia to simulate containment backpressure.

The BAMS contains the following components:

- A *Primary and Secondary Sump* - Simulates the containment compartment volumes below the normal floodup elevation. The Primary and Secondary Sumps are connected with a line at a level simulating the curve overflow level in the AP600. The liquid overflow from the IRWST is also collected in the Secondary Sump. Both tanks are capable of being pressurized to 80 psia to simulate containment backpressure. Return lines to the DVI are connected to the Primary Sump to represent the containment sump recirculation lines.

- *Four Moisture Separators* - Three ADS separators and one break separator sized based on maximum expected flowrates. Separation is primarily accomplished by the use of gravity and a swirl vane moisture separator element. Each separator is provided with a loop seal line on the liquid discharge to ensure vapor flow does not bypass the separator.

- *Containment Sump Return System* - Heated water from a hold-up tank is pumped into the Primary Sump and the IRWST at a mass flow rate equivalent to the mass flow rate of the vented steam. This heated liquid simulates the flow of condensate from the steam vented into the containment building. This steam would be condensed and drain into the IRWST or the containment (primary) sump.

2.4 Instrumentation

A detailed list of all of the instruments and their locations is provided in Appendix A. APEX includes the following types of instruments:

- *Thermocouples (TF/TFM/TH/TW)* are used to measure fluid temperatures. They are also used to measure the temperature distribution in the CMT walls and core heater rods. Premium grade thermocouples have been used and connected to the DAS through controlled purity thermocouple wire.

- *Magnetic Flowmeters (FMM)* are used to measure all single-phase liquid flow rates.

- *Pressure Transducers (PT)* are used to measure the static pressures within the various tanks and piping.

- *Differential Pressure (DP)* transducers are used to measure liquid levels in various tanks and piping. They are also used to determine pressure drops.

- *Vortex Flowmeters (FVM)* are used to measure all steam flow rates.

- *Heat Flux Meters (HFM)* are used to measure heat loss from individual tanks and components.

- *Heated Phase Switches (HPSs)* are used to determine the fluid phase at various points inside system piping. Each HPS consist of three measurements: 1) fluid temperature, 2) T between the fluid and the heater, and 3) a relative heat transfer coefficient.

- *Load Cells (LC)* are used to measure the weight of liquid inside the IRWST, the Primary Sump, and the Secondary Sump.

Ambient air temperature and barometric pressure are also recorded. All of the instruments are monitored and recorded by the DAS. Additionally, a sequence-of-events program is used to monitor various pumps and valves in the test facility.

3. NRC APEX TEST MATRIX

The NRC APEX test matrix primarily focused on Small Break Loss-of-Coolant-Accidents (SBLOCA). The following summarizes the NRC tests being conducted during the first year of the contract. The tests fall into five categories:

1. Design basis accident scenarios intended to provide counterpart to ROSA for very small breaks and transients not covered by the Westinghouse test program.

2. Beyond design basis accident scenarios which are also counterpart to ROSA tests.

3. Tests to examine scaling issues associated with depressurization from the Westinghouse program.

4. Tests intended to help understand the data from the Westinghouse program.

5. PIRT driven tests.

Table 1 lists the tests performed thus far in 1995.

NRC-1 is a one inch cold leg break with failures of all ADS stages 1, 2, and 3 valves to open. Both of the fourth stage ADS trains are fully functional. This is beyond design basis and is counterpart to ROSA test AP-CL-05. The objective was to determine the effect that reduced ADS capability has on the system's ability to depressurize to IRWST injection. The ROSA test stayed at high pressure for an extended period of time. This extended period at high pressure was important since all of the Westinghouse tests were larger breaks, i.e. the break alone was sufficient to remove decay heat. Therefore, limited information was available from OSU on extended PRHR natural circulation, CMT recirculation and heatup, and thermal stratification in the primary system.

NRC-2 is a station blackout and is counterpart to ROSA test AP-SB-01. The purpose is to evaluate the long term PRHR performance including heatup of the IRWST to saturation. The test evaluates ADS performance when the discharge is to a saturated pool. The IRWST injection begins with the IRWST at saturated conditions so the period of subcooling of the primary system is not present. The test has an extended duration at high pressure.

NRC-3 is a two inch cold leg break which duplicates Westinghouse test SB1. The purpose was to remove a check valve in the sump exit, which is an artifact of the facility, to determine its effect on oscillations during the long term cooling phase. The test met its objectives and we were able to conclusively prove that the oscillation prior to sump injection was a facility artifact.

NRC-4 is also a two inch cold leg break repeat of SB1. The purpose was to bypass the break separator, which is an artifact of the facility, to determine its effect on oscillations during the long term cooling phase. Suspicion was directed at the break separator from an examination of the Westinghouse data, however, a mechanistic explanation to connect the two was never found. The test met its objective, showing that the oscillation upon return to saturation was not a result of the break separator. In the meantime a mechanism for the oscillation was developed and explored in NRC12.

Table 1
NRC Tests Performed

NRC TEST	DESCRIPTION	TEST
NRC-3	2" Break, Bottom of Cold Leg #3 with Long Term Cooling without Check Valve CSS-912	2-6-95
NRC-4	2" Break, Bottom of Cold Leg #3 with Long Term Cooling and Direct Discharge to the Primary Sump	2-13-95
NRC-1	1" Break, Bottom of Cold Leg #3 with Failure of ADS Valves 1-3 to Open. ROSA Counterpart Test AP-CL-05.	3-16-95
NRC-11	2" Break, Bottom of Cold Leg #3 with Modified ADS 1-3 Logic and No CMT Refill	5-25-95
NRC-7	1" Break, Bottom of Cold Leg #3 with Modified ADS 1-3 Logic and No Nitrogen Injection	6-8-95
NRC-6	1" Break, Bottom of Cold Leg #3 with Full Pressure ADS Blowdown and no ADS 4 Failures (Transient in Progress Simulation)	6-29-95
NRC-14	1" Break, Bottom of Cold Leg #3 with Full Pressure ADS Blowdown and a Single ADS 4 Failure (Transient in Progress Simulation)	7-19-95
NRC-12	1" Break, Bottom of Cold Leg #4 with Modified ADS 1-3 Logic	7-27-95
NRC-5	½" Break, Bottom of Cold Leg #3 without CMT Refill	8-21-95
NRC-10	1" Break, Bottom of Cold Leg #3 with Failure of 3/4 ADS 4 Valves	8-24-95
NRC-13	Parametric Study of Flow, Pressure and Level Oscillations at Return to Saturation Conditions	10-19-95

NRC-5 is a one-half inch cold leg break and is counterpart to ROSA test AP-CL-04. The purpose is to explore CMT and PRHR natural circulation during extended operation at high pressure characteristic of very small breaks, similar to NRC1 and NRC2. A break of this size is smaller than was considered by the Westinghouse testing.

NRC-6 is a one inch cold leg break at full pressure and is similar to ROSA test AP-CL-03 with the exception that both ADS4 are fully functional and ADS 1-3 are sized at nominal flow areas rather than minimum flow areas. The purpose is to operate the OSU facility at full pressure using initial conditions determined by AP-CL-03. In this test, ADS1 actuated at 3400 seconds at a pressure of 420 psig. Thus it is possible to operate OSU near full pressure rather than as a scaled pressure facility and initialize the conditions to be representative of ROSA at 3400s. This test avoided pressure scaling and provides a different representation of the ADS phase of the transient than the other tests which were based entirely on scaled pressure.

NRC-7 was a one inch cold leg break without nitrogen injection. This is counterpart to Westinghouse SB23. The purpose was to determine the effect of noncondensables on late depressurization and long term cooling,

particularly with regard to PRHR operation and CMT refilling, as well as the possibility to refill other volumes in the absence of noncondensables. As such, it is directed at understanding of phenomenology. It provides information on nitrogen effects, which are identified in the PIRT.

NRC-8 is a one inch cold leg break with failure of CMT drain valves to open. This is beyond design basis and is counterpart to a planned ROSA test. ADS is manually actuated after a time delay. The purpose is to determine the inventory history and ADS depressurization with reduced coolant injection.

NRC-9 is a loss of feedwater with failure of PRHR and is beyond design basis and counterpart to a planned ROSA test. The purpose is to explore system performance in the absence of a principal safety system and to determine CMT performance during extended operation at pressures up to the safety valve setpoint.

NRC-10 is a one inch cold leg break with failure of 3/4 ADS4 valves to open. This is beyond design basis and counterpart to a ROSA test. It is intended to extend the region examined in Westinghouse test SB7. That test had 2/4 ADS4 valves failed and the data showed a significant decrease in the margin to depressurize to allow IRWST injection. On the other hand, it is believed that failure of 4/4 ADS4 valves to open could prevent IRWST injection. This test determines the design margin for one of the most important aspects of the AP600 design, namely the ability to depressurize to allow IRWST injection.

NRC-11 is a two inch cold leg break with rescaled ADS1-3. Examination of the Westinghouse test data revealed that ADS1-3 was overscaled for late phase depressurization. The sizing of ADS1-3 was reduced to obtain better scaling.

NRC-12 was a two inch cold leg break in the PRHR side of the plant. This was the first test with the break on this side. The break drained away the cold returning fluid from the PRHR. The results can be compared to see the effect of break location. The test was run without CMT refill. During the oscillation upon return to saturation, the break was closed at the point in the oscillation when ADS4 flow was at a minimum. The ADS4 flow proceeded through a normal increase in flow, through a maxima, and then settled out immediately at an expected nominal value. When the break was reopened, the oscillation did not reestablish itself.

NRC-13 is a parametric study of the flow, pressure and liquid level oscillations that occur during IRWST liquid injection while the core is at saturated fluid conditions.

NRC-14 is a one inch cold leg break at full pressure similar to ROSA test AP-CL-03 with the exception that the ADS 1-3 flow areas are set to their nominal values rather than their minimum values. This test also assumes that 1 of 4 of the ADS 4 valves fails to open. This test avoided pressure scaling and provides a different representation of the ADS phase of the transient than the other tests which were based entirely on scaled pressure.

NRC-15 is a one inch cold leg break at full pressure. It is the counterpart to ROSA test AP-CL-03. This test assumes that 1of 4 of the ADS 4 valves fails to open. This test avoided pressure scaling and provides a different representation of the ADS phase of the transient than the other tests which were based entirely on scaled pressure.

4. APEX RESULTS

This section briefly summarizes the results obtained thus far from the NRC test program at OSU. In general, the NRC test program at OSU has:

a. Demonstrated APEX test repeatability.

b. Identified and eliminated some sources of non-prototypical behavior caused by APEX facility distortion or measurement systems.

c. Developed APEX counterpart tests for comparisons to other test facilities.

d. Identified phenomena applicable to AP600.

e. Provided data for purposes of benchmarking the NRC's assessment code RELAP5/MOD3.

4.1 APEX Test Repeatability

Figure 3 presents the pressure history for NRC-3, which is typical of an AP600 two-inch cold leg break simulation. The transient can be divided into the following phases:

- Subcooled Blowdown
- Saturation Natural Circulation
- ADS Operation (ADS 1-4)
- IRWST Injection
- Sump Recirculation Cooling

Test NRC-3 (Reference 3), performed on February 6, 1995 was a repeat of the Westinghouse two-inch break simulation (SB-1) performed on June 1, 1994. As shown in Figures 4 through 6, these two tests showed essentially identical results. The minor differences in the test results could be directly attributed to slight differences in initial conditions or improvements to the facility which shall be discussed in the next section.

In general, APEX provides very repeatable results for simulations of AP600 breaks larger than two-inches in diameter. NRC-3, NRC-4 and NRC-11 all demonstrate the excellent repeatability of an AP600 two-inch cold leg break simulation. (Reference 4,5)

For simulations of AP600 breaks smaller than one-inch, the variability of the CMT draining process, inherent to gravity draining under flashing conditions, becomes more significant. Because ADS actuation is dependent on CMT liquid volume, this variability in CMT draining affects the timing of ADS-1 actuation. Subsequent to ADS operation, the system follows the same repeatable event trajectory. The CMT draining phenomena will be the topic of additional study.

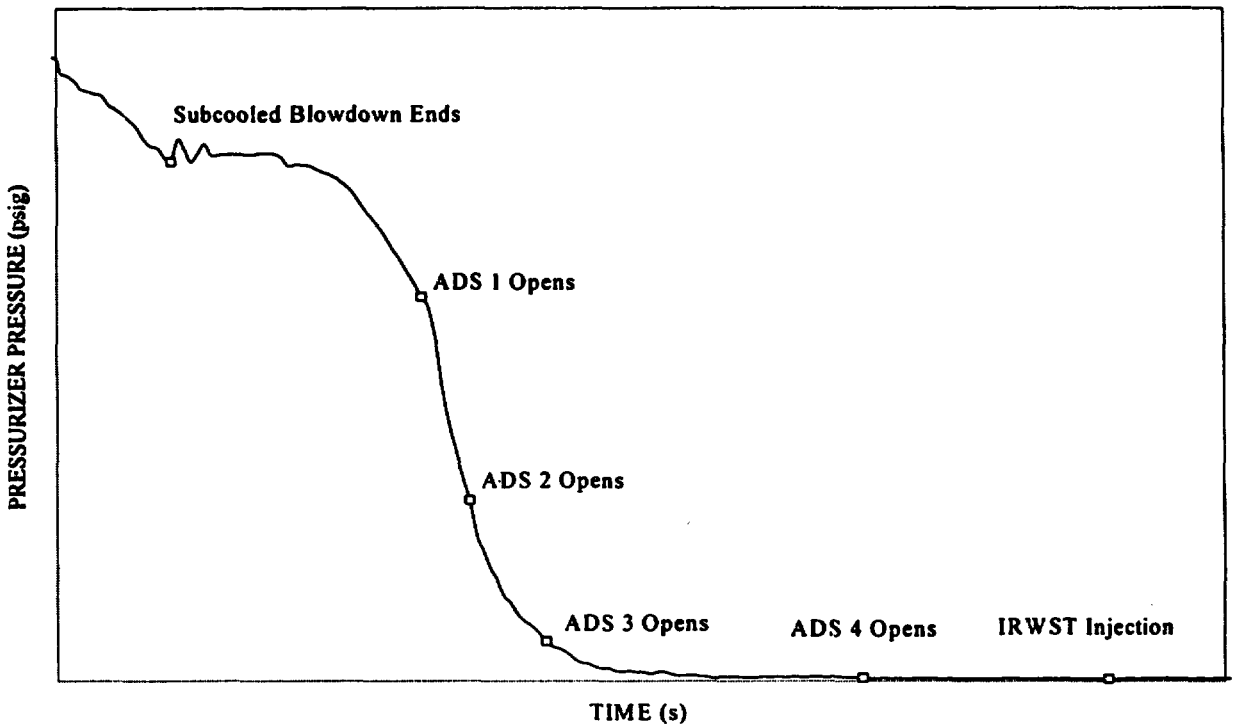

Figure 3. Typical Pressure History for a 2" Cold Leg Break Simulation in APEX

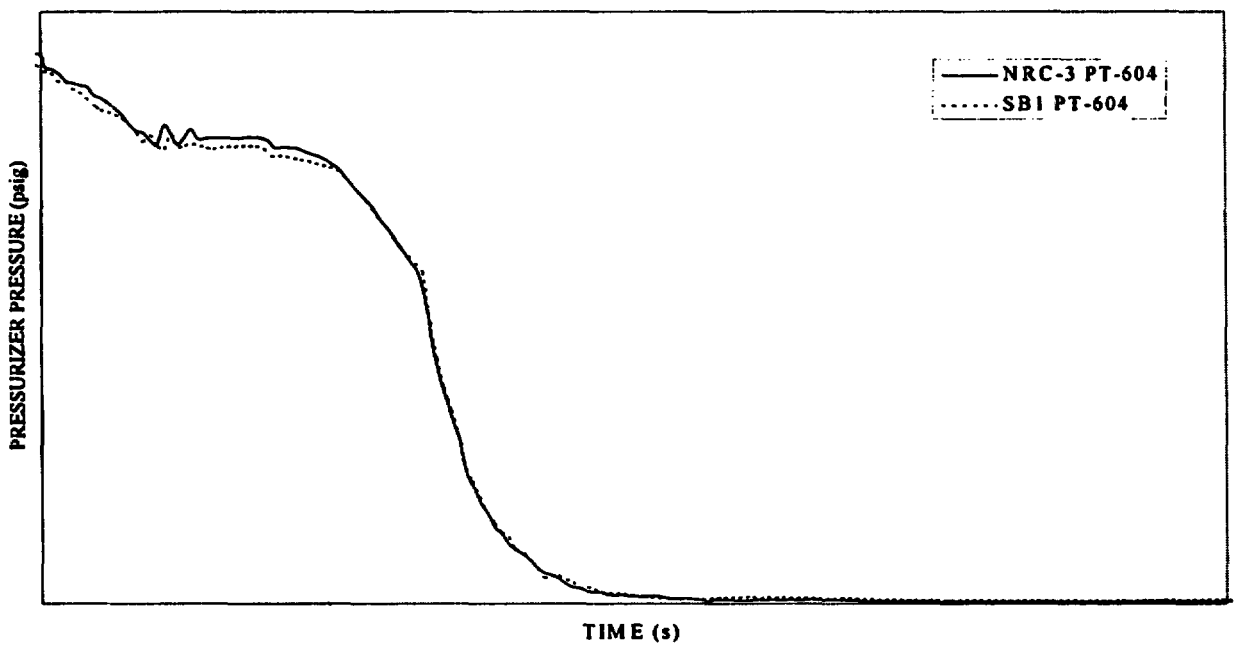

Figure 4. Comparison of NRC-3 (2/95) and SB1 (6/94) Pressurizer Pressure

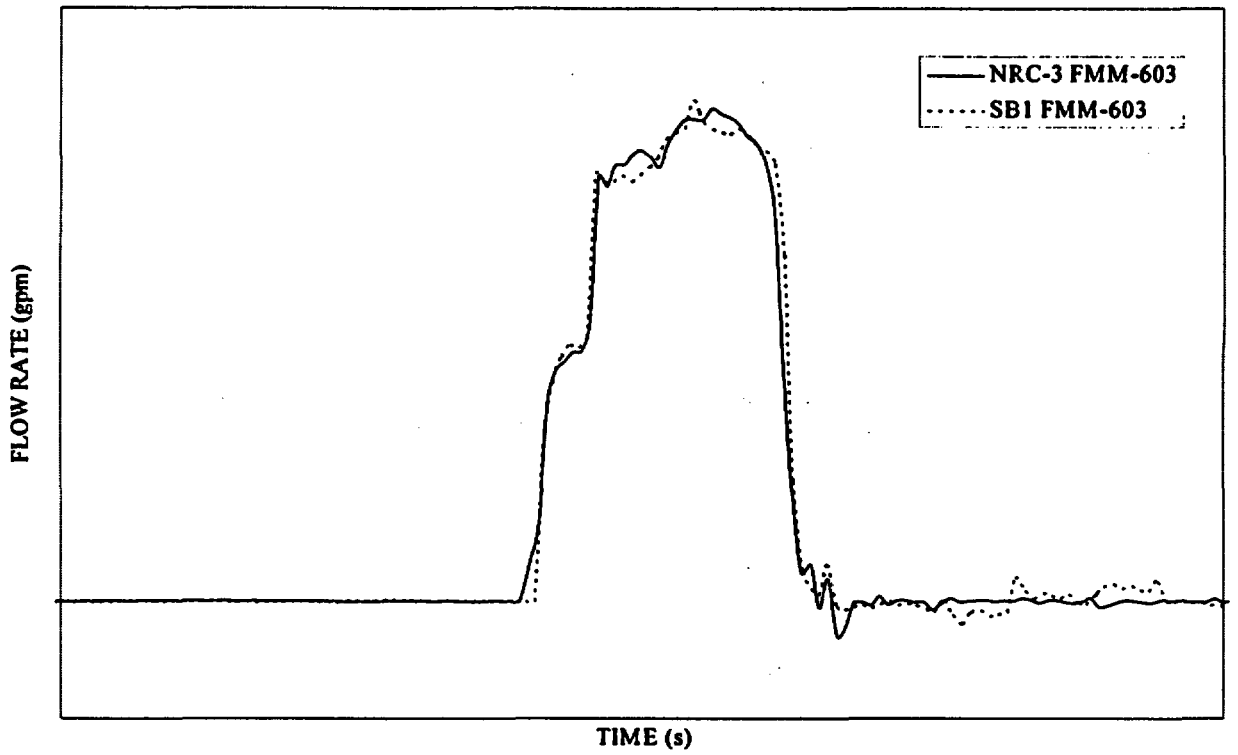

Figure 5. Comparison of NRC-3 (2/95) and SB1 (6/94) Accumulator Flows

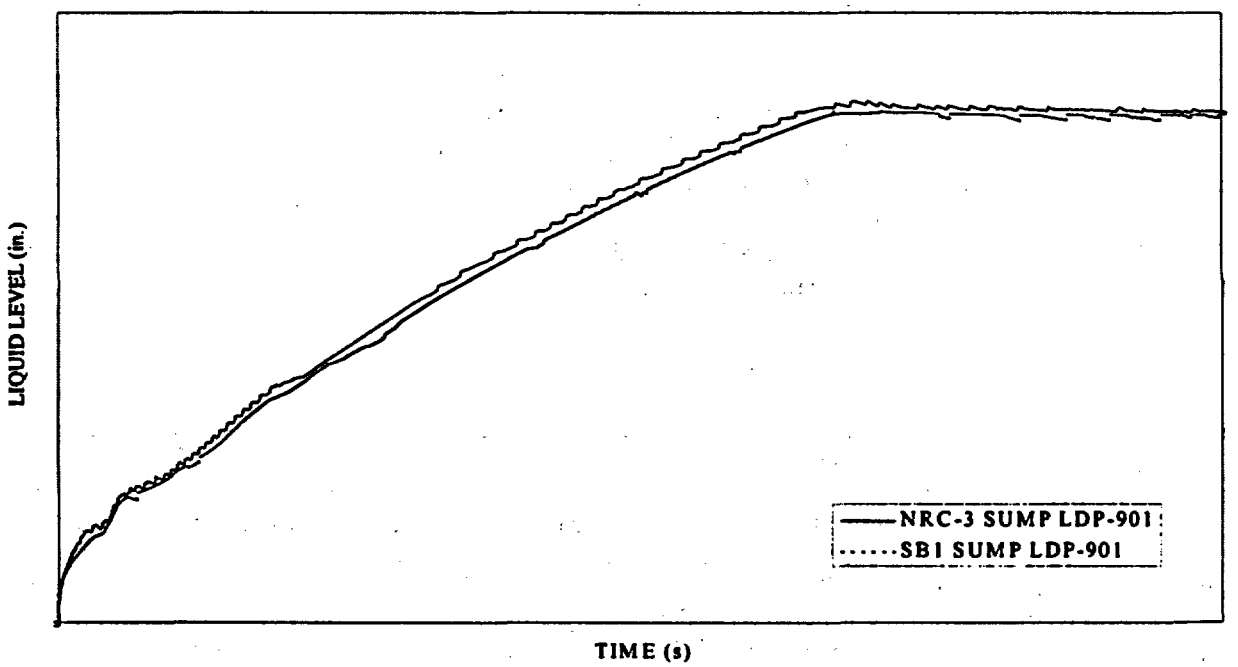

Figure 6. Comparison of NRC-3 (2/95) and SB1 (6/94) Primary Sump Liquid Levels

4.2 APEX Phenomena and Applicability to AP600

The following phenomena of interest have been observed in the APEX facility:

a. Spurious ADS-4 liquid flow oscillations were observed just prior to the onset of long term recirculation cooling.

b. CMT refill was observed subsequent to ADS actuation.

c. CMT asymmetric draining.

d. Low frequency (approximately two minute cycle) oscillations were observed in the DVI flow, the ADS-4 liquid flow, the system pressure, and the reactor vessel liquid level during the IRWST injection phase.

e. Cold leg thermal stratification.

f. Water hammer (low pressure events)

g. Core uncovering (beyond design basis transient)

A concerted effort has been made to determine if these specific phenomena could occur in the full scale AP600 plant. One has been found to be an artifact of the test design. The remainder appear to be feasible phenomena for the AP600 although the event magnitudes are influenced by the effect of scale.

4.2.1 Spurious ADS-4 Liquid Flow Oscillations

Spurious liquid flow oscillations were observed late in the transient, just prior to the transition to the sump recirculation mode of cooling. This is shown in Figure 7. A review of the data revealed that the pressure in the BAMS and the sump were different by 0.3 psi during this portion of the transient. NRC-3 was performed to assess the effect of this pressure difference on the system behavior. For NRC-3, the internals of check valve CSS-912 were removed. This permitted the sump and BAMS pressures to fully equalize. As shown in Figure 8, removal of the check valve internals resulted in an improvement in the BAMS flow measurement and eliminated the spurious ADS-4 liquid flow oscillations.

4.2.2 CMT Refill

For most tests performed in APEX, it was observed that the CMTs would refill subsequent to their initial draining following ADS actuation. This resulted in a temporary decrease in reactor vessel liquid level and therefore was cited as a phenomena of interest to the AP600. This is shown in Figure 9. Figure 10 shows the CMT level as a function of time. The CMTs refill after the system reaches low pressure because of the vacuum produced in the CMTs due to steam condensation. The refill occurs quickly as water is drawn up through the CMT-PBL into the CMTs. However, because the APEX is 1/4 height, it has been determined that CMT refill is not likely to occur in the AP600 because it would require a much greater vacuum to draw water through the CMT-PBL and the condensation process would be limited because external containment temperatures would be elevated during transient conditions. Partial CMT refills can occur at earlier in the transient. No conditions have been observed where CMT refill has resulted in uncovering the core of liquid.

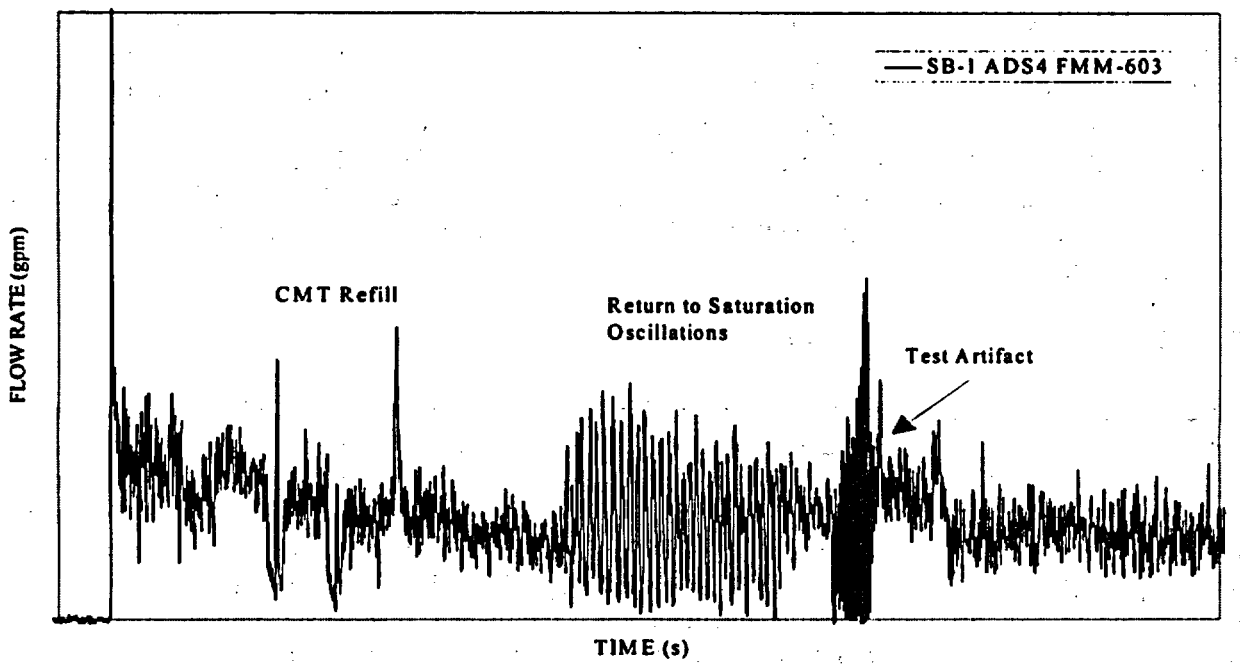

Figure 7. SB1 ADS 4 Liquid Flow Oscillations

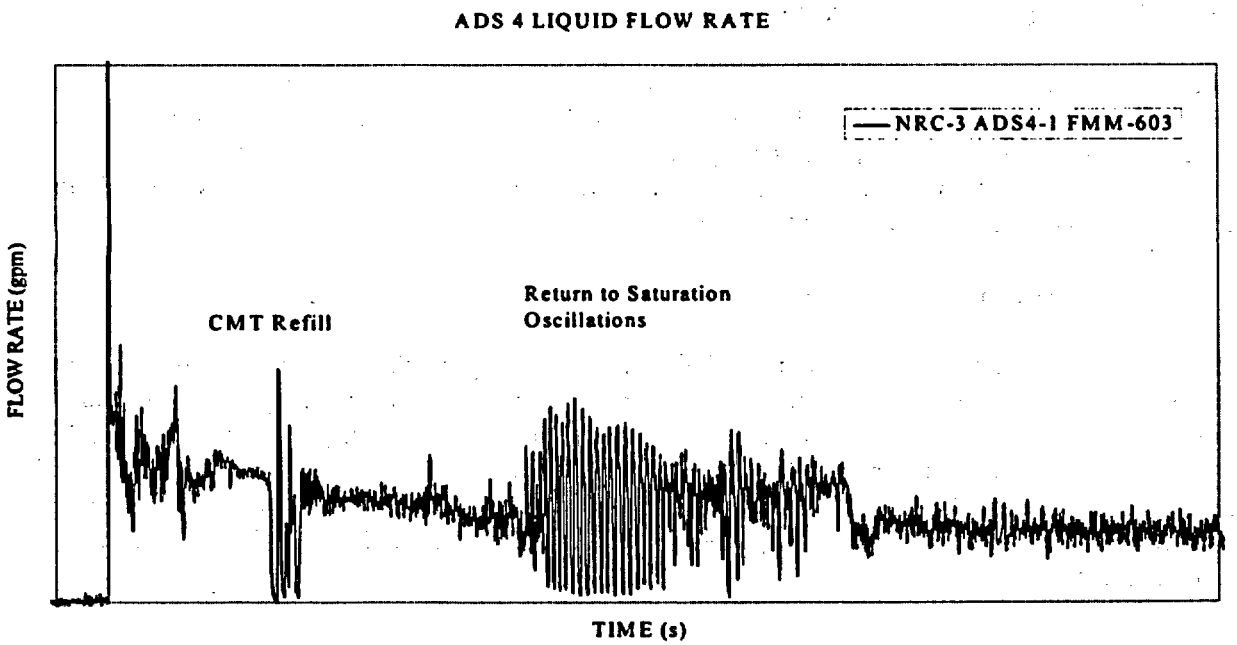

Figure 8. NRC-3 ADS 4 Liquid Flow without Check Valve CSS-912

4.2.3 CMT Asymmetric Draining

Test NRC-1 (Reference 6) was a beyond design basis counterpart test to ROSA AP-CL-05. It simulated a one-inch cold leg break with failure of all of the ADS 1-3 valves to open on demand. A comparison of NRC-1 to AP-CL-05 revealed significant differences in the CMT draining process because of loop geometry. The APEX facility exhibits asymmetric CMT draining which leads to rapid draining of one of the CMTs and early actuation of ADS4. A brief period of liquid holdup in CMT-01 was observed in NRC-1. However, because the ROSA AP600 facility uses a common CMT-PBL, asymmetric CMT draining was not observed in AP-CL-05 test and the CMT draining was significantly delayed. Because the APEX CMT-PBL geometry has been preserved, it is expected that AP600 CMT draining would also be asymmetric leading to an earlier ADS 4 actuation.

4.2.4 Flow, Pressure and Liquid Level Oscillations

Figure 11 shows a set of flow oscillations observed in NRC-3 that occurs after IRWST injection begins. These flow oscillations are associated with system pressure and level oscillations which occur at the same frequency. The onset of these oscillations occurs when the core goes from a subcooled state to a saturated state. Initially it was thought that these oscillations might be induced by holdup in the break flow separators and sump. NRC-4 was designed to test this theory. In test NRC-4, the break separator was bypassed and the flow was piped directly to the primary sump. Test NRC-4 produced identical the same results as NRC-3 demonstrating that the break separator was functioning in a "transparent" manner as designed. It is expected that such oscillations could occur in the AP600. However, the nature of the oscillation mechanisim limits the magnitude of the liquid level oscillations to a region above the top of the hot leg. Therefore uncovering the core of liquid due to this phenomena is not possible.

4.2.5 Cold Leg Fluid Thermal Stratification

All of the tests exhibit fluid thermal stratification in the cold legs during different phases of the SBLOCA. The bottom of the cold leg will typically approach theDVI fluid temperature whereas the top of the cold leg will approach the saturation temperature at system pressure. This phenomenon has also been observed in the ROSA AP600 tests and would be present in the full scale AP600. Figure 12 shows the fluid thermal stratification in cold leg number 4 for test NRC-7.

4.2.6 Condensation Induced Water Hammer

Test NRC-7 (Reference 7) simulated a one-inch AP600 cold leg break. For this test, however, nitrogen carryover from the accumulators was prevented. After the system achieved ambient pressure, a condensation waterhammer event occurred. Because the system was at ambient pressure, it was expected that the peak overpressure from the event was not sufficient to damage piping. An inspection of the facility confirmed that there was no facility damage. The test result agrees with studies that show that the presence of noncondensibles inhibits condensation processes thus reducing the likelihood of a condensation water hammer event.

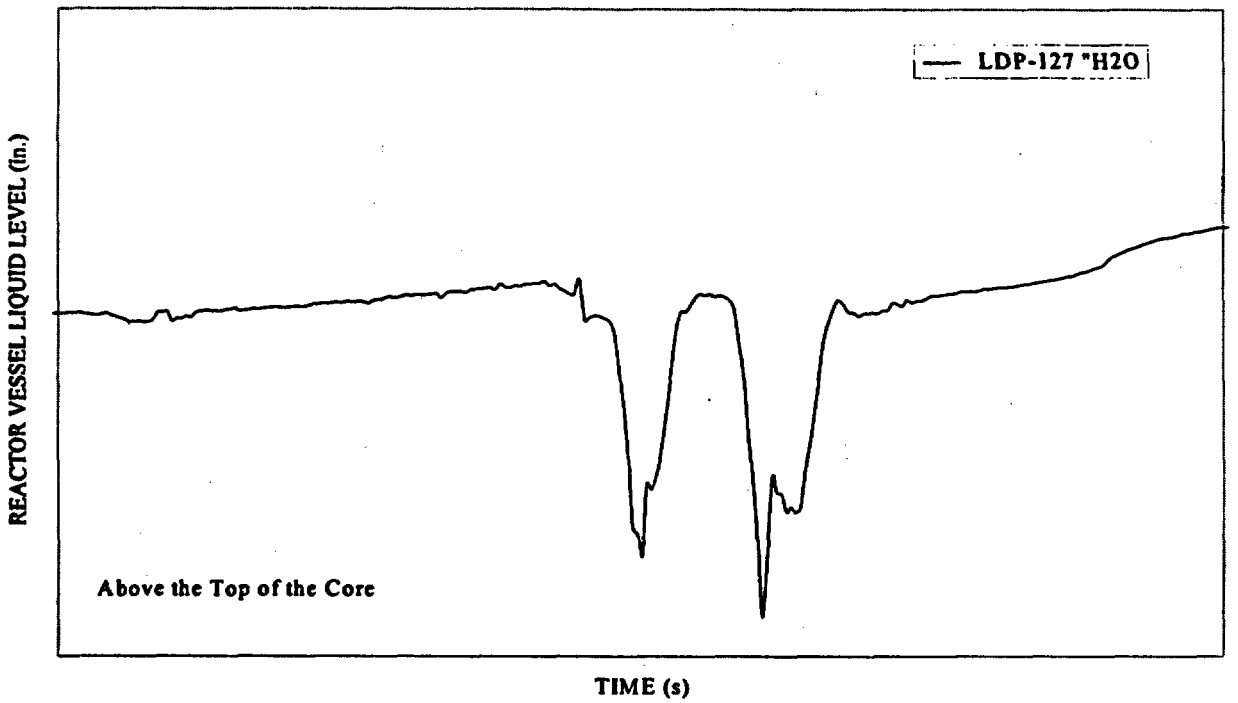

Figure 9. Effect of CMT Refill on Reactor Vessel Liquid Level

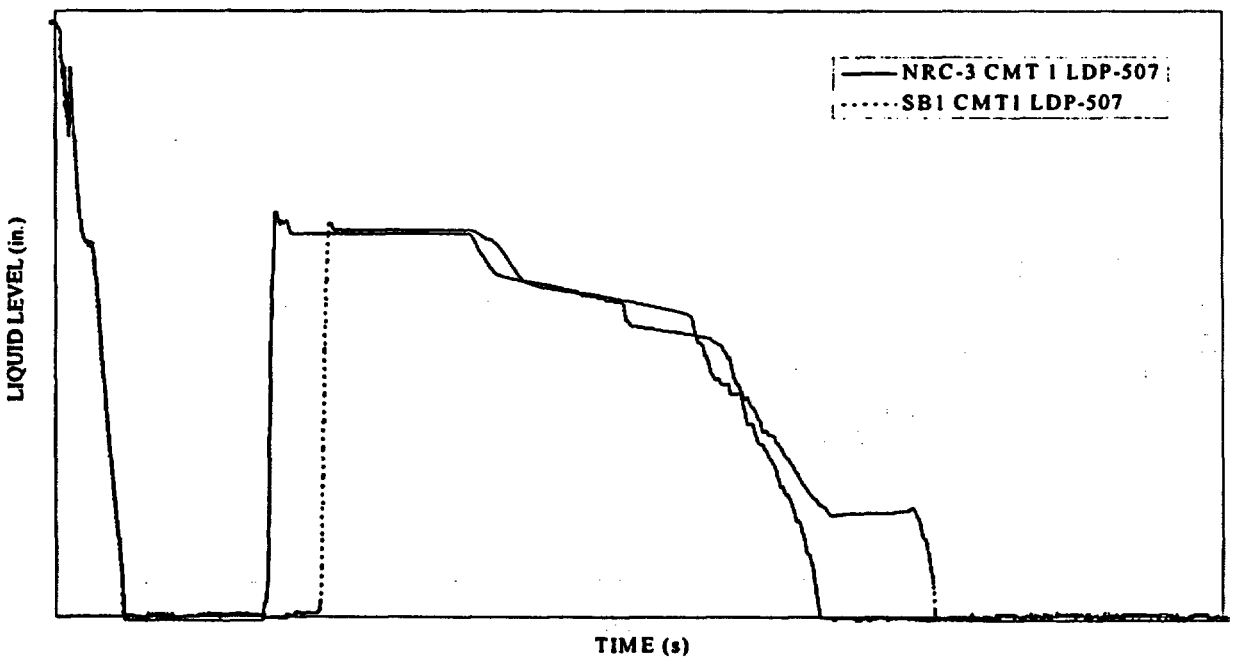

Figure 10. Comparison of NRC-3 and SB1 CMT Draining and Refill Phenomena.

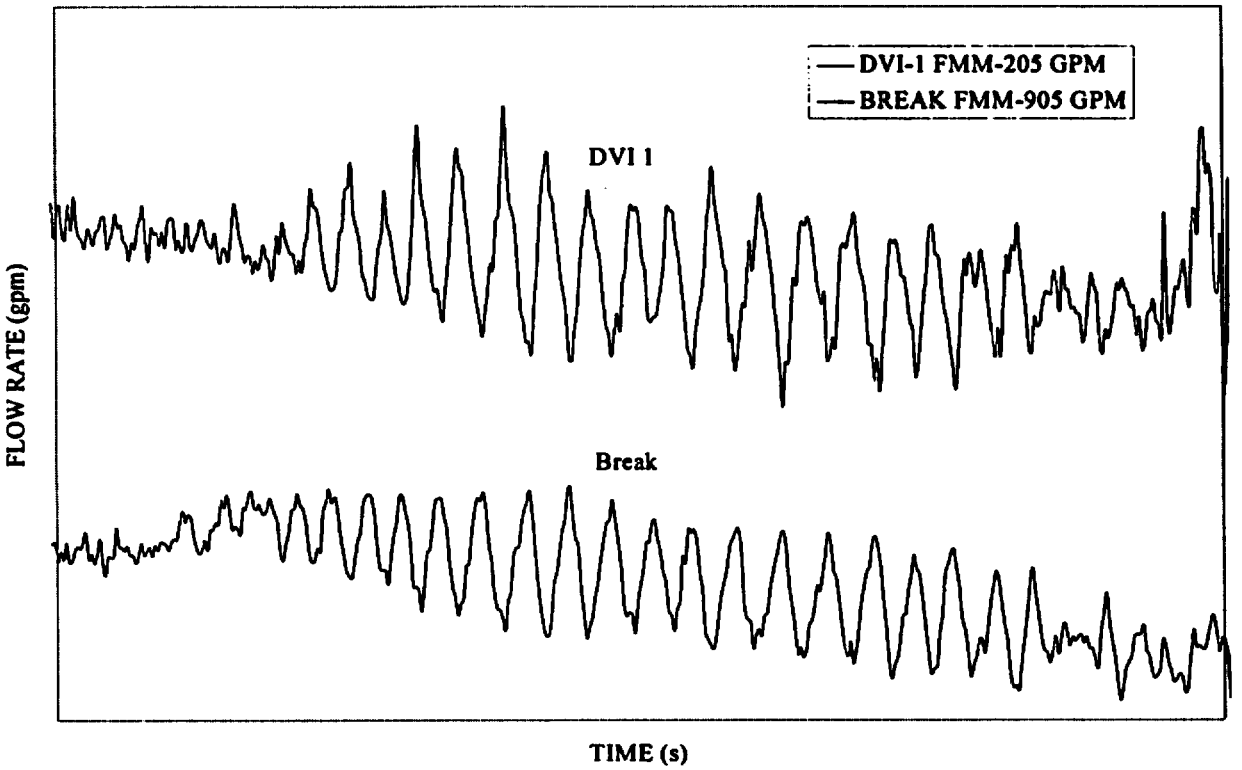

Figure 11. DVI and Break Liquid Flow Oscillations When Core Reaches Saturation Temperature

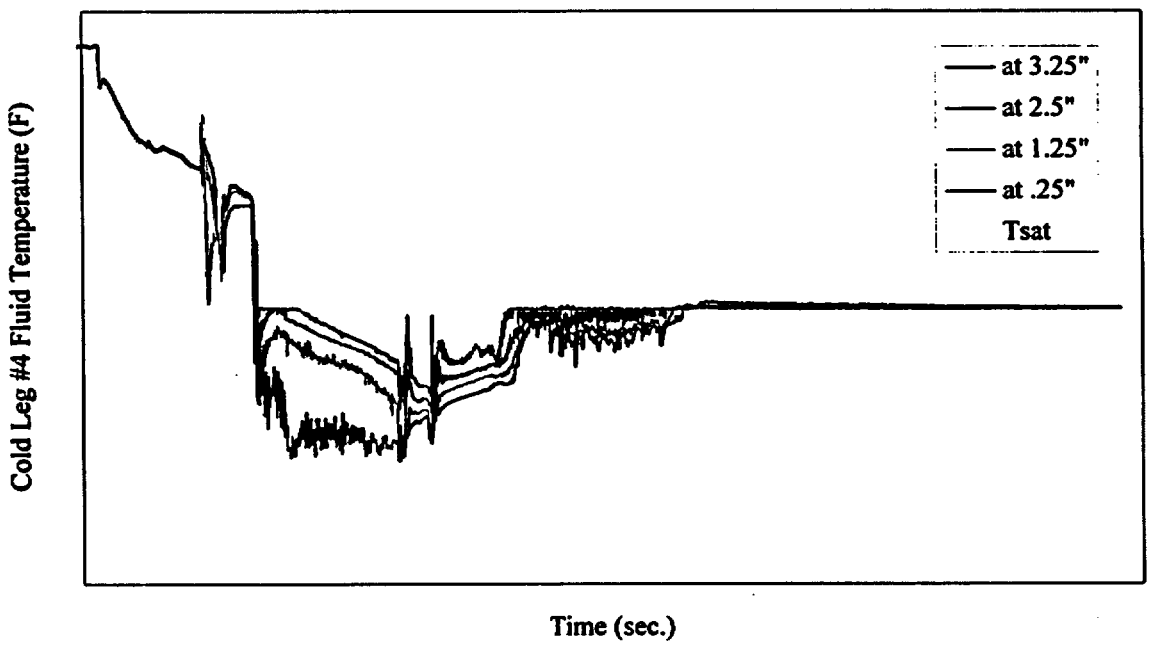

Figure 12. Thermal Stratification in Cold Leg #4 During a 1" Cold Leg Break Simulation

4.2.7 Core Uncovering

None of the design basis accidents simulated thus far have resulted in uncovering the core of liquid. Test NRC-10 was a beyond design basis accident scenario which assumed that three of the four ADS4 valves failed to open on demand. As a result, system depressurization was significantly delayed. This delayed the onset of IRWST injection thus permitting boiloff of core liquid. Test NRC-10 exhibited a temperature excursion due to the uncovering of the top of the core heaters.

This phenomenon is not expected to occur in the full height AP600. The reduced height scale of APEX results in a delay in the onset of the IRWST injection because of the reduced head available to inject against system pressure. Test NRC-10 indicates that the AP600 could reach systems pressures below the head required for IRWST injection in the full height AP600 prior to the liquid level reaching the top of the core; thus preventing core uncovering. NRC-10 is a counterpart test to a ROSA test which supports the conclusion that failure of 3 of 4 ADS4 valves would not cause the core to uncover of liquid.

5. CONCLUSIONS

The NRC test program at Oregon State University has been used to assess a variety of thermal hydraulic conditions for the AP600 design. This includes design basis and beyond design basis accidents that can be used to assess the safety margin afforded by the AP600 design. All of the data has been transmitted to the Idaho National Laboratory for inclusion in the NRC database and comparison to the RELAP5/MOD3 computer code.

Several phenomena of interest have been observed during the course of testing. These phenomena have been assessed to determine their applicability to the AP600. One of these phenomena was conclusively shown to be an artifact of the experiment design. Removal of check valve internals on the BAMS resulted in eliminating the spurious oscillations in ADS 4 liquid flow occuring just prior to long term recirculation.

CMT refill was observed in APEX tests. It is expected that partial CMT refills could occur at higher system pressure earlier in transients. However, because the APEX is 1/4 height, it has been determined that CMT refill is not likely to occur in the AP600 at low pressure because it would require a much greater vacuum to draw water through the CMT-PBL and condensation in the CMTs would be limited because external containment temperatures would be elevated during transient conditions.

Test NRC-1 examined the AP600 response to a one-inch break with failure of all ADS 1-3 valves. Unlike the ROSA AP600 counterpart test, asymmetric CMT draining was observed in APEX test NRC-1. Because the geometry of the APEX CMT-PBL has been preserved, it is expected that the AP600 will exhibit asymmetric draining behavior leading to early ADS 4 actuation for these conditions.

Oscillations in system pressure, DVI flow, core liquid level and ADS 4 liquid flow have been observed during IRWST injection when the core exit reaches the saturation temperature. This phenomena is expected to occur in the AP600 for certain break sizes. The minimum depression in core liquid level due to the oscillations is physically confined to the top of the hot leg.

Thermal stratification of the cold leg fluid was observed in the APEX tests. This phenomenon is expected to occur in the AP600 and has also been observed in ROSA counterpart tests.

Condensation water hammer has been observed at low pressure conditions in APEX. Preventing nitrogen carryover from the accumulators appears to enhance the likelihood of condensation waterhammer late in the transient. This phenomena is applicable to the AP600.

None of the design basis tests performed thus far resulted in uncovering the core. The only test performed for NRC that exhibited core uncovering is NRC-10. NRC-10 was a beyond design basis test that simulated a one inch break with failure of 3 of 4 ADS 4 valves. Core uncovering is not expected to occur in the AP600 because of the additional head available for IRWST injection in the full height plant.

REFERENCES

1. Reyes, J. N., L.E. Hochreiter, L.K. Lau, and A.Y.Lafi. *AP600 Low Pressure Integral Systems Test at Oregon State University Facility Scaling Report*, Westinghouse Electric Corporation, Proprietary, WCAP-14270, January 1995.

2. AP600 Low Pressure Integral System Test at Oregon State University - Facility Description Report, Westinghouse Electric Corporation, WCAP-14124, Vol. I & II, July 1994.

3. Reyes, J.N., A.Y. Lafi, D.A. Pimentel, and J.T. Groome. *Quick Look Report for OSU APEX NRC-3, 2-Inch Cold Leg Break with Long Term Cooling and Check Valve CSS-912 Removed*, Prepared for the USNRC, Oregon State University, March 1995.

4. Reyes, J.N., A.Y. Lafi, O. Stevens, and J.T. Groome. *Quick Look Report for OSU APEX NRC-4, 2-Inch Cold Leg Break with Long Term Cooling and Direct Discharge to Primary Sump*, Prepared for the USNRC, Oregon State University, April 1995.

5. Reyes, J.N., A.Y. Lafi, S.C. Franz, and J.T. Groome. *Quick Look Report for OSU APEX NRC-11, 2-Inch Cold Leg Break with Modified ADS 1-3 Logic and No CMT Refill*, Prepared for the USNRC, Oregon State University, August 1995.

6. Reyes, J.N., A.Y. Lafi, S.C. Franz, and J.T. Groome. *Quick Look Report for OSU APEX NRC-1, 1-Inch Cold Leg Break with Failure of ADS Valves 1-3*, Prepared for the USNRC, Oregon State University, July 1995.

7. Reyes, J.N., A.Y. Lafi, O. Stevens, and J.T. Groome. *Quick Look Report for OSU APEX NRC-7, 1-Inch Cold Leg Break with Modified ADS 1-3 Logic and without Nitrogen Carryover from Accumulators*, Prepared for the USNRC, Oregon State University, October 1995.

PUMA Test Program for SBWR

by

M. Ishii, S.T. Revankar, R. Dowlati, M.L. Bertodano,
V.H. Ransom, R. Viskanta, I. Babelli, W. Wang, Q.A. NguyenLe,
D. Ferry, Y. Me, Z. Xiao, M. Rapp and S.Kelly

School of Nuclear Engineering
Purdue University
West Lafayette, IN 47907-1290

ABSTRACT

The objective of the PUMA integral test program is to obtain confirmatory test data for the SBWR Developed by the General Electric-Nuclear Energy Company. The program was initiated in July 1993 under the sponsorship of the NRC. The SBWR has a simplified coolant circulation system and a passive emergency cooling system. The engineered safety systems and safety-grade systems in the SBWR are: (1) the Automatic Depressurization System (ADS), (2) the Gravity-Driven Cooling System (GDCS), (3) the Passive Containment Cooling System (PCCS), (4) the Isolation Condenser Systems (ICS), and (5) the Pressure Suppression Pool (SP). The GDCS and PCCS are new designs unique to the SBWR and do not exist in operating BWRs. The ICS is similar to those in some operating BWRs. The PCCS is designed for low-pressure operation for the containment cooling, but the ICS is capable of high pressure operation as well to cool the reactor pressure vessel. The PUMA design was completed based on an extensive scaling analysis. The PUMA facility having 1/4 height and 1/400 volume scales is constructed. Various facility characterization tests and instrumentation and data acquisition system checks are performed presently. The facility acceptance test will be performed in November and integral tests will be initiated.

1. INTRODUCTION

The General Electric Nuclear Energy Company (GE) has developed a new boiling water reactor called the Simplified Boiling Water Reactor (SBWR) [1]. Major differences between the current Boiling Water Reactors (BWRs) and the SBWR are in the simplification of the coolant circulation system and the implementation of passive emergency cooling systems. There are no recirculation pumps to drive the coolant in the vessel of the SBWR. The emergency core cooling and containment cooling systems do not have active pump-injected flows.

There are several engineered safety systems and safety-grade systems in the SBWR which are directly related to the relevant issues and objectives of the present program: 1) the Automatic Depressurization System (ADS), 2) the Gravity-Driven Cooling System (GDCS), 3)

the Passive Containment Cooling System (PCCS), 4) the Isolation Condenser Systems (ICS), and 5) the Pressure Suppression Pool (SP). The GDCS and PCCS are new designs unique to the SBWR and do not exist in operating BWR's. The ICS is similar to those in some operating BWRs. Both the GDCS and PCCS are designed for low-pressure operation (less than 1.03 MPa or 150 psia), but the ICS is capable of high pressure operation as well (up to 7.58 MPa or 1100 psia).

The ADS system becomes active at a prescribed vessel condition and depressurizes the reactor vessel so that the gravity driven cooling systems can be activated. The goal of these safety systems is to maintain sufficient core cooling by preventing core uncovery and dryout of the fuel pins.

The performance of these safety systems under a loss of coolant accident (LOCA) and other important transients is a major concern. Since the emergency cooling systems are driven by the gravitational head, interactions between the ADS, GDCS, PCCS and other auxiliary systems are important. The emergency cooling systems depend not only on the gravitational head but also on the relative static pressure differences between the vessel, drywell and wetwell (suppression pool). The safety systems and various natural circulation phenomena encountered after the initial vessel depressurization in the SBWR are somewhat different from the systems and phenomena studied by the nuclear community in existing commercial nuclear reactors.

General Electric has performed tests to assess the GDCS performance in a low pressure full-height GIST facility with a volume scale of 1/508 [2]. Results of this study have demonstrated the feasibility of the GDCS concept. The GIST facility was scaled from an older SBWR design in which the GDCS pools were combined with the SP. The PCCS was absent in the GIST facility, hence parallel operation of the GDCS and PCCS was not observed in the GIST experiments. GE has also performed tests to assess the PCCS performance in the low-pressure, full height Toshiba GIRAFFE facility in Japan with a volume scale of 1/400 [3]. The GIRAFFE tests provided data to help model the prototypic SBWR PCCS units, and demonstrated the feasibility of the noncondensible venting concept. However, the GIRAFFE facility was scaled from an older SBWR design, and it did not investigate GDCS injection in the vessel.

The new PANDA facility in Switzerland is a low-pressure, full-height facility with a volume scale of 1/25 [4]. The main focus of the PANDA facility is on PCCS performance and containment phenomena in a relatively large-scale facility so that three-dimensional effects can be assessed. However, the PANDA facility is not designed for assessing GDCS injection into the vessel. Although GE has performed experimental and analytical studies for the PCCS and GDCS systems and associated phenomena, the U.S. Nuclear Regulatory Commission (NRC) has identified a need to develop additional independent confirmatory data from a well-scaled integral test facility built to reproduce major thermal-hydraulic phenomena at relatively low pressure (< 1.03 MPa or 150 psia) [5]. Purdue University was awarded a research contract, "Confirmatory Integral System Testing for GE SBWR Design," to design, construct and operate PUMA (Purdue University Multi-dimensional Integral Test Assembly) to obtain integral test data.

The major objectives of the PUMA program are to:

1. provide integral data to NRC for the assessment of the RELAP5 code for SBWR applications,
2. assess the integral performance of the GDCS and PCCS systems, and
3. assess SBWR phenomena important to LOCAs and other transients.

The focus of the PUMA integral test program is the reproduction of the important phenomena expected in the SBWR for use in the assessment of the RELAP5 code. The objective of the scaling method is to provide a facility design that will reproduce those phenomena which occur during both the later stages of depressurization of the SBWR pressure vessel and during the functioning of the gravity-driven safety systems. A corollary objective of the scaling will be to preserve, to the extent necessary and possible, the sequence and interrelation of the key phenomena. In this way, comprehensive data which can be related to prototypical conditions will be provided for assessing the code models.

The particular focus of the integral experiments is to obtain data on the performance and interaction of the GDCS and PCCS, particularly as related to the maintenance of the coolant level in the RPV, containment integrity, maintenance of natural circulation, possible occurrence of two-phase natural circulation instabilities, the effect of noncondensible gases on PCCS performance and potential impact on the core cooling and the drywell pressure. Data will also be obtained regarding system interaction between the GDCS, PCCS, auxiliary cooling systems, possible water hammer occurrence during GDCS injection, feedwater injection, and ICS condensate draining into the vessel.

The data collected will provide qualitative as well as quantitative tests of the code models and overall predictive capability of RELAP5. In this way, the uncertainty associated with the calculation of the safety margins predicted to exist for design-basis accidents can be comprehensively assessed by the NRC using the code scaling and uncertainty analysis methodology established several years ago.

2. SCALING METHOD

2.1 General Consideration

Since it is not feasible to build and test a full power prototypical system, a scaled integral test facility is needed. The integral test facility scaling method should provide a rational basis by which to scale-up the integral model test results to the prototype conditions. Therefore, it is necessary to have a rational scaling method that establishes the interrelationship between the important physical variables associated with mass, force and energy of the prototypical system and the model. In view of this, a well balanced and justifiable scaling approach has been developed for the design of the SBWR integral test facility. For this task a three level scaling approach is used. This three level scaling approach consists of, (1) integral scaling, (2) boundary flow scaling, and (3) local phenomena scaling. The integral scaling is derived from the integral response functions for major variables in single and two-phase flow. This scaling

insures that both the steady state and dynamic conditions are simulated. It also determines the geometrical requirements and time scale. The integral scaling results in the simulation of all the major thermal-hydraulic parameters. The boundary flow scaling simulates the mass and energy inventory of each component and flow among these components. The third level scaling is used to insure that key local phenomena can be reasonably scaled. Even under the global simulation of flow, mass and energy, various local phenomena which affect the constitutive relations should be addressed through this third level of scaling. Local phenomena scaling have been carried out in detail. After some distortions in local phenomena and geometry are identified, the impact of the distortions on the integral thermal-hydraulic response of the model facility are evaluated. This three level scaling approach is shown in the Fig. 1.

The scaling criteria for a natural circulation loop under single-phase and two-phase flow conditions have been developed by Ishii, et al. [7-9]. The criteria includes the effects of fluid properties, so one can also apply them for reduced-pressure system scaling. For single-phase flow conditions, continuity, integral momentum and the energy equations in one-dimensional area averaged forms are used. First, relevant scales for the basic parameters are determined, then the similarity groups are obtained from the conservation equations and boundary conditions. The heat transfer between the fluid and structure can be included in the analysis by using the energy equation from the structure. It should be noted that the simulation of a long, large pipe section by a small scale model may encounter some difficulties if the prototype system does not have a reasonably large loss coefficient in addition to the wall frictional loss.

For a two-phase natural circulation system, similarity groups have been developed from a perturbation analysis based on the one-dimensional drift flux model. The set of mass, momentum and energy equations are integrated along the loop, and the transfer functions between the inlet perturbation and various variables are obtained. The scaling parameters developed from the integral transfer functions represent the whole-system similarity conditions, and are applicable to transient thermal-hydraulic phenomena.

The scaling approach that has been used for the design of many existing US-NRC thermal-hydraulic research facilities is summarized in [10]. The so-called "full pressure full-height method" was used for most of these facilities. The scaling approach recommended by the NRC, based on the experience accumulated from extensive LOCA studies in scaled integral test facilities, is summarized in a comprehensive paper by Boucher, et al. [11]. The present scaling method is an extension of the previously developed scaling approach by Ishii, et al. [7-9] and consists of three levels of scaling detail. First, integral scaling methods are applied to the system circulation paths. Second, component boundary flow scaling considerations are applied in order to preserve integral mass and energy inventory. Third, scaling criteria are developed that preserve the similarity of local phenomena such as choking, condensation and bubble rise time. These levels of scaling detail are described below.

2.1 *Integral System Scaling (1st Level)*

It is necessary to have the single-phase flow similarity requirements as a ready reference, since they are needed for a component filled with single phase and also they are needed to simulate the single-phase to two-phase flow transition. The system consists of a thermal

energy source, energy sink and connecting piping system between components. For a natural circulation loop under single-phase flow conditions the similarity parameters are obtained from the integral effects of the local balance equations (continuity, momentum and energy) along the entire loop.

The fluid continuity, integral momentum, and energy equations in one-dimensional, area-averaged forms are used along with the appropriate boundary conditions and the solid energy equation. From the dimensionless forms of these equations, important groups characterizing geometric, kinematic, dynamic and energetic similarity parameters are derived.

If similarity is to be achieved between processes observed in the prototype and in a model, it is necessary to satisfy the following requirements:

$$A_{iR} = (a_i/a_o)_R = 1 \tag{1}$$

$$L_{iR} = (l_i/l_o)_R = 1 \tag{2}$$

$$\left[\sum_i F_i/A_i^2\right]_R = \left[\sum_i \left[f_i \frac{l_i}{d_i} + K_i\right] \Big/ (a_i/a_o)^2\right]_R = 1 \tag{3}$$

$$R_R = (\beta \Delta T_o l_o/u_o^2)_R = 1 \tag{4}$$

$$St_{iR} = (h l_o/\rho_f c_{pf} u_o d_i)_R = 1 \tag{5}$$

$$T^*_{iR} = [(l_o/u_o)/(\delta^2/\alpha_s)_i]_R = 1 \tag{6}$$

$$B_{iR} = (h\delta/k_s)_{iR} = 1 \tag{7}$$

$$Q_{siR} = (q'''_s l_o/\rho_s c_{ps} u_o \Delta T_o)_{iR} \tag{8}$$

where subscript *i* designates a particular component and R denotes the ratio of a value of the model to that of the prototype.

$$\psi_R \equiv \frac{\psi_m}{\psi_p} = \frac{\psi \text{ for model}}{\psi \text{ for prototype}} \tag{9}$$

The reference velocity, u_o, and temperature difference, ΔT_o are obtained from the steady-state solution. If the heated section is taken as the representative section, these characteristic parameters are expressed as follows:

$$u_o = \left[\frac{4\beta g \left[\frac{q'''_o l_o}{\rho_f c_{pf}} \right] \left[\frac{a_{so}}{a_o} \right] l_h}{\sum_i \left[F_i / A_i^2 \right]} \right]^{1/3} \tag{10}$$

and

$$\Delta T_o = \left[\frac{q'''_o l_o}{\rho_f c_{pf} u_o} \right] \left[\frac{a_{so}}{a_o} \right] \tag{11}$$

where the subscript o and so refer to the core flow area and heated surface area, respectively.

For two-phase flow systems, the small perturbation technique and integral response function have been used by Ishii and Kataoka [7] to develop similarity criteria. The important dimensionless groups that characterize the kinematic, dynamic and energetic fields are given as follows:

$$\text{Phase Change No.} \quad N_{pch} \equiv \left[\frac{4q'''_o \delta l_o}{du_o \rho_f \Delta h_{fg}} \right] \left[\frac{\Delta\rho}{\rho_g} \right] = N_{Zu} \tag{12}$$

This phase change number has recently been renamed as the Zuber number, N_{Zu}, in recognition of Zuber's significant contribution to the field.

$$\text{Subcooling No.} \quad N_{sub} \equiv \left[\frac{h_{sub}}{\Delta h_{fg}} \right] \left[\frac{\rho}{\rho_g} \right] \tag{13}$$

$$\text{Froude No.} \quad N_{Fr} \equiv \left[\frac{u_o^2}{g l_o \alpha_o} \right] \left[\frac{\rho_f}{\Delta\rho} \right] \tag{14}$$

$$\text{Drift–Flux No.} \quad N_{di} \equiv \left[\frac{V_{gj}}{u_o}\right]_i \text{ (or Void–Quality Relation)} \tag{15}$$

$$\text{Time Ratio No.} \quad T_i^* \equiv \left[\frac{l_o/u_o}{\delta^2/\alpha_s}\right]_i \tag{16}$$

$$\text{Thermal Inertia Ratio } N_{thi} \equiv \left[\frac{\rho_s c_{ps} \delta}{\rho_f c_{pf} d}\right]_i \tag{17}$$

$$\text{Friction No.} \quad N_{fi} \equiv \left[\frac{fl}{d}\right]_i \left[\frac{1 + x(\Delta\rho/\rho_g)}{(1 + x\Delta\mu/\mu_g)^{0.25}}\right] \left[\frac{a_o}{a_i}\right]^2 \tag{18}$$

$$\text{Orifice No.} \quad N_{oi} \equiv K_i \left[1 + x^{3/2} (\Delta\rho/\rho_g)\right] \left[\frac{a_o}{a_i}\right]^2 \tag{19}$$

where V_{gj}, h_{fg}, h_{sub}, and x are the drift velocity of the vapor phase, heat of evaporation, subcooling and quality, respectively. In addition to the above-defined physical similarity groups, several geometric similarity groups such as (l_i/l_o) and (a_i/a_o) are obtained.

The Froude, friction and orifice numbers, together with the time ratio and thermal inertia groups, have their standard significance. Subcooling, Zuber and drift-flux numbers are associated with the two-phase flow systems. Their physical significance is discussed in detail elsewhere [7-9].

Eqs. (12) through (19) represent relationships between the dimensionless groups and the generalized variables of a two-phase flow system. The dimensionless groups must be equal in the prototype and model if the similarity requirements are to be satisfied. Hence, the following conditions result:

$$(N_{Zu})_R = 1 \,,\ (N_{sub})_R = 1 \,,\ (N_{Fr})_R = 1 \,,\ (N_{di})_R = 1$$

$$(T_i^*)_R = 1 \,,\ (N_{thi})_R = 1 \,,\ (N_{fi})_R = 1 \,, \text{ and } (N_o)_R = 1 \,. \tag{20}$$

Excluding the friction, orifice and drift-flux number similarities from the set of similarity requirements and solving the remaining equations, one obtains the following similarity

requirements:

$$(u_o)_R = (l_o)_R^{1/2} \tag{21}$$

$$(h_{sub})_R = \left[\frac{h_{fg}\rho_g}{\Delta\rho}\right]_R \tag{22}$$

$$(q_o''')_R = \left[\frac{\rho_f\rho_g h_{fg}}{\Delta\rho}\right]_R (\frac{d}{\delta})_R \left[\frac{\rho_s c_{ps}}{\rho_f c_{pf}}\right]_R (l_{oR})^{-1/2} \tag{23}$$

The velocity scale shows that, in contrast to the case of single-phase flow scaling, the time scale for a two-phase flow system is not an independent parameter. From Eq. (30), the time scale in two-phase flow is uniquely established. Thus,

$$\tau_R = \left[\frac{l_o}{u_o}\right]_R = (l_o)_R^{1/2} \tag{24}$$

This implies that if the axial length is reduced in the model, then the time scale is shifted in the two-phase flow natural circulation loops. In such a case, the time events are accelerated (or shortened) in the scaled-down model by a factor of $(l_{oR})^{1/2}$ over the prototype.

2.2 Mass and Energy Inventory and Boundary Flow Scaling (2nd Level)

For integral experiments, accurate simulation of the mass and energy inventory is essential. This requires a separate scaling criteria for the system boundary flows such as the break flow and various ECCS injection flows. Denoting the total volume by V and the mean density by $<\rho>$, the coolant mass inventory balance equation can be written in a dimensionless form that applies to both the model and the prototype system as

$$\frac{d}{dt^*}<\rho^*> = \Sigma\dot{m}_{in}^* - \Sigma\,\dot{m}_{out}^* \tag{24}$$

where

$$t^* \equiv t/(l_o/u_o) \tag{25}$$

and

$$\dot{m}^*_{in} \equiv \frac{\dot{m}_{in}\,\tau_o}{\rho\,V} \sim \frac{\rho_{in}}{\rho}\left[\frac{a_{in}}{a_o}\right]\left[\frac{u_{in}}{u_o}\right] \tag{26}$$

and $\tau_o = (l_o/u_o)$ for either the prototype or the model. The definition for $\dot{m}^*_{out}$ can be given similarly. For equal model and prototype pressure simulation, $(\rho^*_{out})_R = (\rho_{out}/\rho)_R$ is simply unity. Hence, the simulation of the boundary flow requires

$$\left[\frac{a_{out}}{a_o}\,\frac{u_{out}}{u_o}\right]_R = 1 \tag{27}$$

This is a similarity condition for the flow area and velocity combined. Therefore, it is not necessary at discharge points to satisfy the independent conditions for area and flow given by the scaling criteria for circulating flow, which must be satisfied by the other components of the loop. The form of the discharge scaling criterion is very convenient from the standpoint of practical implementation. For example, the break flow velocity, u_{out}, can not be independently controlled if choking occurs. In the case of choking, Mach number similarity is maintained. Thus, for an equal-pressure system the break flow is prototypic in the sense that $(u_{out})_R = 1$, whereas the basic scaling $(u_o)_R = (l_o)_R^{1/2}$ and the criterion given in Eq. (27) predict that the break flow area should be scaled according to

$$\left[\frac{a_{in}}{a_o}\right]_R = (l_{oR})^{1/2} \tag{28}$$

which would result in a reduction of the break flow area beyond the geometrical scale used for the loop flows.

Energy Inventory and Energy Flow Scaling

From the control volume balance, the energy inventory is given in non-dimensional form by

$$\frac{dE^*}{dt^*} = q^* - w^* + \Sigma \dot{m}^*_{in}\, h^*_{in} - \Sigma\, \dot{m}^*_{out}\, h^*_{out} \tag{29}$$

where

$$\dot{m}^*_{in}\, h^*_{in} = \dot{m}_{in}\, h_{in}\, \frac{\tau_o}{\rho V h_o} \sim \left(\frac{\rho_{in}}{\rho}\right)\left(\frac{a_{in}}{a_o}\right)\left(\frac{u_{in}}{u_o}\right)\left(\frac{h_{in}}{h_o}\right) \tag{30}$$

In view of Eq. (30), for a full pressure simulation, i.e. $(h_o)_R = 1$, it is necessary to require

$$(h_{in})_R = 1 \tag{31}$$

This physically implies that the inflow or outflow should have a prototypic enthalpy. The above dimensionless energy equation also shows that the initial energy inventory should be scaled by the volume ratio.

2.3 Pressure Scaling

The work scope and program objectives of the PUMA are focused on the low-pressure region of operation following the initial depressurization of the vessel. This implies that the prototype pressure maximum is about 150 psi (or 1 MPa). In considering the pressure scaling of the integral test facility, two effects should be evaluated separately. These are:

1. System pressure level, which affects all the thermal-hydraulic properties of the liquid, vapor and phase changes.
2. Individual component or inter-component pressure distributions.

Considering the pressure scaling in these two separate effects is somewhat analogous to the well-known Boussinesq assumption. The prototypic pressure is taken as the system pressure scaling base. Hence, the system pressure and all other fluid properties are considered to be prototypic. This will greatly simplify the scaling procedures. Thus, we have the global pressure scaling given by $p_R = 1$

Under the above prototypic system pressure scaling, the thermodynamic and transport properties at every component are considered prototypic. However, the pressure distribution in each component may not be prototypic. It should be noted that the pressure distribution within a component or between components can be the controlling factor in determining the flow by forced convection or natural circulation. This aspect of the pressure effect in a reduced-height system should be considered separately. At the initial blowdown phase of a LOCA or other transient, the major intercomponent flow occurs due to the initial pressure difference between the reactor pressure vessel and the containment. For this initial phase, the pressure difference between these two components should be prototypic at the same elevation, $(\Delta p_{ij})_R = 1$ at $Z_R = l_R$, where the subscripts i and j stand for the reactor vessel and containment, respectively.

However, in the case of natural circulation-dominated flow, such as the reactor vessel internal circulation, GDCS injection or PCCS venting, the hydrostatic head is the essential driving force. For this case, the differential pressure is scaled by the reduced height scaling. Hence,

$$(\Delta p)_R = l_R \quad (\text{at } \Delta Z_R = l_R) \tag{32}$$

For PUMA, the initial differential pressure scaling is set by the initialization process with isolated components. At the later stages of accident simulation, most of the significant liquid flows between components are driven by the hydrostatic head. These flows are accurately simulated by using proper height scaling of all major elements and components based on $\Delta Z_R = l_R$, which implies the complete axial geometrical similarity. This condition, together with the void distribution simulation based on the integral scaling, insures that the differential pressure is scaled by the reduced height scaling.

2.4 Height Scaling

Under the prototypic pressure simulation, the system geometry can be determined from the integral system scaling and the boundary flow scaling discussed above. The dynamic scaling requirements for a two-phase flow system are given by Eqs. (12-19). In general it is difficult to match all these similarity criteria for a scaled down system, so a careful evaluation of each of these requirements should be made.

In considering the dynamics of the system, two conditions should be considered separately. The first is on the quasi-steady flow simulation and the second is the dynamic response of the system, including the inertia effect. It is clear that the Froude number and friction number scale the dynamic response. When the inertia forces are not important, only the balance between the frictional resistance and gravitational force should be considered. This can be achieved by taking the product of these two numbers. Thus, natural circulation number is defined as

$$N_{nc} = N_f N_{Fr} = \left[\frac{\text{friction}}{\text{interia}}\right]\left[\frac{\text{inertia}}{\text{gravity head}}\right] \tag{33}$$

This equation can be extended to include the minor loss coefficient as

$$N_{nc} = (N_f + N_o)N_{Fr} \tag{34}$$

Using kinematic and energy similarities, a less restrictive requirement, $(N_f + N_o)_R = 1$, is obtained for an approximate dynamic similarity between the inertia term and flow resistance. The advantage of this requirement relative to the two independent requirements of $(N_f)_R = 1$ and $(N_o)_R = 1$ is significant. Under a homogeneous flow assumption, the above less restrictive requirement can be approximated by

$$(N_f + N_o)_R \approx \left[\frac{fl}{d} + K\right]_R \left[\frac{a_o}{a_i}\right]_R^2 = 1 \qquad (35)$$

By using the geometrical similarity criteria, $(a_o/a_i)_{R=1}$, it follows that

$$\left[\frac{fl}{d} + K\right]_R = 1 \qquad (36)$$

These two scaling criteria apply to the gravity driven flow. A careful analysis of Eq. (36) clearly indicates the great advantage of using the reduced-height system for a given volume scale in satisfying the dynamic similarity criteria. By reducing the flow area, the hydraulic diameter is reduced by $d_R = \sqrt{a_R}$, except at bundle sections such as the core. For most small integral test facilities, it is necessary to have $l_R > d_R$ in order to maintain a reasonably large axial height so that the naturally existing two-phase level fluctuations do not adversely affect various transient phenomena. In general, the ratio of the first friction term itself is always larger than unity. However, by reducing the height of a facility, this ratio can be made closer to unity by increasing d_R for a fixed value of v_R. The second significant point is that the minor loss coefficient is an easy parameter to adjust through small design modifications in such a way that $K_R < 1$ to compensate for increased friction. Hence by properly modifying the K value, Eq. (36) can be achieved.

In view of the above and the cost consideration, the volume scale of 1/400 and the height scale of 1/4 appear to be most desirable for the PUMA. This implies the general area ratio of 1/100, and the transverse length ratio of 1/10.

2.5 Local Phenomena Scaling (3rd Level)

Although the global scaling criteria satisfy the system response similarity, the local phenomena may not be satisfied. Hence it is important to study the local phenomena scaling in detail. In the local phenomena (1) reactor vessel flow dynamics and instability scaling, (2) choked flow case, (3) unchoked flow case, (4) relative velocity and flow regime, (5) critical heat flux scaling (CHF), (6) flashing in the chimney, (7) condensation in suppression pool, (8) vent phenomena in suppression pool, (9) mixing in stratified fluid volumes, (10) natural circulation, (11) heat source and sink, (12) PCCS venting into suppression pool, (13) condensation in PCCS condensers, (14) stratification in the drywell, and (15) stratification in the suppression pool are considered. The scaling of these phenomena are considered in detail and appropriate scaling criteria and design implementations are discussed in Ref. [12].

3. SCALE OF THE PUMA FACILITY

To determine the overall size of the proposed facility, it is necessary to consider four essential factors; (1) the need to scale relations to the existing facility, (2) the need to compensate for the shortcomings of existing facilities or complement the overall data base, (3) the need for a

stand-alone justifiable rationale for the choice of a_R and l_R, and (4) the overall impact on the total cost.

For the PUMA facility, the above factors have been examined in detail. Based on these considerations, a quarter height and 1/400 volume scale have been chosen as the most desirable design. The existing or under-construction integral facilities for the SBWR are all full height. The GE GIST facility [2] is a low pressure, full-height facility, thus $l_R = 1$ and $a_R = 1/400$. The GIRAFFE facility [3] in Japan has $l_R = 1$ and $a_R = 1/400$. The planned PANDA facility [4] has $l_R = 1$ and $a_R = 1/25$. The aspect ratio, l_R/d_R, for these facilities are 22.5, 20 and 5, respectively. In view of the overall cost and the volume scale of these facilities, a new facility at the volume scale of about 1/400 appears to be optimum. This will match the mass and inventory of the GIST and GIRAFFE facilities.

Since the existing facilities are all full-height, the impact of the actual total height on various phenomena can be evaluated sufficiently. However, the existing facilities fall into the category of thin and tall systems, which have some major shortcomings. The present quarter-height system with the volume scale of 1/400 has the advantage of well-matched gravity to frictional forces. Furthermore, due to relatively large cross-sectional areas, the important phenomena of two or three dimensional flow in the drywell and suppression pool and voiding patterns and flow regimes in the core and chimney can be better simulated. This is considered to be particularly important for assessing the effects of two or three dimensional flow circulations and various instabilities such as manometer oscillation, density wave instability, geysering and flashing-induced cyclic phenomena on the natural circulation cooling and stability of the GDCS.

4. PUMA DESIGN AND CONSTRUCTIION

The PUMA project was initiated on July 26, 1993. The preliminary scientific design was reviewed by the NRC on November 29, 1993. The NRC approved the design of the PUMA on April 6, 1994 after extensive review by the NRC staff, BNL and INEL. The engineering design of the facility was approved on August 15, 1994 and the construction was initiated. On March 31, 1995 the basic loop construction was completed and the leak tests were performed on April 11, 1995. The first functional test was performed after required minimum instrumentations were installed. Several malfunctions of components were found and these were fixed. The second functional test was performed successfully. The installation of all the instrumentations, wiring, data acquisitions systems and control room took approximately six months after the completion of the loops. The system characterization tests were initiated in August and are presently underway together with the checking of the data acquisition systems.

The schematic of the PUMA facility is shown in Figure 1. The facility includes models for all the major components of SBWR safety and non-safety systems that are important to the transient response to a postulated LOCA and other transients. Thus it includes the reactor pressure vessel, drywell, suppression pool, GDCS, ICS, PCCS, and auxiliary system like feed water line, CRD line and RWCU/SDC.

The present scaled model cannot represent all detailed geometrical features of the SBWR. The model design was based on a number of considerations. First, the requirements of global scaling were met. Then, important phenomena were identified and scaled for local scaling. In some cases, both global and local scaling cannot be satisfied simultaneously. In such cases, the requirement on global scaling was kept intact and certain compromises on local scaling were made. In addition to scaling considerations, hardware components were evaluated for ease of construction, operation and cost. Certain geometrical features in the model for some components were thus distorted in PUMA. Details on these distortions and their impact on the loop thermal-hydraulics have been discussed in [12].

From the scaling analysis, the various scaling criteria for the PUMA were obtained. The most fundamental groups are for the geometry, power, time and flow. These are given below.

$$v_R = 1/400 \ , \ a_R = 1/100 \ , \ d_R = 1/10 \text{ and } l_R = 1/4$$

$$q'''_R = 1/200$$

$$\tau_R = 1/2 \ , \ u_R = 1/2$$

From these criteria the reactor pressure vessel was scaled and the PUMA RPV dimensions were obtained. The total height is 613 cm, ID 60 cm, volume 1.76 m^3. The material is stainless steel 405 to comply with the ASME boiler code. The PUMA core power has a capacity of 400 kW through a total of 38 heater rods which are grouped into three power regions. The schematic of the RPV is given in Fig. 4. It has an annulus downcomer, three rings of heater rod arrays with 6 for the inner ring, 12 for the middle ring and 20 for the outer ring. There are two bypass regions in the core. The chimney is divided into two axial sections as in the SBWR. The lower section consists of nine flow channels of equal flow area. The details of the design are given in the design report [12].

The PUMA has three GDCS tank volumes, three PCCS condensers, and three ICS condensers. The drywell has a total height of 6.75 m and the volume of each section in the drywell is properly scaled. The suppression pool has a total height of 2.8 m and diameter of 2.8 m. The automatic depressurization system is simplified to two SRVs and four DPVs. Two of the DPVs are located in the main steam lines.

The PUMA has approximately 400 instruments that will provide detailed measurements of the mass and energy inventory in each vessel, various flows between components, pressure, pressure drop, temperature, void fraction, gas concentration and heat transfer.

5. Test Matrix

The facility acceptance test is planned for November 1995. Upon a successful acceptance test, the integral tests will be initiated. The first year test matrix is divided into phase 1 consisting of 15 tests and phase 2 consisting of 9 tests.

The phase 1 test matrix includes several main steam line break LOCAs, bottom drain line break LOCAs, GDCD line break LOCAs, loss of feedwater, feedwater line break LOCA and several PANDA and GIRAFFE counterpart tests.

The phase 2 test matrix includes two helium tests, several bottom drain line break LOCAs with reduced safety system functions and a station blackout scenario.

6. Conclusions

The scaling method, scientific design, engineering design and construction of the PUMA facility for the SBWR integral tests are discussed in detail. The facility is based on the application of a three-level scaling method which incorporates both the top-down and bottom-up scaling approaches in systematic manner. In the integral scaling (i.e.: level one), the steady-state and dynamic characteristics of circulating flow within each component are simulated. The level two scaling based on the control volume balances of mass and energy insures that the mass and energy inventories and inter-components flow of mass and energy are simulated. The level three scaling examines the scaling of various local phenomena which affects the transfer mechanisms and constitutive laws.

The resulting design is a 1/4 height 1/400 volume scaled test facility, where all the major safety and non-safety thermal-hydraulic components of the SBWR are simulated. The power is scaled by 1/200 and the test facility is operated at the prototypic pressure. However, the PUMA is focused on the various transients following the initial stage of the blow down which brings the RPV pressure to about 150 psi. The facility has the capability to simulate various LOCAs and other transients important to the safety analysis of the SBWR. It can simulate both the GDCS action phase and later the PCCS dominated phase in consistent manner.

Acknowledgements

The authors wish to acknowledge the comments and support provided by the following individuals. NRC: M.W. Hodges, T.L. King, F.Eltawila, L.M. Shotkin, D.E. Bessett and J.T. Han (PUMA Program Manager), BNL: U.S. Rohatgi, G. Slovik, Y. Parlatan and J.Jo, INEL: J.L. Anderson and K.G. Condie, and GE Nuclear Energy personnel.

REFERENCES

1. GE Nuclear Energy, "SBWR Standard Safety Analysis Report 25A5113 Rev. A, August (1992).
2. Billig, P.F., "Simplified Boiling Water Reactor (SBWR) Program Gravity-Driven Cooling System (GDCS) Integral Systems Test-Final Report," GEFR-00850, October (1989).
3. Tsunoyama, S., Yokobori, S., Arai, K., "Development of Passive Containment Cooling System," Proc. International Topical Meeting on Advanced Reactor Safety, Hyatt Regency, Pittsburgh, April 17-21 (1994).
4. Yadigaroglu, G., "Scaling of the SBWR Related Test," Report NEDC-32258, November (1993).

5. Han, J.T., Bessett, D.E., Shotkin, L.M., "NRC Confirmatory Testing Program for SBWR," Proceedings of the Twenty-First Water Reactor Safety Information Meeting, Bethesda, MD, October 25-27 (1993).

6. NRC Draft Report, "Compendium of ECCS Research for Realistic LOCA Analysis - Draft Report for Comment," NUREG-1290 (1987).

7. Ishii, M., Kataoka, I., "Similarity Analysis and Scaling Criteria for LWRs under Single Phase and Two-Phase Natural Circulation", NUREG/CR-3267, ANL-83-32 (1983).

8. Kocamustafaogullari, G., Ishii, M., "Scaling Criteria for Two-Phase Flow Natural and Forced Convection Loop and their Application to Conceptual 2x4 Simulation Loop Design", ANL-82-61, NUREG/CR-3420 (1983).

9. Kocamustafaogullari, G., Ishii, M., "Reduced Pressure and Fluid to Fluid Scaling Laws for Two-Phase Flow Loop", NUREG/CR-4584, ANL-86-19 (1986).

10. Condie, K.G., Larson, T.K., Davis, C.B., McCreery, G.E., "Evaluation of Integral Continuing Experimental Capability (CEC) Concepts for Light Water Reactor Research-PWR Scaling Concepts", NUREG/CR-4824, EG&G 2494 (1987).

11. Boucher, T.J., DiMarzo, M., Shotkin, L.M., "Scaling Issues for a Thermal-Hydraulic Integral Test Facility", NPC Paper.

12. Ishii, M., Revankar, S.T., Dowlati, R., Bertodano, M.L., Babelli, I., Wang, W., Pokharna, H., Ransom, V.H. and Viskanta, R., "Scientific Design of Purdue University Multi-Dimensional Integral Test Assembly (PUMA) for GE SBWR," Purdue University Report PU-NE 94/1, NUREG/CR-6309, 1995.

Nomenclature

A	Flow area scale
a	Cross-sectional area [m^2]
B_i	Biot number
c_p	Specific heat [J/kg-C]
D,d	Diameter [m]
E	Energy [J]
F	Total pressure loss coefficient
f	Friction factor, friction
G	Mass velocity [kg-m/s^2]
Gr	Grashof number
g	Gravitational acceleration [m/s^2]
j	Superficial velocity [m/s]
H	Height [m]
h	Enthalpy [J/kg]
K	Minor loss coefficient
L	Axial length scale
l	Length [m]
m,M	Mass [kg]
$\dot{m}$	Mass flow rate [kg/s]
n,N	Number
N_d	Drift flux number
N_{Fr}	Froude number
N_f	Friction number
N_{flash}	Flashing phase change number
N_{nc}	Natural circulation number
N_o	Orifice number
N_{pch}	Phase change number (= Zuber number)
N_{sub}	Subcooling number
N_{th}	Thermal inertia ratio
Nu	Nusselt number
N_{Zu}	Zuber number
p,P	Pressure [Pa]
q	Power [W]
q″	Heat flux [W/m^2]
Qs	Heat source number
R	Richardson number
St	Modified Stanton number
t	Time [s]
T	Temperature [°C]

T^*	Time ratio number
u	Velocity [m/s]
u_f	Internal energy of liquid
v,V	Volume [m^3]
V_{gj}	Drift velocity [m/s]
w	Work [J]
x	Quality
Z	Distance [m]

Greek Symbols

β	Volumetric thermal expansion coefficient [K^{-1}]
δ	Conduction depth [m]
Δ	Difference
α_s	Thermal diffusivity [m^2/s]
α	Void fraction
ρ	Density [kg/m^3]
τ	Time Constant [s]

Subscripts

e	Exit
f	Fluid
g	Gas
i	ith component
in	Inlet
m	Model
o	Reference point/component
out	Outlet
p	Prototype
R	Ratio
s	Surface, solid

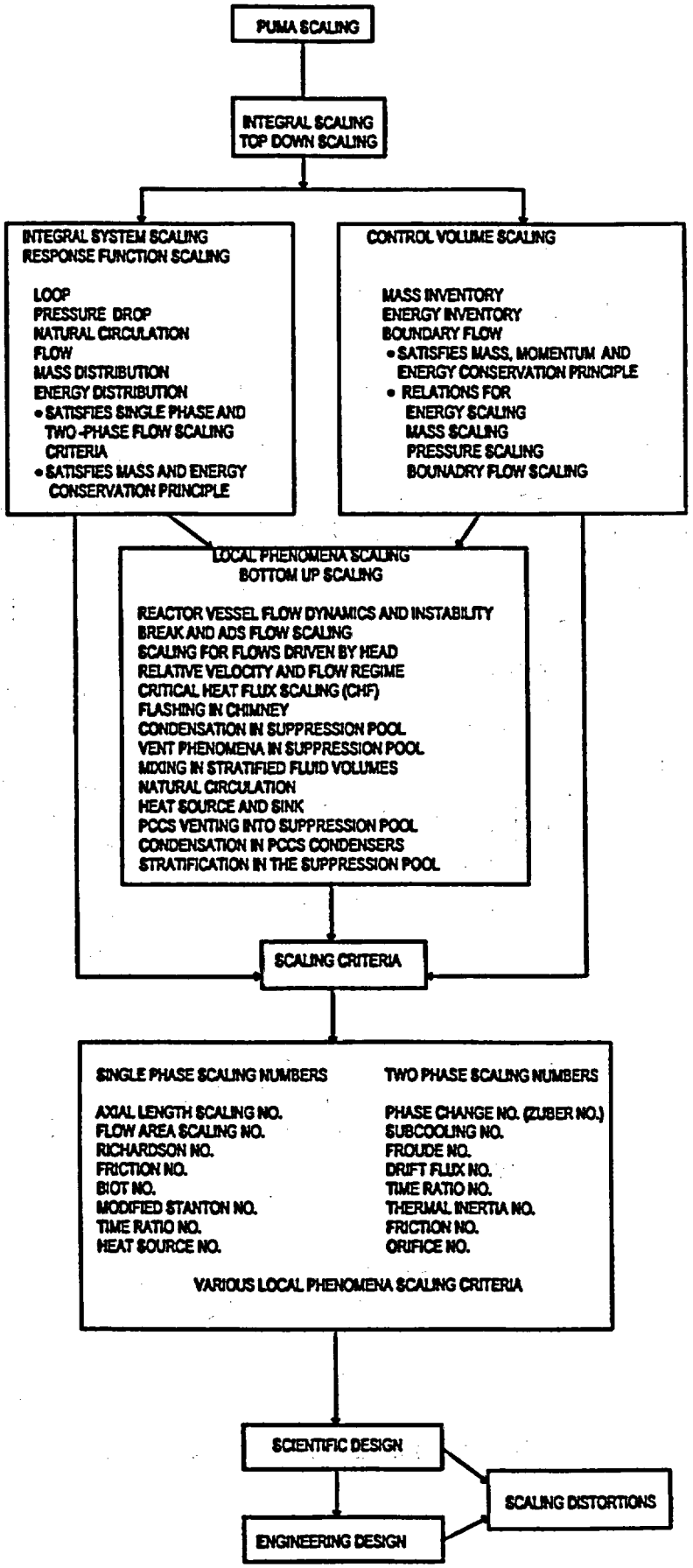

Fig. 1 Schematic Diagram for PUMA Scaling Procedure

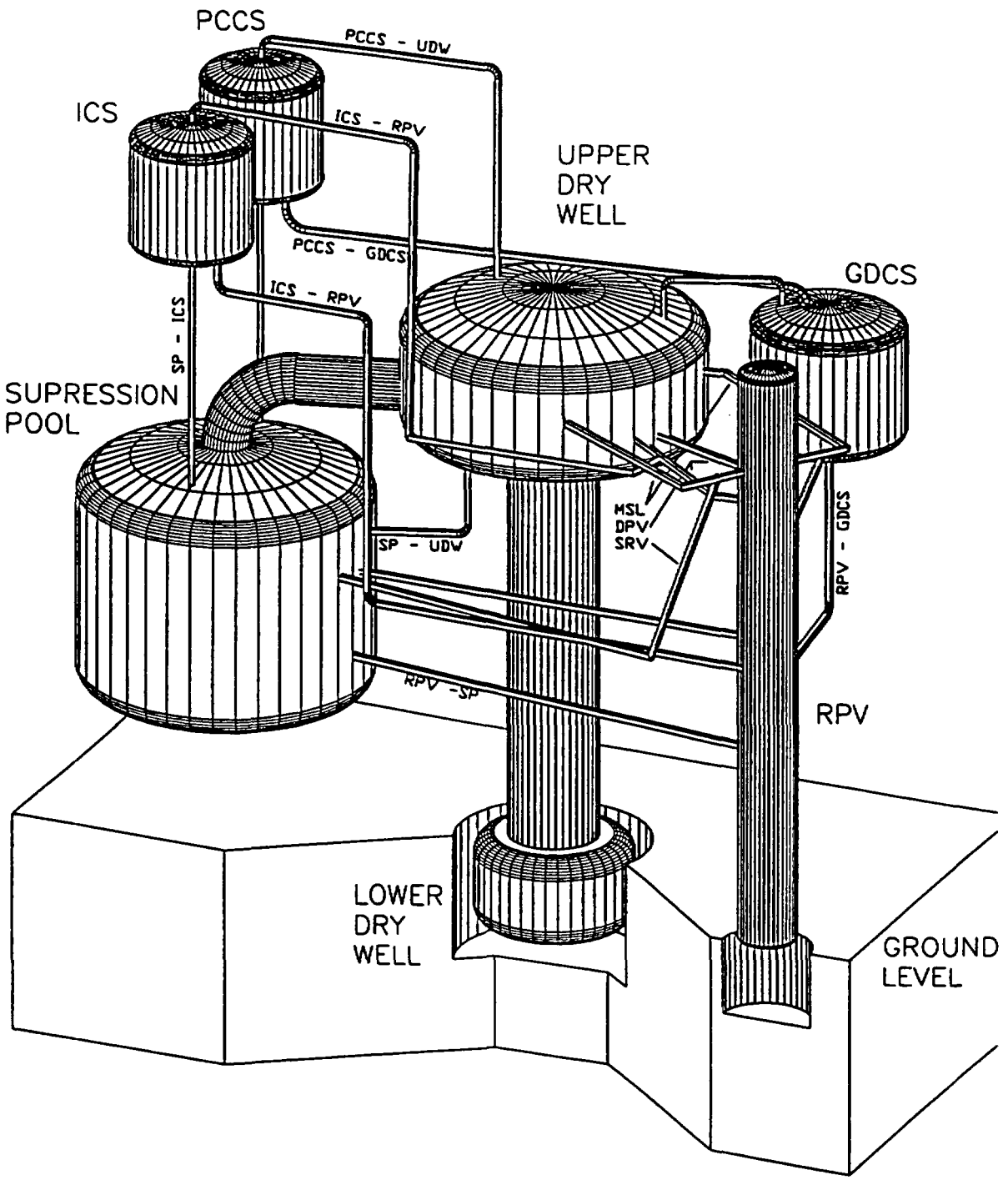

Figure 2. PUMA Three Dimensional Schematics

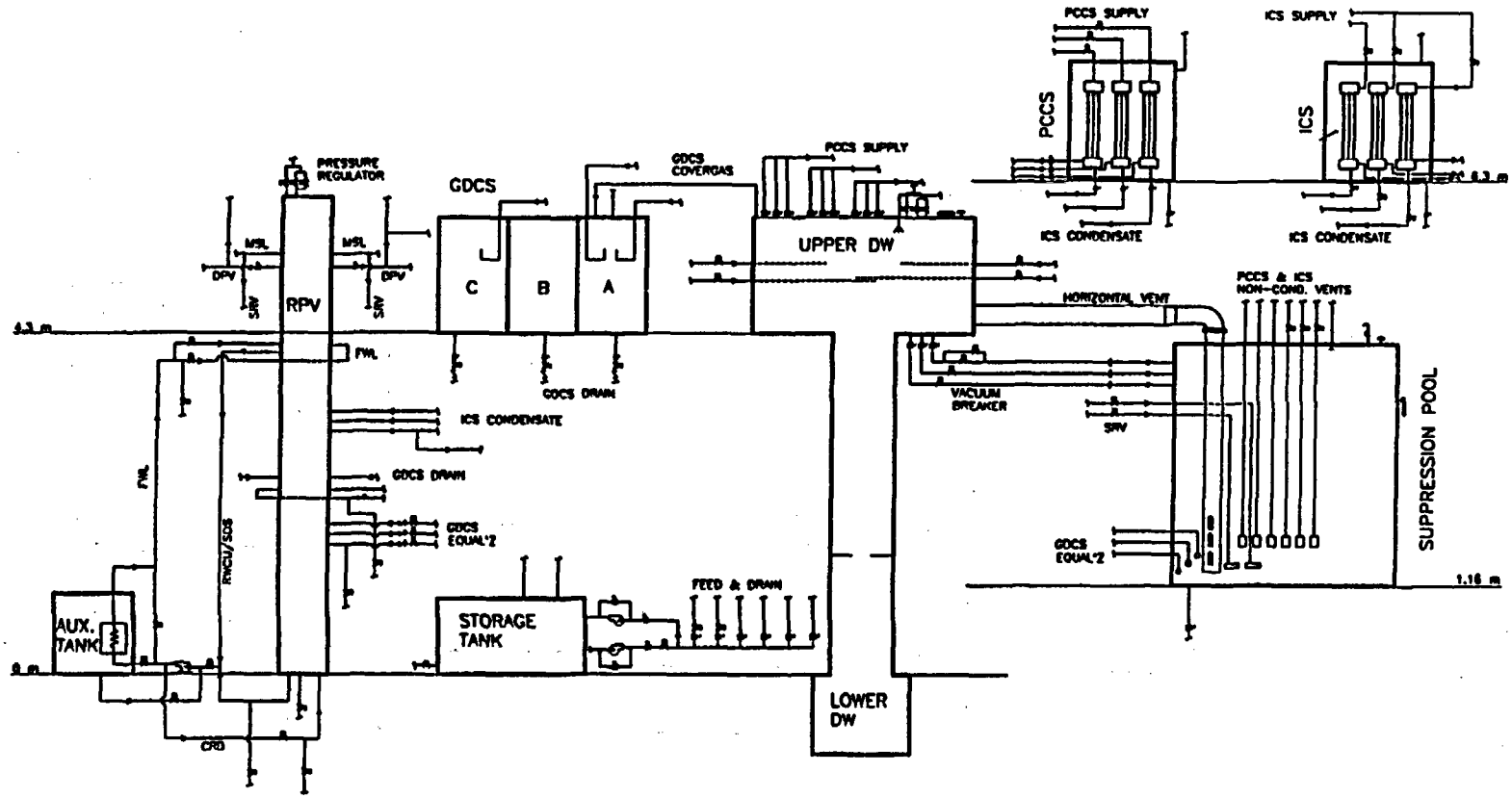

Figure 3. Schematics of PUMA Components and Connecting Lines

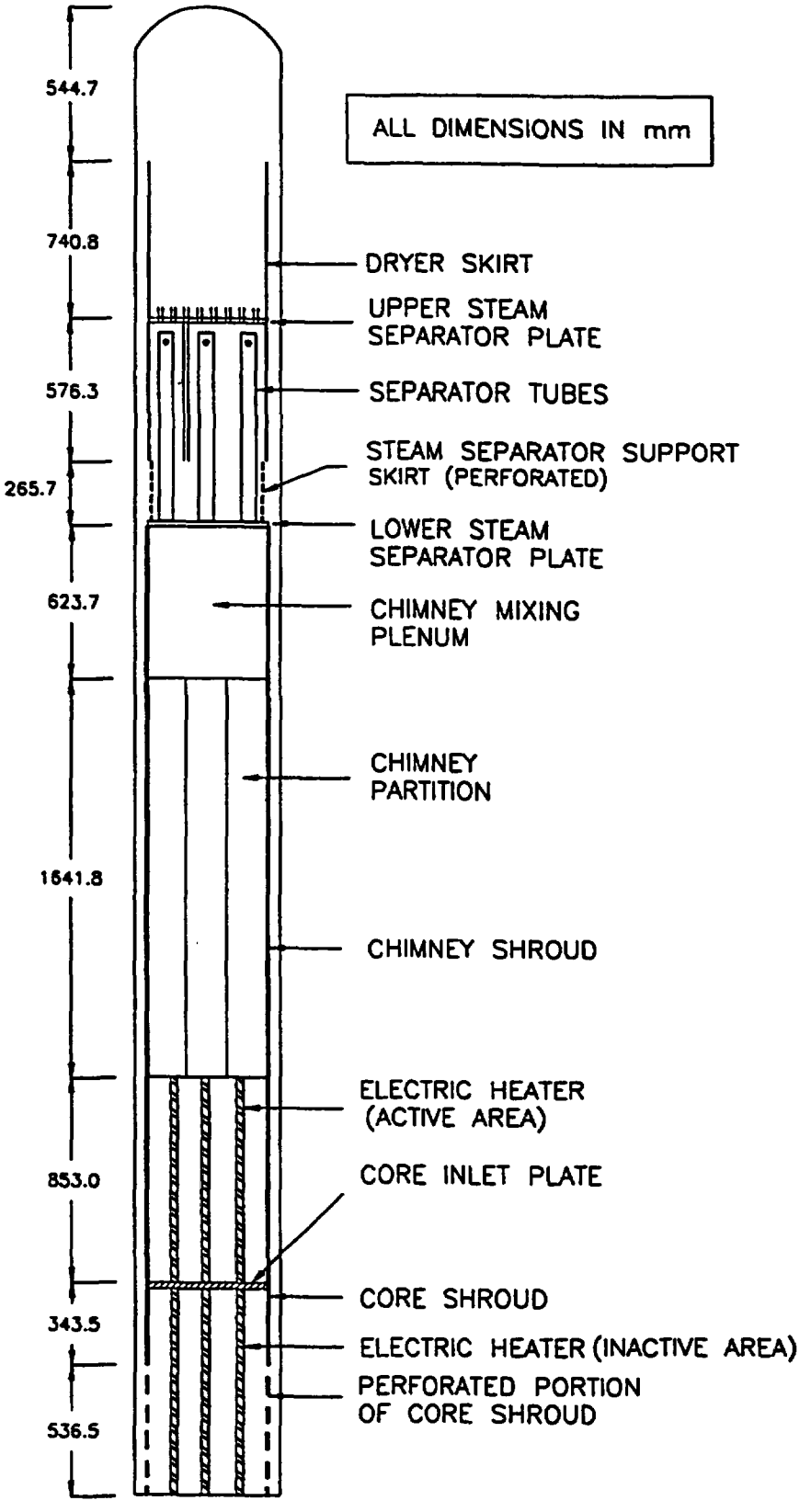

Fig. 4 Schematics of PUMA Reactor Pressure Vessel Internals

The PANDA Tests for SBWR Certification

G. Varadi, J. Dreier, Th. Bandurski,
O. Fischer, M. Huggenberger, S. Lomperski, and G. Yadigaroglu*

Thermal Hydraulics Laboratory
Paul Scherrer Institute (PSI), CH-5232 Villigen PSI, Switzerland

Abstract

The ALPHA project is centered around the experimental and analytical investigation of the long-term decay heat removal from the containments of the next generation of "passive" ALWRs. The project includes integral system tests in the large-scale (1:25 in volume) PANDA facility as well as several other series of tests and supporting analytical work. The first series of experiments to be conducted in PANDA have become a required experimental element in the certification process for the General Electric Simplified Boiling Water Reactor (SBWR).

The PANDA general experimental philosophy, facility design, scaling, and instrumentation are described. Steady-state PCCS condenser performance tests and extensive facility characterization tests were already conducted. The transient system behavior tests are underway; preliminary results from the first transient test M3 are reviewed.

1 Introduction: The ALPHA Project and PANDA

In 1991, the Paul Scherrer Institute (PSI) in Switzerland, initiated the ALPHA project for the experimental and analytical investigation of the long-term decay heat removal from the containment of the next generation of "passive" ALWRs; the effects of aerosols on containment performance are also considered. The dynamic containment response of

---

* main affiliation: Swiss Federal Institute of Technology (ETH), CH-8092 Zurich, Switzerland

such systems, as well as containment phenomena, are investigated. The ALPHA project includes integral system tests in the large-scale (1:25 in volume) PANDA facility; the smaller-scale separate-effects LINX series of tests related to various passive containment mixing, stratification, and condensation phenomena in the presence of non-condensable gases; the AIDA tests on the behavior of aerosols in Passive Containment Cooling Systems (PCCS); and supporting analytical work. The project has been, so far, mainly directed to the investigation of the General Electric (GE) Simplified Boiling Water Reactor (SBWR) PCCS and related phenomena.

The PANDA integral-test results discussed here were initially expected to bring only confirmatory information for the certification of the SBWR by the United States Nuclear Regulatory Commission (US NRC). Recent developments have made the first series of experiments to be conducted in PANDA a *required* experimental element in the certification process; thus, the tests are now performed according to the NQA-1 Quality Assurance procedure.

The SBWR confirmatory research and later the certification effort have been conducted in collaboration with a large international team. The closest PSI partners in this team have been the Electric Power Research Institute (EPRI), the General Electric Company (GE) and the University of California-Berkeley (UCB) in the US, the Netherlands Energy Research Foundation (ECN) and KEMA in the Netherlands, the Toshiba Corporation in Japan, the Instituto de Investigaciones Eléctricas (IIE) in Mexico, and the Italian national utility ENEL, as well as ENEA, Ansaldo, and SIET in Italy.
Elements of the SBWR international program closely linked to the ALPHA project are:

- Single-tube condensation experiments at UCB (Vierow and Schrock, 1991; Kuhn et al., 1995) and at MIT (Siddique et al., 1993).
- The smaller scale (1:400) integral test facility GIRAFFE, operated by Toshiba (Yokobori et al., 1991).
- The full-scale PCCS condenser qualification PANTHERS experiments performed by SIET in Italy (Botti et al., 1994).

Tests in all major PSI facilities started in 1995. The very first series of PANDA experiments conducted at the beginning of 1995 were steady-state PCCS condenser performance tests, as counterpart tests to those conducted at the PANTHERS and GIRAFFE facilities. Extensive facility characterization tests were completed in July 1995: the facility leak rates, heat losses, as well as the pressure-drop–flow-rate characteristics of the various lines were obtained. These are needed for the accurate description of the facility in computations. The first transient system behavior test was conducted in early October 1995 and the remaining series of transient tests intended for SBWR certification are underway and should be completed at about the end of 1995.

In addition to the large-scale PANDA tests, small-scale experiments and numerous analyses were conducted at PSI to better understand basic phenomena and SBWR

system behavior, to provide preliminary data for the development of computational models, etc.

2 The PANDA Large-Scale Facility

The PANDA general experimental philosophy, facility design, scaling, and measurement concepts were defined in early 1991 (Coddington et al., 1992). At that time it was decided to design a large-scale facility capable of simulating SBWR behavior during the long-term (or PCCS-cooling) phase of the postulated Loss-of-Coolant Accident (LOCA). The tests cover the LOCA phase that starts typically one hour after scram. They are intended to investigate mainly any three-dimensional effects that may be present during this phase. Thus, in relation to the SBWR certification effort, the PANDA transient test objectives are to demonstrate that:

- Containment performance is similar in a larger-scale, multidimensional system to that previously demonstrated with the smaller-scale GIRAFFE tests.
- Any non-uniform distributions in the containment do not create significant adverse effects.
- There are no adverse effects associated with multi-unit PCCS operation and interactions with other reactor systems.
- The tests also extend the data base available for code qualification and serve to further validate the system code TRACG (Andersen et al., 1993).

2.1 Conceptual Design

Early during the conceptual design phase of the facility, it was recognized that it was neither possible nor desirable to preserve exact geometrical similarity between the SBWR containment volumes and the experimental facility (Coddington et al., 1992), in spite of the fact that multidimensional containment phenomena such as mixing of gases (steam and noncondensables) and natural circulation between compartments may depend on the particular geometry of the containment building. Any attempt to reproduce the complex geometry of the SBWR in the PANDA facility would have been futile; the various phenomena taking place in the containment are complex and simple linear geometric scaling would have rather produced serious scaling distortions.

The various containment volumes were instead represented by interconnected simple cylindrical vessels. The general philosophy followed in designing the experimental facility was to allow any multidimensional effects to take place by dividing the main containment compartments (Drywell and Suppression Chamber) in two to allow for spatial distribution effects to manifest themselves. A variety of well-controlled boundary conditions (e.g., imbalances) can be imposed during the experiments, to study the various phenomena under well-established conditions, and in certain cases establish

an envelope for the behavior of the system. Carefully conducted "parametric" or sensitivity experiments can also provide more valuable data for code qualification, than attempts to simulate geometrically, but to a necessarily limited degree, the rather complex reactor system. Boundary conditions and the interconnections between containment volumes and their behavior can be controlled to study various system scenarios and alternative accident paths.

Following this general philosophy, the SBWR Reactor Pressure Vessel (RPV) and the Gravity-Driven Cooling System (GDCS) pools are represented each by one vessel. The Drywell (DW) and Suppression Chamber (SC or Wetwell) are represented both by *two* separate, interconnected vessels (Figures 1 and 2). The RPV contains a 1.5 MW electrical heat source. The electric "core" geometry and the heat rod dimensions are not intended to match those of the SBWR reactor core; they merely provide the necessary amount of heat to the RPV. The RPV internals (chimney height, etc.) also resemble those of the SBWR. The parameters of importance for global system behavior, namely, the RPV water inventory and water level are accurately scaled.

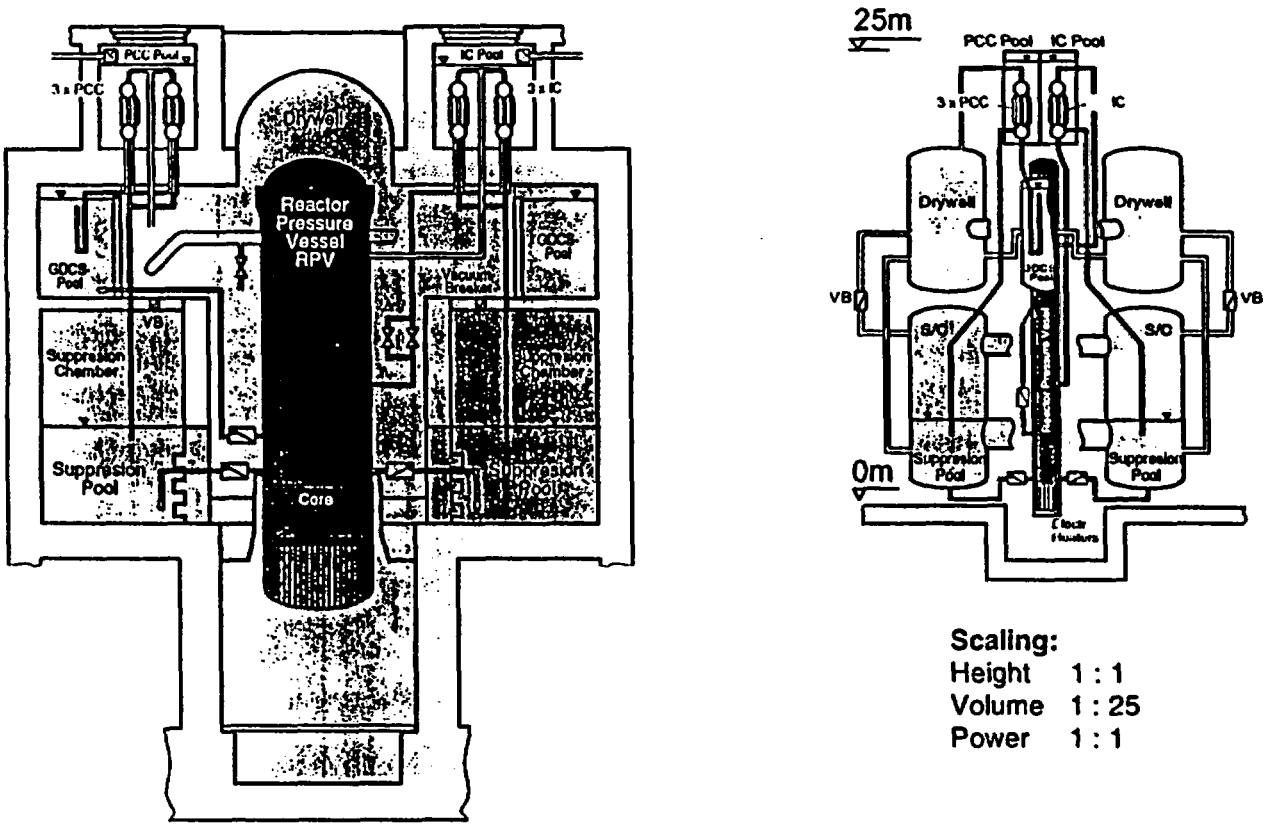

Figure 1 Schematic Illustration of the SBWR and of the PANDA Facility (at the same scale)

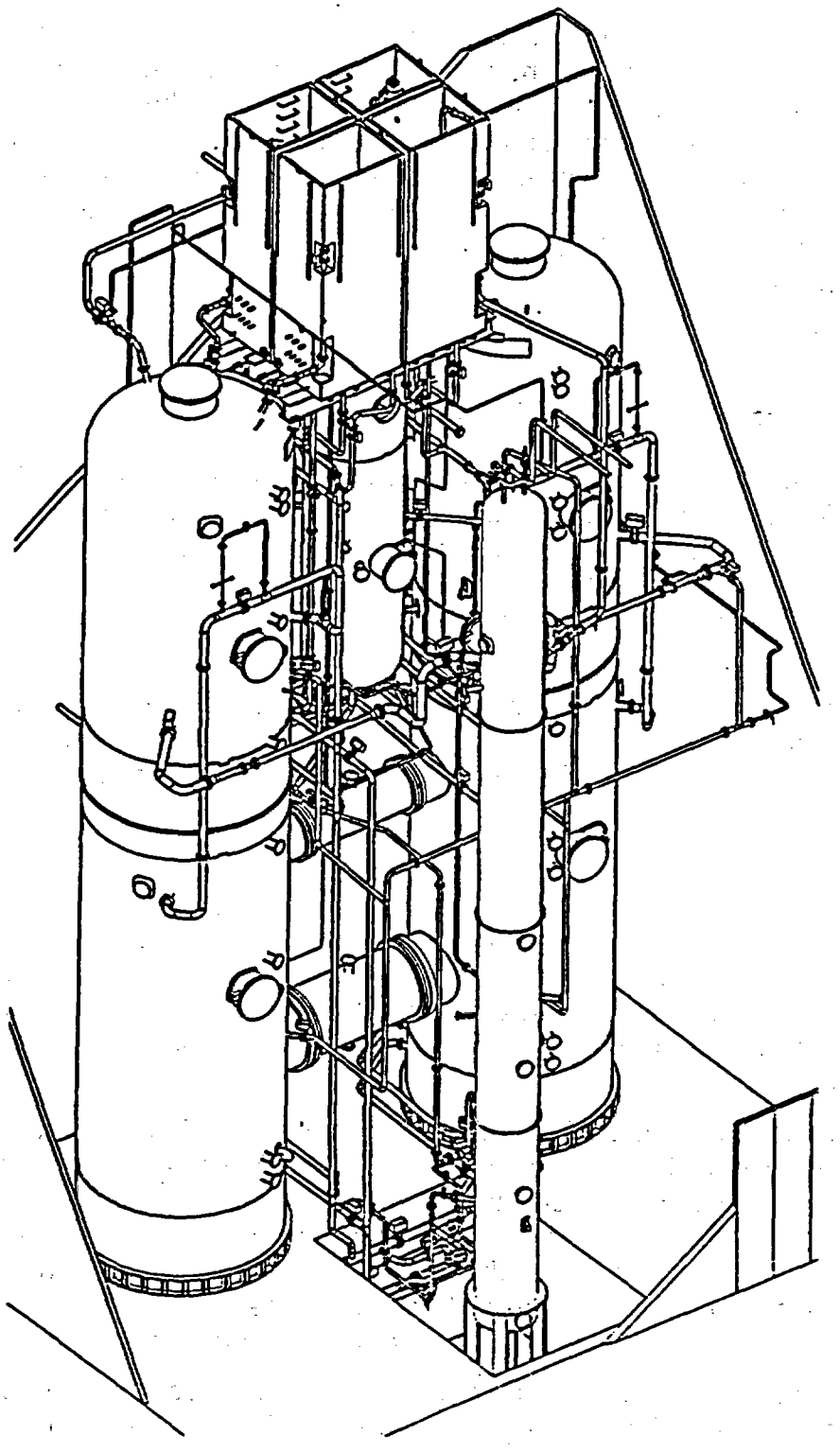

Figure 2 Isometric View of the PANDA Test Facility

There is a total of three PCCS condensers representing the corresponding three units in the SBWR and a single Isolation Condenser System (ICS) condenser representing two of the three corresponding SBWR units. (The two SBWR ICS condenser units correspond to the 2x50 % design value of the cooling capacity; the third ICS condenser is an extra 50 % redundant unit.) The condensers are connected to the two DW vessels, as shown in Figure 3. The fact that there are three PCC units and only two DW volumes allows some degree of asymmetric behavior or creates flows between the two DWs, even with equal flow areas from the RPV to the two DW volumes. The details of the system and its scaling rationale are described by Huggenberger (1991), and Coddington et al. (1992). Figure 3 shows details of the piping interconnecting the various volumes.

2.2 Scaling of the PANDA Facility

In relation to scaling, both "top-down" and "bottom-up" (Zuber, 1991) scaling considerations and criteria were developed. General, "top-down," scaling criteria are derived by considering the processes controlling the state of classes of containment sub-systems (e.g., containment volumes, pipes, etc.). Close examination of specific phenomena or system components (e.g., thermal plumes, vents, etc.) leads to "bottom-up" scaling rules.

A rigorous scaling study (Yadigaroglu, 1994) describes the scaling rationale and scaling details of the PANDA facility. Additional work (Coddington and Andreani, 1995; Andreani and Tokuhiro, 1995) covers certain particular aspects of scaling.

2.2.1 Top-Down Scaling

Generic scaling criteria for thermal-hydraulic facilities, such as those proposed by Ishii and Kataoka (1983) are not specific to the combined thermodynamic and thermal-hydraulic phenomena taking place inside containments. Thus, specific scaling criteria for the design of facilities simulating the dynamic operation of BWR containments such as PANDA were derived.

The SBWR containment is particularly complex and thermo-hydraulically coupled to the primary system. In addition to the usual BWR pressure suppression system and its various components, such as the main vents, one must now also consider the operation of the particular PCCS system and its components. According to the "top-down" approach, general scaling criteria were derived by considering the processes (rate of pressurization, heat and mass transfers) controlling the state of classes of containment subsystems (e.g., containment volumes, pipes, etc.).

In essence, mass and energy transfers take place between containment volumes through their junctions. Heat may also be exchanged between volumes by conduction through the structures connecting them. These exchanges lead to changes in the thermodynamic condition of the various volumes; this, in particular, leads to changes of

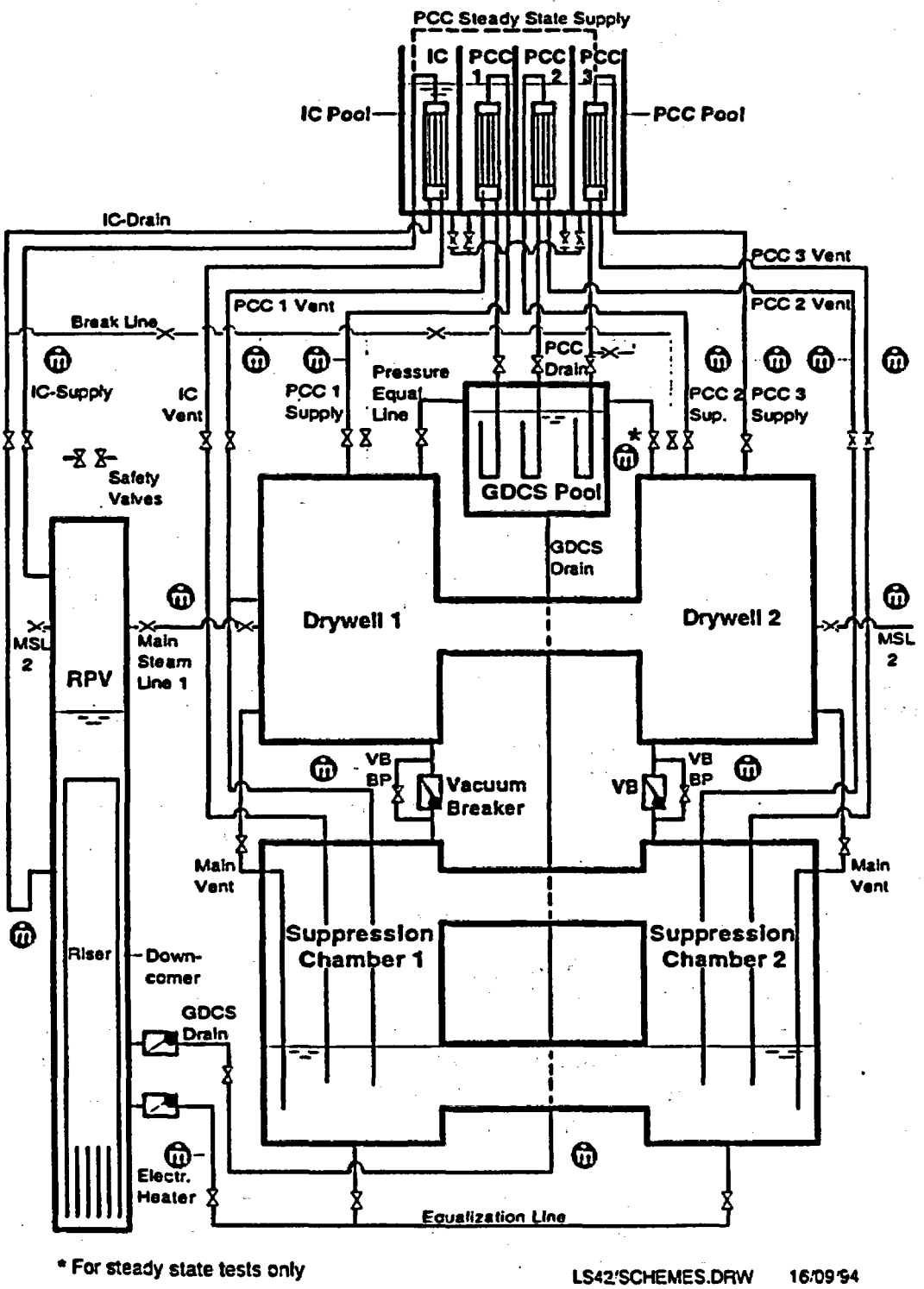

Figure 3 Piping Connections and Process Lines of the PANDA Facility (the symbols m in a circle denote flow rate measurements)

the volume pressures. The junction flows (flows between volumes) are driven by the pressure differences between volumes. Thus, the thermodynamic behavior of the system (essentially, its pressure history) is linked to its thermal-hydraulic behavior (the flows of mass and energy between volumes).

Prototypical fluids under prototypical thermodynamic conditions are used in PANDA; the nitrogen filling initially the containment is, however, replaced by air - the difference is of no importance. The fact that the fluids are expected to be in similar thermodynamic states and have similar composition in the prototype and the model, can be used to simplify the analysis and scaling of the facility.

The top-down scaling study confirmed the validity of the (familiar) scaling of all the following variables with the "system scale," R:

$$(\text{power})_R = (\text{volume})_R = (\text{horizontal area in volume})_R = (\text{mass flow rate})_R = (\text{heat transfer areas})_R = R$$

where the subscript R denotes the ratio between the corresponding scales of prototype and model. The system scale R can be defined as the ratio of prototype to test facility power input. For PANDA, R = 25.

In the BWRs, and particularly during the PCCS-cooling phase of the LOCA considered here, the important pressure drops and the corresponding junction flows are controlled by the submergence depth of vents in the Pressure Suppression Pool or by hydrostatic pressure differences between interconnected liquid volumes (e.g., the RPV and GDCS pool liquid spaces). The analyses of these processes justify the choice of 1:1 scaling for the vertical heights in general and for the submergence depths in particular (Yadigaroglu, 1994).

The pressure evolution resulting from the thermodynamics of the system and the pressure drops between volumes must clearly scale in an identical fashion. Considering the fact that prototypical fluids are used, this requirement links the properties of the fluid (in particular the latent heat and the specific volumes of water and steam) to the pressure differences between volumes (and to water levels or submergence depths of vents), resulting in 1:1 scaling for pressure drops. Thus, the above considerations result in:

1:1 scaling for pressure differences, elevations, levels, and submergences

This scaling rule determines the pipe diameters, lengths, and hydraulic resistances, and indirectly dictates the transit times between volumes. These transit times should, in principle, have the same (1:1) time scale as the time constants controlling the filling or pressurization rates of system volumes. This matching cannot be perfect, but the distortion is shown to be negligible, since the transit times are much shorter than the volume filling or pressurization times.

For the types of transients taking place in the SBWR, the average pressure drops between containment volumes are not expected to be dominated by inertial effects (very rapid changes in flow rates). Thus, the inertial characteristics of the piping (i.e., the lengths of piping and the velocities in these pipes), do not have to be scaled exactly. Usually (and fortunately), the total pressure drops in the piping are dominated

by local losses, so that the total pressure drops in the scaled facilities and in the prototype can be matched by introducing adequate local orifice losses.

2.2.2 Scaling of Specific Phenomena - Bottom-Up Approach

Close examination of the *specific* phenomena governing the operation of certain system components (e.g., vents immersed in the Pressure Suppression Pool of the SBWR) led to "bottom-up" scaling rules. Bottom-up scaling (Yadigaroglu, 1994) was applied for phenomena and facility components that were selected as being of particular importance by a Phenomena Identification and Ranking Table (PIRT) exercise. These include the scaling of thermal plumes, mixing and stratification phenomena in the Pressure Suppression Pool, as well as in the Drywell volume, of heat and mass transfers at liquid-gas interfaces, of the heat capacity of containment structures, etc. Of particular importance is also the scaling of the various vents discharging mixtures of steam and noncondensable gases into the Pressure Suppression Pool. The importance of heat losses was considered in detail and the facility was very heavily insulated to minimize losses.

Heat and mass transfer in the PCCS and ICS condensers must also be properly scaled. Condensation in the presence of noncondensables inside the tubes is perfectly scaled since the PANDA condenser tubes have prototypical dimensions and are expected to work under prototypical conditions. Heat transfer on the secondary, pool side may be affected by natural circulation in the pool. Although the PANDA PCCS and ICS pools have smaller scaled surface areas than the SBWR pools, water can be added during the experiments in a controlled manner to compensate for the smaller water inventory.

In summary, the PANDA model is essentially a 1:25 "vertical slice" of the SBWR. The heat capacity and heat losses of the experimental facility cannot be made to match those of the SBWR. This issue can be addressed, however, during data reduction by an accurate system heat balance based on measurements and heat loss calibrations.

3 Instrumentation and Data Acquisition

The facility is heavily instrumented with some 600 sensors for temperature, pressure, pressure difference, level or void fraction, flow rate, gas (oxygen or air) concentration, electrical power, valve position, and conductivity (presence of phase) measurements. Thus, the instrumentation includes, beyond the classical instruments, also non-condensable fraction (oxygen) sensors, phase detectors, "floating thermocouples" measuring the surface temperature of pools, etc.

A very large number of thermocouples measure not only fluid temperatures, but also facility component temperatures (vessel and pipe wall temperatures); these are used to obtain accurate heat balances and to estimate the heat losses from the various facility components.

The data acquisition system can sample and store all instrumentation channel readings continuously with a frequency of 0.5 Hz and for short periods of time with a "burst" frequency of 5 Hz. The facility is operated and controlled remotely and interactively by a computer-screen-based system. Very few operator interventions need to take place during the tests.

4 Preconditioning: Establishment of the Proper Initial Conditions for the Tests

The PANDA facility is equipped with auxiliary air and water supply systems for preconditioning the contents of the various system components. In particular with

1. An *auxiliary air supply system* (connected to the top of each vessel), used to pressurize any vessel.

2. A *demineralized water supply system* (that can be connected to the RPV and to the auxiliary water system), used to initially fill any system volume.

3. An *auxiliary water system* connectable to top and bottom filling ports in all vessels and pools. The system includes cooling and heating capability; for heating, heat is drawn from the RPV via a heat exchanger. Draining ports are also provided in all vessels and pools.

4. An *auxiliary steam system*: steam from the RPV can be directed to any vessel for preheating its structure or its gas space.

5. An *auxiliary vent system* that can be connected to any vessel; the system includes a pressure or temperature controlled vent valve.

Systems 4 and 5 in combination can be used for venting vessels (to establish, for example a pure-steam atmosphere). Directing the water supplied by the auxiliary water system to either the top or the bottom filling port of a vessel allows the establishment of both stratified and well-mixed initial conditions in its water space at the beginning of the tests.

According to typical preconditioning procedures, before test initiation, the various containment volumes are isolated, filled with the required fluids, and heated using heat from the RPV via a preconditioning-system heat exchanger. When the required initial conditions are reached, the vessel connections are opened and the test begins. Experience from the first tests has shown that the specified initial conditions can be matched very precisely (e.g., for temperatures within less than $\pm$ 2 K).

5 Steady-State PCCS Condenser Qualification Tests

The very first series of PANDA experiments conducted at the beginning of 1995 were steady-state PCCS condenser performance tests, as counterpart tests to certain tests conducted at the PANTHERS and GIRAFFE facilities. In this first series of tests, the effect of noncondensables on the condenser performance was investigated. Thus, the tests were conducted mostly at constant steam flow rate and variable noncondensable mass fraction.

For these tests, one of the PCCS condenser units (the most extensively instrumented one) was connected directly to the RPV by a specially built line. Thus, the RPV provided the required steam flow rate. The required noncondensable gas flow rate was injected directly into the pipe connecting the RPV to the PCCS condenser, well above the inlet of the condenser to insure adequate mixing. The liquid drain flow was discharged via the PCC drain to the GDCS pool and from there it was returned to the RPV. The vent flow was directed to the SC that had no liquid in it. The DWs were isolated. The GDCS and the SCs were connected and preheated to avoid subcooling of the condensate and condensation of any steam vented from the condensers. The pressure downstream of the condensers, in the SC and the GDCS, was controlled by venting to the atmosphere. For pure-steam tests, the condenser vent line was closed and the pressure in the RPV was allowed to find its own equilibrium value; this was the pressure level needed to achieve full condensation rate.

After achieving the required condenser inlet and downstream pressure conditions and assuring that stable operation had been achieved, the test data were recorded for at least 10 minutes. The test was considered successful when the specified test conditions were met in an average sense within a given tolerance (e.g., ± 5 % for the steam flow), during 10 minutes of the recording period, and when the standard deviation of any oscillations also did not exceed the same tolerance level. Repeatability tests showed differences in condenser performance of only a few percent.

Figure 4 shows the condenser efficiency, defined as the fraction of inlet steam condensed, as a function of the noncondensable mass fraction, at the reference steam flow rate. As expected, the condenser efficiency diminishes as the noncondensable mass fraction increases. The figure contains also blind pre-test predictions obtained with the TRACG code. These TRACG predictions were completed and submitted to the US NRC before running any of the tests. The trends predicted by TRACG are in excellent agreement with the experimental ones. The TRACG values are quantitatively slightly conservative (i.e., they tend to underpredict condenser performance).

6 Facility Characterization Tests

Extensive facility characterization tests were completed in July 1995: the facility leak rates, heat losses, as well as the pressure-drop–flow-rate characteristics of the various

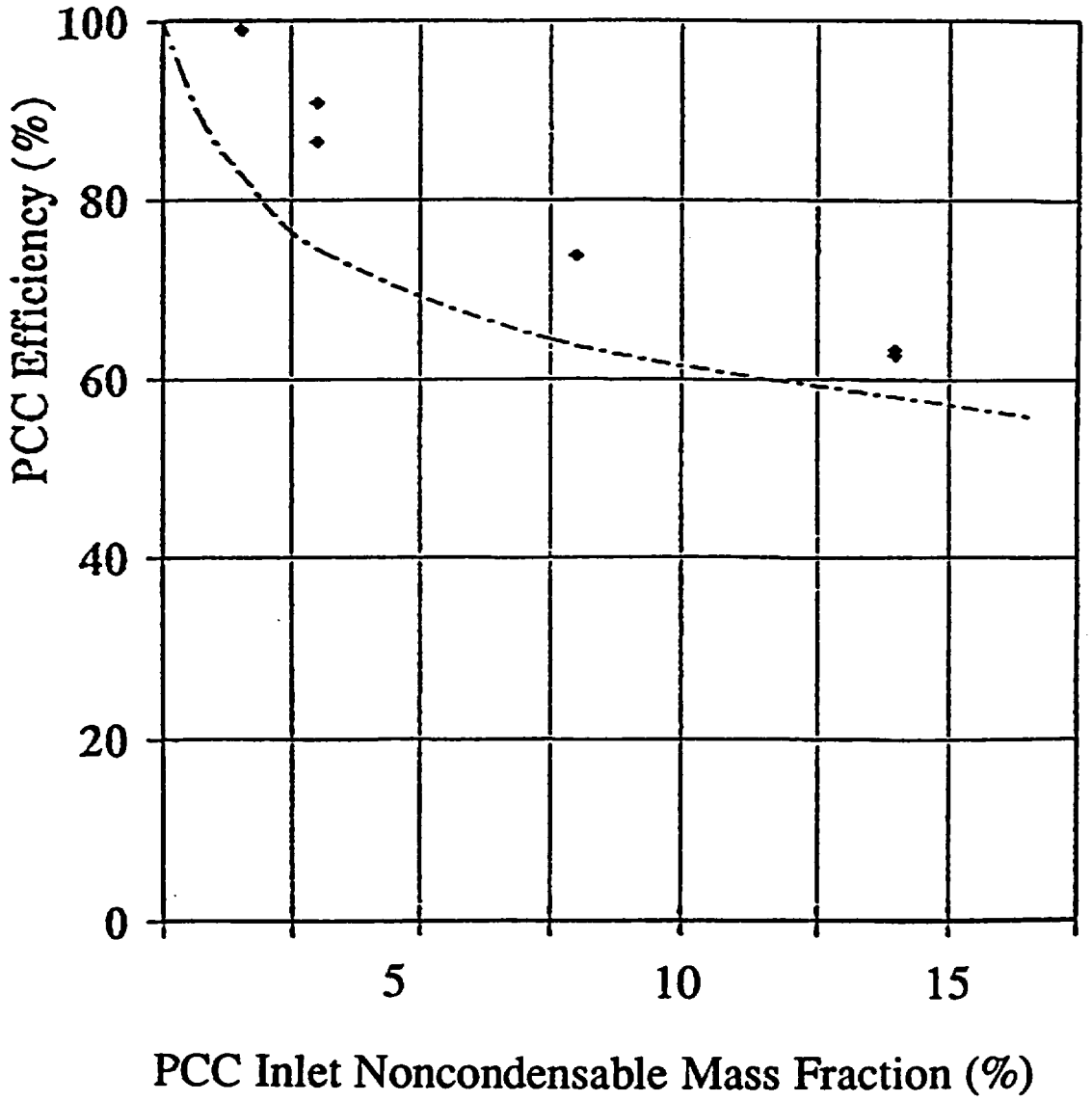

Figure 4 Steady-State Condenser Characterization Tests: Condenser Efficiency as a Function of the Noncondensable Mass Fraction at Constant Steam Flow Rate.

lines were obtained. These are needed for the accurate description of the facility in computations.

The facility was first pressurized with air to a pressure of 5 bars. The various system vessels where than isolated by closing the valves on the lines connecting them. The facility was left at that state for 62 hrs. The pressure decrease in each individual vessel due to any leakage was recorded and corrected for air temperature effects. The cold-system losses measured this way were lower than 0.08 % vessel volumes per day for all vessels except for the RPV, that had a higher leak rate (3.7 % per day).

The cold leakage tests were followed by heat loss tests. For these tests, the vessels were initially interconnected, purged of any air by steam injection and finally filled with saturated steam at 4 bars. The vessels were than valved off and isolated from each other and from the environment and left to cool down due to heat losses. The recorded vessel gas-space and wall temperatures allowed estimation of the heat losses.

Figure 5 shows the sum of all the heat losses from the facility measured this way as a function of vessel (essentially vessel wall) temperature. The measured total facility losses met and exceeded the heat loss criteria initially established to design the facility: they did not exceed about 7 % of the expected scaled reactor decay heat power at 24 hrs after scram (the design target was 10 %). In reality, the actual losses during a typical test will be even lower, since the SCs will be at a lower temperature.

The PANDA facility includes flow rate instruments in practically all its lines, as shown in Figure 3. As a final facility characterization test, the flow rates and the line pressure losses were measured simultaneously in all instrumented lines. For most lines, these tests were conducted in a quasi-steady state fashion with air (by using the air stored under pressure in one of the facility vessels). Since the vessels are very large, the variation of the pressure during recording of the characteristics was very small. For the two Main Steam Lines and the three PCCS feed and vent lines, the tests were also conducted using steam produced in the RPV. Water tests have been carried out for the GDCS return line to the RPV and the equalization line between the WW's and the RPV.

The flow-rate vs pressure-drop tests showed that the total pressure losses in the various system lines had been correctly estimated (in comparison to the SBWR values) and "built-in." They also provide the exact loss coefficients that can be used in computer models of the system.

In summary, the facility characterization tests described summarily here demonstrated that the facility mass and heat leakages were below the maximum acceptable values set earlier and that the pressure-drop flow-rate characteristics of the lines matched the ones of the SBWR system.

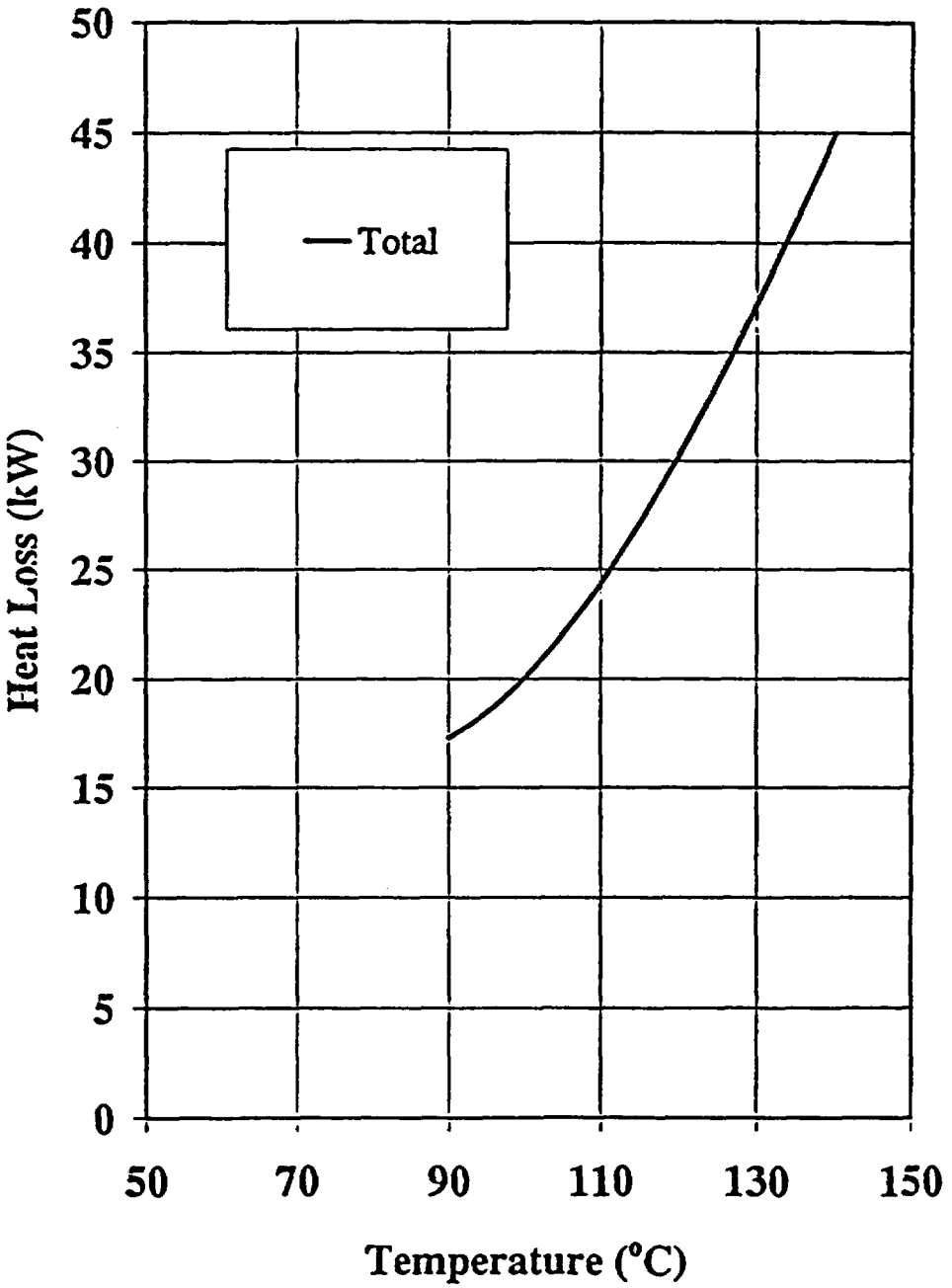

Figure 5 Measured PANDA Facility Heat Losses as Functions of Vessel Temperature.

7 Transient System Behavior Tests

A series of nine transient system tests have been planned as the primary containment and systems interaction data base for SBWR certification. The test matrix is set in a way investigating parametric variations around a base test, that is a counterpart test to one of the GIRAFFE tests. Thus, any effects of system scale and of non-uniformities in the system will become apparent.

This transient test series includes several Main Steam Line Break (MSLB) tests. The initial conditions for these tests are the state of the system one hour after scram during the LOCA; at that time the DW contains mostly steam and almost all the air has been pushed into the SC. One test is similar to a GIRAFFE MSLB test with uniform Drywell conditions, while a second one maximizes the influence of DW asymmetries on the operation of the PCCS condensers. Uniform and asymmetric DW conditions can be created in PANDA by varying the fraction of steam flow that is injected into each of the interconnected Drywell vessels and by modifying the number of condenser units directly connected to each vessel.

Another test is designed to investigate the startup of the PCCS system. In this case, the DW contains initially a large amount of air. Tests investigating the effect of the Isolation Condensers on global system performance and the effects of Vacuum Breaker openings are also planned. Finally, there are tests designed to explore the effect of DW to WW leakage which bypasses the Suppression Pool.

The actual transient system behavior tests are underway. The first transient Test M3 was conducted successfully at the beginning of October 1995. This test has demonstrated the following:

- the facility can be operated and controlled very well, and very narrowly defined initial test conditions and boundary conditions (initial states of various containment volumes, power input, etc.) can be achieved
- the pre-conditioning equipment worked very successfully in this respect
- the instrumentation performed with high accuracy and reliability; certain very difficult flow rate measurements are still under scrutiny; a combination of measurements and analysis will be needed to resolve problems related to these.

The data from the M3 test are being analyzed. *Preliminary and necessarily limited and tentative* findings concerning the SBWR long-term containment cooling system are:

- The overall global behavior of the containment was very favorable; the system exhibits great "robustness." The PCCS units were able to accommodate themselves in sharing the cooling load, regardless of any observed dissymetries and three-dimensional effects.

- There are possibly interesting findings regarding the distribution of noncondensables and their effects on the PCCS system. Small amounts of noncondensables seem to affect the status of the condensers operating in parallel. The global operation of the PCCS system does not, however, seem to be influenced by such possible dissymetries and three-dimensional effects, as noted above.

This is reassuring since, indeed, PANDA was built to investigate such effects.

Definite conclusions will be obtained after examination and analysis of all the data; this is underway.

8 Pre-Test Calculations

Blind pre-test calculations are performed and submitted to the US NRC, as stated earlier. The first such calculations were conducted in collaboration with GE, IIE in Mexico, and KEMA and ECN in the Netherlands using the TRACG code. The pre-test calculations for the steady-state PANDA PCCS condenser tests showed very good agreement between the calculated condenser performance and the test data, the TRACG calculations being only slightly conservative, as already stated.

Pre-test calculations for the first transient Test M3 predicted the peak containment pressure very well. Comparison of the code predictions with the detailed test data are just beginning.

Acknowledgments

The ALPHA project, conducted at PSI in cooperation with the Electric Power Research Institute (EPRI) and the General Electric Company (GE), receives financial support from the Nuclear Power Committee of the Swiss Utilities (UAK), the (former) Swiss National Energy Research Foundation (NEFF) and GE; these financial contributions are gratefully acknowledged. Particular technical contributions from international collaborations are mentioned in the text.

This paper results from the collaboration of a large number of persons both inside PSI as well as outside. The authors particularly acknowledge the contributions of PSI collaborators P. Coddington and B. Uebelhart during the early phases of the project, of L. Voser for design, construction and resolution of many instrumentation problems, of J. Healzer for pre-test analyses and general advice, of C. Aubert for test planning and data analysis, of H.-J. Strassberger for facility operation, and of P. Gritsch, W. Bulgheroni and P. Rasmussen for facility controls and data acquisition systems. The authors are also indebted to J. Yedidia of EPRI who was instrumental in organizing the ALPHA program and to their numerous GE colleagues who contributed time and effort,

in particular to A. Rao, J. Fitch, B. Shiralkar, J. Torbeck, A. Arretz, B. Usry and B. Wingate.

References

Andersen, J.G.M. et al., 1993, "TRACG Qualification," Licensing Topical Report, NEDE-32177P, Class 3 (February 1993).

Andreani, M. and Tokuhiro, A., 1995, "Condensation in the Spout Region of a Gas-Vapour Plume Rising in a Subcooled Water Pool," pp. PC2-17-24 in *Proceedings, The 2nd Int. Conference on Multiphase Flow '95, Kyoto*, April 3-7, 1995, Kyoto, Japan, Vol. 2.

Botti, S. et al., 1994, "Tests on Full Scale Prototypical Condensers for SBWR Application," European Two-Phase Flow Group Meeting, SIET, June 6-8, 1994.

Coddington, P., Huggenberger, M., Güntay, S., Dreier, J., Fischer, O., Varadi, G., and Yadigaroglu, G., 1992, "ALPHA: The Long-Term Decay Heat Removal and Aerosol Retention Programme," pp. 203-211 in *5th International Topical Meeting on Nuclear Reactor Thermal Hydraulics (NURETH-5)*, Salt Lake City, USA, Sept. 1992.

Coddington, P. and Andreani, M., 1995, "SBWR PCCS Vent Phenomena and Suppression Pool Mixing," pp. 1249-1271 in *Proceedings of the 7th Int. Meeting on Nuclear Reactor Thermal-Hydraulics NURETH-7*, Saratoga Springs, New York, September 10-15, 1995, NUREG/CP-0142, Vol. 2.

Huggenberger, M., 1991, "PANDA Experimental Facility Conceptual Design," PSI internal report AN-42-91-09, ALPHA-105.

Ishii, M. and Kataoka, I., 1983, "Similarity Analysis and Scaling Criteria for LWR's Under Single-Phase and Two-Phase Natural Circulation," NUREG/CR-3267 (ANL-83-32).

Kuhn, S.Z., Schrock, V.E. and Peterson, P.F., 1995, "An Investigation of Condensation from Steam-Gas Mixtures Flowing Downward Inside a Vertical Tube," pp. 312-335 in *Proceedings of the 7th Int. Meeting on Nuclear Reactor Thermal-Hydraulics NURETH-7*, Saratoga Springs, New York, September 10-15, 1995, NUREG/CP-0142, Vol. 1.

Siddique, M., Golay, M.W., and Kazimi, M.S., 1993, "Local Heat Transfer Coefficients for Forced Convection Condensation of Steam in a Vertical Tube in the Presence of a Non-condensable Gas," *Nucl. Technol.*, Vol. 102, p. 386.

Vierow, K.M. and Schrock, V. E., 1992, "Condensation in a Natural Circulation Loop with Non-Condensable Gases, Part I Heat Transfer," *Proc. Int. Conf. Multiphase Flows*, Tsukuba, Japan, September 1991.

Yokobori, S., Nagasaka, H., Tobimatsu, T., 1991, "System Response Test of Isolation Condenser Applied as a Passive Containment Cooling System," *1st JSME/ASEM Joint International Conf. on Nuclear Engineering (ICONE-I)*, Nov. 1991, Tokyo.

Yadigaroglu, G., 1994, "Scaling of the SBWR Related Tests", GE Nuclear Energy report NEDC-32288 (July 1994).

Zuber N., 1991, "Hierarchical, Two-Tiered Scaling Analysis," Appendix D to "An Integrated Structure and Scaling Methodology for Severe Accident Technical Issue Resolution," Nuclear Regulatory Commission Report NUREG/CR-5809, EGG-2659 (November 1991).

NRC CONFIRMATORY AP600 SAFETY SYSTEM PHASE I TESTING IN THE ROSA/AP600 TEST FACILITY

Gene S. Rhee, U.S. Nuclear Regulatory Commission
Yutaka Kukita, Japan Atomic Energy Research Institute
Richard R. Schultz, Idaho National Engineering Laboratory

ABSTRACT

The NRC confirmatory phase I testing for the AP600 safety systems has been completed in the modified ROSA (Rig of Safety Assessment) test facility located at the Japan Atomic Energy Research Institute (JAERI) campus in Tokai, Japan. The test matrix included a variety of accident scenarios covering both design and beyond-design basis accidents. The test results indicate the AP600 safety systems as reflected in ROSA appear to perform as designed and there is no danger of core heatup for the accident scenarios investigated. In addition, no detrimental system interactions nor adverse effects of non-safety systems on the safety system functions were identified. However, three phenomena of interest have been identified for further examination to determine whether they are relevant to the AP600 plant. Those three phenomena are: (1) a potential for water hammer caused by rapid condensation which may occur following the actuation of the automatic depressurization system (ADS), (2) a large thermal gradient in the cold leg pipe where cooled water returns from the passive residual heat removal system and forms a thermally stratified layer, and (3) system-wide oscillations initiating following the ADS stage 4 actuation and persisting until the liquid in the pressurizer drains and steam generation in the core becomes insignificant.

I. Introduction

Westinghouse Electric Corporation submitted the Advanced Passive 600 MWe (AP600) nuclear power plant design to the Nuclear Regulatory Commission (NRC) for design certification. In contrast to the current generation of reactors, this new design features passive safety systems for mitigating accidents and operational transients. Since these passive safety systems rely on gravity-driven flow, most of the driving forces for the safety functions are small compared to those available under conventional pumped systems. Thus, the performance of these new safety systems may be adversely affected by small variations in thermal hydraulic conditions. Also, the computer analyses of the passive safety systems pose a challenge for current thermal-hydraulic

system analysis codes in that the current codes were not sufficiently assessed for conditions of low pressure and low driving heads and for the system interactions that may occur among the multiple flow paths used in the AP600 design. Therefore, integral effects test data have been obtained under the ROSA/AP600 Confirmatory Test Program for evaluation of AP600 safety system performance and for independent assessment and validation of computer analysis codes. Other integral effects test data were also obtained from the NRC low pressure confirmatory test program at the Oregon State University (OSU) test facility and by Westinghouse from its integral test programs in the SPES-2 (Simulatore Per Espriencze di Sicurezza-2) and OSU test facilities. SPES-2 is a full-pressure, full-height test facility in Italy but much smaller in scale (1/395 by volume) than ROSA which represents a 1/30 volume-scale for AP600. The OSU facility is a low pressure, reduced 1/4 height facility with a considerably smaller volumetric scale (1/200 by volume) as compared to ROSA. NRC confirmatory safety system testing is not required for design certification but would provide additional technical bases for the NRC licensing decisions.

The ROSA/AP600 testing was conducted in cooperation with the JAERI. The arrangement of this cooperative effort was reported earlier in the 1994 International Topical Meeting on Advanced Reactors Safety (Ref. 1).

This paper provides an overall look at the testing program. Figure 1 shows how the ROSA/AP600 Test Program fits in the overall objective of predicting the behavior of the AP600 safety systems under various accident conditions. All of the test results related to the AP600 system behavior, namely the results obtained from ROSA/AP600, SPES, and OSU test facilities, are integrated, and a consistent model is synthesized. After scaling aspects are taken into account appropriately, the AP600 safety system behavior is finally predicted. It should be noted that what is observed in ROSA may not necessarily occur in the AP600.

II. Facility Description

The ROSA facility is a full-height, full-pressure facility and includes two primary loops, each containing one cold leg, one hot leg, an active inverted-U tube steam generator, and an active reactor coolant pump. The reactor pressure vessel includes an annular downcomer and contains full-length electrically heated rods capable of generating 10 MW or 16 percent of the scaled full power of the AP600.

The facility configuration and the relative height of each component are shown in Figure 2. The ROSA facility was originally designed after a Westinghouse 4-loop plant with the simplification of each loop representing two loops of a 4-loop plant. In order to implement the AP600 design, the facility was extensively modified, resulting in the configuration shown in Figure 2. In particular, all of the AP600 safety systems were implemented in the ROSA facility. However, there were still some discrepancies between ROSA and AP600

configurations. These discrepancies were considered to have a minor effect on the system behavior. In any case, the main discrepancies are in the following three areas:

1. ROSA has one cold leg in each loop whereas AP600 has two cold legs in each loop. This means that in ROSA the pressure balance lines (PBLs) of both core makeup tanks (CMTs) are supposed to be connected to the same cold leg, unlike in AP600 where each CMT PBL is connected to a different cold leg, and thus in ROSA what happens in one CMT may unduly affect the other CMT through the common cold leg connection. For instance, a break in the PBL of one CMT may cause rapid fluid loss in the cold leg which in turn affects the PBL of the other CMT. In order to avoid undue influence of one CMT on the other, the CMT PBL is connected to the cold leg of its own loop for the tests involving PBL breaks. Figure 2 shows the usual configuration, i.e., both PBLs connected to the same cold leg through a common offtake pipe.

2. The ROSA cold legs have a shallow loop seal whereas AP600 has no loop seals. The depth of the loop seal was much reduced from the original value. However, it could not be eliminated completely because of hardware constraints. A loop seal bypass was installed to examine the effect of a loop seal. When a loop seal is present and contains liquid, it would hinder the vapor flow from the steam generator to the downstream break or to the PBL take-off point in the cold leg. Thus, the loop seal may affect the system behavior somewhat. However, it turned out that the effect was not appreciable.

3. The ROSA cold legs and hot legs are at the same elevation whereas in AP600 the cold legs are at a slightly higher elevation than the hot legs. This discrepancy is not expected to cause much difference in the system behavior.

The details of the facility configuration and modification were reported earlier (Ref. 1, 2, and 3).

III. Test Matrix

Since the ROSA facility is a full-pressure test facility, it is particularly good for studying the system behavior under high pressure conditions. The types of accident scenarios chosen for the ROSA/AP600 test matrix were those which would provide high pressure conditions for a relatively long period of time during which the system behavior and the interactions among subsystems could be studied. Each accident scenario chosen encompassed a multitude of phenomena, some of which occurred at the same time while others appeared sequentially. Any one test was not chosen to see a particular phenomenon but to examine many phenomena and their interactions. These tests were integral effects tests and not separate effects tests and covered both design and

beyond-design basis accident scenarios. In all cases the important objective of the test was to obtain data for the computer code assessment under AP600-like conditions.

The specific test matrix is shown in Table 1. It can be divided into two categories; 1) design basis accidents with a single failure criterion, and 2) beyond-design basis accidents involving multiple failures. The first category consists of loss-of-coolant accidents (LOCAs) of small to medium size breaks ranging from a 1/2" break in the cold leg to a double-ended guillotine break in the direct vessel injection line and the inadvertent opening of a stage 1 valve of the ADS. The second category involves multiple failures of various components such as steam generator tubes, ADS valves, and CMT discharge valves. In all cases except for Test No. 5 (APCL05) where all ADS stage 1-3 valves failed shut but all four ADS stage 4 valves were operational, one of the ADS stage 4 valves was assumed to have failed as the worst single failure.

Table 1 shows two different configurations, either AP600 or SPES. The AP600 configuration refers to the case where the orifices in the ADS lines were set to obtain the best-estimate flows whereas the SPES configuration refers to the case where the ADS orifices were set corresponding to the minimum ADS valve areas following practices used in SPES tests. The reason for following the SPES practices was to use the same test conditions in order to run counterpart tests. For non-counterpart tests, the objective was to use the best-estimate test conditions to investigate the best-estimate behavior of the safety systems.

IV. Test Results

The test results discussed in this paper are the ones directly related to the question of how effectively the core is cooled under various accident conditions. One of the key accident mitigation strategies used in the AP600 design is the effective depressurization of the primary system to the containment pressure to allow long term coolant injection from the in-containment refueling water storage tank (IRWST). Figure 3 shows system depressurization behavior as a function of time for various accident conditions. As expected, the depressurization rate increased as the break size increased. Even if there was no break as in the case of a station blackout event, the system depressurized effectively as a result of cooldown by steam generators, the passive residual heat removal (PRHR) system, CMTs, and the accumulators (ACC). The precipitous decline of pressure near the end of the transient was due to actuation of ADS.

The best way for assuring the cooling of the core is to show that the core is always covered with single phase liquid or two-phase mixture. Such is the case for all 14 tests conducted so far covering a wide variety of accident scenarios. Figure 4 shows collapsed liquid levels in the vessel as a function of time for representative cases. Only a double-ended guillotine break in the direct vessel injection (DVI) line showed that a significant part of the upper region of the core was above the collapsed liquid level. However, even in

this case two-phase mixture covered the entire region of the core as suggested by the fact that the upper plenum had a significant amount of liquid throughout the transient.

The effective core cooling is also evidenced by a clad temperature plot a representative of which is shown in Figure 5. All of the heater rod surface temperatures are either below or at the saturation point throughout the transient.

Although ROSA/AP600 tests suggest that the AP600 safety systems appear to perform as designed and there is no evidence of core heatup for a variety of accident conditions, three phenomena of interest have been identified for further investigation to determine whether they are relevant to AP600.

One of the phenomena identified for further investigation is the rapid condensation and potential for water hammer which may occur following the actuation of the ADS. Prior to actuation of ADS, a significant amount of liquid would be lost in a LOCA event. As an example, Figure 6 shows the liquid inventory distribution some time before ADS actuation. In this particular test a small break was located in the pressure balance line of one of the CMTs. As can be seen in Figure 6, vapor-liquid interfaces existed in the upper plenum and the core among other places. However, there was a substantial amount of subcooling in the bulk region of the cold legs, core, and the upper plenum as a result of efficient cooling mainly by the PRHR system and the CMTs. Upon actuation of ADS, large valves in the ADS line were opened particularly when the ADS stage 2 was actuated. A large amount of fluid then rushed out of the pressurizer to the IRWST, causing a large amount of liquid and vapor to be drawn up toward the pressurizer from the other parts of the system. This action created a breakup of vapor-liquid interfaces and allowed vapor and subcooled liquid to come in contact, causing the rapid condensation of steam and the generation of pressure spikes and possibly water hammer. A tremendous potential for fluid motion due to rapid condensation of steam following the ADS actuation is reflected in Figure 5, which indicates that the entire upper half of the core was occupied by the fluid of the same temperature.

The second phenomenon identified for further investigation is the occurrence of a large temperature gradient in the cold legs because of thermal stratification between the existing coolant and the cooled water returned from the PRHR. Figure 7 shows a temperature profile in the cold leg in the PRHR side. These temperatures were taken from a thermocouple rake which contained 5 equally spaced thermocouples across the cold leg. A large temperature gradient also existed in the other cold leg (the CMT side cold leg) as shown in Figure 8 even though the magnitude is less than that in the PRHR side cold leg. The extent and duration of the thermal stratification in the cold leg may not be representative of AP600 since similar tests in OSU showed a different behavior. For instance, a 1" cold-leg break in OSU did not show any thermal stratification even though a 2" cold-leg break test showed a thermal stratification. One of the major differences between ROSA and OSU is the arrangement of the PRHR return line. In ROSA the return line is connected to the cold leg about 85 cm downstream from the steam generator outlet plenum

whereas in OSU the return line enters the steam generator outlet plenum itself. This and other factors should be considered in extending the ROSA results to the AP600 plant.

The above two phenomena do not appear to affect any safety system functions seriously even though the thermal stratification in the cold leg would have some effect on other phenomena such as the recirculation around the CMT and the removal of mass and energy from the system through the break. The important thing is to recognize that they may be important to structural integrity, and thus they must be evaluated to determine whether they are relevant to the AP600.

The last phenomenon identified for further investigation is the occurrence of system-wide oscillations which were initiated following the actuation of the ADS stage 4 and which persisted until the liquid in the pressurizer drained out and the steam generation in the core became insignificant. During this particular time period, practically everything oscillated even though the amplitude was different for different variables. The oscillation was slow with the period varying from about 300 sec at the outset of the oscillation to about 100 sec near the end of the oscillation period. For example, Figure 9 through 12 show the collapsed liquid levels in the upper plenum and in the pressurizer, the pressure in the upper plenum, core temperatures, the mass flow rate through the ADS stage 4A line, and the injection flow rate from the IRWST to the downcomer. Some of these are in-phase while the others are out-of-phase with each other. For instance, the pressurizer liquid level is in-phase with the IRWST injection flow rate while it is out-of-phase with the upper plenum liquid level, upper plenum pressure, core temperatures, and the ADS4 flow rate. The causes for these oscillations have not been completely determined yet. However, some plausible explanations are described below.

The basic components involved in the characteristic, slow system-wide oscillations are shown in Figure 13. On close examination, one notices that there are two forcing functions which cause the oscillations to occur. One of them is that the liquid mass in the pressurizer needs to drain out. The other is that the steam generated in the core needs to vent out.

The liquid inventory shown in Figure 13 represents the condition shortly after the ADS stage 4 valves opened. Previously when the ADS stage 1 valves opened, a large amount of flow started passing through the ADS line connected to the top of the pressurizer. As the ADS stage 2 and 3 valves opened, the flow increased even more and carried a large mass of liquid from the vessel and the hot leg to the pressurizer which was soon filled completely with liquid. The liquid level in the pressurizer slowly decreased as the flow through the ADS1-3 line decreased as a result of decreasing pressure. When the liquid level in either of the two CMTs decreased to a set point, the ADS stage 4 valves opened, forcing a large amount of flow through the ADS4 line and drastically reducing and eventually eliminating the flow through the ADS1-3 line. When there was not enough upward flow in the pressurizer, the liquid mass in the pressurizer could not be supported and thus had to drain out. However, this draining process was not smooth because the space vacated by the draining liquid had to be occupied by the steam which had to come from the hot leg

below since the ADS stage 1-3 line was closed for the vapor flow. Since the surge line pipe was not big enough to allow steam and water to have a stable countercurrent flow, the liquid downflow was intermittent; the liquid downflow first followed by the steam upflow. This oscillatory draining process continued until all of the liquid drained out from the pressurizer. The upward steam flow carried liquid with it, and thus the liquid draining process was prolonged.

The other cause for the oscillations is due to the fact that two-phase flow must go through restricted openings of the ADS stage 4 valves in order to vent. In other words, if these openings are large enough to avoid any significant interference with two-phase flows, the venting process would not cause any oscillations. When two-phase flows vent through restricted openings such as ADS stage 4 lines, they may exhibit oscillatory behavior particularly when the upstream pressure is lower than that which would produce choked flow. The postulated reason is as follows. At the restricted openings the liquid piles up as a result of preferential passage of vapor, and eventually the openings may be filled up completely with the liquid at which time steam still being generated in the core would start raising the pressure. When the pressure is high enough, a liquid plug formed at the restricted openings would be expelled, clearing the way for steam to vent again with the accompanying reduction in pressure. This alternate blockage and clearing of two-phase flow would produce oscillations in pressure which in turn would affect many other system variables.

The two mechanisms giving rise to oscillations as described above are not independent of each other because they both affect the common variables which in turn provide a feedback to the driving variables. For instance, as the pressurizer liquid drains, it would tend to increase the liquid level in the hot leg which in turn would tend to increase the probability of forming a liquid plug in the ADS4 line which would increase the pressure in the hot leg and the vessel, which would reverse the liquid downflow in the pressurizer as steam would now try to fill the space that had just been vacated by the draining liquid.

The system-wide oscillations described above did not seriously affect any safety functions nor core coolability. However, if such oscillations are to occur in the AP600, the operator should be made aware of when and why such oscillations would occur.

For the scenarios investigated, a concern about the possible violent condensation taking place in the top region of CMTs did not materialize. Instead, the ROSA/AP600 tests showed that recirculation between cold legs and CMTs warmed up cold liquid in CMTs which eventually flashed as the system depressurized to allow the CMTs to drain. If flashing did not generate enough pressure to overcome the downstream pressure, draining would be delayed until the cold leg was uncovered such that steam could flow up to the top of the CMT through a pressure balance line. In this latter case, a violent condensation did not occur because the top part of the CMT liquid had already been warmed up.

The test matrix also included tests for investigating the effect of non-safety systems on safety system functions. Specifically, the effect of a makeup pump on the system behavior was investigated and found to be insignificant. Interactions among the subsystems were also investigated, and no detrimental interactions were identified.

V. Conclusion

The AP600 safety systems, as reflected in ROSA, seem to function as designed, and there is no evidence of core heatup in all of the accident scenarios which were investigated. However, three phenomena of interest have been identified for further examination to determine whether they are relevant to the AP600.

VI. References

1. Rhee, G., Bessette, D., and Shotkin, L., "NRC Confirmatory Safety System Testing in Support of AP600 Design Review," Proc. of ARS '94 International Topical Meeting on Advanced Reactors Safety, 1994, Pittsburgh, PA, pp. 977-984.

2. Boucher, T.J., et al., "Design Modifications of LSTF for AP600 Testing," INEL-95/0200, July 1995.

3. Kukita, Y., et al., "ROSA/AP600 Testing: Facility Modifications and Initial Test Results," Proc. of 22nd Water Reactor Safety Information Meeting, 1994, Washington D.C.

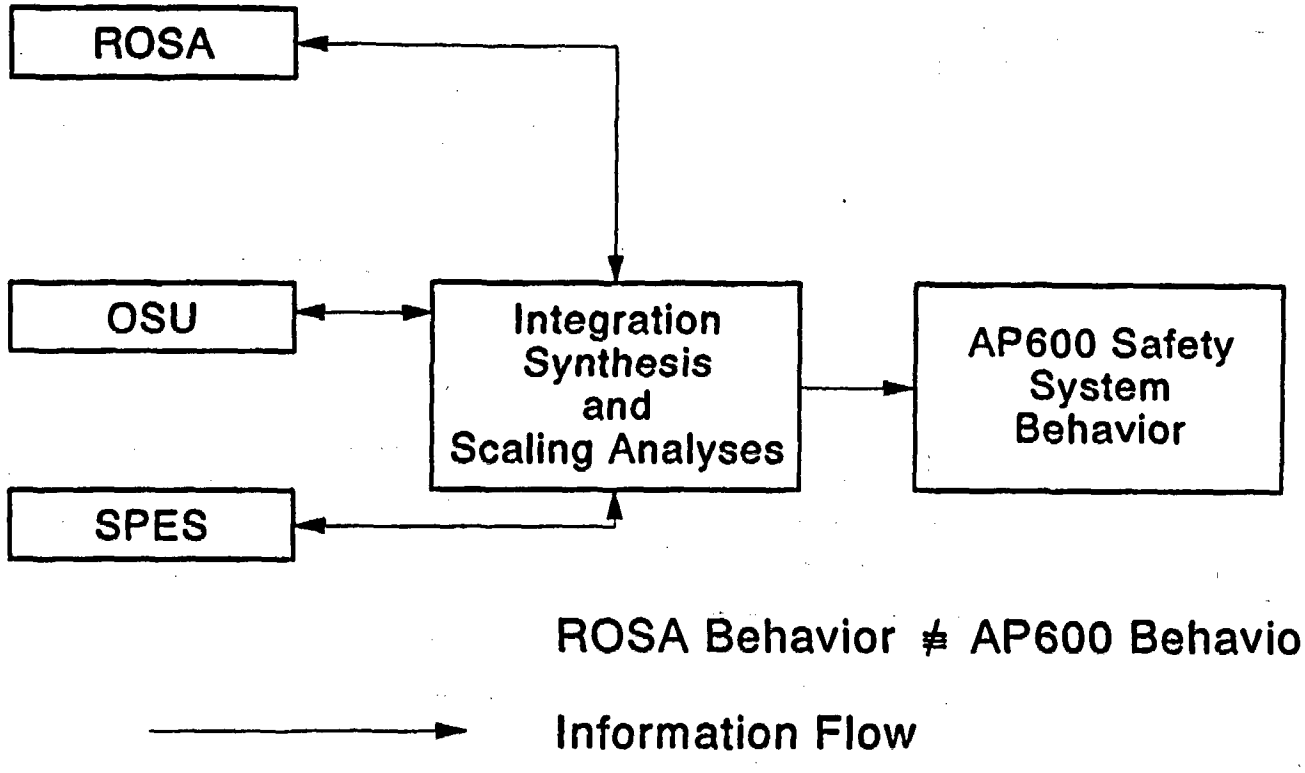

Figure 1 ROSA/AP600 Test Program as Part of Overall Program for Predicting AP600 Safety System Behavior

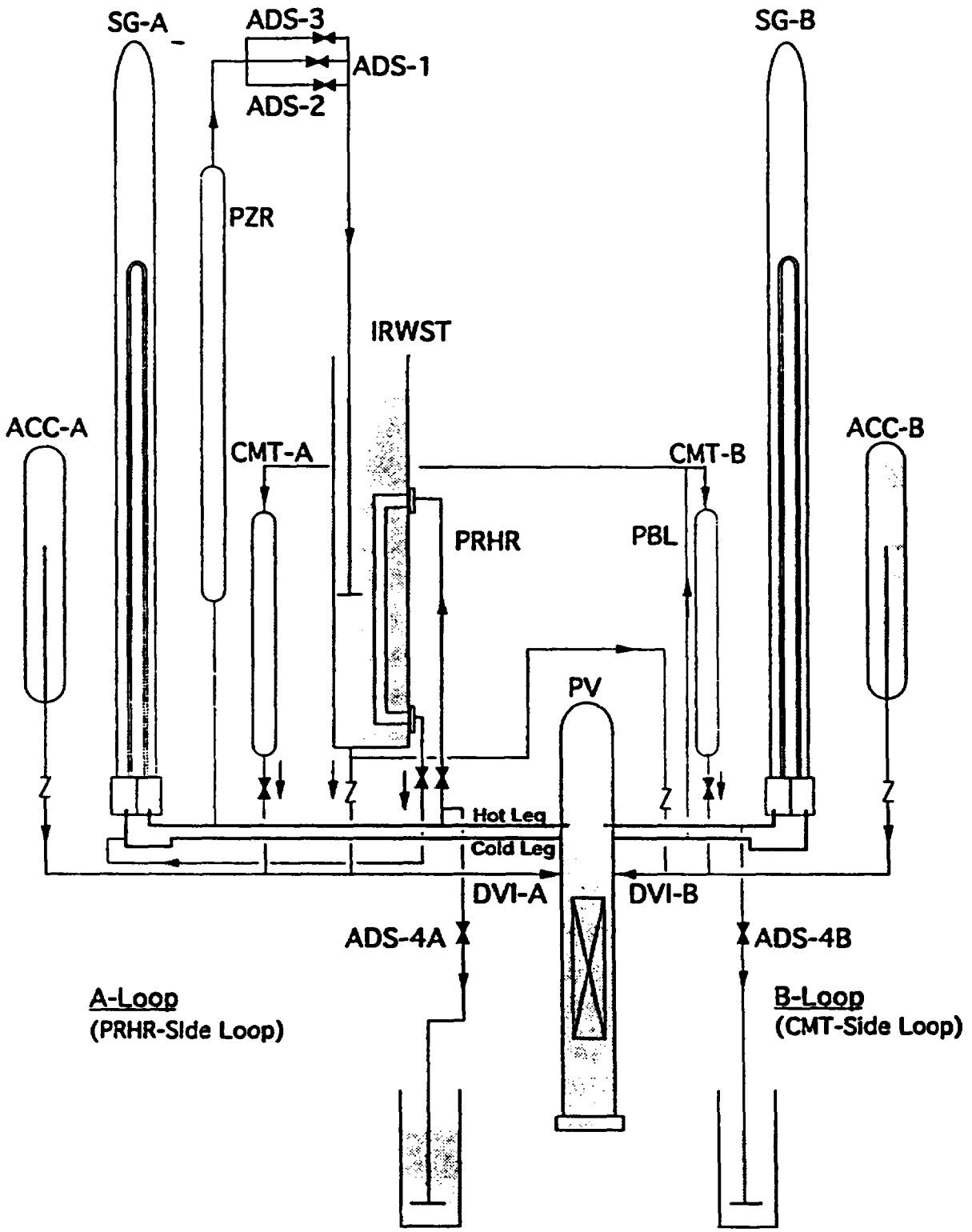

FIGURE 2 ROSA/AP600 TEST FACILITY LAYOUT

Table 1 ROSA-AP600 Program Test Matrix

No	Test	Date	Test Description
1	AP-CL-03	April 14, '94	1-Inch Bottom-Oriented Cold Leg (CL) SBLOCA[1]. SPES Configuration & ADS Stages 1, 2, 3 One-Valve Operation.
2	AP-AD-01	May 17, '94	Inadvertent Opening of ADS Stage[1]. SPES Configuration.
3	AP-CL-04	June 7, '94	1/2-Inch Bottom-Oriented CL SBLOCA[1]. AP600 Configuration.
4	AP-PB-01	June 28, '94	2-Inch Pressure Balance Line (PBL) SBLOCA[1]. SPES Configuration.
5	AP-CL-05	August 2, '94	1-Inch Bottom-Oriented CL SBLOCA with Failure of ADS Stages 1, 2, & 3. AP600 Configuration.
6	AP-PB-02	Sept 20, '94	1-Inch PBL SBLOCA, A-Loop CMT Check Valves Failed Closed, B-Loop Loop Seal Bypass Open. AP600 Configuration.
7	AP-DV-01	Oct 11, '94	Direct Vessel Injection (DVI) Line Double-Ended-Guillotine Break (DEGB)[1]. AP600 Configuration with revised coolant pump coastdown.
8	AP-CL-06	Nov. 1, '94	1-Inch Top-Oriented CL SBLOCA[1]. SPES Configuration & ADS Stages 1, 2, 3 One-Valve Operation.
9	AP-BO-01	Nov. 24, '94	Station Blackout[1,2]. AP600 Configuration with revised coolant pump coastdown.
10	AP-SG-01	Dec. 17, '94	Steam Generator Tube Rupture (SGTR): 1-3/4 Tubes Ruptured[1]. AP600 Configuration with revised coolant pump coastdown.
11	AP-SL-01	April 18, '95	Main Steam Line Break with 5-Tube SGTR[1]. AP600 Configuration.
12	AP-CL-07	May 16, '95	1-Inch Bottom-Oriented CL SBLOCA with Failure of 75% of ADS Stage 4 (Only 25% of ADS Stage 4 in B-Loop)[3]. SPES Configuration & ADS Stages 1, 2, 3 One-Valve Operation.
13	AP-CL-08	June 6, '95	2-Inch Bottom-Oriented CL SBLOCA[1,4,5]. AP600 Configuration with revised coolant pump coastdown.
14	AP-CL-09	June 27, '95	1-Inch Bottom-Oriented CL SBLOCA with Chemical Volume Control System (CVCS) Makeup Pump Injecting Into A-Loop Crossover Leg, 1 Accumulator (A-Loop), No CMTs, 50% of ADS, & 1 of 2 IRWST Gravity Drain Lines (A-Loop). AP600 Configuration with revised coolant pump coastdown.

1 One Stage 4 ADS valve failed in B-Loop.
2 Core power decay curve includes G-Factor henceforth.
3 PRHR heat exchanger bundle reduced from 45 tubes to 21 tubes.
4 Steam separators installed on ADS Stage 4 discharge lines.
5 IRWST Feed & Bleed system used.

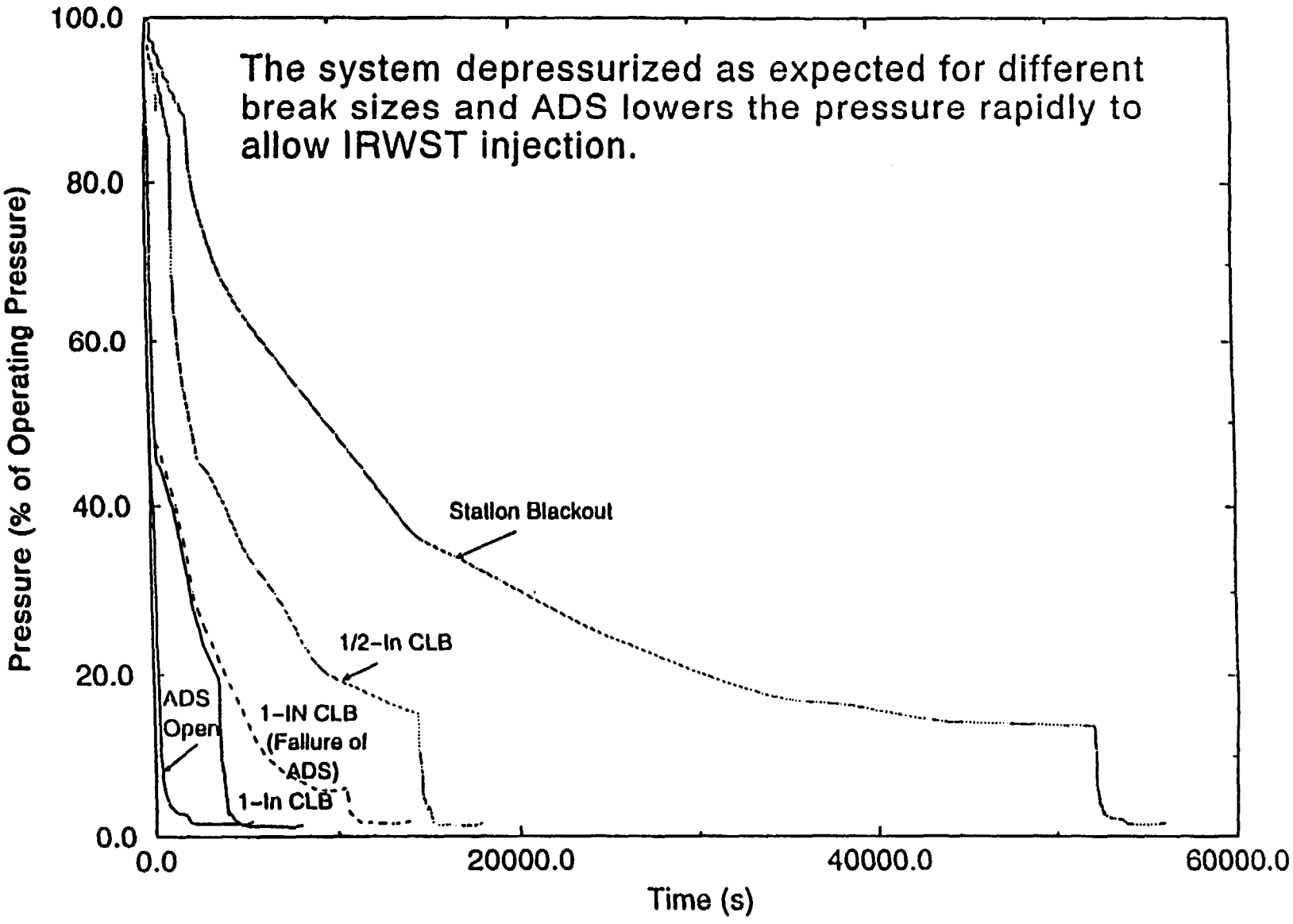

Fig. 3 Primary Pressure

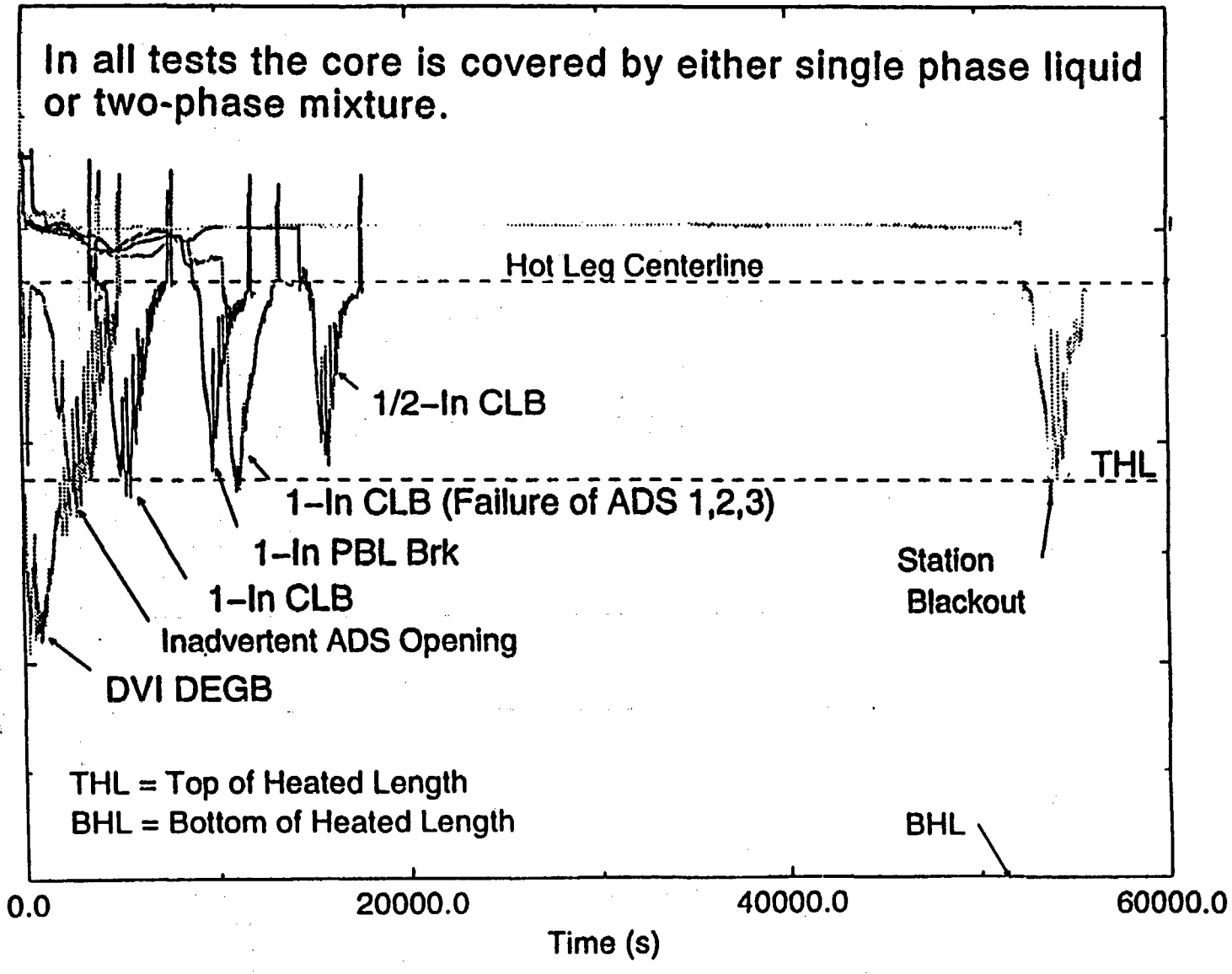

Fig. 4 Collapsed Liquid Levels in Core and Upper Plenum

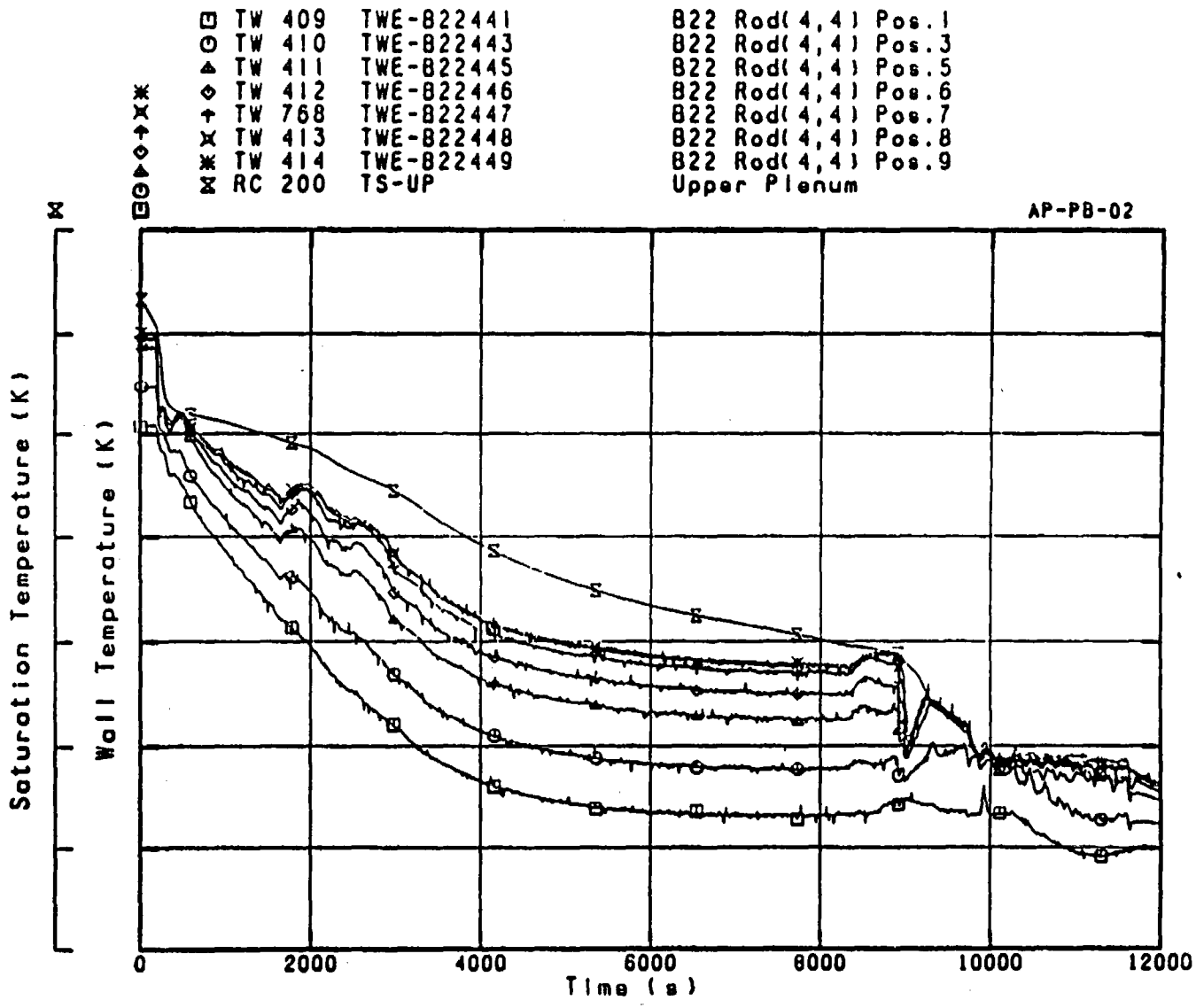

Fig. 5 Fuel Rod Surface Temperatures in Core

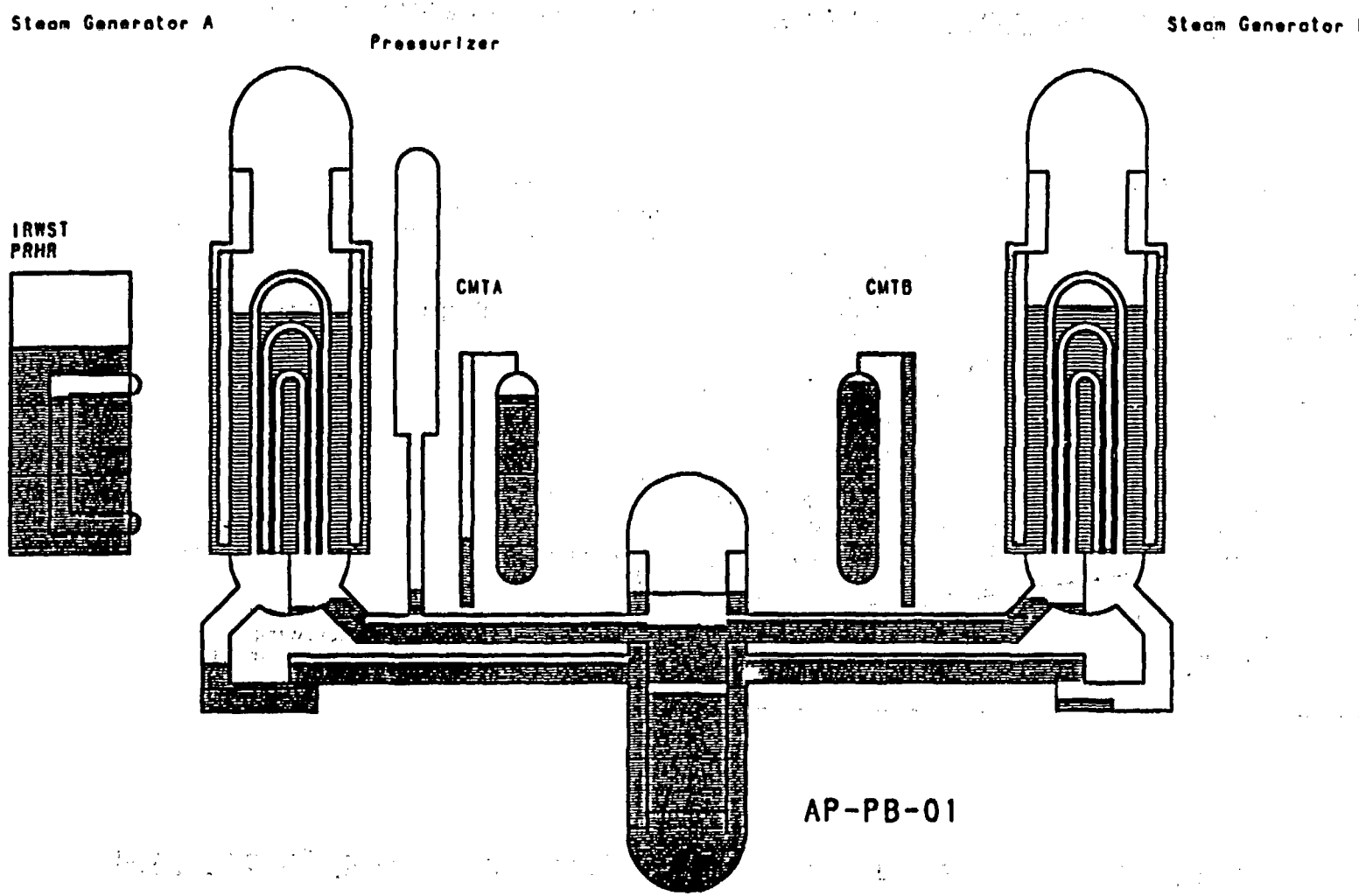

Fig. 6 Coolant Mass Inventory Distribution (At 1000 s)

PRHR Cooling Resulted in a Large Temperature Gradient Across Cold Leg

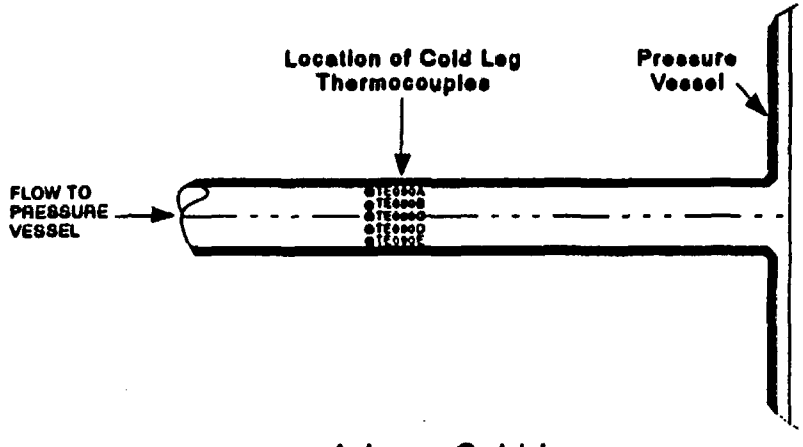

A-Loop Cold Leg

NOTE: Temperature traces are shown in order given in legend.

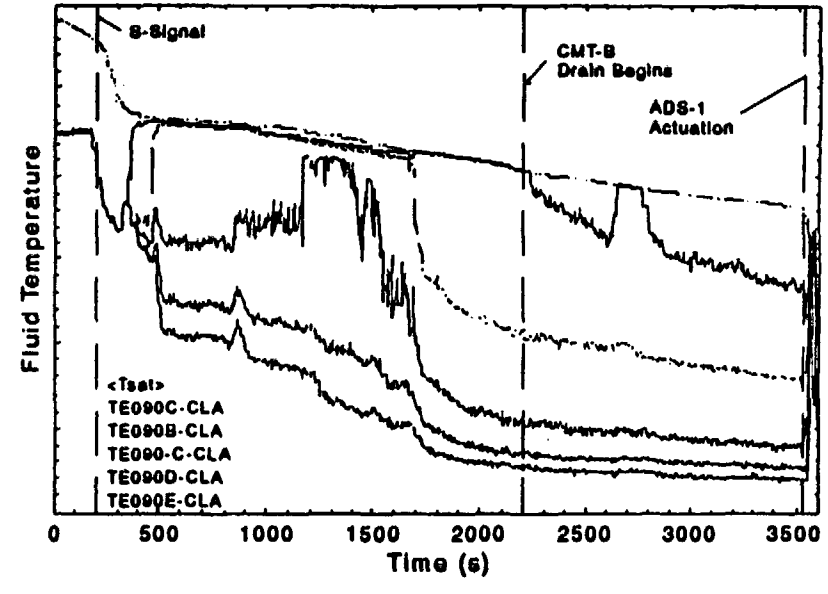

A-Loop Cold Leg Temperatures

Fig. 7 Fluid Temperature Behavior in ROSA-AP600 PRHR Side Cold Leg

PRHR, CMT and Accumulator Flows Result in Large Temperature Gradients in Cold Leg

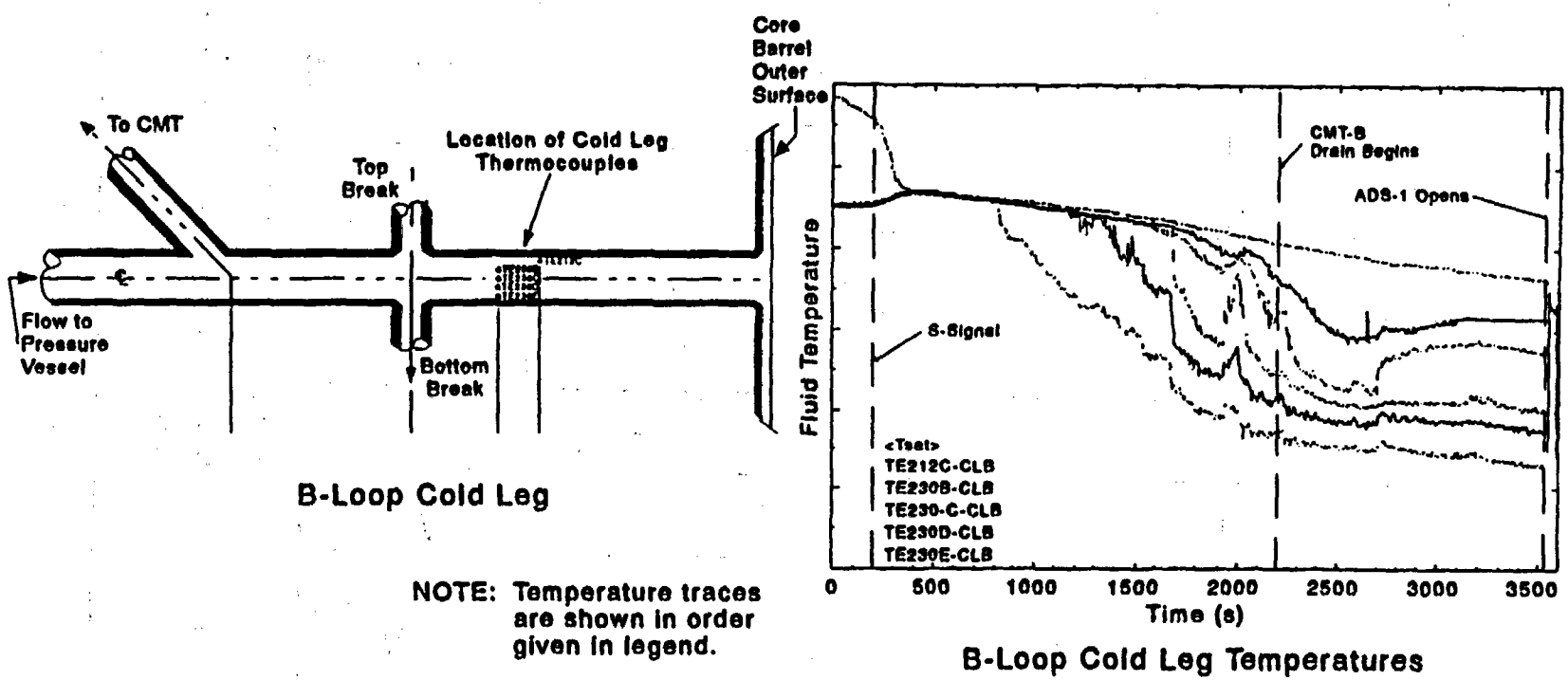

Fig. 8 Fluid Temperature Behavior in ROSA-AP600 CMT Side Cold Leg

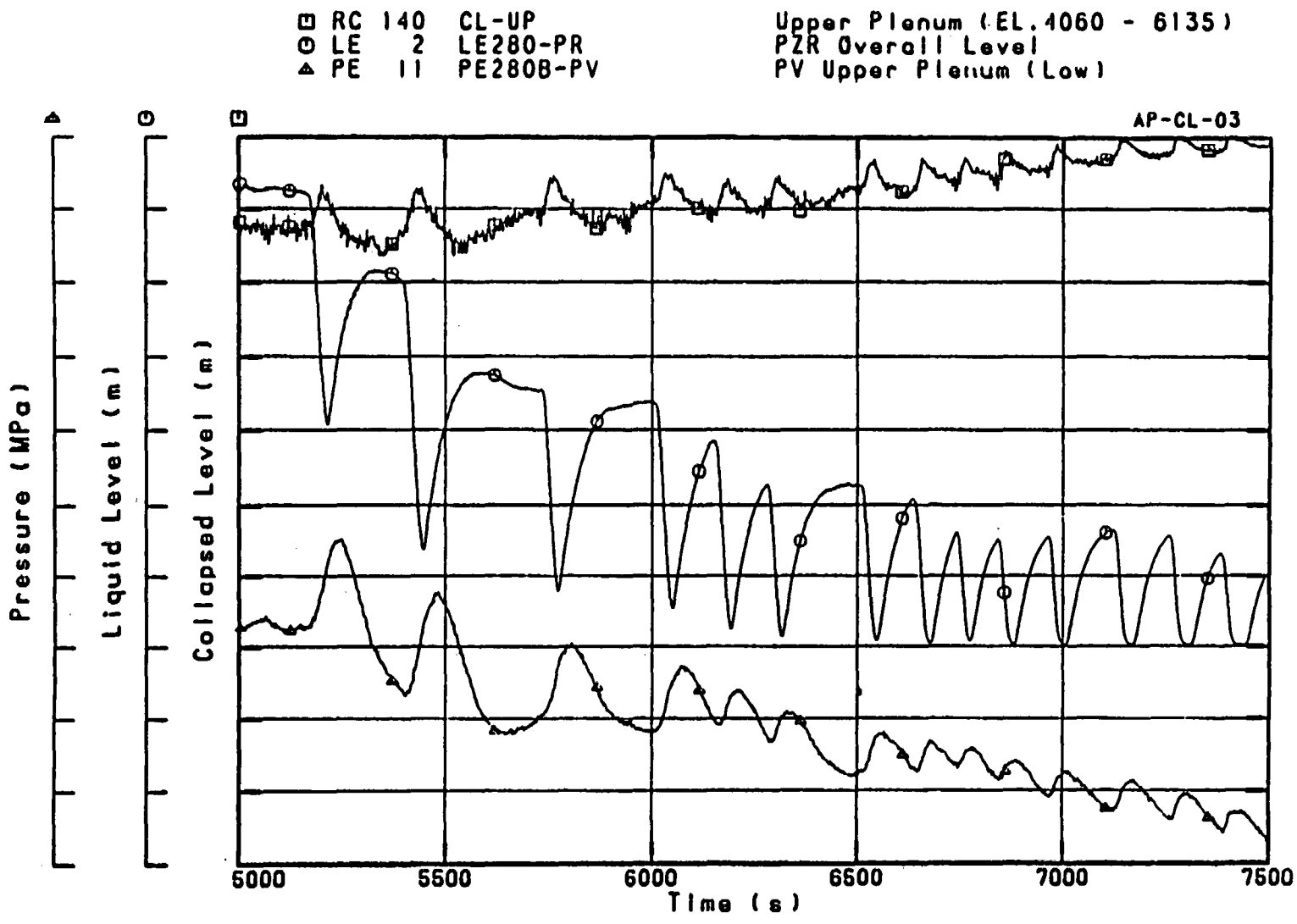

Fig. 9 UP Pressure, UP and Pressurizer Liquid Levels

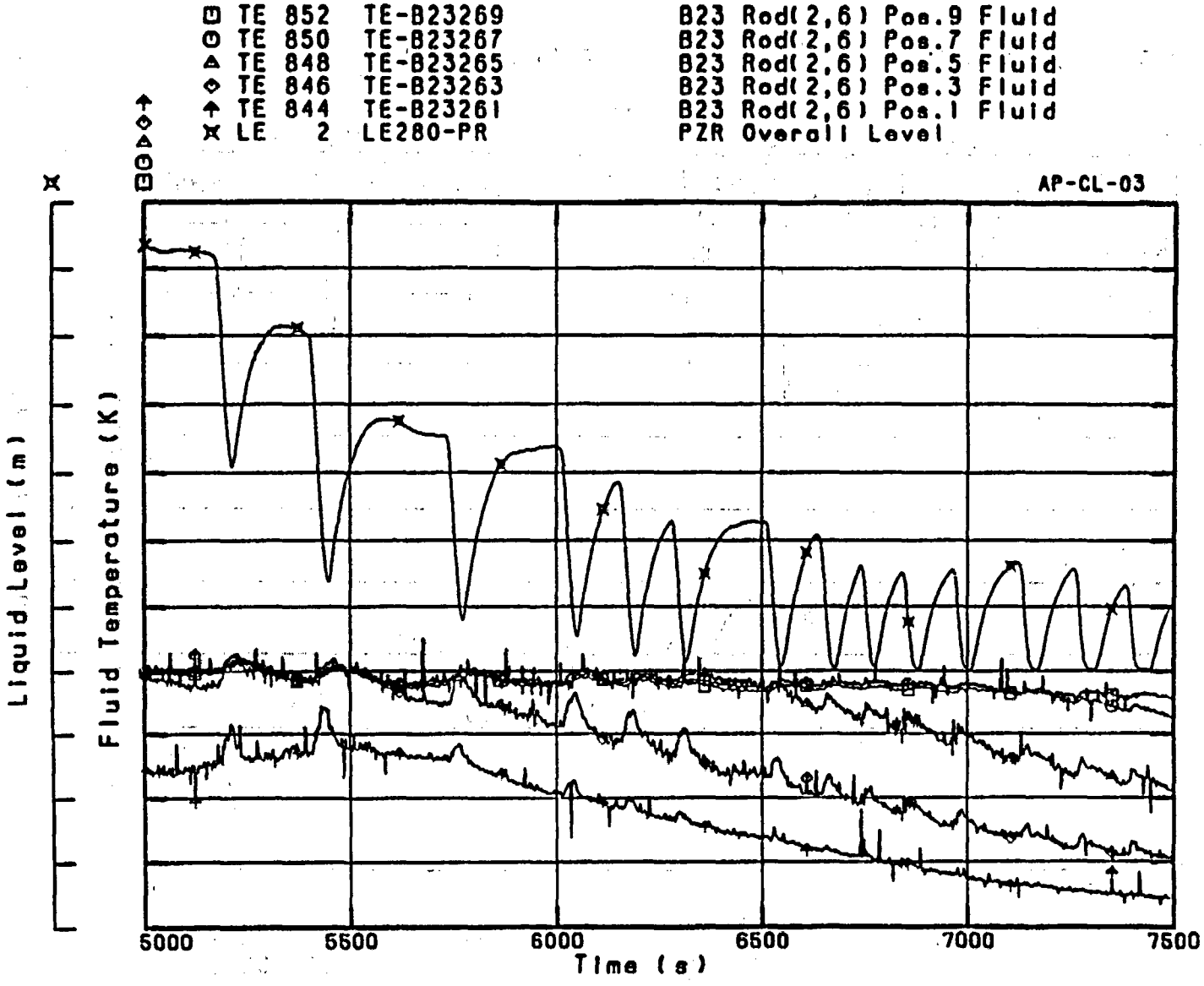

Fig. 10 Core Fluid Temperatures and PZR Liquid Level

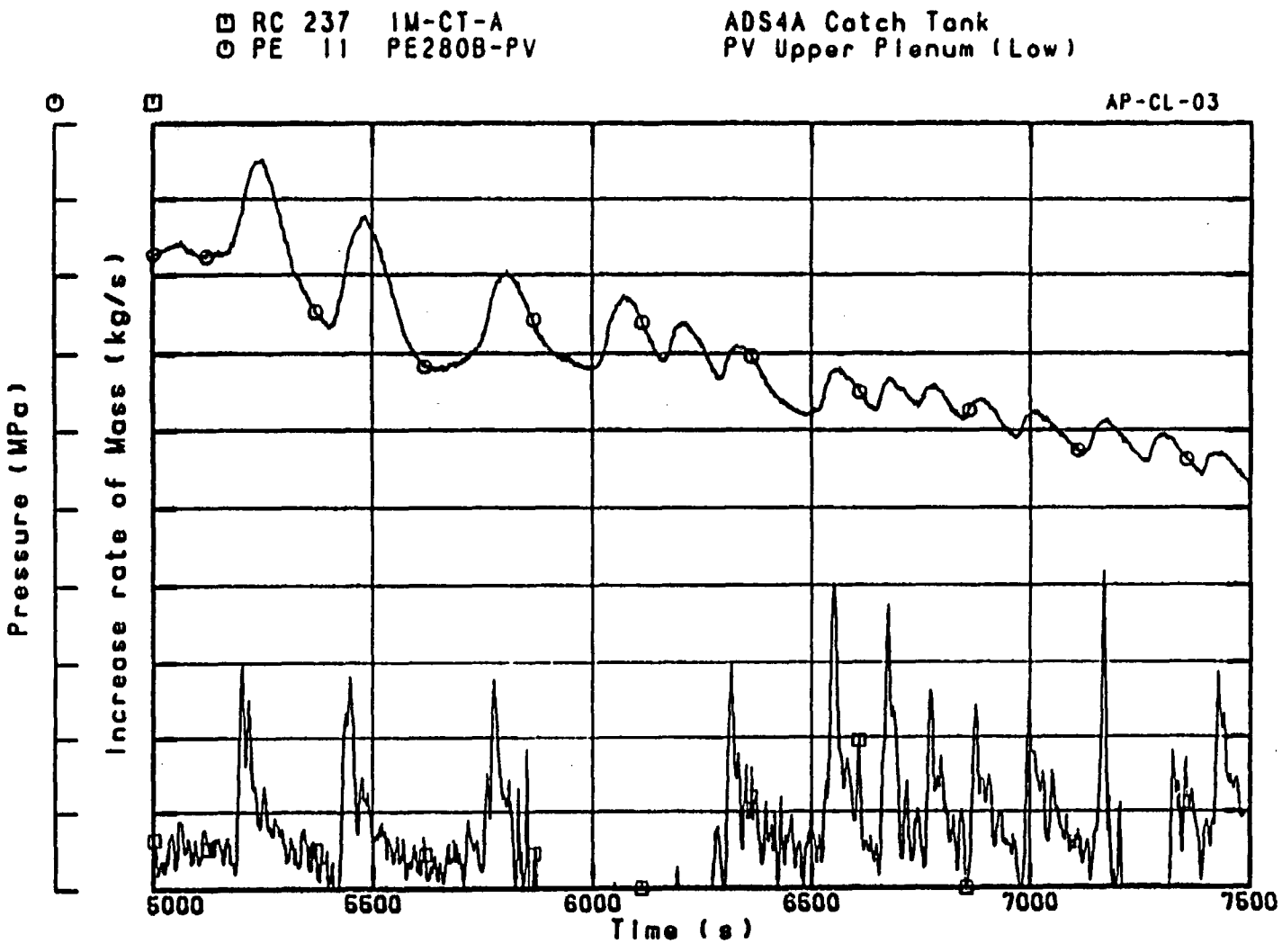

Fig. 11 ADS-4A Flowrate and Upper Plenum Pressure

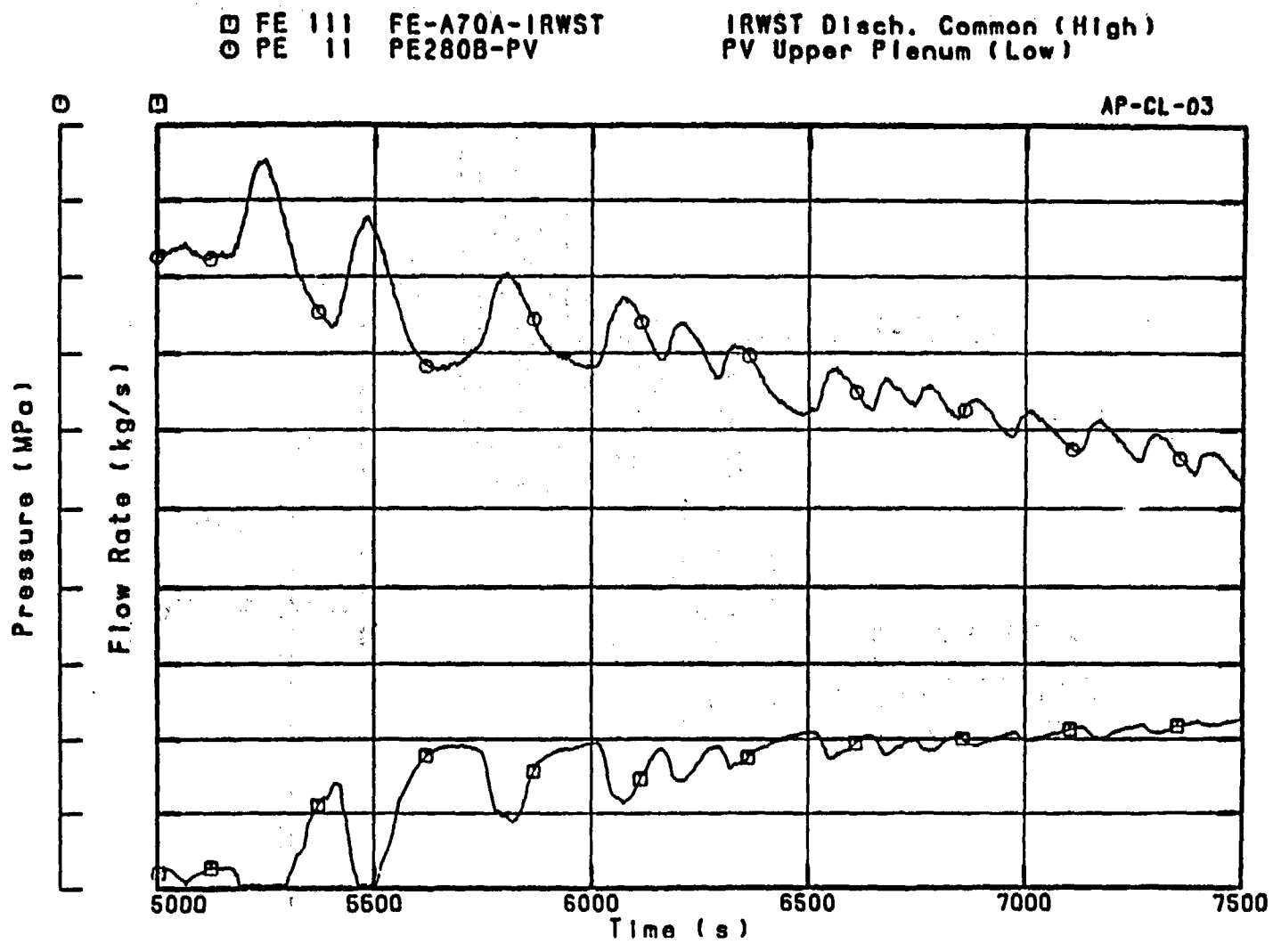

Fig. 12 IRWST Discharge and Upper Plenum Pressure

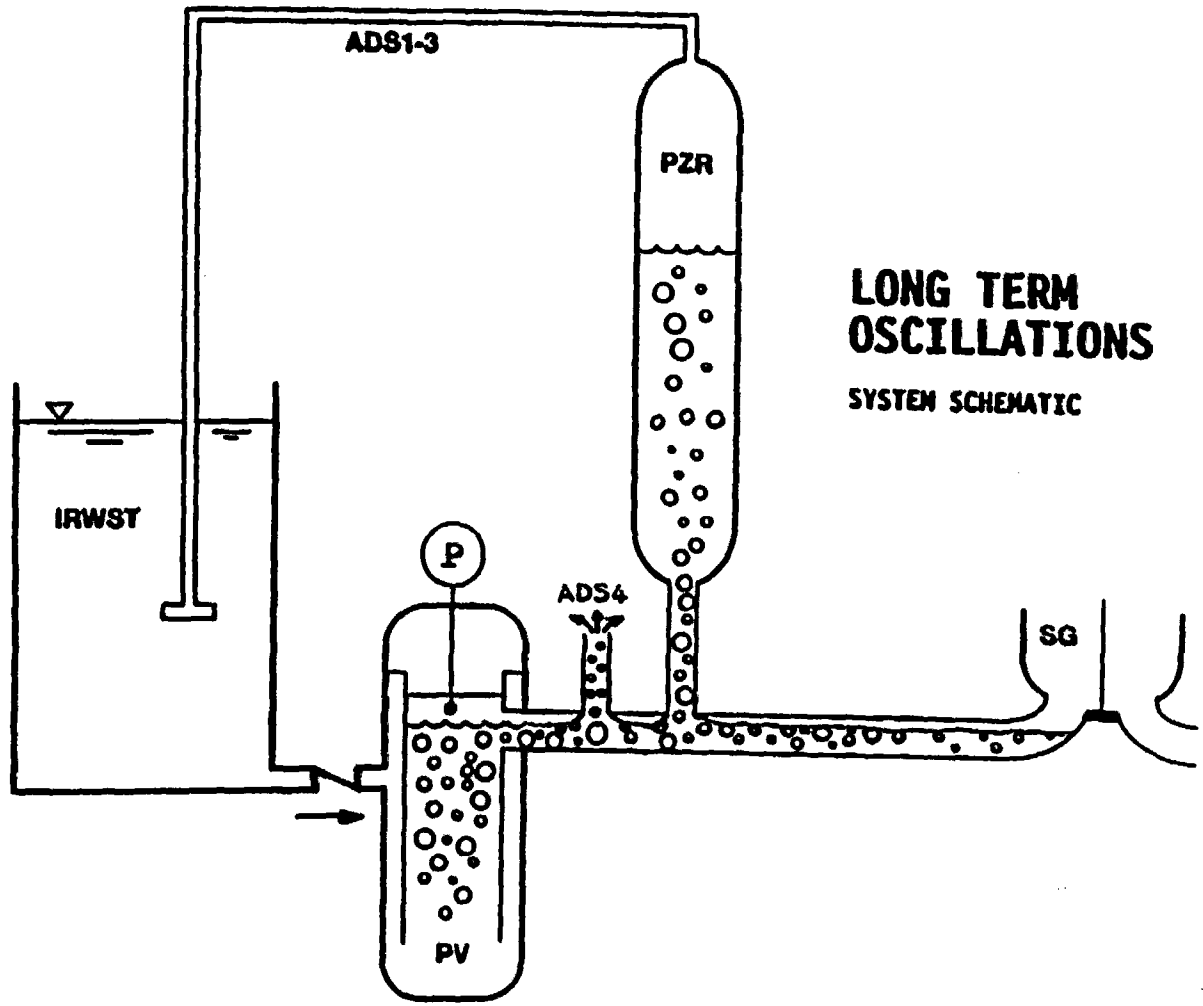

FIGURE 13 SCHEMATIC DIAGRAM OF PRIMARY SYSTEM INVOLVED IN SLOW SYSTEM-WIDE OSCILLATIONS

NRC FORM 335 (2-89) NRCM 1102, 3201, 3202

U.S. NUCLEAR REGULATORY COMMISSION

BIBLIOGRAPHIC DATA SHEET

(See instructions on the reverse)

1. REPORT NUMBER (Assigned by NRC, Add Vol., Supp., Rev., and Addendum Numbers, If any.)

NUREG/CP-0149
Vol. 1

2. TITLE AND SUBTITLE

Proceedings of the Twenty-Third Water Reactor Safety Information Meeting

Plenary Session, High Burnup Fuel Behavior, Thermal Hydraulic Research

3. DATE REPORT PUBLISHED

MONTH	YEAR
March	1996

4. FIN OR GRANT NUMBER

A3988

5. AUTHOR(S)

Compiled by Susan Monteleone, BNL

6. TYPE OF REPORT

Conference Proceedings

7. PERIOD COVERED *(Inclusive Dates)*

October 23-25, 1995

8. PERFORMING ORGANIZATION – NAME AND ADDRESS *(If NRC, provide Division, Office or Region, U.S. Nuclear Regulatory Commission, and mailing address; if contractor, provide name and mailing address.)*

Office of Nuclear Regulatory Research
U.S. Nuclear Regulatory Commission
Washington, DC 20555-0001

9. SPONSORING ORGANIZATION – NAME AND ADDRESS *(If NRC, type "Same as above"; if contractor, provide NRC Division, Office or Region, U.S. Nuclear Regulatory Commission, and mailing address.)*

Same as Item 8 above.

10. SUPPLEMENTARY NOTES C. Bonsby, NRC Project Manager
Proceedings prepared by Brookhaven National Laboratory

11. ABSTRACT *(200 words or less)*

This three-volume report contains papers presented at the Twenty-Third Water Reactor Safety Information Meeting held at the Bethesda Marriott Hotel, Bethesda, Maryland, October 23-25, 1995. The papers are printed in the order of their presentation in each session and describe progress and results of programs in nuclear safety research conducted in this country and abroad. Foreign participation in the meeting included papers presented by researchers from France, Italy, Japan, Norway, Russia, Sweden, and Switzerland. The titles of the papers and the names of the authors have been updated and may differ from those that appeared in the final program of the meeting.

12. KEY WORDS/DESCRIPTORS *(List words or phrases that will assist researchers in locating the report.)*

BWR type reactors-reactor safety, international organizations-meetings, PWR type reactors-reactor safety, water cooled reactors-proceedings, Human Factors, Reactor Control Systems, Reactor Instrumentation, Probabilistic Estimation, Risk Assessment

13. AVAILABILITY STATEMENT

Unlimited

14. SECURITY CLASSIFICATION

(This Page) Unclassified

(This Report) Unclassified

15. NUMBER OF PAGES

16. PRICE

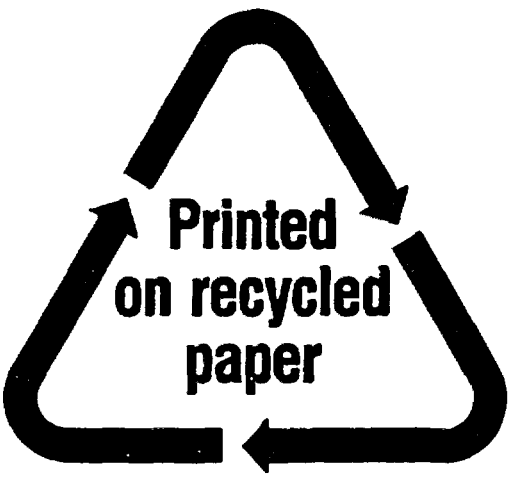

Federal Recycling Program

UNITED STATES
NUCLEAR REGULATORY COMMISSION
WASHINGTON, D.C. 20555-0001

OFFICIAL BUSINESS
PENALTY FOR PRIVATE USE, $300

SPECIAL FOURTH-CLASS RATE
POSTAGE AND FEES PAID
USNRC
PERMIT NO. G-67